JAERI-M
82-120

COMPARISON REPORT FOR CSNI INTERNATIONAL STANDARD PROBLEM 12 (ROSA-III RUN 912)

September 1982

Kanji TASAKA, Yoshinari ANODA, Hiroshige KUMAMARU
Hideo NAKAMURA, Masanori IRIKO,* Taisuke YONOMOTO
and Masayoshi SHIBA

日本原子力研究所
Japan Atomic Energy Research Institute

JAERI-Mレポートは，日本原子力研究所が不定期に公刊している研究報告書です。
入手の問合わせは，日本原子力研究所技術情報部情報資料課（〒319-11茨城県那珂郡東海村）あて，お申しこしください。なお，このほかに財団法人原子力弘済会資料センター（〒319-11 茨城県那珂郡東海村日本原子力研究所内）で複写による実費頒布をおこなっております。

JAERI-M reports are issued irregularly.
Inquiries about availability of the reports should be addressed to Information Section, Division of Technical Information, Japan Atomic Energy Research Institute, Tokai-mura, Naka-gun, Ibaraki-ken 319-11, Japan.

編集兼発行　日本原子力研究所
印　　刷　いばらき印刷㈱

JAERI-M 82-120

Comparison Report for CSNI International Standard Problem 12 (ROSA-III Run 912)

Kanji TASAKA, Yoshinari ANODA, Hiroshige KUMAMARU,
Hideo NAKAMURA, Masanori IRIKO*,
Taisuke YONOMOTO and Masayoshi SHIBA

Division of Nuclear Safety Research,
Tokai Research Establishment, JAERI

(Received August 9, 1982)

ROSA-III Run 912 was identified as International Standard Problem 12 by the Committee on the Safety of Nuclear Installations. Run 912 simulated a 5% split break LOCA condition in a BWR at the pump suction in the recirculation line with the HPCS failure. Comparisons between the test data and the calculations by eight international participants were made and discussed.

Keywords:
ROSA-III, RUN912, 5% Split Break, HPCS Failure, BWR, LOCA, ISP-12, CSNI Calculation, Open Problem, System Pressure, Break Flow Rate, Heater Rod Surface Temperature, Liquid Level, Peak Cladding Temperature

---

* On leave from Computer Service Corporation (CSK)

JAERI－M 82－120

CSNI 国際標準問題 12 番（ROSA－Ⅲ Run 912）比較レポート

日本原子力研究所東海研究所安全工学部
田坂　完二・安濃田良成・熊丸　博滋
中村　秀夫・入子　真規*・与能本泰介
斯波　正誼

（1982 年 8 月 9 日受理）

Organization for Economic cooperation and Development の committee on Safety of Nuclear Installations において，ROSA－Ⅲ実験 RUN 912 が国際標準問題 No. 12 に選定された。ROSA－Ⅲ実験 RUN 912 は，1981 年 5 月 19 日に日本原子力研究所において行われた。ROSA－Ⅲ装置は，沸騰水型原子炉（BWR）の冷却材喪失事故（LOCA）を模擬実験するための装置であり，RUN 912 では再循環ポンプ吸込側配管の小破断実験を行った。破断面積は 27.3 mm^2 で，これは BWR の再循環ポンプ吸込側配管の 5 %破断に相当する。

RUN 912 は，蒸気ドーム圧力 7.35 ± 0.1 MPa，下部プレナム温度 552 ± 1 K，下部プレナム未飽和度 10.5 K，炉心入口流量 16.0 Kg／s，炉心出口クォリティ 13.5 %，最大線出力 16.7 kW／m の初期条件から実験が開始された。高圧炉心スプレイ系は故障していると仮定された。

8 機関の参加者より，5 つの異なる計算コードを使用して計算結果が提出され，それらの計算結果と ROSA－Ⅲ実験 RUN 912 の実験結果との比較が行われた。破断流の計算結果と実験結果の一致はあまり良くないが，安全弁モデルを組み込んだ解析では，圧力の時間変化の計算結果と実験結果との一致は，満足できるものであった。燃料棒表面温度の時間変化は，炉心の水位変化と相関している。炉心の水位および燃料棒表面温度についての各参加者からの計算結果は，相当に大きなばらつきがあった。参加者によっては，水位および燃料棒表面温度の傾向をよく計算できたが，参加者によっては，水位および燃料棒表面温度の計算結果と実験結果の一致はよくなかった。

---

* 外来研究員：コンピューターサービス（株）（CSK）

The following conclusions were arrived at for ISP-12 OECD/NEA CSNI LOCA International Standard Problems.

1. In general the computer codes used for the analysis of the ROSA-III international open standard problem had the capability to predict the important features of the small break transint.

2. Prediction of the mixture level transient inside the shroud was found to be important in the code having the ability to calculate the measured core temperature. To correctly predict the mixture level it was found that the codes needed the ability to accurately calculate the core inlet flow, depressurization rate, ECCS actuation, and interphase drag in the advanced codes or bubble rise in the first generation computer codes.

3. Prediction of the vessel pressure and downcomer mixture level transients were found to be important factors in predicting the correct performance of ECCS and therefore the correct primary system response.

4. Energy balance in the form of steam flows are of primary importance in the BWR small break LOCA especially to predict the system pressure accurately.

Summary

The Committee on the Safety of Nuclear Installations of the Organization for Economic Cooperation and Development designated ROSA-III Test Run 912 as International Standard Problem 12. ROSA-III Test Run 912 was conducted on May 19, 1981 at Japan Atomic Energy Research Institute. The ROSA-III test system was assembled to represent a small break in the recirculation pump suction line of a commercial boiling water reactor (BWR). The break size was 27.3mm^2 which is equivalent to about a 5% break of the recirculation suction line in a commercial BWR.

RUN 912 was indicated from primary coolant system initial conditions of: steam dome pressure, 7.35±0.1 MPa; lower plenum temperature, 552±1 K; lower plenum subcooling, 10.5 K; core inlet flow rate, 16.0 kg/s; core exit quality, 13.5% and the maximum linear heat rate, 16.7 kW/m. The high pressure core spray system was assumed to have failed.

Calculations were submitted by eight participants using five different computer codes and a comparison was made between participants calculations and measurements from ROSA-III Test Run 912. Although relatively poor agreement occured between the calculated and measured break mass flow rate, the agreement between the measured and calculated system pressure responce was in general satisfactory in those analyses with the built-in model for the safety relief valve. The heater rod surface temperature transient can be corrected to the liquid level transient in the core. There was large scatter among the calculated results of the liquid level and heater rod surface temperature transients in the core. However, several participants were able to calculate the trends of the liquid level and heater rod surface temperatures well. Agreement between measured and calculated transients of the liquid level and heater rod surface temperatures was poor for some participants.

Contents

目　　次

List of Tables

List of Figures

1. Introduction

At the seventh CSNI* LOCA/ECC and Fuel Behavior Working Group meeting held on June 23rd through 25th, 1980 in Paris, it was approved that Run 912 test of ROSA-III program be the international standard problem number twelve (ISP-12). ROSA-III program is an experimental program to conduct system effect tests concerning a loss-of-coolant accident (LOCA) with emergency core cooling (ECC) in a BWR.
The program has been carried out at Tokai Research Establishment of the Japan Atomic Energy Research Institute (JAERI) since 1976 as a part of Japanese research programs on light water reactor safety. Since Run 912 was the first standard problem concerning a BWR LOCA, it was decided that ISP-12 be categorized as an open problem and the test results released before conducting the analyses.

The ROSA-III program's primary objective is to study the thermal hydraulic response of a BWR during a LOCA with ECC and to provide a base data to evaluate the predictability of computer codes developed for BWR LOCA/ECC analyses. The test facility used in the program is called the ROSA-III facility and is a volumetrically scaled (1/424) BWR system with an electrically heated core. The facility is heavily instrumented such that various thermal hydraulic transients during the tests can be measured.

A detailed description of the ROSA-III test facility, the test conditions of Run 912, and the specification of plot out had been transmitted from JAERI to the participants before conducting the test. Run 912 was successfully conducted on May 19, 1981. Run 912 is a simulated LOCA test with the 5% split break condition at the pump suction in the recirculation line piping. The high pressure core spray system (HPCS) was assumed to fail. The entire core was uncovered and exposed to a steam enviroment. The core was cooled after ECC injection. The cladding temperature increased and then decreased one time.
The peak cladding temperature reached in the test was 839 K. All the cladding was quenched after the low pressure coolant injection system (LPCI) started injecting water into the core bypass and the effectiveness of the ECCS was confirmed.

---

* OECD/NEA Committee on Safety of Nuclear Installations

All the Run 912 data was processed by computer and released to the participants in July, 1981.

Eight participants submitted the calculations of Run 912 transients by April 20th, 1982. Table 1.1 lists the participants names and computer codes. Each participant listed in Table 1.1 submitted the calculations and about one hundred plots in accordance with the specification prepared by JAERI.

Each calculation has been reviewed and compared to the experimental data by the JAERI staff. Comparison plots for the transients of important variables are shown and discussed in this report.

Table 1.1 List of Contributors

Country (Organization)	Identification	Computer Code	Time Interval [s]
USA (INEL*1)	U	TRAC-BD1	0 ∿ 500
Switzerland (EIR*2)	S	RELAP4/MOD6	0 ∿ 328
Sweden-Finland (Studsvik-VTT*3)	F	RELAP5/MOD1 (cycle 014)	0 ∿ 285
Netherlands (ECN*4)	N	RELAP4/MOD6	-2 ∿ 166
Japan (JINS*5)	J	RELAP4/MOD6/ U4/J3 (modified)	0 ∿ 472
Japan (JAERI-C*6)	C	THYDE-B1	0 ∿ 396
Japan (JAERI-A*7)	A	RELAP4/MOD6/ U4/J3	0 ∿ 469
Japan (JAERI-R*8)	R	RELAP5/MOD1 (cycle 001)	0 ∿ 372

*1 Idaho National Engineering Laboratory

*2 Swiss Federal Institute for Reactor Research

*3 Studsvik Energiteknik Ab
Technical Research Center of Finland

*4 Netherlands Energy Research Foundation

*5 Institute of Nuclear Safety, Japan

*6 Japan Atomic Energy Research Institute
Division of Nuclear Safety Evaluation
Nuclear Safety Code Development Laboratory

*7 Japan Atomic Energy Research Institute
Division of Nuclear Safety Evaluation
Nuclear Safety Analysis Laboratory

*8 Japan Atomic Energy Research Institute
Division of Nuclear Safety Research
Reactor Safety Laboratory 1

2. Brief Description of ROSA-III Test Run 912

The ROSA-III program was initiated in 1976 to investigate the thermal hydraulic behavior of a BWR during a postulated LOCA and to provide a base data to evaluate computer codes developed for LOCA analyses.
In order to meet these objectives, the ROSA-III test facility was designed and fabricated in 1978 to simulate major components of the primary system of a BWR except a nuclear core[1].

ROSA-III Run 912, performed on May 19, 1981, was conducted as the CSNI ISP-12 test simulating a 5% split break LOCA condition at the pump suction in the recirculation line with HPCS failure[2][3].

The description of the test facility and the test results are given in this section.

2.1 Test Facility

The ROSA-III facility is a volumetrically scaled (1/424) BWR system with an electrically heated core designed to study the response of a BWR system during a postulated LOCA[1].

The test facility consists of four major subsystems which have been instrumented such that desirable parameters can be measured and recorded during LOCE (Loss of Coolant Experiment) transients.
These subsystems are: (a) a pressure vessel, (b) a steam line and a feedwater line, (c) a coolant recirculation system and (d) the ECCS.
The system instrumentation is described in Section 2.2. The ROSA-III major components and the pressure vessel internal structure are shown schematically in Figs. 2.1 and 2.2, respectively. The ROSA-III piping system is shown in Figs. 2.3, and the major characteristics of the ROSA-III facility are compared with those of a LBWR (large BWR) in Table 2.1.

The pressure vessel simulates that of a BWR. It has a simulated core, a lower plenum, an upper plenum, an annular downcomer, a steam separator, a simulated steam dryer plate and a steam dome.
The core is composed of four half-length simulated fuel assemblies and a control rod simulator. Each fuel assembly containes 62 fuel rods and two water rods which are spaced and supported in a square (8 × 8) array by lower and upper tie plates. The simulated fuel rod is heated electrically with a chopped cosine axial power distribution. The effective heated length is 1880 mm, one half of the active length of a BWR fuel

rod. An orifice plate assembly at the core inlet simulates the flow resistance of a nuclear core.

The steam line and the feedwater line simulate those of a BWR. Steam is discharged into the atmosphere through the steam line connected to the steam dome. The steam line has three branches. The first branch has a control valve to control the steady state pressure of the steam dome before blowdown. The second branch simulates the ADS (automatic depressurization system). The third branch has an orifice to simulate the flow resistance of the steam turbine-generator. The feedwater line is connected to a feedwater sparger located above the downcomer region. Feedwater is supplied from a FWT (feedwater tank).

The coolant recirculation system simulates the BWR recirculation loop. The system consists of two loops, each provided with a recirculation pump and two jet pumps. One is an intact loop which simulates the unbroken loop of a BWR and the other is a broken loop which simulates the broken loop of a BWR. The broken loop has two break simulators and a quick shutoff valve to simulate a double-ended shear break or a split break. Each break simulator consists of a flow nozzle or a sharp edged orifice which determines the break area, and a quick opening blowdown valve. The break type, position, and area are experimental variables. The standard condition is a 200% double-ended shear break at the recirculation pump inlet side with a nozzle diameter of 26.2 mm.

The ECCS of ROSA-III facility simulates that of a BWR. The ECC systems include HPCS, LPCS, LPCI and ADS. The spray systems, the HPCS and the LPCS, spray emergency cooling water on the top of the core. The LPCI system supplies emergency cooling water into the core-shroud directly. Each ECCS is provided with a tank, a pump, a valve and a control system to control a valve trip delay, a valve opening speed, and a flow rate.

2.2 Instrumentation

The instrumentation system of the ROSA-III facility was designed to obtain thermal hydraulic data to contribute to assessing analytical codes for BWR LOCA evaluation. In order to fulfill the objectives, various types of detectors are used in the facility. Table 2.2 summarizes the number of instruments and Fig. 2.4 shows the measurement locations. Detailed descriptions of the ROSA-III instrumentation system

can be found in References (1) and (4). It should be noted however that some of the instruments are still deyelopmental and further improvement will produce more accurate and reliable test data.

The data acquisition system (DATAC 2000B) was designed to record the test data of 700 channels on a magnetic tape at rates up to 30 KHz. The data is later processed by a FACOM M200 system computer at JAERI by off-line control using conversion factors determined from examination of the test data and the sensors.

2.3 Test Conditions and Experiment Procedure

The test conditions of Run 912 are summarized in Table 2.3. Run 912 simulated a 5% break condition of the cross sectional area of the piping at the pump suction in the recirculation line. The break area was determined by inserting an orifice with the diameter of 5.9 mm.

The initial fluid conditions of Run 912 before the break initiation were as follows. The steam dome pressure was 7.35 MPa. The fluid temperature in the lower plenum was 551.8 K and the degree of subcooling was 10.5 K. The electric power supplied to the core was 3969 kW corresponding to 44% core power if the power/volume ratio were the same in the ROSA-III core as in a BWR core. The maximum linear heat generation rate of the simulated fuel rods in the core was 16.7 kW/m. The core inlet flow rate is 16.0 kg/s and the estimated steam quality at the outlet of the core is 13.5% assuming that 5% of the coolant flowing into the lower plenum bypassed the core.

The test was initiated by opening a quick opening valve located downstream of the orifice to blow off steam and water from the break. The main recirculation pumps were tripped at the break initiation. The major events observed during the Run 912 transient are shown sequentially in Table 2.4.

The core power was not changed in the first 8.8 s after the break initiation and was decreased afterwards in accordance with the decay curve of the stored heat release and the heat generation rate after the reactor scram at the time of break as shown in Fig. 2.5. The fuel rod power and the axial power distributions in the core shown in Figs. 2.6(a), 2.6(b), and 2.7 were maintained the same in the transient as in steady state.

The steam line and the feedwater line were not coupled in the present test. The steam flow was controlled to maintain the system pressure constant using the control valve, CV-130, installed in the steam line (see Fig. 2.3) in the steady state before the break initiation. The control valve, CV-130, was fully opened at the break initiation and the steam flow rate was then controlled by an orifice in the steam line with a diameter of 18.0 mm to simulate the flow resistance of the steam turbine. Closure of the feed water line was initiated at 2,0 s and completed at 3.1 s after the break initiation. CV-130 was closed manually simulating the main steam line isolation valve (MSIV) closure 3 s after the liquid level in the downcomer decreased to 4,76 meters above the bottom of pressure vessel (L2 level). The MSIV closure was initiated at 22 s and completed at 24 s after the break initiation. The control valve, CV-130, was opened between 80 s and 110 s after the break initiation simulating the pressure relief valve actions after the main steam line isolation valve closure. The automatic depressurization system (ADS) was actuated at 158 s after break or 120 s after the liquid level in the downcomer had decreased to 4.25 m. A 15.5 mm orifice was inserted in the ADS line to simulate the steam flow rate in the ADS line in a BWR. The system pressure was decreased sharply by actuation of the ADS and the low pressure core spray system (LPCS) was started to apply spray water from the top of the core at a pressure of 2.38 MPa at 318 s after the break initiation. The low pressure injection system (LPCI) started to inject water into the core bypass at a pressure of 1.81 MPa at 406 s after the break initiation to reflood and to cool the core.

Sequence of the valve control is given in Table 2.5.

2.4 Brief Description of Test Results

The system pressure transient in the lower plenum is shown in Fig. 2.8. The pressure decrease during the first 21 s was due to the discharge of fluid from the break and from the steam line. Immediately after the MSIV closure at 24 s, the pressure increased and reached the opening pressure of the relief valve. The pressure is maintained between 8.3 MPa and 8.4 MPa by the relief valve from 80 s to 110 s after the break initiation. As soon as the ADS was actuated at 158 s, the pressure decreased rapidly. The lower plenum fluid reached the saturation condition at 159 s and started to flash.

The LPCS and the LPCI started to provide water at 318 s and 406 s after the break initiation, respectively. Decrease in the depressurization rate was observed from 325 s due to flashing of steam in the core and in the feedwater line,

Figure 2.9 compares the cladding temperature transient at several different elevations of the heater rod A11. The earliest Dryout occurred at 131 s after the break initiation at the top of the core (Position 1). Rewetting of the heater rod surface was observed at Position 1 at 170 s after the break initiation due to the flashing of steam in the lower plenum. The heater rod surface was dried out from 206 s to 261 s as the flashing was diminished and the cladding temperature started to increased again. Rewetting observed at Position 1 between 266 s and 294 s was probably due to the break through of the counter current flow limiting (CCFL) at the upper tie plate.
All the surfaces were quenched between 328 s and 433 s after the break initiation. The quench front progressed from both the top and the bottom of the core. The peak cladding temperature (PCT) observed was 839 K at Position 4 of the heater rod A88.

The liquid level transient data was obtained by reducing on-off signals detected by conductivity probes located at various elevations in the upper and lower plenums, the core, the core inlet, the guide tube, and the downcomer. It can be recognized from Fig. 2.10 that the liquid in the core and the downcomer region decreased due to the discharge of fluid from the break and recovered one time due to flashing in the lower plenum. The whole core was uncovered as the flashing decreased. Figure 2.10 shows that the liquid level was formed above the upper tie plate during the core uncovering due to CCFL.
The liquid level quickly recovered in the core as the LPCI started to inject water to reflood the core.

The discharge flow rate was measured by a gamma densitometer and high and low range drag disks. Figure 2.11 shows the discharge flow transient measured by a low range drag disk and a gamma densitometer.

2.5 Variables to be Calculated

Selected variables which are essential for the description of the transients in the test are presented in Table 2.6. It was not necessary for participant to calculate all of the variables listed in Table 2,6. In was sufficient to submit the limited results which were calculated by the model and the code they used. The calculated results are, submitted by each participant as transient data from 0 s to 1000 s with an interval of 0.5 s.

A list of the variables which were calculated by each participant is also presented in Table 2.6.

Table 2.1 Primary Characteristics of BWR-6 and ROSA-III

	BWR-6	ROSA-III	BWR/ROSA
No. of Recirc. Loops	2	2	1
No. of Jet Pumps	24	4	6
No. of Separators	251	1	251
No. of Fuel Assemblies	848	4	212
Active Fuel Length (m)	3.76	1.88	2
Total Volume (m^3)	621	1.42	437
Power (MW)	3800	4.4	864
Pressure (MPa)	7.23	7.23	1
Core Flow (kg/s)	1.54×10^4	36.4	424
Recirculation Flow (l/s)	2970	7.01	424
Feedwater Flow (kg/s)	2060	4.86	424
Feedwater Temp (K)	489	489	1

Table 2.2 Instrumentation List

TYPE	SENSOR	NUMBER	NOTE	
PRESSURE	PRESSURE TRANSDUCER	20		
DIFFERENTIAL PRESSURE	DP CELL	60	PV AND LOOP	44
			LEVEL MEASUREMENT	5
			FLOW METER	11
FLUID TEMPERATURE	CA THERMOCOUPLE	129	PRIMARY LOOP	23
			DTT	4
			TIE ROD	28
			UPPER PLENUM	10
			LOWER PLENUM	10
			TIE PLATE	40
			BY PASS	14
FUEL ROD TEMPERATURE	CA THERMOCOUPLE	213		
SLAB SURFACE TEMPERATURE	CA THERMOCOUPLE	70	CORE BARREL	24
			PRESSURE VESSEL	3
			CHANNEL BOX	35
			SHROUD SUPPORT	8
SLAB INNER TEMPERATURE	CA THERMOCOUPLE	9	JP DIFFUSER	4
			PV WALL	5
VOLUMETRIC FLOW RATE	TURBINE METER	3	ECCS LOOP	3
	VENTURI METER	4	PRIMARY LOOP	10
	ORIFICE METER	6		
MASS FLOW RATE	TURBINE METER	4	RECIC. LOOP	4
	ORIFICE METER	3	STEAM LINE	3
LIQUID LEVEL	CONDUCTIVITY PROBE	138		
	CAPACITANCE PROBE	2		
DENSITY	GAMMA DENSITOMETER	10	2 BEAM GD	2
			3 BEAM GD	2
MOMENTUMR FLUX	DRAG DISK	7		
SIGNAL	ON/OFF SWITCH	14		
PUMP SPEED	REVOLUTION COUNTER	2		
ELECTRIC POWER	VA METER	2		
TOTAL		696		

Table 2.3 Test Conditions

Parameter	Specified Value	Measured Value
Break Conditions		
Location	MRP suction	MRP suction
Type	Split	Split
Break Orifice Diameter (mm)	5.9	5.9
Initial System Conditions		
Steam Dome Pressure (MPa)	7.35	7.30
Lower Plenum Temperature (K)	551.7	551.8
Lower Plenum Subcooling (K)	10.5	10.8
Core Inlet Flow Rate (kg/s)	16.0	16.4
Core Outlet Quality (%)	13.8**	13.5**
Power Level (kW)	1260 + 2700	1262+2707
Maximum Linear Heat Rate(kW/m)		
Channel A P.F.=1.1	16.65	16.67
P.F.=1.0	15.13	15.16
P.F.=0.875	13.24	13.26
Channel B-D P.F.=1.1	11.89	11.92
P.F.=1.0	10.81	10.84
P.F.=0.875	9.46	9.48
Water Level in PV* (m)	5.0	5.0
Feedwater Conditions		
Temperature (K)	489	489
Flow Rate (kg/s)	2.39	Fig.3.11
Initiation of Line Closure(s)	2.0	2.0

* note, L3 Level for Scram : 5.0 m from PV Bottom

** not include core bypass flow
core bypass flow is assumed to be 0.8kg/s

Table 2.3 Test Conditions (contd.)

Parameter	Specified Value	Measured Value
Steam Discharge Conditions		
Steady State Flow Rate(kg/s)	2.39	2.04
Transient Flow Rate (kg/s)	keep steady value	Fig.3.10
Orifice Diameter (mm)	18.0	18.0
Initiation of Line Closure(s)	L2*+3(s)	24.0
Safety Relief Valve Setting Pressure (MPa)	$8.24 \leqq P \leqq 8.34$	$8.40 \leqq P \leqq 8.47$
ECCS Conditions		
HPCS	not-used	not-used
LPCS		
Injection Location	Upper Plenum	Upper Plenum
Initiation Conditions	L1*+40(s) and $\leqq$ 2.16 (MPa)	318(s) at PV Pressure 2.38(MPa)
Coolant Temperature (K)	313	313
Injection Flow Rate(m^3/s)	1.13×10^{-3}	Fig.3.12
LPCI		
Injection Location	Top of Core Bypass	Top of Core Bypass
Initiation Conditions	L1*+40(s) and $\leqq$ 1.57 (MPa)	406(s) at PV Pressure 1.81 (MPa)
Coolant Temperature (K)	313	315
Injection Flow Rate (m^3/s)	3.50×10^{-3}	Fig.3.13
ADS Conditions		
Initiation Time (s)	L1*+120 (s)	158 (s)
Flow Rate	Scaled Flow of BWR	Fig.3.8 through 3.10
Orifice Diameter (mm)	15.5	15.5

* note : Each trip level is as follows;

L3 Level for Scram : 5.0 m from PV Bottom

L2 Level for MSIV and HPCS : 4.76 m from PV Bottom

L1 Level for LPCS, LPCI and ADS : 4.25 from PV Bottom

Table 2.4 Sequence of Events

Time after Break (s)	Events
0.0	Break
	Initiate core power control
	Terminate recirculation pump power
2.0	Initiation of feed water line valve closure
3.1	Closure of feed water line
8.8	Initiation of core power curve reduction
19.0	L2 (4.76m) signal
24.0	Closure of steam discharge line
38.2	L1 (4.25m) signal
80.0	Safety relief valve actuation
98.8	Jet pump suction nozzle uncovery
117	Dryout at the top of the core
156	Recirculation pump suction nozzle uncovery
158	ADS valve opens (at system pressure 8.03 MPa)
159	Initiation of lower plenum flashing
275	Whole core uncovery
318	LPCS Initiation (at system pressure 2.38 MPa)
406	LPCI Initiation (at system pressure 1.81 MPa)
440	Completion of core reflooding
444	All heater rods quenched

Table 2.5 Valve Control Sequence of Steam Discharge Line

Time	t < 0	0 (Break) ≦ t	L2 + 3 ≦ t	---	p ≧ 8.24 MPa	---	L1 + 120
CV-1	Open	Close (Manual)	Close		Close		Close
CV-2 (see Fig.2.3)	Open	Close (Manual)	Close		Close		Close
CV-130	Control to maintain steady state pressure	Open (Manual)	Close (Manual)		Control to maintain pressure between 8.24 MPa and 8.34 MPa (Manual)		Close (Manual)
AV-168	Open	Open	Open		Open		Close (Auto)
AV-169	Close	Close	Close		Close		Open (Auto)

t = 0 : Break

t = L2 + 3s : MSIV closure

t = L1 + 120s : ADS valve opening

Table 2.6 Variables to be Calculated

No.	Item*1	ID*2		Location*3	Unit	Data*4		Submitted Data *5							
								U	S	F	N	J	C	A	R
1	PRESS.	PA	1	LOWER PLENUM	Pa	PA	1								
2	PRESS.	PA	2	STEAM DOME	Pa	PA	3								
3	PRESS.	PA	3	BREAK B UPSTREAM	Pa	PA	14	X							
4	DIFF.P.	PD	4	LOWER PL.-UPPER PL.	Pa	PD	21								
5	DIFF.P.	PD	5	UPPER PL.-STEAM DOME	Pa	PD	22								
6	DIFF.P.	PD	6	LOWER PLENUM HEAD	Pa			X	X			X			
7	DIFF.P.	PD	7	DOWNCOMER HEAD	Pa	PD	24		X						
8	DIFF.P.	PD	8	PV BOTTOM-TOP	Pa	PD	25								
9	DIFF.P.	PD	9	INTACT LOOP JP DISCH.-SUC.	Pa	PD	26								
10	DIFF.P.	PD	10	INTACT LOOP JP DRIVE.-SUC.	Pa	PD	27								
11	DIFF.P.	PD	11	BROKEN LOOP JP DISCH.-SUC.	Pa	PD	30								
12	DIFF.P.	PD	12	BROKEN LOOP JP DRIVE.-SUC.	Pa	PD	31						X		
13	MASS.F.	FM	13	MAIN STEAM LINE	kg/s	FM	71								
14	MASS.F.	FM	14	ADS LINE	kg/s	FM	71								
15	MASS.F.	FM	15	TOTAL CORE INLET FLOW	kg/s	FM	716	Δ				Δ	Δ		
16	MASS.F.	FM	16	HIGH POWER CH. INLET FLOW	kg/s	FM	711		X				X		
17	MASS.F.	FM	17	AVE. POWER CH. INLET FLOW	kg/s	FM	713		X				X		
18	MASS.F.	FM	18	GUIDE TUBE	kg/s	FM	715	Δ					X		
19	MASS.F.	FM	19	FROM CORE TO BYPASS	kg/s			X	X				X		
20	MASS.F.	FM	20	INTACT LOOP JP OUTLET	kg/s										
21	MASS.F.	FM	21	BROKEN LOOP JP OUTLET	kg/s										
22	MASS.F.	FM	22	VESSEL SIDE BREAK FLOW	kg/s	FM	706	X							
22'	MASS.F.	FM	22	VESSEL SIDE BREAK FLOW	kg/s	FM	708	X							
23	MASS.F.	FM	23	PUMP SIDE BREAK FLOW	kg/s	FM	705	X	X						
23'	MASS.F.	FM	23	PUMP SIDE BREAK FLOW	kg/s	FM	707	X	X						
24	MASS.F.	FM	24	BREAK FLOW	kg/s	FM	709								
24'	MASS.F.	FM	24	BREAK FLOW	kg/s	FM	710								
25	VOL.F.	FV	25	HPCS	m^3/s	FV	73	X				X			
26	VOL.F.	FV	26	LPCS	m^3/s	FV	74	Δ				Δ			
27	VOL.F.	FV	27	LPCI	m^3/s	FV	75	Δ		Δ		Δ			
28	VOL.F.	FV	28	FEED WATER	m^3/s	FV	76	Δ				X			
29	VOL.F.	FV	29	INTACT LOOP JP DISCHARGE	m^3/s	FV	78	Δ					X		
30	VOL.F.	FV	30	BROKEN LOOP JP DISCHARGE	m^3/s	FV	80	Δ					X		
31	VOL.F.	FV	31	INTACT LOOP REC. PUMP	m^3/s	FV	88	X					X		
32	VOL.F.	FV	32	BROKEN LOOP REC. PUMP	m^3/s	FV	89	X		Δ			X		
33	POWER	WE	33	CORE POWER	kW	WE	103								X
34	REV.	SR	34	INTACT LOOP REC. PUMP	R.P.M	SR	104			X			X		X
35	REV.	SR	35	BROKEN LOOP REC. PUMP	R.P.M	SR	105			X			X		X
36	DIFF.P.	PD	36	INTACT LOOP REC. PUMP HEAD	Pa	PD	34								
37	DIFF.P.	PD	37	BROKEN LOOP REC. PUMP HEAD	Pa	PD	35								
—	TEMP.	TE	—	HIGH POWER CH.(L.P.F.=1.1)	K	TE	—	*6	X	X	X		X	X	
—	TEMP.	TE	—	HIGH POWER CH.(L.P.F.=1.0)	K	TE	—	*6	X					X	
—	TEMP.	TE	—	HIGH POWER CH.(L.P.F.=0.875)	K	TE	—	*6	X	X	X		X	X	X
—	TEMP.	TE	—	AVE. POWER CH.(L.P.F.=1.0)	K	TE	—	*6							

Table 2.6 Variables to be Calculated (contd.)

No.	Item*1	ID*2		Location*3	Unit	Data*4	Submitted Data *5							
							U	S	F	N	J	C	A	R
108	LEVEL	LM	108	UPPER PLENUM	m		Δ						X	Δ
109	LEVEL	LM	109	HIGH POWER CHANNEL	m		Δ						X	Δ
110	LEVEL	LM	110	AVERAGE POWER CHANNEL	m		Δ							Δ
111	LEVEL	LM	111	CORE INLET	m		Δ				X			Δ
112	LEVEL	LM	112	LOWER PLENUM	m		Δ							Δ
113	LEVEL	LM	113	CORE BYPASS	m		Δ							Δ
114	LEVEL	LM	114	DOWNCOMER	m		Δ							Δ
115	DENSITY	DE	115	INTACT LOOP JP OUTLET	kg/m^3	DE 701								
116	DENSITY	DE	116	BROKEN LOOP JP OUTLET	kg/m^3	DE 702								
117	DENSITY	DE	117	PUMP SIDE BREAK	kg/m^3	DE 703	*7	X						
118	DENSITY	DE	118	VESSEL SIDE BREAK	kg/m^3	DE 704	*7							
119	MO.FLUX	MF	119	INTACT LOOP JP OUTLET	kg/ms^2		X	X	X	X	X		X	X
120	MO.FLUX	MF	120	BROKEN LOOP JP OUTLET	kg/ms^2		X	X	X	X	X		X	X
121	MO.FLUX	MF	121	PUMP SIDE BREAK	kg/ms^2	MF 132	X	X	X	X	X		X	X
122	MP.FLUX	MF	122	VESSEL SIDE BREAK	kg/ms^2	MF 133	X	X	X	X	X		X	X
123	FLUID.T.	TE	123	LOWER PLENUM	K	TE 138								
124	FLUID.T.	TE	124	UPPER PLENUM	K	TE 139								
125	FLUID.T.	TE	125	STEAM DOME	K	TE 140								
126	FLUID.T.	TE	126	UPPER DOWNCOMER	K	TE 141								
127	FLUID.T.	TE	127	LOWER DOWNCOMER	K	TE 142								
128	FLUID.T.	TE	128	ABOVE UPPER TIEPLATE	K	TE 456					X			
129	FLUID.T.	TE	129	BELOW UPPER TIEPLATE	K	TE 466					X			

*1 PRESS. : Pressure
DIFF.P. : Differential Pressure
MASS.F. : Mass Flow Rate
VOL.F. : Volumetric Flow Rate
REV. : Rotational Speed
TEMP. : Heater Rod Surface Temperature
MO.FLUX : Momentum Flux
FLUID.T : Fluid Temperature

*2 Identification codes of variables for ISP-12 calculation

*3 PL. : Plenum
JP : Jet Pump
DISCH. : Discharge
SUC. : Suction
DRIVE. : Drive
CH. : Channel
AVE. : Average
REC. : Recirculation
L.P.F. : Local Peaking Factor
PV : Pressure Vessel

*4 Symbols in the experiment data report; see Table in Ref.(3)

*5 blank: calculated variable
X : variable not calculated
Δ : variable calculated at JAERI from other variables and/or data

*6 Center part of core (Position 4) is represented by two volumes.

*7 Density at upstream of break.

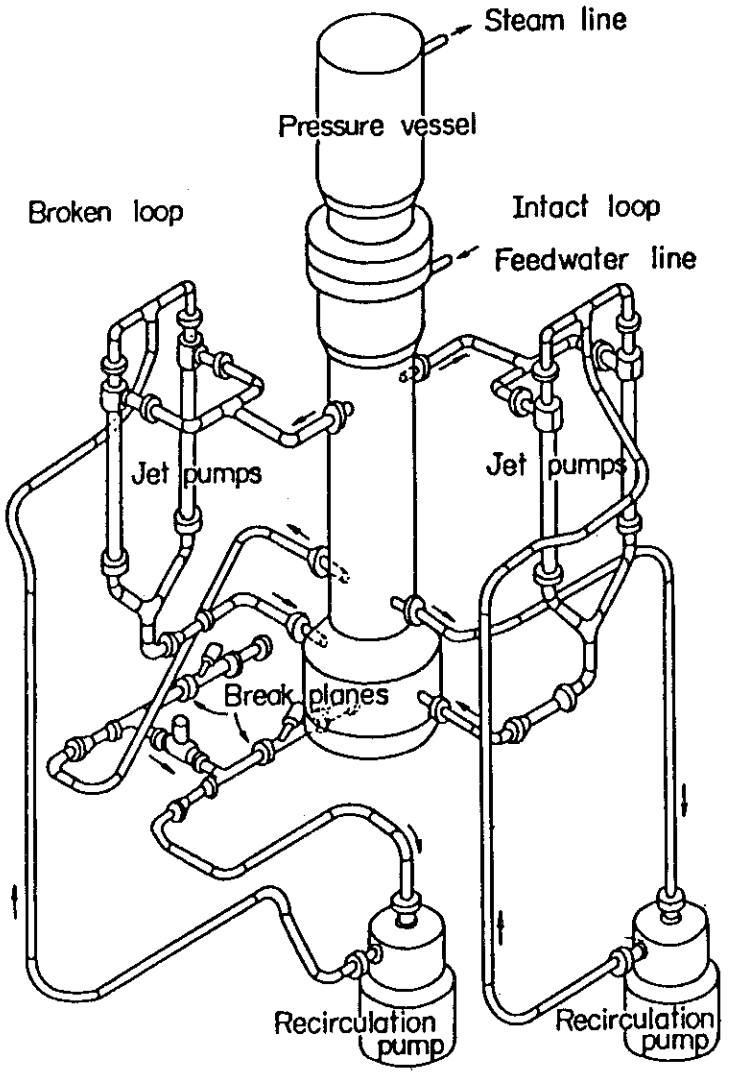

Fig. 2.1 Schematic Diagram of ROSA-III Test Facility

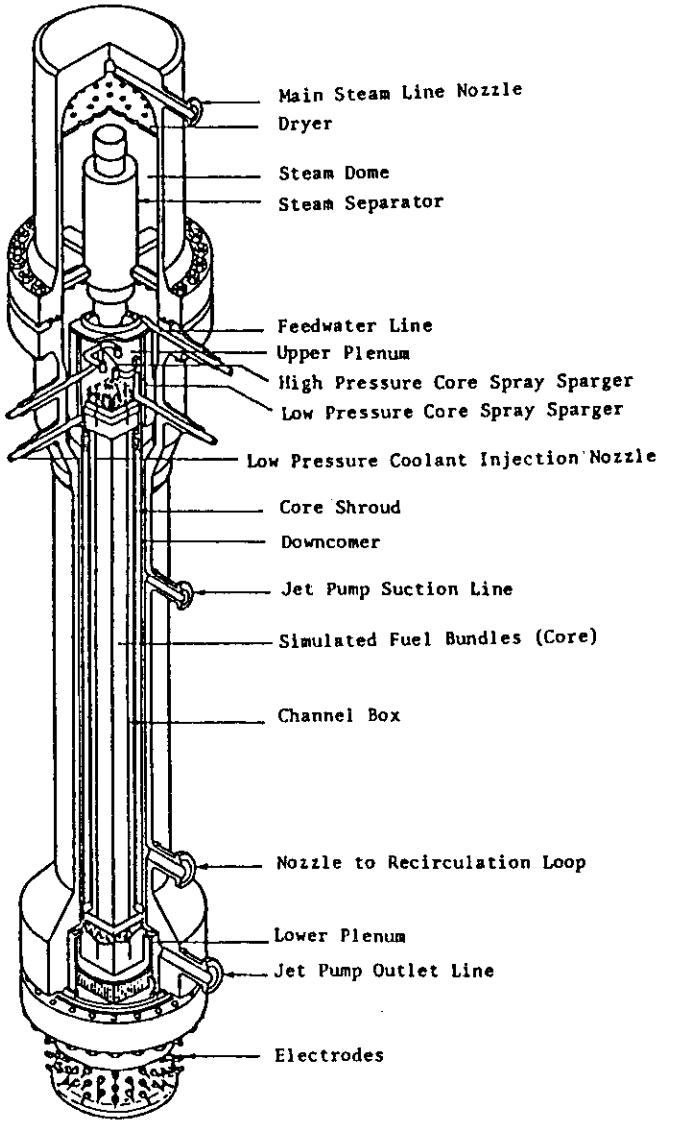

Fig.2.2 Internal Structure of Pressure Vessel of ROSA-III Test Facility

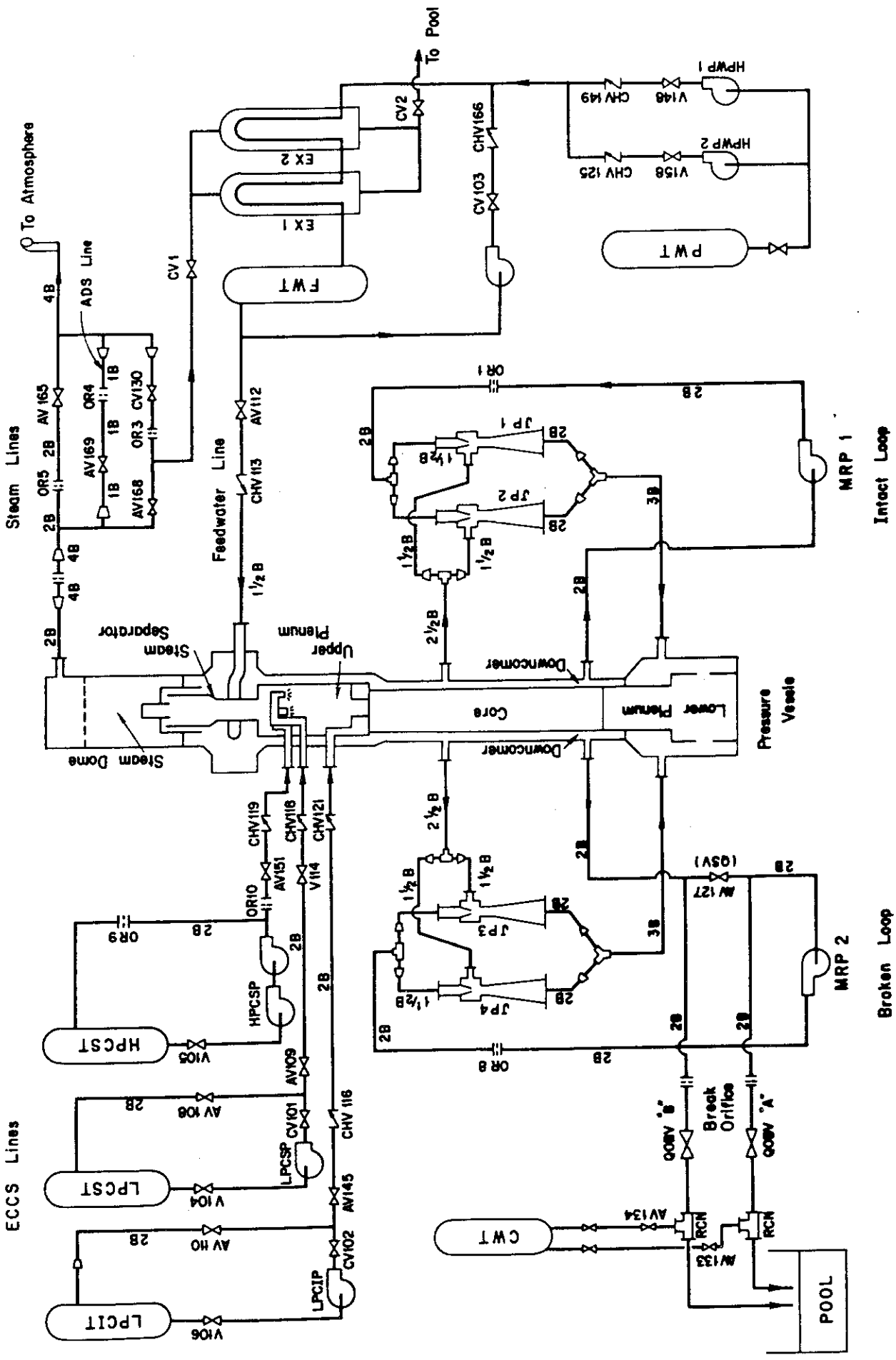

Fig. 2.3 ROSA-III Piping Schematic

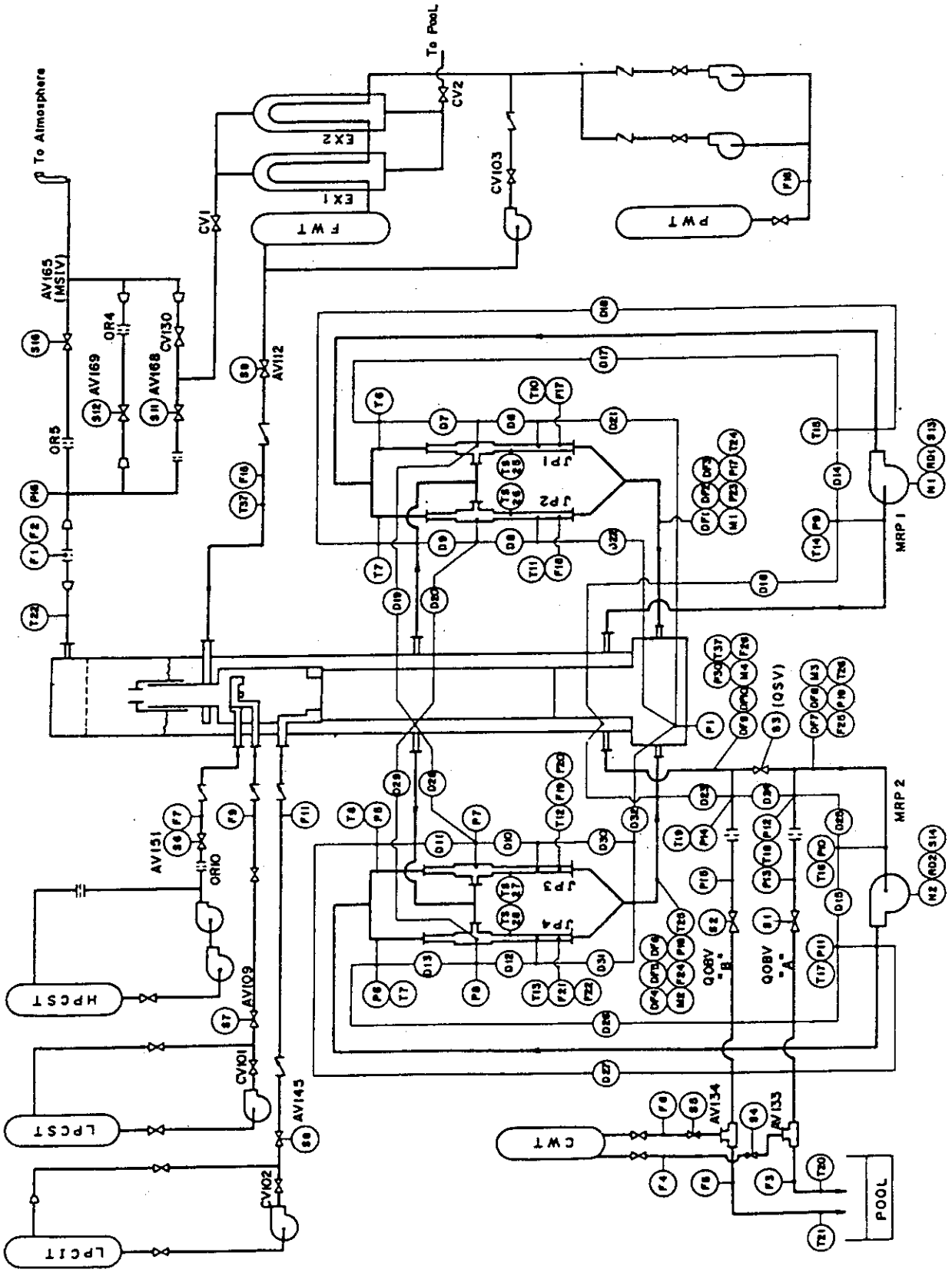

Fig. 2.4(a) Flow Diagram and Instrumentation Location of ROSA-III Test Facility

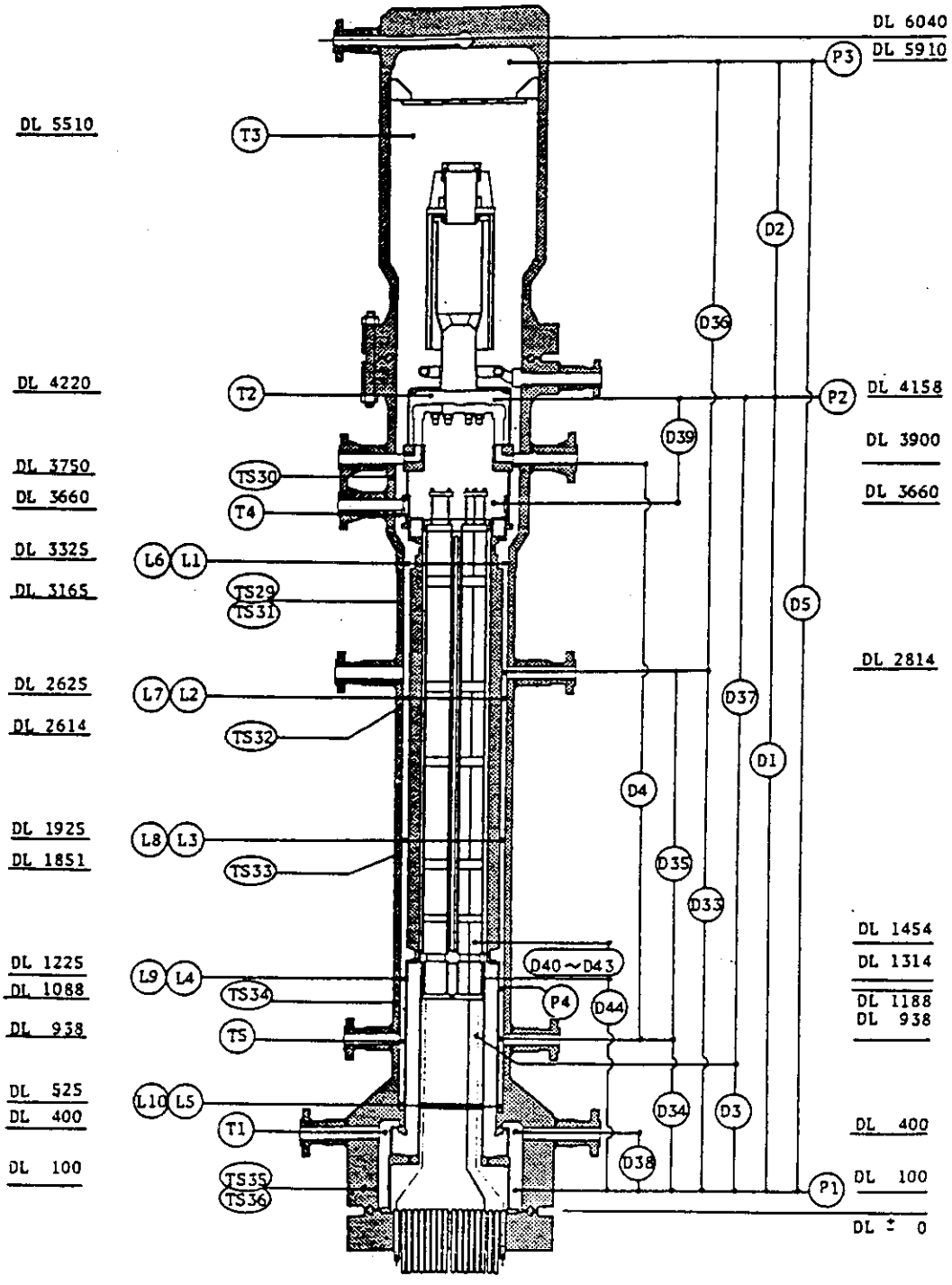

Fig. 2.4(b) Instrumentation Location in Pressure Vessel of ROSA-III Test Facility

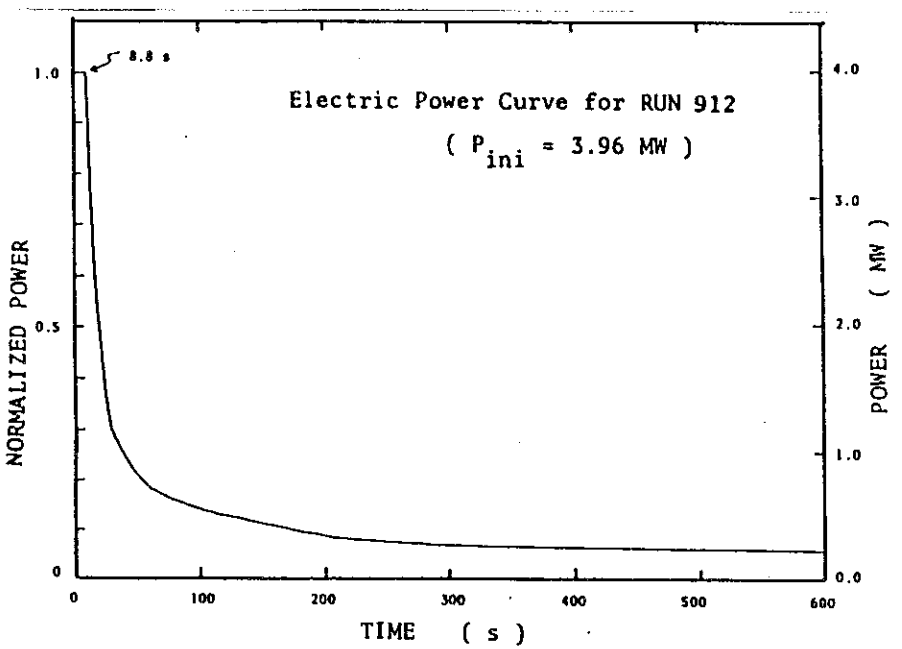

Fig. 2.5 Power Transient

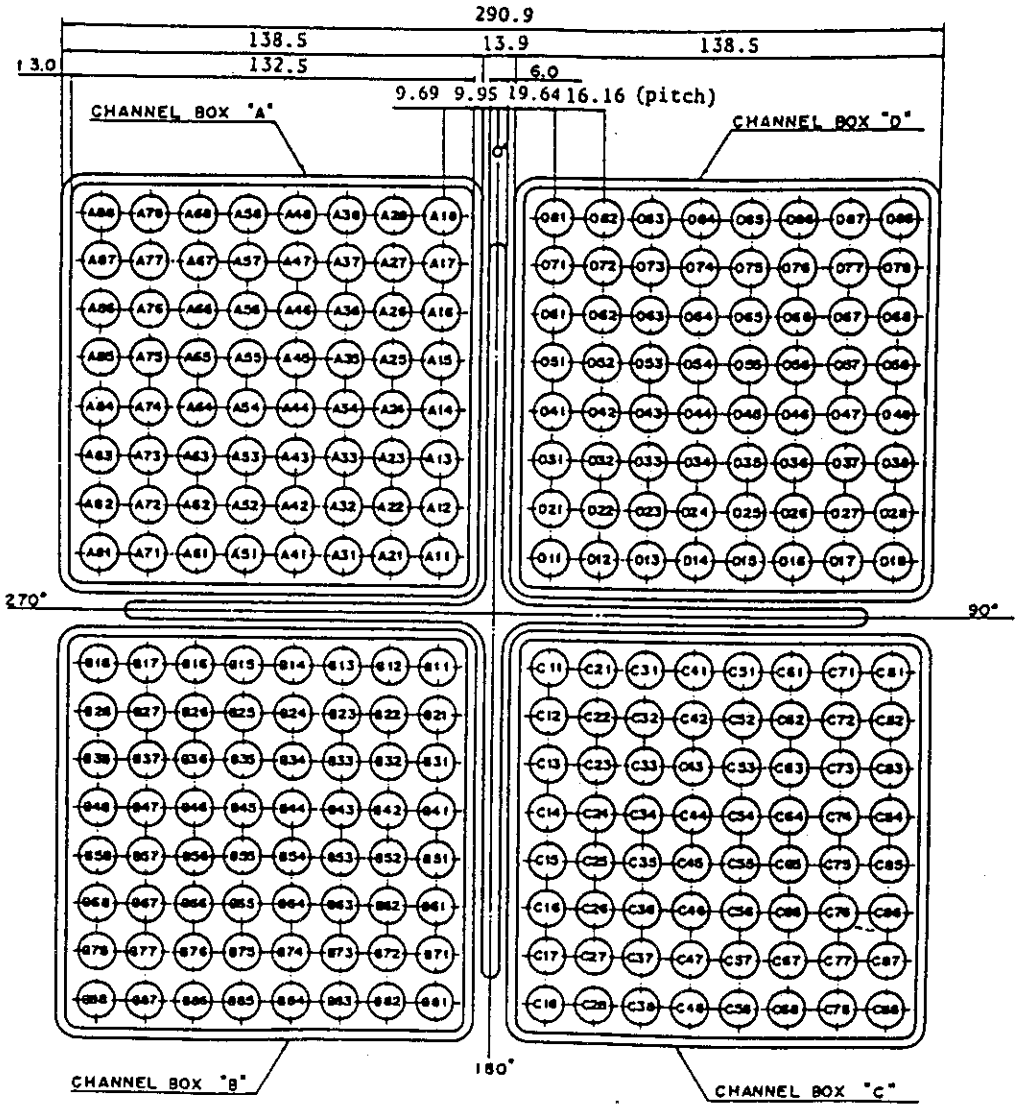

Heater rod O.D. is 12.27mm

AS4,BS4,CS4 and DS4 are water rod simulators with void probes, O.D.= 15.01mm

A4S,B4S,C4S and D4S are water rod simulators with thermocouples, O.D.= 15.01mm

Fig. 2.6(a) Arrangement of Heater Rods

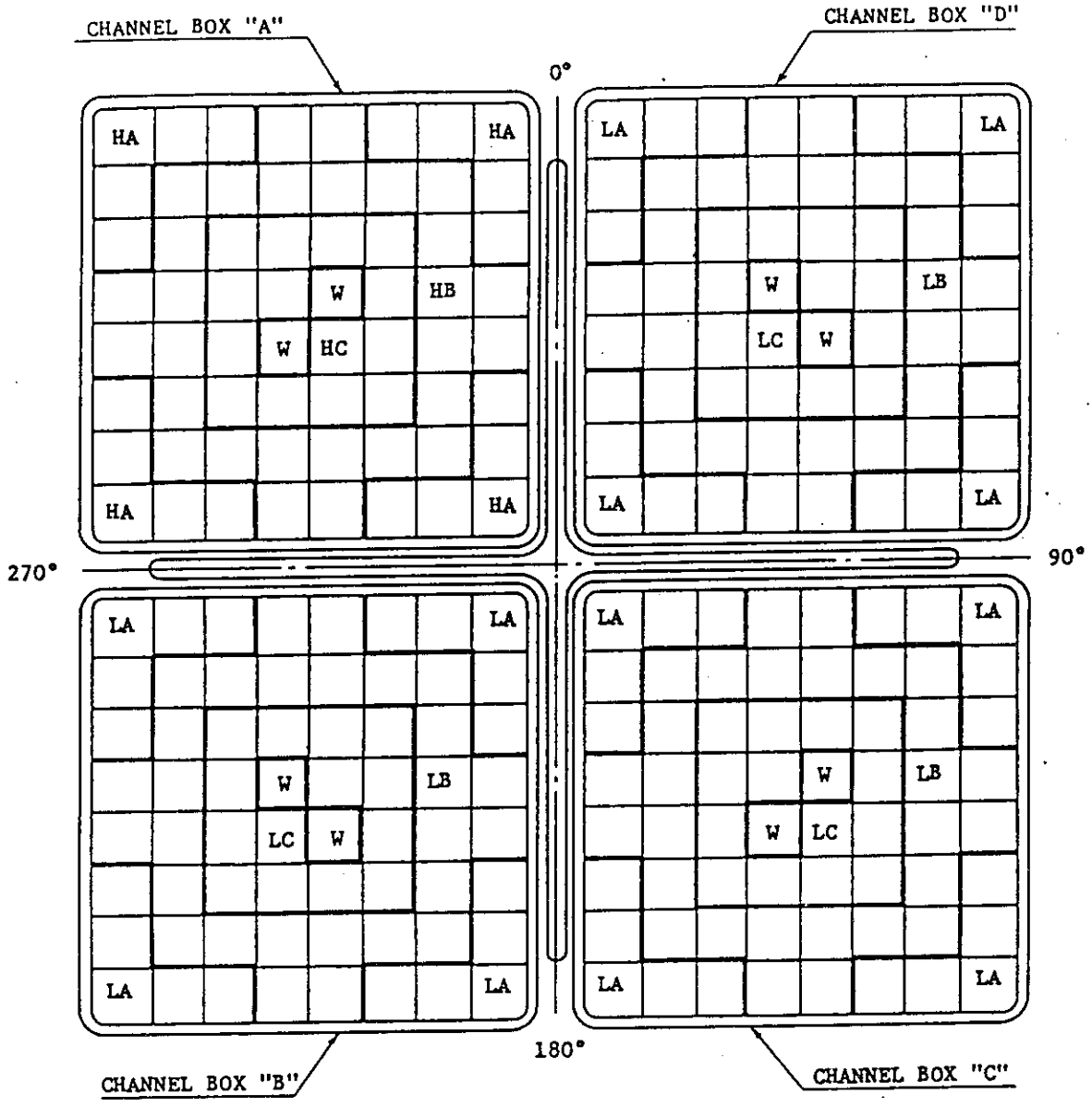

Region	HA	HB	HC	LA	LB	LC	W
Linear Heat Rate (kw/m)*	18.5	16.81	14.41	13.21	12.01	10.29	0.0
Local Peaking factor	1.1	1.0	0.875	1.1	1.0	0.875	0.0
No. of Rods	20	28	14	60	84	42	8

note : Radial Peaking factor is 1.4

* in the case of power = 4.4MW

Fig. 2.6(b) Radial Power Distribution

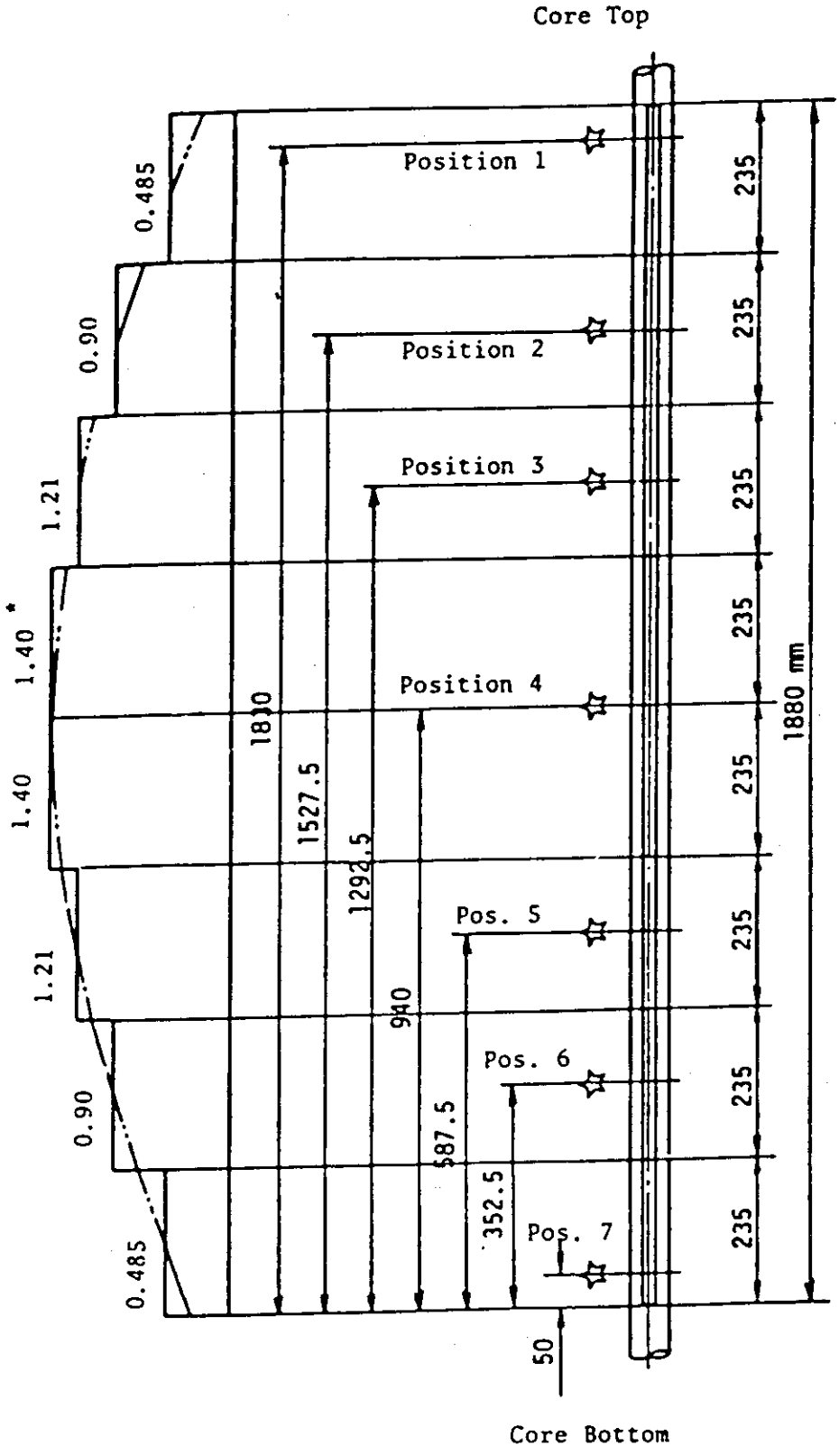

Fig. 2.7 Axial Power Distribution

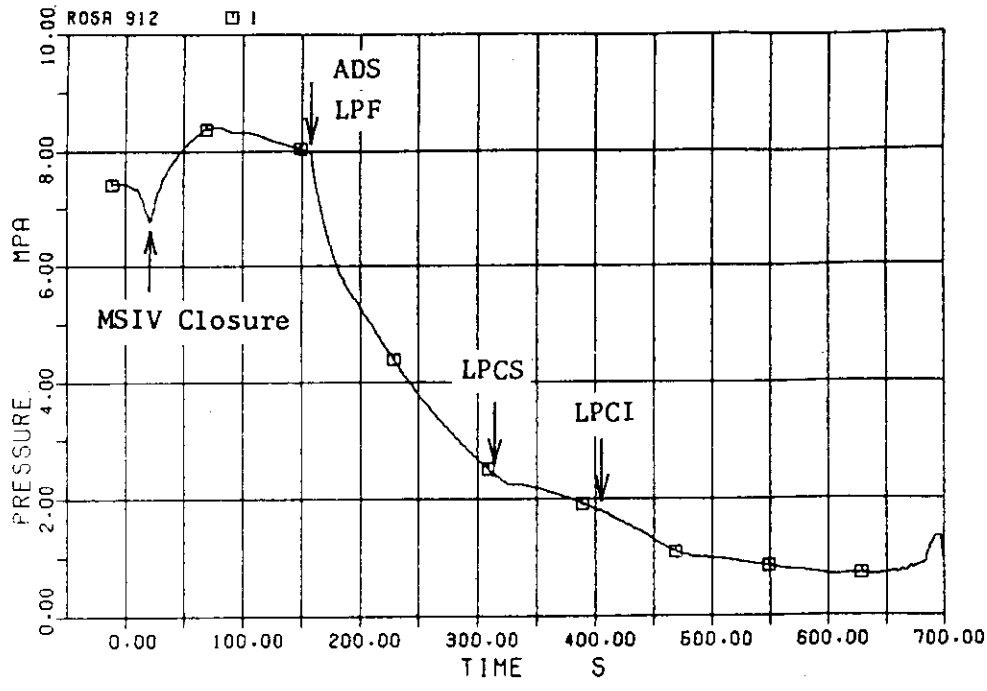

Fig. 2.8 System Pressure in Lower Plenum

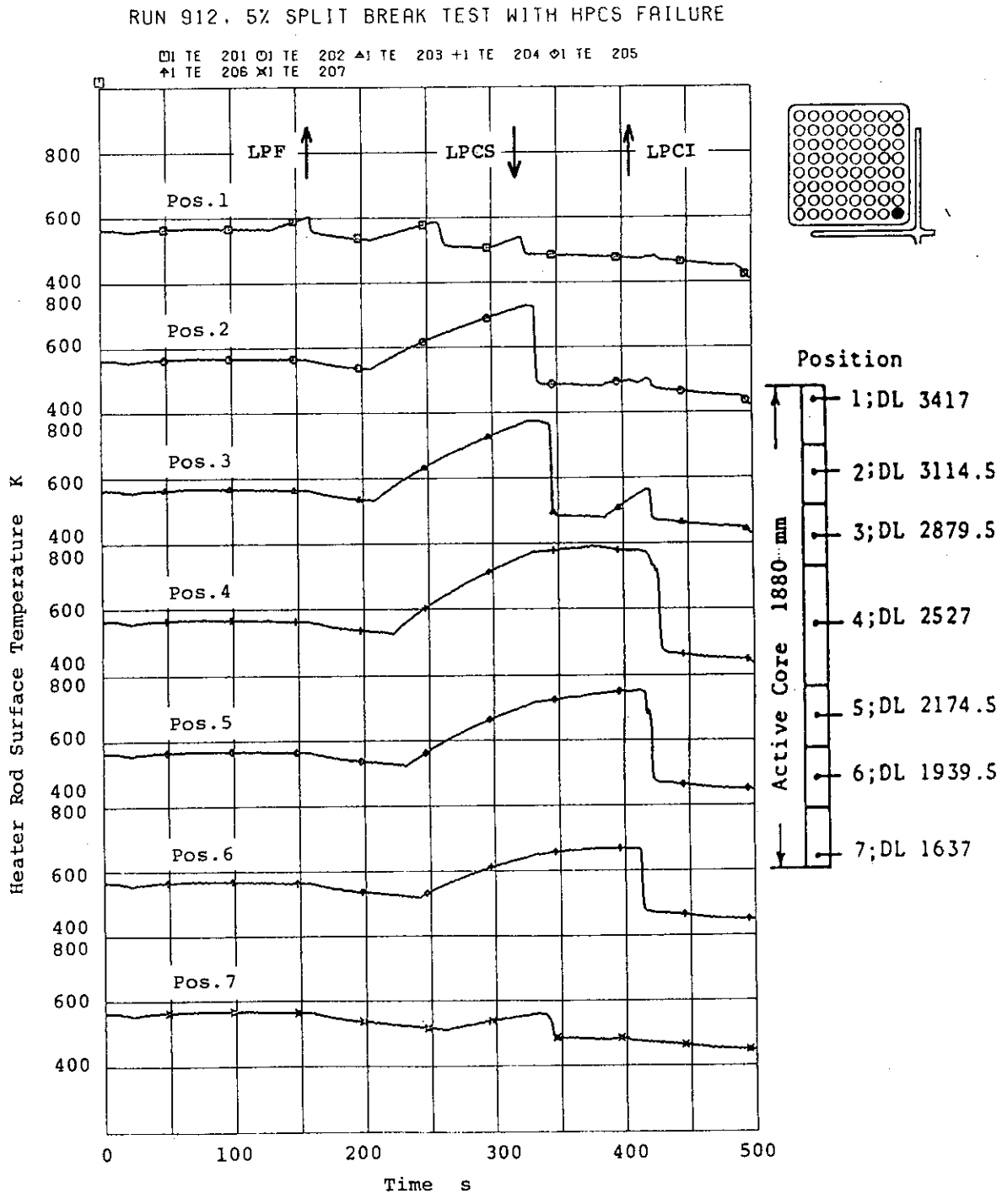

Fig. 2.9 Surface Temperature of All Rod

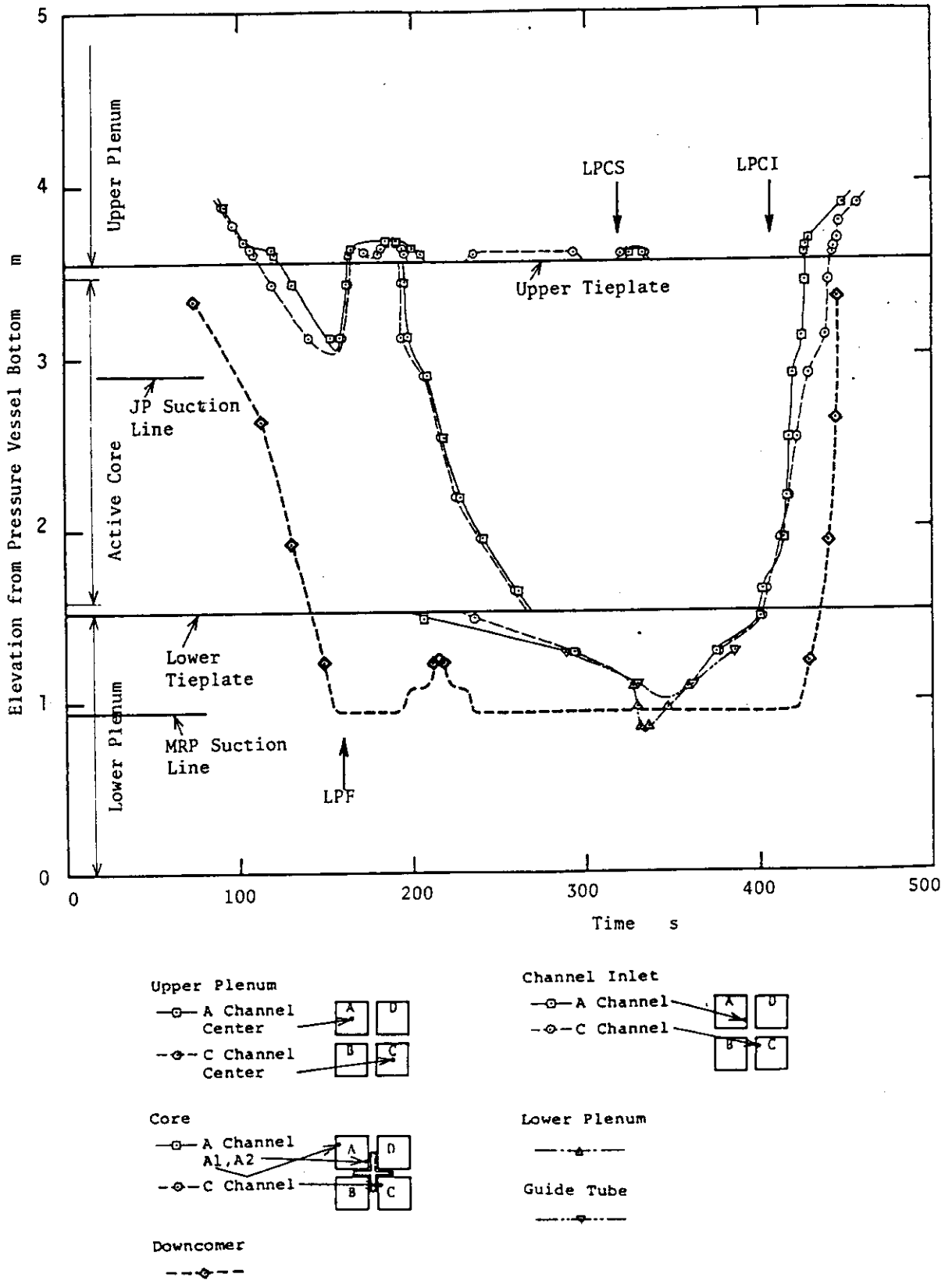

Fig. 2.10 Estimated Liquid Level in Upper Plenum, Core, Channel Inlet, Lower Plenum, Guide Tube and Downcomer

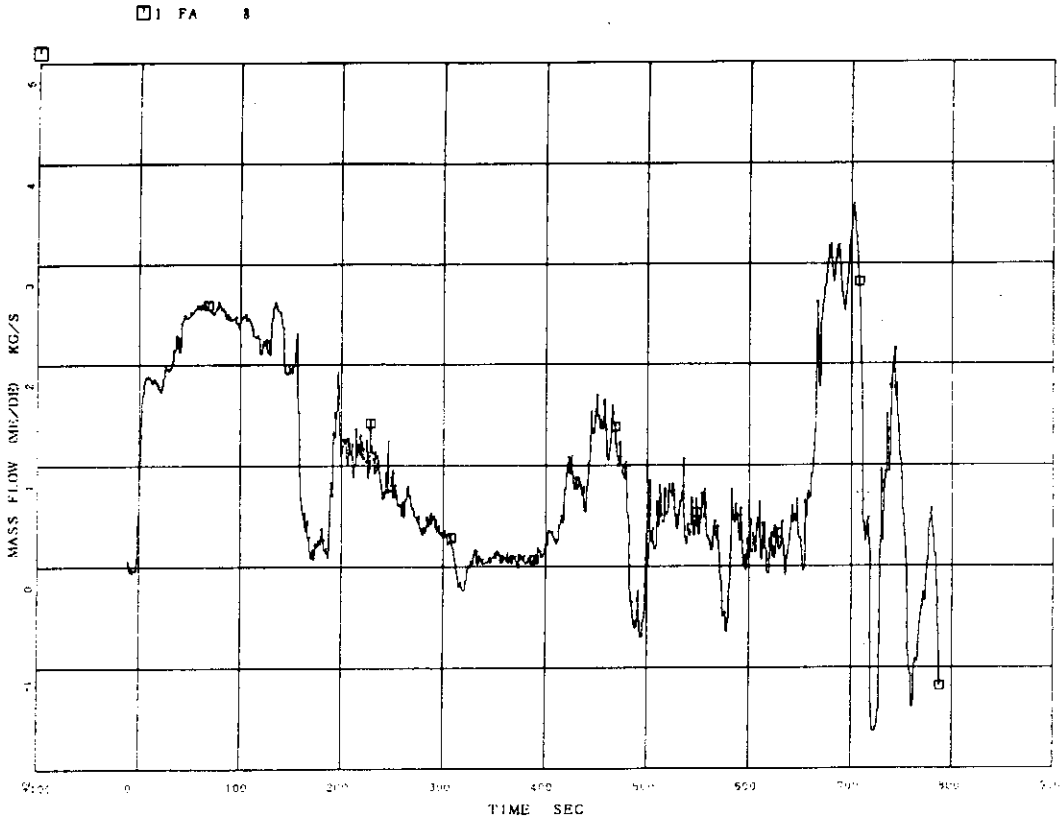

Fig. 2.11 Discharge Flow Rate from Break

3. Summary of Participant Models

In this chapter, important characteristics of the codes and models used by the participants are summarized. The important characteristics presented in this section, however, are limited to the information which was sent by the participants.

Computers used by the participants, CPU times and storages required to perform the calculations are listed in Table 3.1. It is not easy to directly compare the CPU times and storages presented in Table 3.1, due to the differences of computer systems.

Important characteristics of the codes used by the participants are summarized in Table 3.2. USA used TRAC-BD1 code[6], and Sweden-Finland and JAERI-R utilized RELAP5/MOD1 code[8] to perform the calculations. These two codes are so-called advanced codes based on nonhomogeneous nonequilibrium hydrodynamic models. JAPAN-C used THYDE-B1 code[10] which was developed at JAERI for BWR small LOCA analysis and has a three-region node model with moving boundaries originally used in SAFE code. The other participants utilized RELAP4/MOD6 code[7] or RELAP4/MOD6/U4/J3 code[9]. The latter is an improved version of RELAP4/MOD6 revised at JAERI including improvements for analysis of refill and reflood phases of not only large break but also small break LOCAs in a BWR.

Table 3.3 presents important characteristics of the models used by the participants: (a) number of components, (b) models of injection and discharge and (c) special features and comments. Nodalization schemes of USA, Switzerland, Sweden-Finland, JINS, JAERI-C, JAERI-A and JAERI-R are given in Figs. 3.1(a), (b), (c), (d), (e), (f) and (g), respectively.

(To date, the nodalization scheme of Netherlands has not been received.)

Table 3.1 Computer and CPU Time

Country (Organization)	Computer Code	Computer	CPU Time [h]	Storage
USA (INEL) U	TRAC-BD1(6)	CDC 176	9	240K Words (Octal)
Switzerland (EIR) S	RELAP4/MOD6(7)	CDC 6600	10.9	300KB (Octal)
Sweden-Finland (Studsvik-VTT) F	RELAP5/MOD1(8) (cycle 014)	?	?	?
Netherlands (ECN) N	RELAP4/MOD6(7)	CDC Cyber 175	7.94	354.6KB
Japan (JINS) J	RELAP4/MOD6 /U4/J3(9) (modified)	IBM 3033	1.5	2060KB
Japan (JAERI-C) C	THYDE-B1(10)	FACOM M200	1.5	912KB
Japan (JAERI-A) A	RELAP4/MOD6/ U4/J3(9)	FACOM M200	1.4	1088KB
Japan (JAERI-R) R	RELAP5/ MOD1(8) (cycle 001)	FACOM M200	30	1604KB

Table 3.2 Important Characteristics of Codes Used by Each Participant*

Country (Organization) Identifier	Computer Code	Classification	Number of Equations: Mass Conservation	Number of Equations: Momentum Conservation	Number of Equations: Energy	Vertical Slip Model	Horizontal Slip Model	Flooding Model	Remarks
USA (INEL) U	TRAC-BD1 *1b	UVUT	2	2	2	UVUT Separator-dryer model at the vertical junctions of the separator-dryer region	UVUT Separator-dryer model at the holizontal junctions of the separator-dryer region	UVUT CCFL model *1a at side entry orifices, lower tieplates and upper tieplates	*1a CCFL model is described by Kutateladze-type correlation. *1b Version 11 plus updates (nearly Version 12)
Switzerland (EIR) S	RELAP4/ MOD6	One-dimensional homogeneous model	1	1	1	At all of the junctions in core except the junction in SS *2a outlet	Not used	Not used	*2a SS: Steam separator
Sweden-Finland F	RELAP5/ MOD1 (cycle 014)	UVUT *3a	2	2	1 *3a				*3a It is assumed that the least massive phase be at saturation.
Netherlands (ECN) N	RELAP4/ MOD6	One-dimensional homogeneous model	1	1	1	?	?	?	
Japan (JINS) J	RELAP4/ MOD6/U4/ J3	One-dimensional homogeneous model	1	1	1	Used in vertical junctions CIO, UT, GTI, BO and DC junctions. *5a Slip model was not used at UT during short period after break.	Not used	CCFL fill junction model.	*5a CIO: Core Inlet Orifices which contain the effect of the low tieplate UT : Upper tieplate BO : Bypass outlet GTI: Guide tube inlet DC : Downcomer
Japan (JAERI-C) C	THYDE -B1	One-dimensional homogeneous and three -region *6a models	1	1 *6b	1	. Separator . Separation efficiency is specified by the user as a function of mixture level in the downcomer	Not used	Not used	*6a Three region model A node is divided into three subnodes (Vapor, Mixture, Liquid). In each subnode, mass and energy conservation equations are solved. *6b Momentum flux terms are neglected.
Japan (JAERI-A) A	RELAP4/ MOD6/U4/ J3	One-dimensional homogeneous model	1	1	1	Used in vertical junctions, SEO, LT, UT, SP inlet and DC junctions. *7a	Not used	CCFL fill junction model.	*7a SEO: Side entry orifice LT : Lower tieplate UT : Upper tieplate SP : Separator DC : Downcomer
Japan (JAERI-R) R	RELAP5/ MOD1 (cycle 001)	UVUT *8a	2	2	1 *8a				*8a It is assumed that the least massive phase be at saturation.

Table 3.2 Important Characteristics of Codes Used by Each Participant (contd.)*

Country	Bubble Rise Model	Critical Flow Model	Recirculation Pump Model	Jet Pump Model	Vapor Generation Model	Remarks
U		. Characteristic analysis after 111 sec . Break model till 111 sec	Speed-time table	Modified TEE component Momentum source term obtained by considering the momentum balance is used.	Complete nonequilibrium package plus subcooled boiling Simplified thermal energy jump condition	
S	. Wilson's correlation (0.0) . In LP, C, UP, SS and DC*2b	. Henry-Fauske and HEM . Multipliers for HEM : 1.0 Subcooled (extended) Henry: 1.0 . Transition quality: 0.02	?	Momentum Mixing (MUMIX=2)		*2b LP: Lower Plenum SS: Steam Separator C : Core DC: Downcomer UP: Upper Plenum
F		Characteristic analysis	?	Not used*3b	Correlations based on data from the Moby Dick experiment and the work of Jones et al.	*3b The code has no jet pump model
N	?	?	Normal pump model in RELAP4 Values and homologous curves were given	Normal jet pump in RELAP4		
J	Phase separation model including bubble rise model in shroud . Wilson model; core(1.0), LD(0.8), LP(0.0), UP(0.0), UD(0.0) and Bypass and GT(0.0).*5b . Bubble velocity=0; STD(1.0)*5b	Henry-Fauske and HEM . Multipliers for Henry-Fauske: 1.0 HEM : 0.85 . Transition Quality: 0.02	. Rated values and homologous curve data for ROSA-III recirculation pump.	. Mixing model in the junctions for the jet pump drive and suction flow . Reverse flow form loss coeff. K_R.*5c	Equilibrium model and steam table	*5b LD: Lower downcomer LP: Lower plenum UP: Upper plenum UD: Upper downcomer GT: Guide tube STD: Steam dome JP: Jet pump *5c K_R. Recirculation pump-JP: 1.4 JP suction-JP discharge: 1.763 DC-JP suction: 1.24
C	. Bubble rise velocity Wilson's correlation . Phase separation In shroud: Calculated with a sweep-out length*6c Out of shroud: Calculated with a sweep-out length*6d	. Moody and orifice models . Coefficient Moody: 0.6, Orifice: 0.61 . Transition quality: 0.02	. Rated values and head-vs-flow table as a function of quality	. Modelled as a set of three special junctions.	Equilibrium model	*6c A sweep out length is calculated from the steady state heat balance *6d A sweep out length is input,
A	. Wilson model in Core(0.8), UDC(0.1938157), LP(0.0), UP(0.0) and JP(0.0) . Complete Phase separation in MDC and LDC.*7b	. Henry-Fauske and HEM . Multipliers for Extended Henry: 1.0 Henry-Fauske: 1.2, HEM: 1.0 . Transition quality: 0.3	. Rated value and homologous curve data for ROSA-III recirculation pump	. Mixing model in the junctions for the jet pump driving flow and suction flow.		*7b UDC: Upper downcomer MDC: Middle downcomer LDC: Lower downcomer LP : Lower plenum UP : Upper plenum JP : Jet pump
R		Characteristic analysis	. Rated values and homologous curves were given.	. Pumps which posses the same coast down and homologous curves as the recirculation pump were added to the jet pump suctions*8b.	Correlations based on data from the Moby Dick experiment and the work of Jones et al.	*8b The code has no jet pump model

Table 3.2 Important Characteristics of Codes Used by Each Participant (contd.)*

Country	Interphase Drag	Wall Friction	Separator Model	Remarks
U	. Interfacial shear coeff. and interfacial area based on Ishii correlation . Wallis annular flow model for a wavy film shear.	. Single-phase friction factor correlation with the effect of the wall surface roughness. . Standard homogeneous correlation: Pfann correlation	Separator-dryer model*1c Empirical model 100% separation	*1c Separator-dryer model set axial and radial friction factors for the liquid and vapor phase, respectively
S		?	?	
F	Dynamic drag*3c and steady drag*3d were considered	. HTFS modification of Baroczy two-phase friction multiplier correlation . Colebrook correlation for single-phase friction factor	?	*3c due to virtual mass acceleration *3d arises from viscous shear between phases and depends on flow regime
N		Fanning-friction	No separator model	
J		. Fanning friction . Baroczy two-phase friction multiplier	. Phase separation in upper plenum and upper downcomer	
C		. Calculated using a pressure loss coefficient . Two-phase multiplier Thom-Martinelli	. Normal junction model modified to allow slip between vapor and liquid.	
A		. Fanning friction . Baroczy two-phase friction multiplier	. Homogeneous flow in separator . Phase separation in upper downcomer	
R	Dynamic drag*8c and steady drag*8d were considered	. HTFS modification of Baroczy two-phase friction multiplier correlation . Colebrook correlation for single-phase friction factor	Not used*8e Modeled by using a downward junction	*8c due to virtual mass acceleration *8d arises from viscous shear between phases and depends on flow regime *8e The code has a separator model (100% separation)

Table 3.2 Important Characteristics of Codes Used by Each Participant (contd.)*

Country	Heat Transfer Correlation (*HTC: heat transfer coefficient [W/m^2K])					
	Steady state	Blowdown initiation	flashing (rewet)	Core uncovery (dryout)	LPCS (rewet)	LPCI (reflood)
U	. Forced convection to singel-phase liquid: Dittus-Boelter Chen F factor=1.0 . Saturated nucleate boiling Chen (α<0.96, vapor HTC=0)	. Forced convection (Dittus-Boelter) and natural convection to single-phase liquid. . Saturated nucleate boiling Chen (α<0.96, vapor HTC=0)	Iloeje minimum stable film boiling for rewet	. Transition boiling* . Film boiling* . Convection to single-phase vapor Max(Dittus-Boelter, turbulent natural convection)	Not used	Not used
S	. Subcooled liquid forced convection: Dittus Boelter . Subcooled nucleate boiling: Modified Chen . Saturated nucleate boiling: Chen			. Transition boiling : Modified Tong Young . Film boiling : New Groeneveld		
F	. Subcooled nucleate boiling : Modified Chen . Saturated nucleate boiling : Chen	. Saturated nucleate boiling: Chen . Subcooled laminar and turbulent natural convection . Pool nucleate boiling : Foster-Zuber	. Saturated nucleate boiling : Chen . Pool nucleate boiling : Foster-Zuber	. High flow film boiling : Condie-Bengston . Two-phase laminar natural convection . Superheated laminar natural convection etc.	Superheated Laminar Natural Convection High Flow Film Boiling : Condie-Bengston Saturated Nucleate Boiling : Chen etc.	
N						
J	. Subcool forced convection : Dittus-Boelter . Nucleate boiling : Thom			. Free convection + radiation . Superheated vapor forced convection : Dittus-Boelter	Hdry: Convective HTC(FLECHT)=17.0,20.0, 5.5 Hwet: Top down liquid film nucleate boiling=5678 with Duffey-Porthouse's quench front velocity correlation	Hflood: Film boiling HTC=142 quality≥0.05
C	. Subcool forced convection : Dittus-Boelter . Nucleate boiling : Thom	. Nucleate boiling: Thom	. Pool film boiling : Berenson	. Forced convection in vapor : Dittus-Boelter	Forced Convection in Vapor : Dittus-Boelter Pool Film Boiling : Berenson	Pool film boiling: Berenson transition boiling : Mcdonough-Milich-King Nucleate boiling: Thom
A	. Nucleate boiling : Thom	. Nucleate boiling: Thom	. Nucleate boiling : Thom	. Adiabatic	Hdry: convective HTC*=17.0, 20.0, 8.5 (FLECHT) Hwet(by Topdown liquid film) Nucleate boiling HTC=5678	Hflood: Film boiling HTC=142 quality=0.05
R	. Subcooled nucleate boiling : Modified Chen . Saturated nucleate boiling : Chen	. Saturated nucleate boiling: Chen . Subcooled laminar and turbulent natural convection . Pool nucleate boiling : Foster-Zuber	. Saturated nucleate boiling : Chen . Pool nucleate boiling : Foster-Zuber	. High flow film boiling : Condie-Bengston . Two-phase laminar natural convection . Super heated laminar natural convection etc.	Superheated laminar natural convection High flow film boiling : Condie-bengston Saturated nucleate boiling : Chen etc.	

Table 3.2 Important Characteristics of Codes Used by Each Participant (contd.)*

Country	CHF correlation	Comments
U	Nucleate boiling transition . Critical quality ∿ Biasi Minimum stable film boiling temperature Henry-Berenson or Iloeje . Temperature corresponding to CHF point Biasi	Film boiling: Void fraction weighted between Dougall-Rohsenow and Bromley H_{ℓ}: Radiative contribution with Stefan-Boltzmann Transition boiling: Bjornard-Griffith
S	Blowdown . High flow subcooled DNB correlation Tong . High flow saturated DNB correlation Hsu and Beckner . Low flow DNB correlation Modified Zuber	
F	. High flow subcooled DNB correlation Tong . High flow saturated DNB correlation Hsu and Beckner . Low flow DNB correlation Modified Zuber	
N	. High flow subcooled DNB correlation Tong . High flow saturated DNB correlation Hsu and Beckner . Low flow DNB correlation Modified Zuber	
J		
C	. Babcock & Wilcox Company, B & W-2 . Barnet . Modified Barnet	
A		
R	. High flow subcooled DNB correlation Tong . High flow saturated DNB correlation Hsu and Beckner . Low flow DNB correlation Modified Zuber	

* In the case where each code has several model options, only the model used by each participant is presented in this table.

Table 3.3 Important Characteristics of Models Used by Each Participant (a) Number of Components

Country (Organization) Identification	Computer Code	Volume					Junction			Heat Slab					Remarks
		System				Containment	Junction (except Fill and Leak Junctions)	Fill and Leak Junctions	The Others	Vessel Wall	Pipe Wall	Internal Structure	Core		
		Inside Shroud	Downcomer	Recirculation Line	The Others								Core (Axial x Radial)	Comments (L.P.F.: Local Peaking Factor)	
USA (INEL) U	TRAC-BD1	57	11	53	18	1	140	18	0	12	39	38	32 (8 × 4)	① Average Power Channel (L.P.F.=1.0) ② High Power Channel (L.P.F.=1.1) ③ High Power Channel (L.P.F.=1.0) ④ High Power Channel (L.P.F.=0.875)	
Switzerland (EIR) S	RELAP4/ MOD6	8	3	14	0	0	30	7	0	4*2a	0	2	8 (8 × 1)	① Single Channel	*2a Heat Loss from Vessel Wall is not Considered
Sweden-Finland F	RELAP5/ MOD1/ (cycle 014)	27	12	17	12	7	72	7	0	10	6	4	16 (8 × 2)	① Average Power Channel (L.P.F.=1.0) ② High Power Channel (L.P.F.=1.0)	
Netherlands (ECN) N	RELAP4/ MOD6	12	4	12	6	3	44	6	0	0	0	0	7 (①5 + ②2)	① High Power Channel (L.P.F.=1.272) ② Average Power Channel (L.P.F. =0.9094)	
JAPAN (JINS) J	RELAP4/ MOD6/ U4/J3 (modified)	6	3	11	0	1	25	9	6*5a	4	0	4	28 (7 × 4)	① Average Power Channel (L.P.F.=1.0) ② High Power Channel (L.P.F.=1.1) ③ High Power Channel (L.P.F.=1.0) ④ High Power Channel (L.P.F.=0.875)	*5a Special Junction to Calculate Top-down Quenching Dummy Fill Simulating ECC Injection to Lower Plenum
Japan (JAERI-C) C	THYDE -B1	1	1	4	0	0	11	8	0	2	0	2	14 (7 × 2)	① Average Power Channel (L.P.F.=1.0) ② High Power Channel (L.P.F.=1.0)	
Japan (JAERI-A) A	RELAP4/ MOD6/ U4/J3	7	4	14	0	1	31	9	2*7a	5	14 (include pump casing)	11	13 (13 × 1)	① Single Channel	*7a Special Junction to Calculate Top-Down Quenching
Japan (JAERI-R) R	RELAP5/ MOD1 (cycle 001)	35	15	38	7	3	100	6	0	19	0	0	21 (7 × 3)	① Average Power Channel (L.P.F.=1.0) ② High Power Channel (L.P.F.=1.1) ③ High Power Channel (L.P.F.=1.0 and 0.875)	

Table 3.3 Important Characteristics of Models Used by Each Participant (b) Models of Injection and Discharge

Country	Main Steam		SRV		ADS		Feed Water		LPCS		LPCI		
	Signal of Closure	Input of Flow Rate	Signals of Actuation and Closure	Input of Flow Rate	Signal of Actuation	Input of Flow Rate	Signal of Closure	Input of Flow Rate	Signal of Actuation	Input of Flow Rate	Signal of Actuation	Input of Flow Rate	
U	Time	Fill Model (Time -Velocity	Actuated at Steam Dome Pressure above 8.4MPa	Fill Model (Pressure-Velocity) Maintained Pressure below 8.47MPa	L1+120s	Fill Model (Pressure-Velocity)	Time 4s	Fill Model (Time-Velocity) Feedwater Line Flashing Occurred at The Bipe between PV and FW Fill.	L1+40s and Pressure	Fill Model (Pressure-Velocity)	L1+40s and Pressure	Fill Model (Pressure-Velocity)	PV: Pressure Vessel FW: Feedwater
S	L2 Mixture Level	Program Calculated?	Actuated at Pressures above 8.34MPa?	?	Experimental Pressure at Which ADS was Actuated	Program Calculated Flow Rate?	Neglected?						
F	L2+3s	?	Actuated at Pressure above 8.47MPa	?	L1+120s	?	?	?	?	?			
N	Mixture Level	Time-Pressure	Actuated at Pressure above 8.24MPa	Controlled to Maintain Pressure below 8.34MPa	Mixture Level	Time-Pressure	Time 3.1s	Time-Velocity	Pressure	Pressure-Velocity	Pressure	Pressure-Velocity	
J	Time (Table) 24s	Time-Mass Flow Rate	Actuated at Steam Dome Pressure above 8.47MPa Closed at Steam Dome Pressure below 8.40MPa	Pressure-Mass Flow Rate	L1+120s	Henry-Fauske(1.0) and HEM(0.85) Time-Areas (0.3sec Full Opened)	Time (Table) 3.1s	Time -Mass Flow Rate	L1+40s	Pressure -Volumetric Flow Rate	L1+40s	Pressure -Volumetric Flow rate	
C	L2+3s	Choked Flow Model	Actuated at Pressure above 8.12MPa	Pressure-Mass Flow Rate	L1+120s	Choked Flow Model	Time 2s	Time -Mass Flow Rate	L1+40s and Pressure (2.16MPa)	Pressure -Mass Flow Rate	L1+40s and Pressure (1.57MPa)	Pressure -Mass Flow Rate	
A	L2	Time-Mass Flow Rate	Actuated at Pressure above 8.4MPa	Closed at Pressure below 8.4MPa	L1+120s	HEM Time-Area	Neglected		L1	Pressure -Volumetric Flow Rate (Const. Enthalpy)	L1+40s	Pressure -Volumetric Flow Rate (Const. Enthalpy)	
R	Time 24s	Time-Velocity	Actuated at Pressures above 8.34MPa	Controlled to Maintain Pressure at 8.34MPa	Time 158s	Time-Velocity	Time 2s	Time-Velocity	Time 318s	Time-Velocity	Time (406s)	Time-Velocity	

Table 3.3 Important Characteristics of Models Used by Each Participant (c) Special Features and Comments

Country	Special Features and Comments
U	Ambient heat loss modeled. Correct feedwater line volume modeled: O Flashing affected system pressure
S	1 Leak hole is not modeled 2 Standard RELAP4/MOD6 was used together with some changes of the code errors. The errors corrected were related to leak junction area calculations, fluid property calculations at leak junctions and time step calculations.
F	
N	
J	
C	The degree of the mixing between the injected liquid and the steam in the system is determined by the mixing efficiency given by the user.
A	
R	

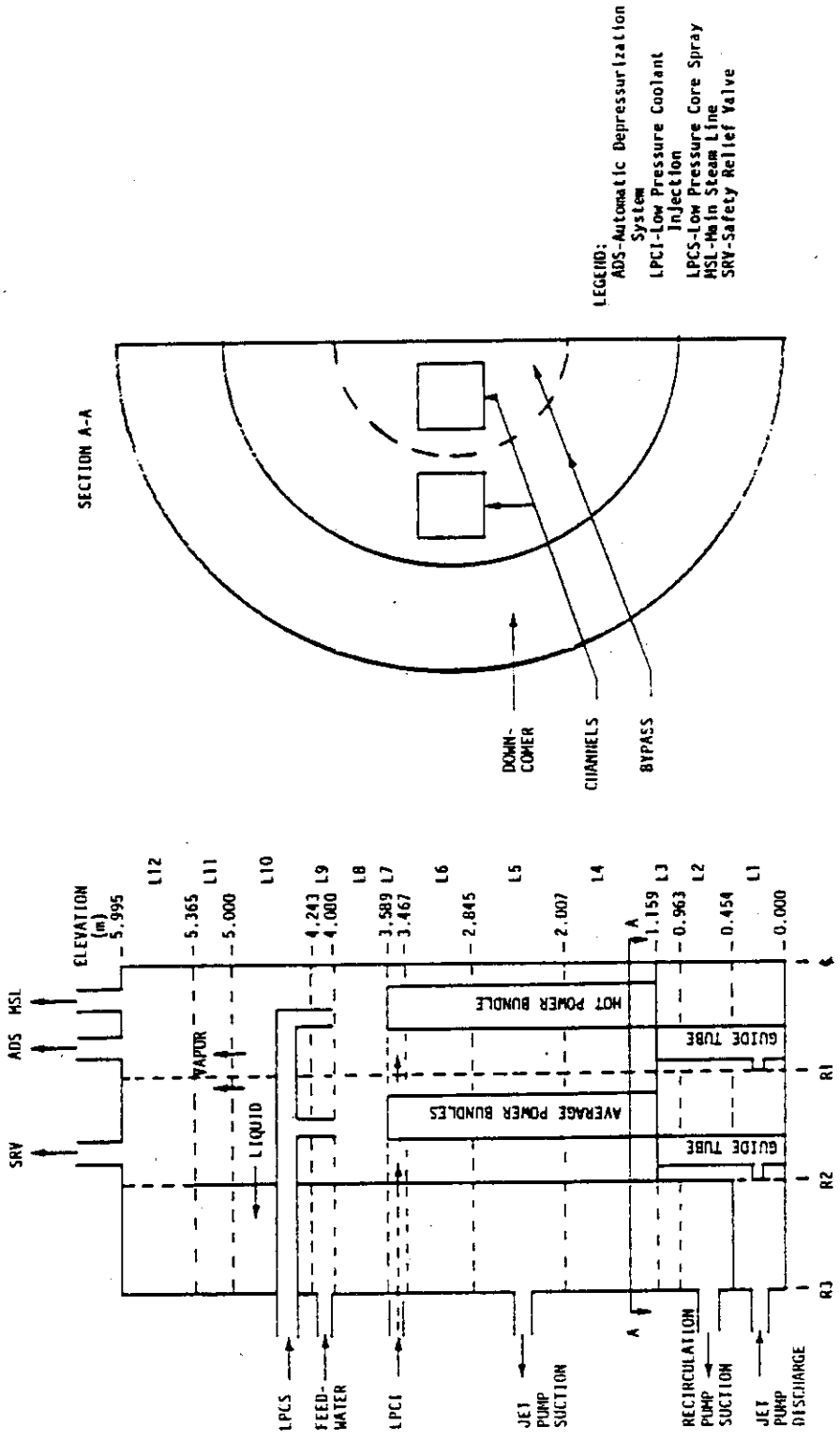

Fig. 3.1(a) System Nodalization Diagram of USA (1)

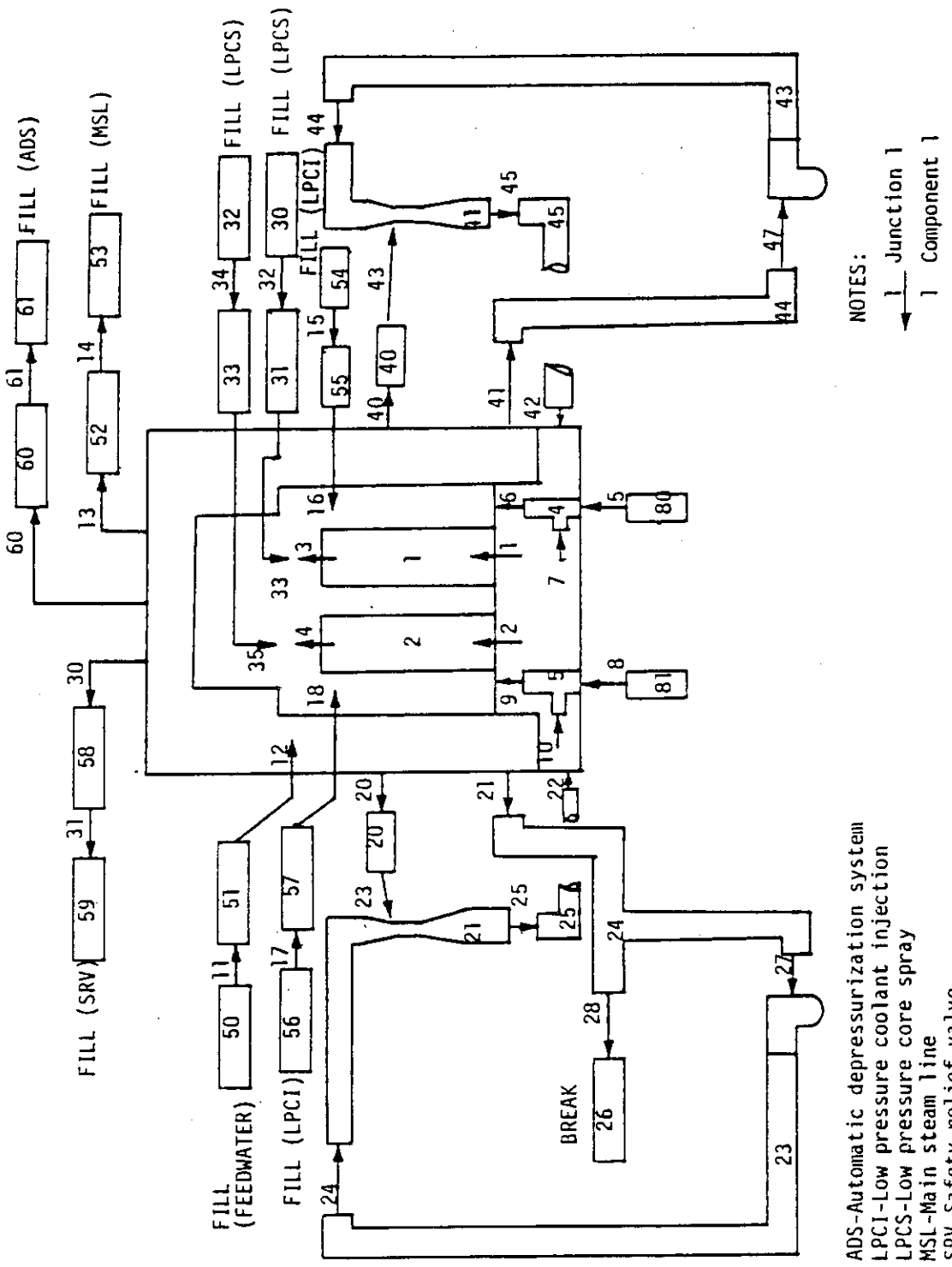

Fig. 3.1(a) System Nodalization Diagram of USA (2)

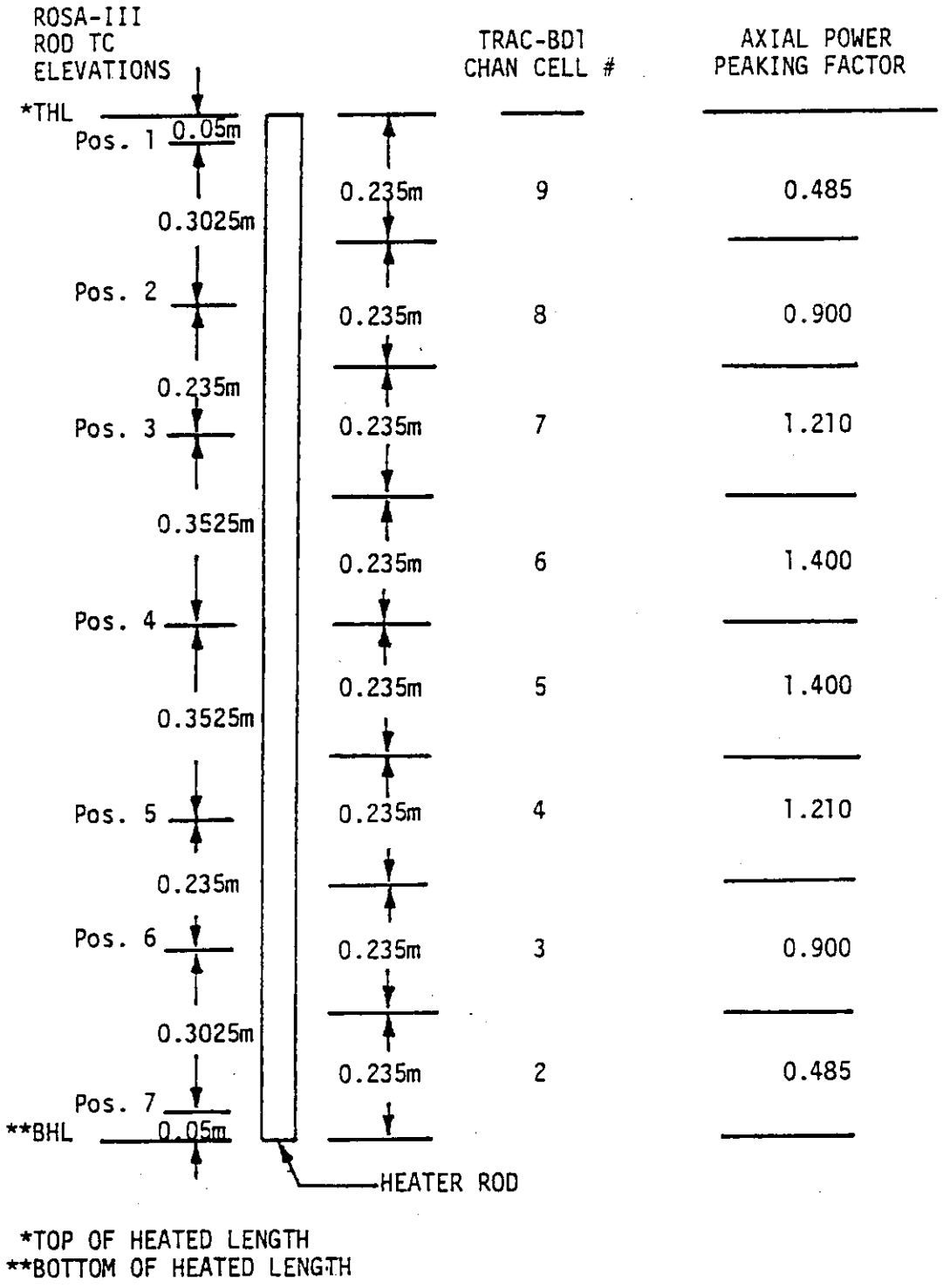

Fig. 3.1(a) System Nodalization Diagram of USA (3)

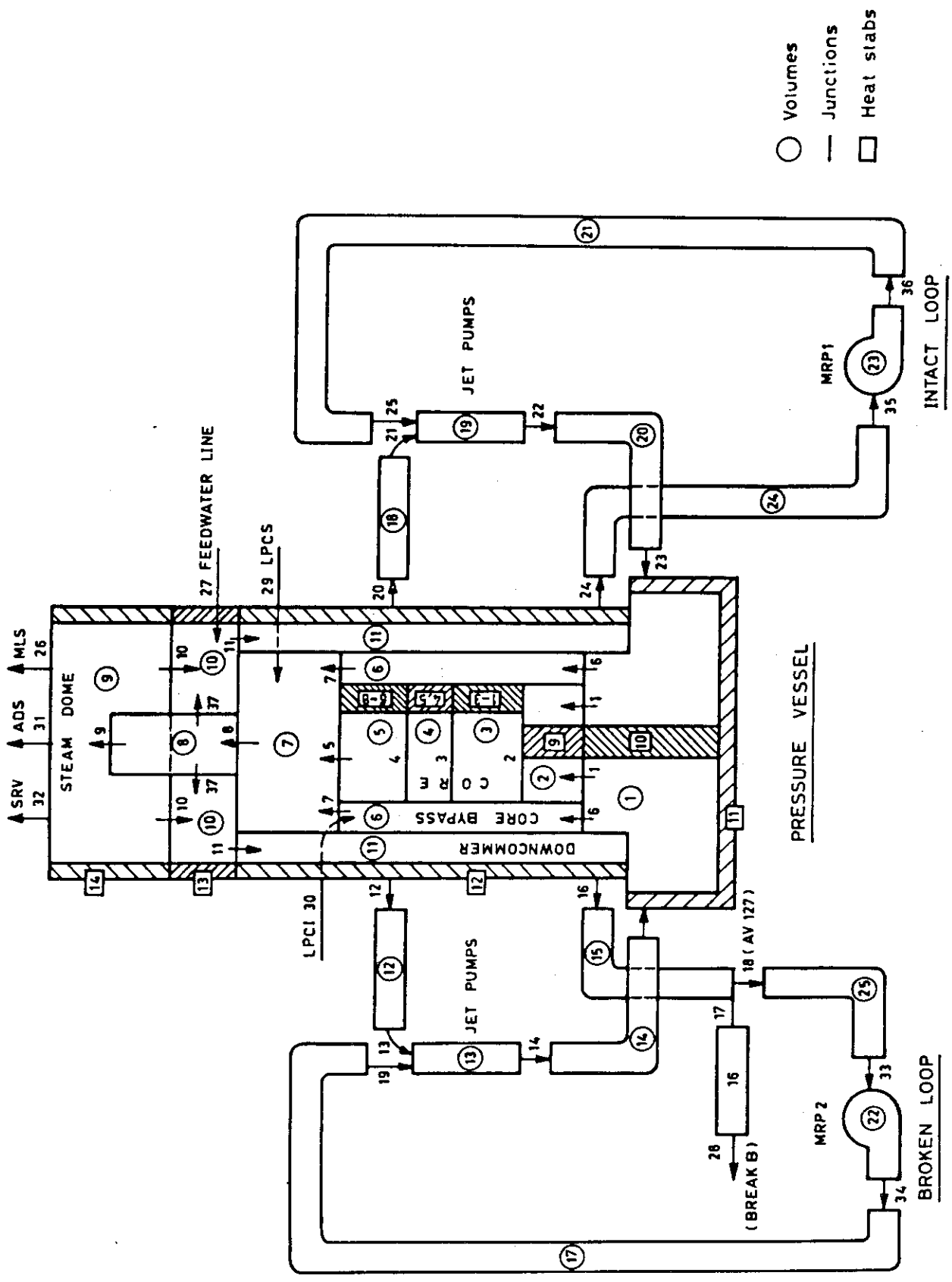

Fig. 3.1(b) System Nodalization Diagram of Switzerland

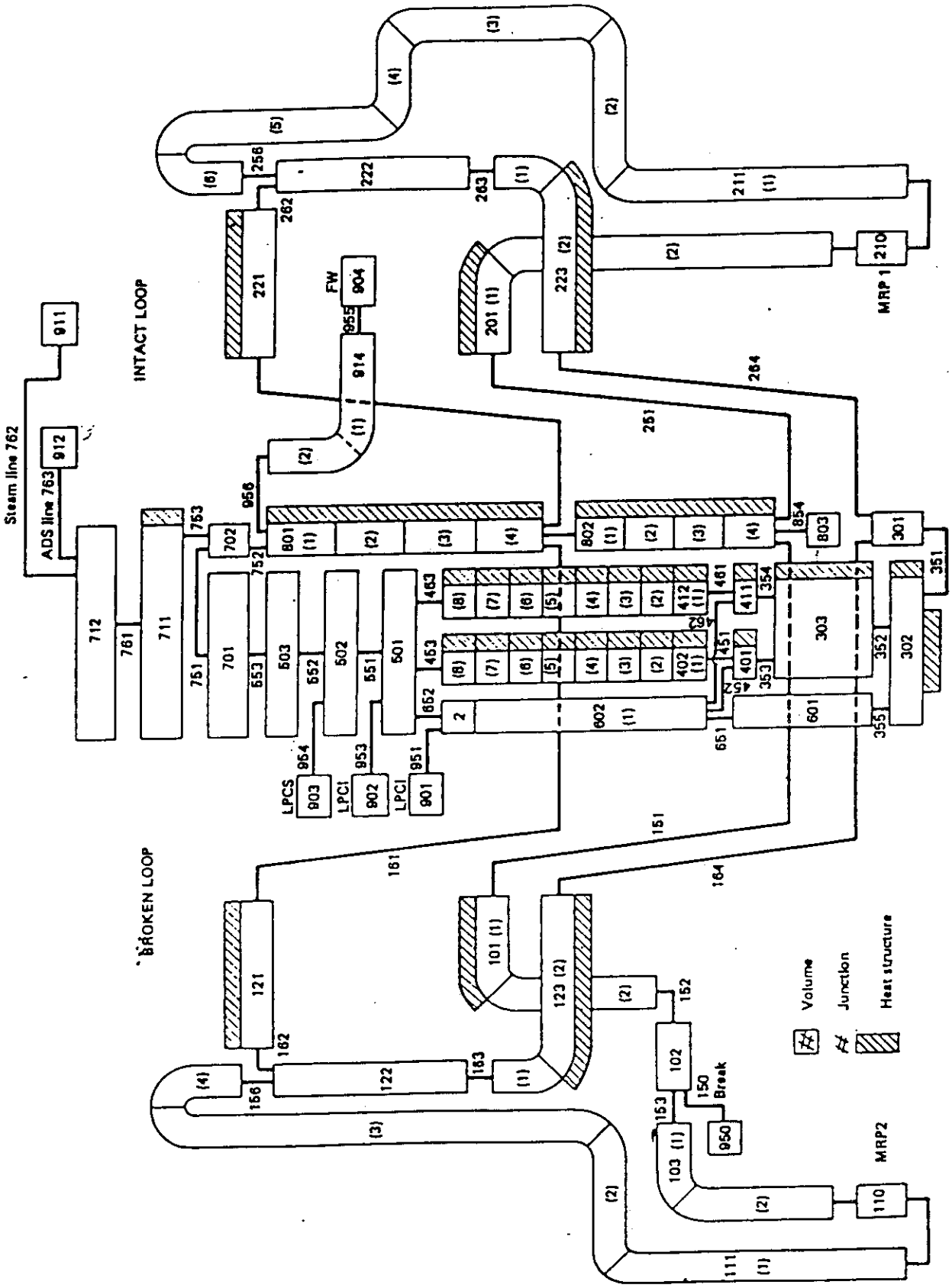

Fig. 3.1(c) System Nodalization Diagram of Sweden-Finland

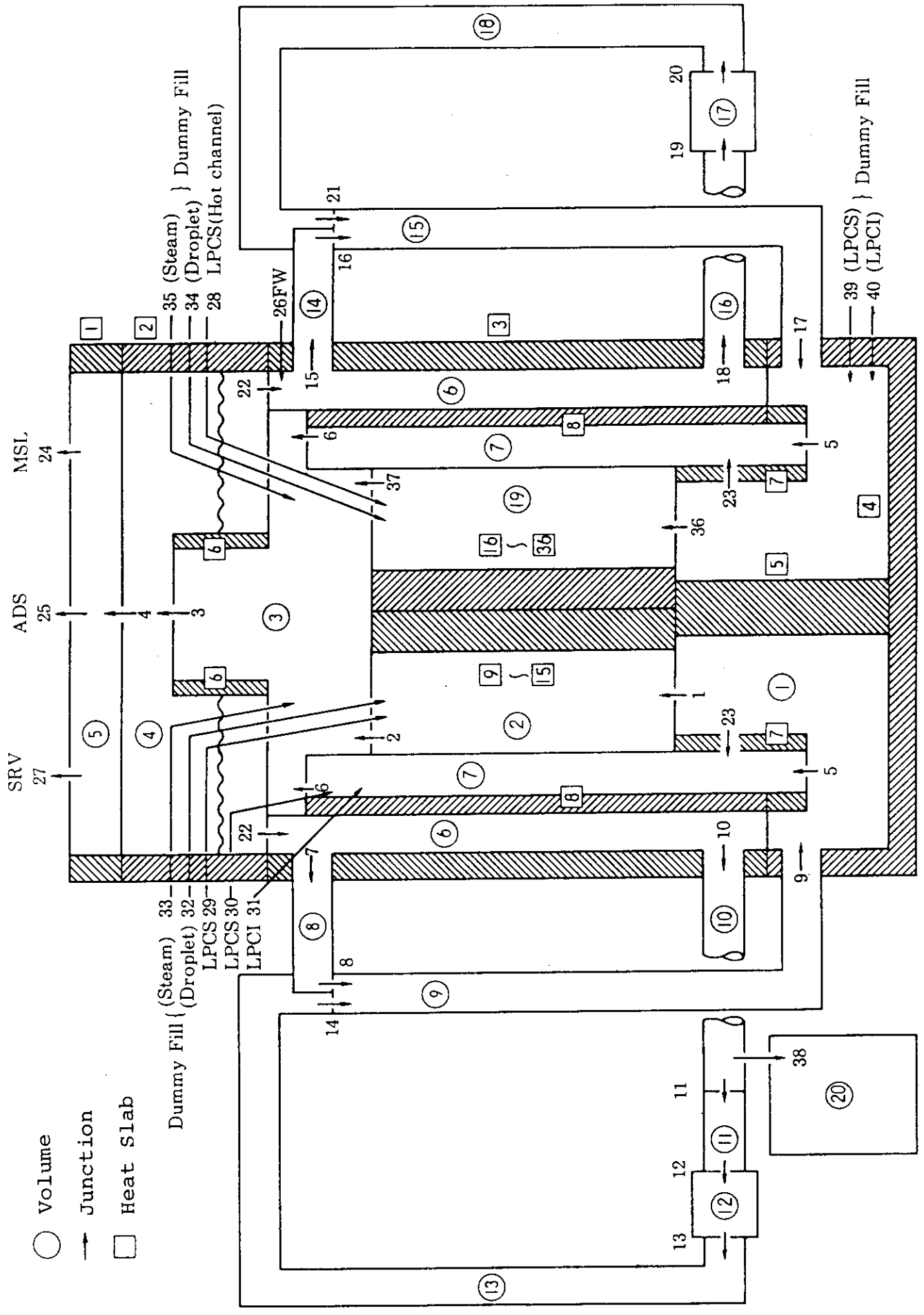

Fig. 3.1(d) System Nodalization Diagram of JINS

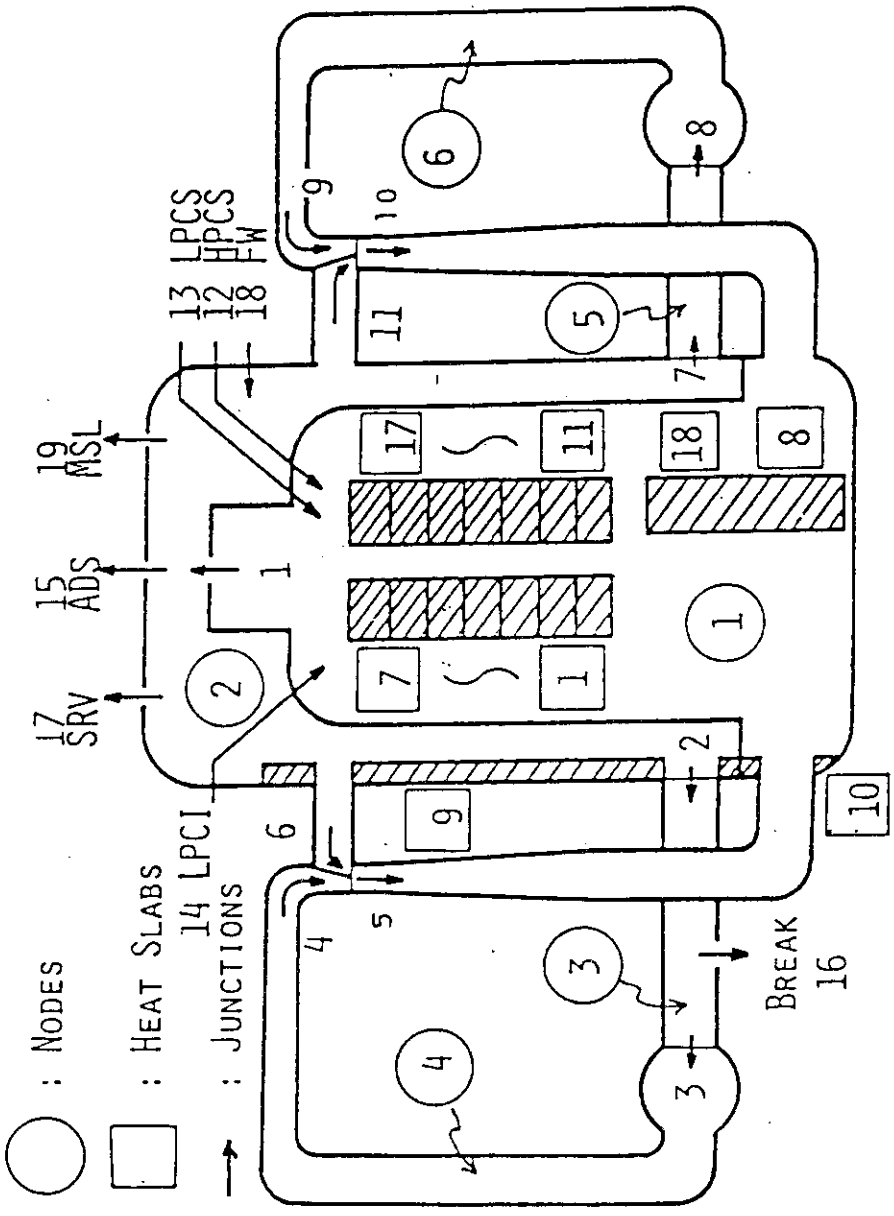

Fig. 3.1(e) System Nodalization Diagram of JAERI-C

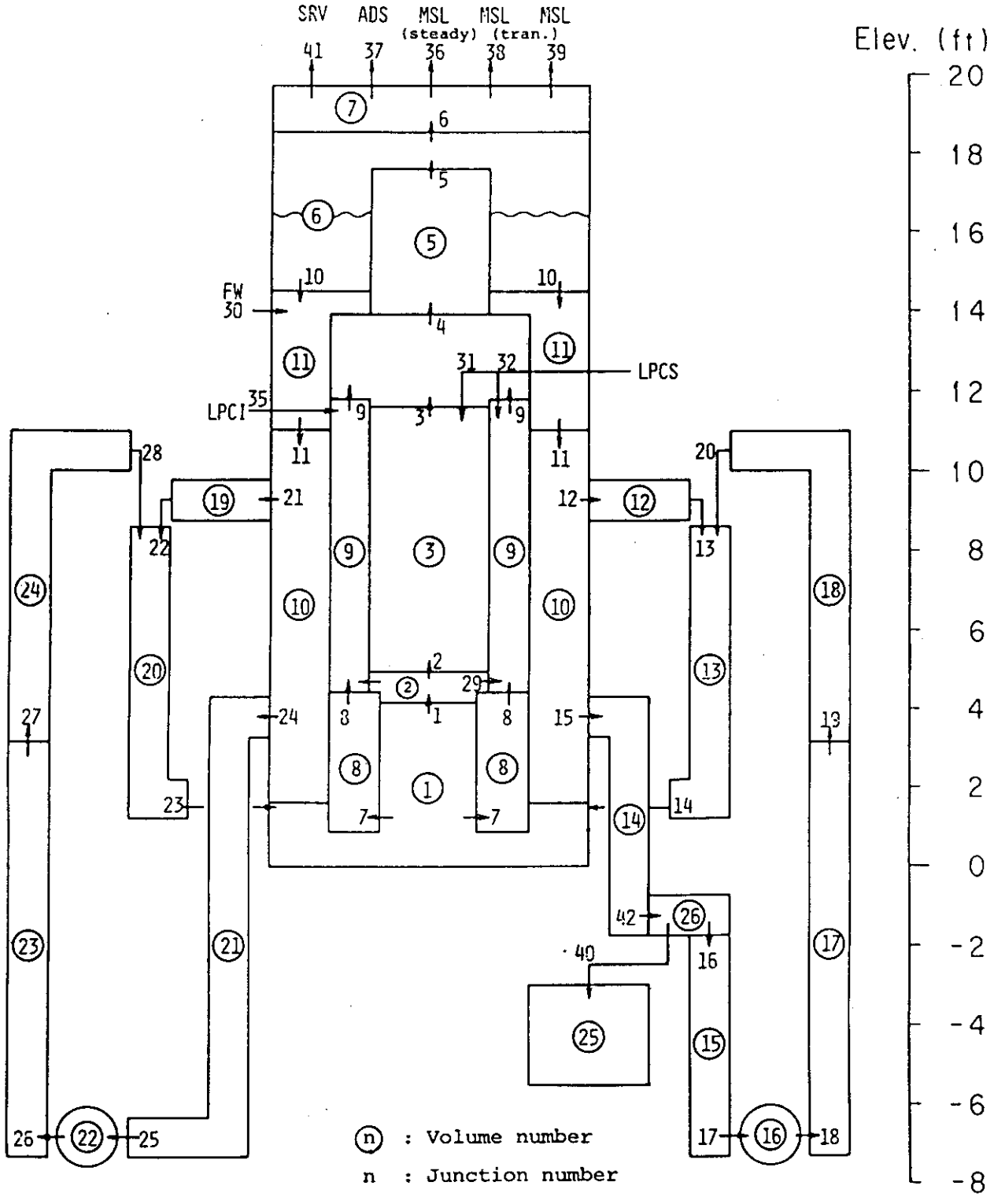

Fig. 3.1(f) System Nodalization Diagram of JAERI-A

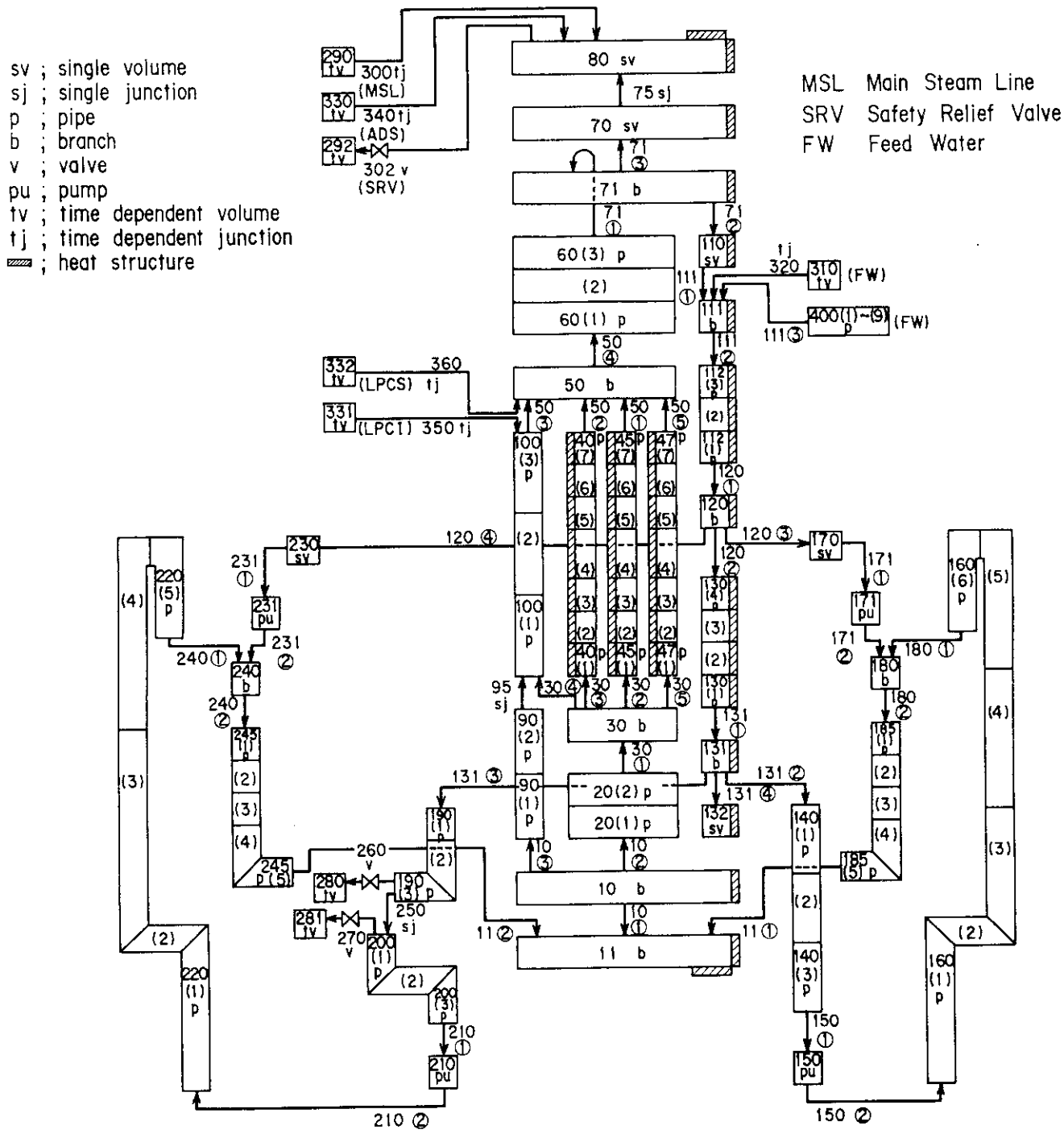

Fig. 3.1(g) System Nodalization Diagram of JAERI-R

4. Comparison of Results

The participants calculated results of major variables are compared with the experimental results in this section. Scenario of the 5% break LOCA test Run 912 is shown in Fig. 4.1 and scenarios calculated by the participants are shown in Fig. 4.2 through 4.9.
Comparisons are shown for calculated and measured pressure in Figs. 4.10 through 4.12, flow rates in Figs. 4.13 through 4.34 and 4.39 through 4.48, densities in Figs. 4.35 through 4.38, pump performances in Figs. 4.49 through 4.52, differential pressures in Figs. 4.53 through 4.66, mixture levels in Figs. 4.67 through 4.79, core power in Fig. 4.80, heater rod surface temperatures in Figs. 4.81 through 4.108, dryout and quench fronts in Figs. 4.109 through 4.111, and fluid temperatures in Figs. 4.112 through 4.118.

4.1 System Pressure Transient

Comparison of system pressure calculations and data is shown in Fig. 4.10. The USA calculation with TRAC-BD1 gave an excellent agreement with the data of the system pressure transient because of an excellent agreement between calculated results and the data on the steam flow rate through the main steam line, the safety relief valve, and the ADS line (see Figs. 4.13 and 4.14). Temporary hold of the pressure after 328 s was calculated by USA. However, the pressure began to decrease at 86 s after break, 34 s earlier than the data. The liquid level decrease in the core began at 68 s in the calculation 42 s earlier than the data and the calculated steam generation rate in the core became smaller than the data. Therefore, the calculated pressure started to decrease 34 s earlier than the data. Differences between the calculated and the measured flow rates from the break had little influence on the calculation of the pressure.

Swiss and Dutch calculations with RELAP4/MOD6 showed a continuous increase in the system pressure after the MSIV closure giving a much higher pressure than the data since the steam flow rate through the safety relief value was not properly modelled.

Swedish-Finnish calculation and JAERI-R calculation with RELAP5/MOD1, JINS, JAERI-A calculations with RELAP4/MOD6/U4/J3, and JAERI-C calculation with THYDE-B1 agreed with each other on the system pressure transient and showed excellent agreement with the data before the ADS

actuation at 158 s.

JINS and JAERI-C calculations gave very good agreement with the data after the ADS actuation. JINS calculation gave higher flow rate in the ADS line than the data. It is supposed that the reason why JINS obtained good agreement with the data might be that the amount of steam generated during the lower plenum flashing period was larger in their calculation, JAERI-C calculation gave lower ADS flow rate but a higher break flow than the data. Accordingly, their effects were compensated giving good agreement with the data on the pressure decrease. Large oscillation occurred after 336 s in JAERI-C pressure calculation which was not observed in the test. JAERI-A calculation gave higher pressure than the data after the ADS actuation due to higher steam generation in the core because of the delay in core uncovery.

Swedish-Finnish calculation and JAERI-R calculation gave lower pressure than the data because of the higher ADS flow rate in the calculations. JAERI-R calculation of ADS flow showed a peculiar trend after 270 s due to improper modelling of the ADS line in the analysis. Temporary hold of the pressure at 2,2 MPa was calculated by JINS and JAERI-A. RELAP4/MOD6/U4/J3 includes provisions for calculating top-down quench in the core after the LPCS is initiated to provide spray to the core and the pertinent increase in the steam generation rate was calculated by JINS and JAERI-A.

4.2 Break Flow

Break flow measurement using drag disks and a gamma densitometer involved an error of at least ±20%. Accordingly, in this review, emphasis was made on the calculation of the incipient time of the break flow decrease due to the uncovering of the recirculation line inlet. Comparisons of calculated and measured break flows are shown in Figs. 4.23 through 4.34.

The USA calculation gave very early decrease of the break flow at 111 s after break compared to 156 s in the test. This was due to too large of a break flow rate because no critical flow model was used in the USA analysis by TRAC-BD1 before 111 s after break (see Fig. 4.27). Calculated break flow was adjusted to approach data curve for first 111 s by adjusting the wall friction, although the data had large uncertainties.

The other calculation results of break flow using choking models scattered within the range of 1.4∿1.8 kg/s until uncovering of the recirculation line and the timings of the recirculation line uncovering agreed with the timing in the experiment within an error range of -20 s ∿+10 s.

The break flow rate of JAERI-A did not decrease sharply after the recirculation line uncovering. The reason may be that the transition quality from the Henry-Fauske critical flow model to HEM was specified as 0.3, whereas the transition quality of 0.02 is usually used.

The recirculation line uncovering time in the calculation of Switzerland was earlier than the experiment, while the break flow rate was smaller than the other calculation results except for the JINS result. This was probably due to the smaller initial mass inventory in the downcomer.

4.3 Total Core Inlet Flow Rate

The total core inlet flow decreases to a very low value at 50 s after the break when there remains still enough water in the pressure vessel for core cooling. Therefore, the models for the recirculation pump and the jet pump are not so important in a small break LOCA as in a large break LOCA. However, the core cooling can be deteriorated before 50 s after break if the calculated core inlet flow becomes considerably lower than the measured flow resulting in the fall of the mixture level or the increase in the void fraction at the upper part of the core. Comparisons of calculated and measured core inlet flows are shown in Figs. 4.15 through 4.18.

The recirculation pump coastdown data (pump speed vs. time) was used in the analyses by USA, Sweden-Finland, Switzerland and Netherlands in which the trend of the core inlet flow was well calculated (ef. Figs. 4.49 and 4.50). However, the USA results and the Switzerland results became less than the experimental flow rate for the time ranges between 5 s and 22 s and beyond 10 s, respectively (see Fig. 4.16). The calculated core inlet flow rate by Sweden-Finland decreased rapidly after the break because of no jet pump model in their analysis and the core inlet flow became substantially less than the measured flow until 3 s after break. The Netherlands results of the core inlet flow coast-down was delayed from the measured flow because of the delay in the

input data for the pump coastdown. The calculated core inlet flow rate by Netherlands exceeded the measured flow rate after 10 s.

The calculated core inlet flows by JINS, JAERI-A and JAERI-R were considerably higher than the measured flow because they used the incomplete recirculation pump data of ROSA-III without the measured torque data. The JAERI-R results were higher than the measured flow rate because JAERI-R modelled the jet pump by incorporating a pump in each suction line of the jet pump due to a limitation in the capability of RELAP5/MOD1 for simulating a jet pump.

4.4 Mixture Level

Since advanced codes like TRAC-BD1 and RELAP5/MOD1 do not predict the mixture level transient, it is assumed in this comparison work that the mixture level passed downward through the volume if the void fraction exceeded 95 %. If the void fraction became lower than 95 %, it is assumed that the mixture level passed upward through the volume. Calculated mixture levels in the pressure vessel are compared with measured levels in Figs. 4.67 through 4.79.

The USA calculation gave a faster decrease of the mixture level in the downcomer than the data since the break flow rate was higher in their calculation (see Fig. 4.74). Consequently, it gave earlier uncovering of the inlet of the recirculation line and earlier initiation of the rapid pressure decrease. The mixture level decrease in the core was initiated at 68 s in the USA calculation about the same time the mixture level decrease in the downcomer was initiated.
The level reached below the midplane of the core. The mixture level increase due to flashing of fluid in the lower plenum, initiated at 168 s, was slower in the calculation than the data. And the mixture level decrease after the lower plenum flashing (LPF) was also slower in the calculation. The minimum level reached after LPF in the USA calculation was at the midplane of the core, whereas, the whole core was uncovered in the test. The mixture level begain to recover at 368 s after break, after the LPCI started to provide water.
The level oscillated during the recovery period and the whole core was reflooded at 414 s in the USA calculation. In summary, the USA calculation followed the overall trend of the liquid level transient observed in the test. However, the minimum mixture level reached was much higher

in the calculation than the data.

The Swiss calculation gave a faster decrease of the mixture level in the downcomer than the data giving earlier uncovering of the recirculation line inlet at 135 s, which is 20 s earlier than the data (see Fig. 4.75). This was probably due to the smaller initial inventory of the coolant assumed in the calculation. The upper part of the core was uncovered between 9 s and 48 s. This was probably due to too low of a flow rate at the inlet of the core in the calculation (see Fig. 4.16). The calculation gave earlier initiation of the mixture level decrease in the core at 57 s after break, approximately 55 s earlier than the data. The mixture level reached a minimum at the midplane of the core at the start of LPF. Recovery of the mixture level due to LPF was smaller in the calculation than the data. The mixture level decrease after LPF was slower in the calculation than the data. The whole core was uncovered at 275 s in the test, however, the calculation did not give the whole core uncovering at that time or even after, although the calculation was terminated at 328 s.

The JINS calculation followed the overall trend of the mixture level transient in the test (see Fig. 4.76). The calculation followed the mixture level decrease in the core and the downcomer in the test before LPF. The downcomer mixture level temporarily recovered at 138 s in the calculation which could not be readily interpreted. The level did not reach the outlet to the recirculation line in the calculation before LPF. Temporary recovery of the mixture level in the core due to LPF was calculated well. However, recovery of the mixture level in the downcomer was much larger in the calculation than the data. This was probably due to improper modelling of the bubble rise velocity and the void distribution in the analysis. The calculation gave fast reflood of the core after the LPCI was initiated at 406 s. The mixture level decreased again after 433 s and the upper one third of the core was uncovered. This was due to provisions incorporated in RELAP4/MOD6/U4/J3 to model the counter current flow limit. The mixture level in the downcomer was maintained low even after the core reflood in JINS calculation.

The JAERI-A calculation gave a 16 s delay for the initiation of LPF (see Fig. 4.78). The calculation gave good agreement with the trend of the data on the mixture level decrease after LPF. Quantitatively, a considerable difference existed between calculated

and measured results. The whole core was uncoyered at 366 s in the calculation compared to 275 s in the test.

The THYDE-B1 code was developed with special emphasis on the capability of predicting the mixture level transient during a BWR small break LOCA.

The JAERI-C calculation with THYDE-B1 followed the overall trend of the mixture level transient in the core and in the downcomer (see Fig. 4.77). The calculation gave a higher mixture level in the downcomer although it followed the trend of the level decrease very well. Change of the cross-sectional area of the flow path was pertinently taken into account. The calculation also gave an excellent agreement with the data on the mixture level transient in the core before LPF. Recovery of the mixture level by LPF was underpredicted. This might be due to modeling of the shroud inside region with one volume. Momentum transfer to the core and the counter current flow limiting at the core inlet orifice can not be predicted by one volume representation.

The whole core uncovering was well calculated at 264 s giving excellent agreement between the data and the calculation. The pressure decrease was accelerated by the injection of water by the LPCS at 310 s and the LPCI was initiated to provide water at 330 s in the calculation. Consequently, the reflood of the core was calculated at approximately 391 s, 49 s earlier than the experiment. Large oscillations of the mixture level were given in the calculation due to gereration of steam bubbles in the core flowing upward.

The JAERI-R calculation followed the overall trend of the mixture level transient in the test (see Fig. 4.79). This was due to the excellent two-phase flow model incorporated in the RELAP5/MOD1 code. The mixture level decrease in the downcomer was calculated very well giving excellent agreement on the uncovering of the outlet to the recirculation line. The calculation gave a slightly earlier decrease of the mixture level in the core by approximately 20 s. The recovery of the mixture level by LPF was calculated but the top part of the core remained uncovered. The calculation followed the mixture level decrease well after LPF. The whole core uncovering at 265 s was calculated well. The mixture level increase in the downcomer due to LPF was peculiarly large. The calculation with RELAP4/MOD6/U4/J3 showed the same trend. The JAERI-R calculation gave a faster decrease of the mixture level in

the downcomer after LPF compared with the results with RELAP4/MOD6/U4/J3. The level started to recover from the bottom of the core at 328 s after LPCS actuation at 318 s. The start of reflooding was approximately 70 s earlier than the test. The calculation was terminated at 372 s after break.

4.5 Heater Rod Surface Temperature

Transient of the heater rod surface temperature, and those of dryout, rewet and quench fronts are closely related to the liquid level transient in the core. The heater rod surface temperatures in the high power channel and in the average power channels are shown in Figs. 4.81 through 4,108. The dryout and quench fronts of the heater rod in the high power channel (L,P.F.=1.1 and 1.0) and in the average power channel (L,P,F.=1,0) are shown in Figs, 4.109 through 4,111.

(1) Dryout, Rewet and Quench

Temporary dryout and rewet within 40 s after the break initiation is ovserved in the calculations of USA (TRAC-BD1), Switzerland (RELAP4/MOD6) and Sweden-Finland (RELAP5/MOD1), which did not occur in the experiment (see Figs. 4.109 through 4.111). This is because the liquid levels in the core decreased temporarily or the void fractions in the upper part of the core increased above 0.95 due to a temporary decrease of core inlet flow rates below the experimental result (see Fig. 4.16).

The calculated liquid level in the core by the USA and Switzerland decreased much earlier than the experiment and the liquid level decreased below the midplane of the core before the LPF initiation (see Figs. 4.74 and 4.75). The heater rod surface above the midplane of the core dried out before the LPF initiation. In the experiment, however, only the top part of the heater rod dried out for a short time period. While rewetting by LPF was calculated by every participant, rewetting to the top of the core, observed in the experiment, was calculated only in the analyses by RELAP5/MOD1 (Sweden-Finland, JAERI-R) and RELAP4/MOD6/U4/J3 (JINS, JAERI-A). Dryout after rewetting by LPF was calculated well by RELAP5/MOD1 (Sweden-Finland, JAERI-R), RELAP4/MOD6/U4/J3 (JINS) and THYDE-B1 (JAERI-C). Uncovering of the whole core in the calculation of JAERI-A occurred at 366 s, 91 s later than the experiment. Uncovering of the whole core was not calculated in the analyses of the USA and Switzerland and the lower part of the core did not dryout.

The heater rod surface quenched after ECCS actuation from the top and the bottom of core simultaneously in the experiment. Top-down quench was calculated by RELAP4/MOD6/J4/J3 (JINS, JAERI-A), however, the heater rod surface dried out again after reflooding due to small hat transfer coefficients used in the calculation. Bottom-up quench was calculated by TRAC-BD1, RELAP5/MOD1 and THYDE-B1, however, JAERI-R analysis by RELAP5/MOD1 stopped before quench after turnaround of the heater rod surface temperature. RELAP4/MOD6 analyses were terminated before the actuation of ECCS.

(2) TRAC-BD1 Analysis by USA

USA results by TRAC-BD1 showed the cladding temperature rise after the early dryout due to the temporary increase in the void fraction in the upper part of the core up to 40 s after break (see Figs. 4.81 through 4.84). In spite of the short dryout period, short time after the break the cladding surface temperature rose to 824 K at Position 3 of the peak power rod due to the high heating rate .

The top part of the core did not rewet by LPF. The dryout front propagation to the lower part of the core was slower than the experimental results after temporary recovery of the level by LPF.
No dryout was calculated below Position 5.

The USA results showed rapid quench front propagation to the top of the core after the initiation of LPCI and the whole core was quenched at 414 s after break.

(3) RELAP5/MOD1 Analyses by Sweden-Finland and JAERI-R

The trends of the heater rod surface temperatures were calculated in the analyses of Sweden-Finland and JAERI-R (RELAP5/MOD1) because of the good agreement between the measured and calculated liquid levels. However, in the calculation of Sweden-Finland, temporary dryout occurred at the upper part of the core 20 s after the break initiation, whereas no dryout was observed in the experiment during this time period (see Figs. 4.88 and 4.89).

The trend of dryout and rewet before LPF agreed with that of the experiment. The timing of uncovering the whole core agreed with the uncovering time in the experiment and the trend of temperature turnaround by ECC water was calculated thereafter. The increasing temperature rate after dryout was smaller than the experiment probably due to the higher heat transfer coefficient calculated by the heat transfer correlation for the two-phase laminar natural convection, mode 25 in RELAP5/MOD1.

The applicability of this correlation in this region should be studied.

The calculation of Sweden-Finland stopped during the temperature rise and quenching was not calculated (see Fig. 4.91).
In the calculation of JAERI-R, the bottom part of the core quenched due to accumulation of ECC water from LPCS started at 318 s, and the temperature at the higher part of the core turned around due to falling water from LPCS and upward steam flow in the core (see Figs. 4.81 through 4.87).

(4) RELAP/MOD6 Analyses by Netherlands and Switzerland

Netherlands results calculated with RELAP4/MOD6 showed no dryout within the limited calculation time of 166 s after break being different from the experimental trend which showed dryout before LPF in the upper part of the core (see Fig. 4.88). Therefore, the calculated liquid level in the core is expected to be in poor agreement with the measured level. The higher system pressure of Netherlands results or the higher saturation temperature could influence the cladding temperature.

The trend of the heater rod surface temperature of Switzerland was similar to that of USA in the following respects: (1) early dryout and rewet, which were not observed in the experiment, (2) earlier dryout before LPF than the experiment, and (3) slower liquid level decrease after LPF without dryout at the lower part of the core (see Fig. 4.111). The heater rod surface temperature was calculated only for the average power channel until 328 s after the break initiation. No quenching of the heater rod was calculated.

(5) RELAP4/MOD6/U4/J3 Analyses by JINS and JAERI-A

The dryout and quench front trend of JINS and JAERI-A results calculated by RELAP4/MOD6/U4/J3 agreed well with that of the experiment (see Fig. 4.111). The temperature increase rate of the cladding was larger than that of the experiment after dryout following LPF possibly due to a lower heat transfer rate after dryout calculated by the RELAP4/MOD5 heat transfer package used in the analysis.

JINS and JAERI-A results showed the top-down quench begining immedoately after the initiation of LPCS (see Figs. 4.95 through 4.101). The top-down quench was based on the spray heat transfer model in RELAP4/MOD6/U4/J3. LPCS water penetrating into the core was limited by the Wallis flooding correlation and flowed down along the clad surface. The top-down quench velocity was calculated with the Duffey-Porthouse correlation. The heat transfer coefficient in the rewetted region clad

surface was 5678 W/m^2K (1000 $Btu/h.ft^2°F$).

The cladding surface did not quench by bottom-up reflooding after LPCI initiation because of the small heat transfer coefficient of 142 W/m^2K (25 $Btu/h.ft^2°F$) used in Relap4/MOD6/U4/J3 based on the BWR-FLECHT experiment. The cladding temperature began to decrease slowly after reflooding when the temperature was still high and it began to rise again if the heater rod surface had been quenched by the top-down quench after LPCS initiation.

(6) THYDE-B1 Analysis by JAERI-C

The trend of the heater rod surface temperature calculated by JAERI-C (THYDE-B1) agreed well with the trend of the experimental results due to satisfactory calculation of the liquid level in the core. However, the steam in the core cannot be superheated, since the region inside the shroud was represented by one node. The heater rod surface temperature was lower than the experimental results and the increasing rate of the heater rod surface temperature was also smaller than the measured results. Reflooding occurred earlier than the experimental results due to earlier actuation of LPCI. The direct cooling effect by LPCS water sprayed on the top of core cannot be taken into account by THYDE-B1. The spray water from LPCS contributed only to raise the liquid level from the bottom of core.

(7) Peak Clodding Temperature (PCT)

The heater rod surface temperature at the midplane of the peak power rod with a local peaking factor of 1.1 in the peak power channel A, corresponding to PCT, was calculated by USA, JINS and JAERI-R (see Fig. 4.84).

The USA results of the cladding temperature increase rate after dryout agreed well with that of the experiment. However, the PCT of the USA results was 664 K, calculated at Position 2, 370 s after break (see Fig. 4.82). The PCT occured at the midplane of core (Position 4) in the experiment, whereas the calculated PCT occured at top part of the core (Position 2). The calculated peak temperature at the midplane of the core after reflooding by LPCI was 609 K, much lower than the measured PCT of 839 K which occured at 410 s after break during the reflood period after LPCI initiation. Two peaks other than the PCT were calculated in the USA analysis. The first peak was caused by the core uncovering due to a decrease in inlet flow during the early period of blowdown. The second peak was due to the core uncovering before LPF,

Theforst and the second peaks were 824 K (Position 3, 25 s) and 807 K (Position 4, 171 s), respectively, which were closer to the measured PCI of 839 K than the calculated PCT of 664 K.

The PCT calculated by JINS with RELAP4/MOD6/U4/J3 was higher than the measured PCT. JINS selected the RELAP4/MOD5 heat transfer correlations. This selection resulted in a higher rate of cladding temperature rise than the experimental result before LPCS initiation at 308 s. After LPCS initiation, the cladding temperature rise was accelerated because a lower heat transfer coefficient of 17 W/m^2K (3.0 $Btu/h.ft^{2\circ}F$) was used for the dry rods before being wetted by LPCS based on the GE-FLECHT experiment. The PCT calculated by JINS was 964 K being 125 K higher than the measured PCT of 839 K. The PCT was calculated below the midplane of core (Position 5) immediately after wetting by LPCS.

The PCT in the calculatation of JAERI-R, 665 K, occurred at Position 4 of the peak power rod 320 s after break. The calculated PCT was considerably lower than the measured one.

Table 4.1 Comparison of Major Events

Country / Identifier	Computer Code	L2 Signal [s]	Closure of MSIV [s]	L1 Signal [s]	Actuation of SRV [s] ~ [s]	JP Suction Nozzle Uncovery [s]	MRP Suction Nozzle Uncovery [s]	Actuation of ADS [s]	Lower Plenum Flashing [s]	Dryout at the Top of the Core [s]	Whole Core Uncovery [s]
Experiment	——	19	24	38	66 ~ 126	99	156	158	159	198	275
USA U	TRAC-BD1	——	24	44	48 - 85	92	(108)	164	168	——	——
Switzerland S	RELAP4/ MOD6	?	9	?	?	34	135	?	(158)	——	——
Sweden-Finland F	RELAP5/ MOD1(014)	?	23	?	73 ~ 137	——	——	158	?	——	——
Netherlands N	RELAP4/ MOD6	2	21	?	?	?	?	139	149	——	——
JINS J	RELAP4/ MOD6/U4/J3	16.2	24	41.5	76 ~ 138	107	325	161.5	171	192	312
JAERI-C C	THYDE-B1	22	25	24	72 ~ 132 152 ~ 158	125	224	158	(158)	——	264
JAERI-A A	RELAP4/ MOD6/U4/J3	19	19	38	?	93	156	158	175	227	366
JAERI-R R	RELAP5/ MOD1(001)	?	24	?	71 ~ 158	80	162	158	(162)	192	265

* SRV : Safety Relief Valve,

JP : Jet Pump,

MRP : Main Recirculation Pump.

Table 4.1 Comparison of Major Events (contd.)

Identifier	Actuation of LPCS		Actuation of LPCI		Initiation of Core Reflooding	Completion of Core Reflooding	Quenching of All Heater Rods	PCT				
								Temp.	Time	Position		
	[s]	[MPa]	[s]	[MPa]	[s]	[s]	[s]	[K]	[s]	Channel	L.P.F.	Position
Exp.	318	2.38	406	1.81	399	440	444	839	410	A	1.1 (Corner)	4
U	328	2.34	368	1.82	—	420	414	824	25	High Power	1.1	3
S	—	—	—	—	—	—	—	—	—	—	—	—
F	265	2.43	—	—	—	—	—	—	—	—	—	—
N	—	—	—	—	—	—	—	—	—	—	—	—
J	308	2.37	406	1.80	408	(433)	—	964	430	High Power	1.1	5
C	310	2.16	330	1.57	350	391	384	810	337	High Power	1.0	4
A	367	2.4	458	1.8	458	—	—	—	—	—	—	—
R	318	1.59	—	—	328	—	—	665	320	High Power	1.1	4

* PCT : Peak cladding Temperature, L.P.F. : Local Peaking Factor

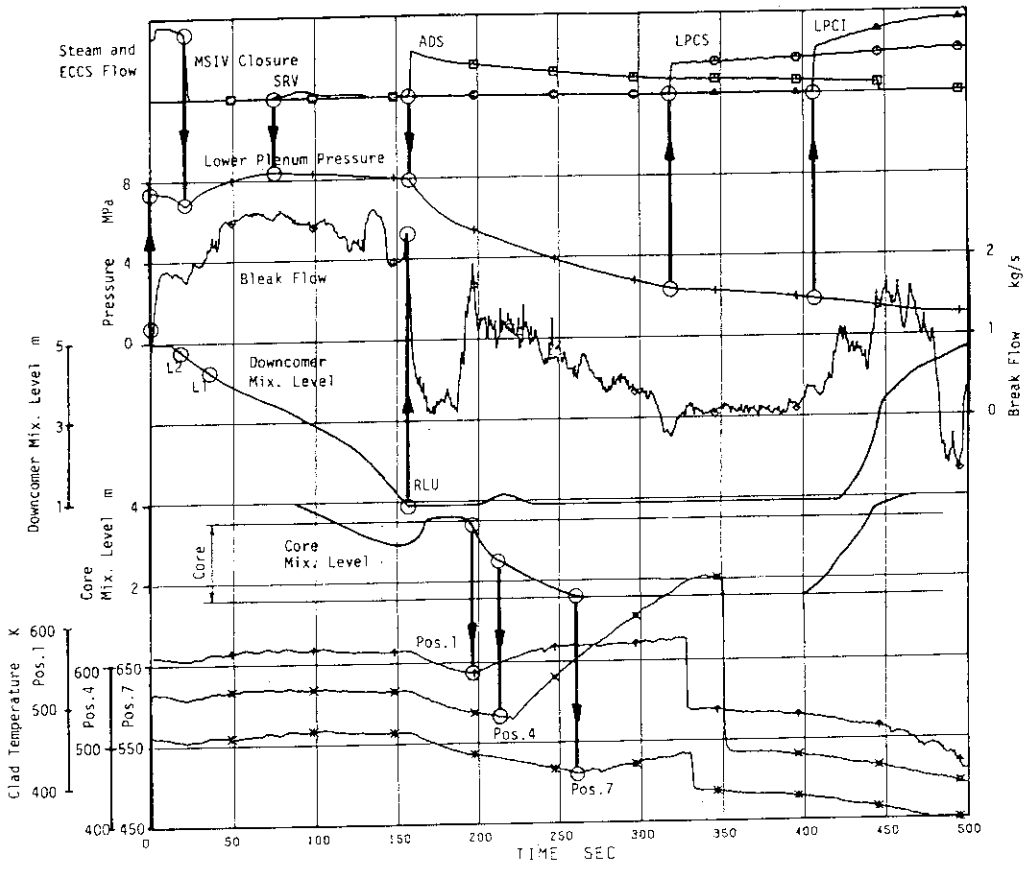

Fig. 4.1 Scenario in Experiment

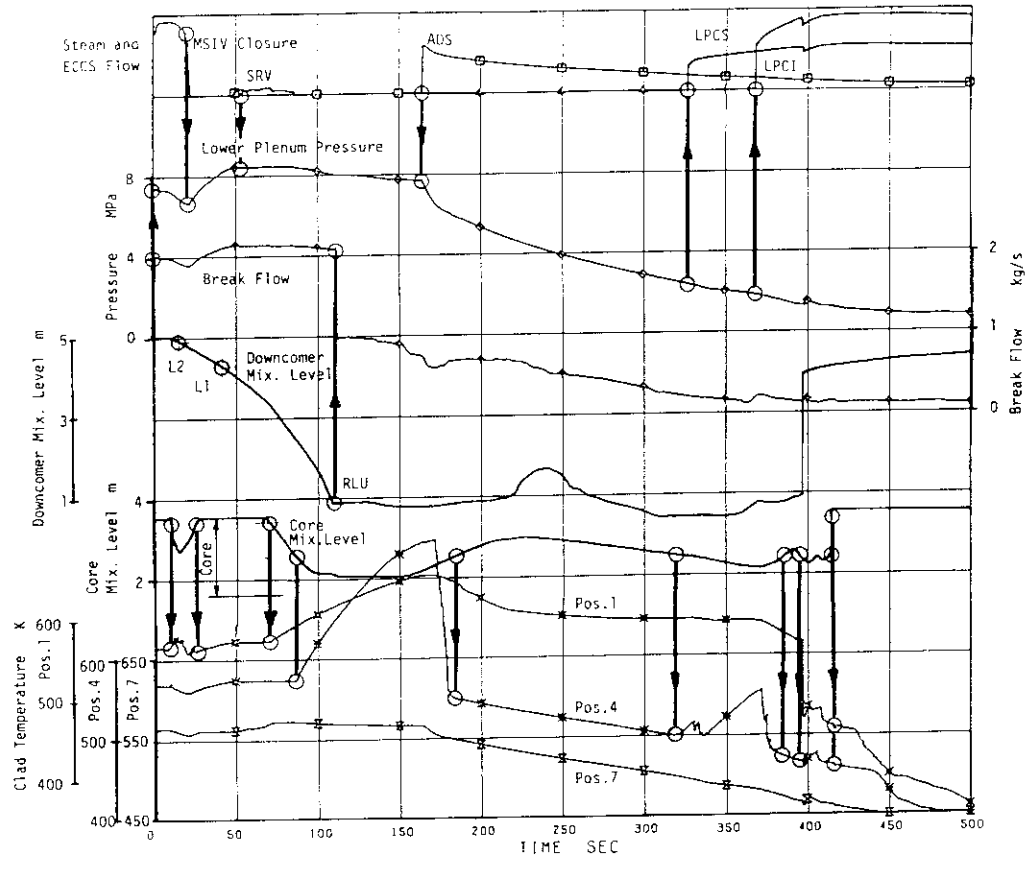

Fig.4.2 Scenario in USA Calculation

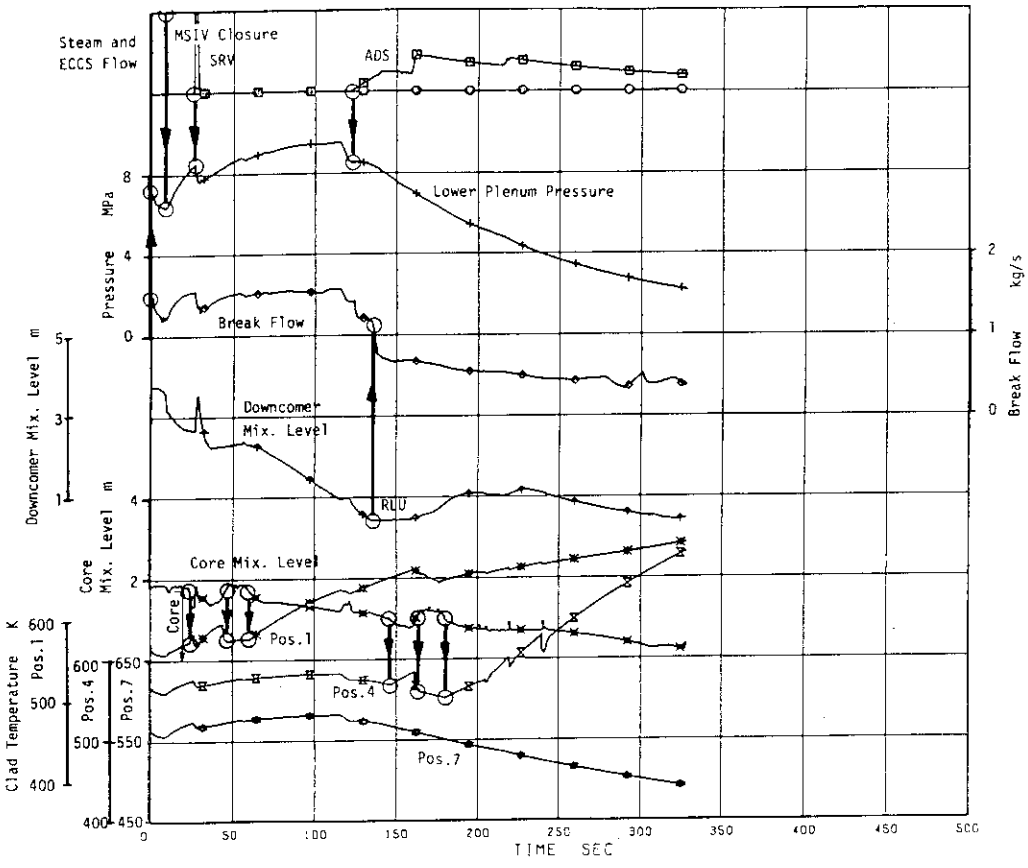

Fig.4.3 Scenario in Switzerland Calculation

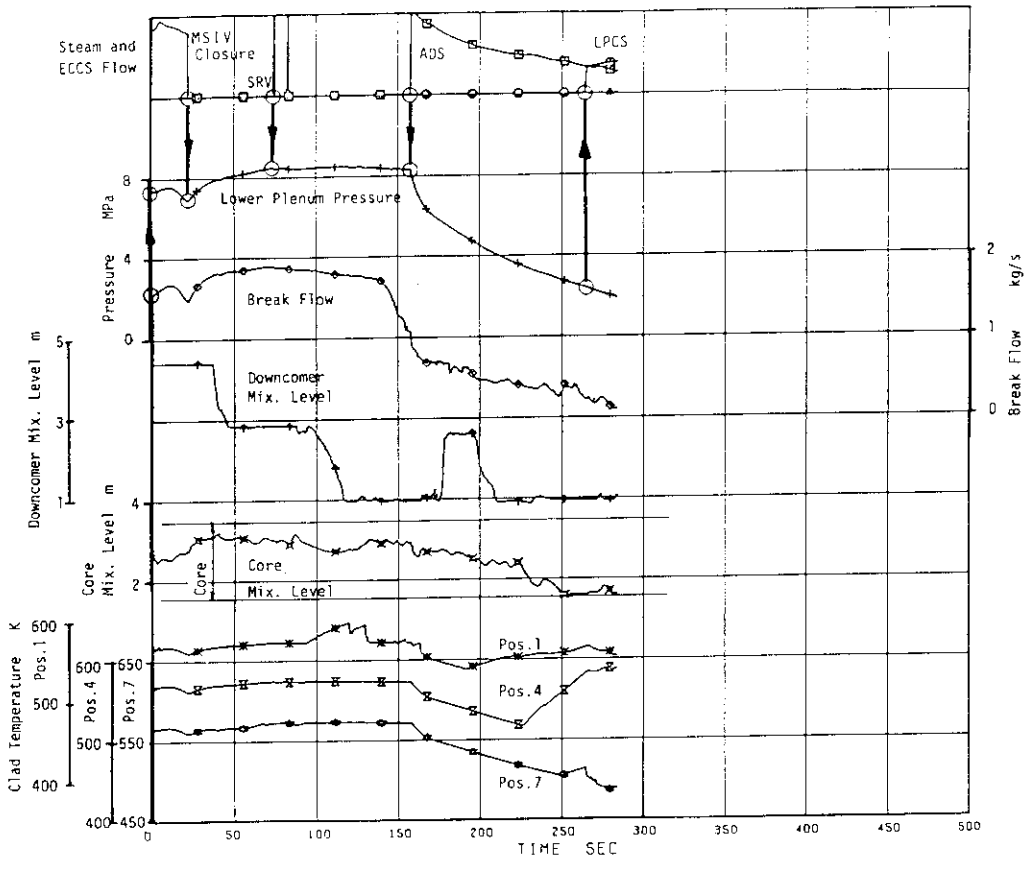

Fig.4.4 Scenario in Sweden-Finland Calculation

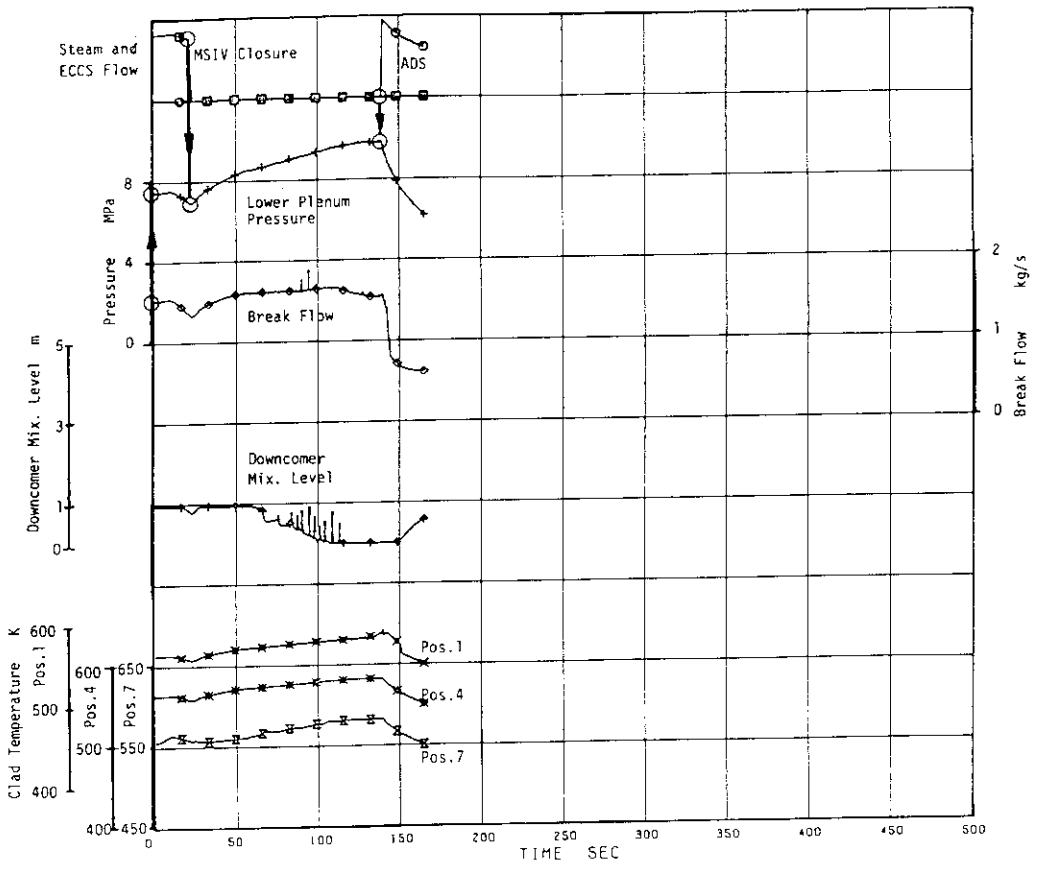

Fig.4.5 Scenario in Netherlands Calculation

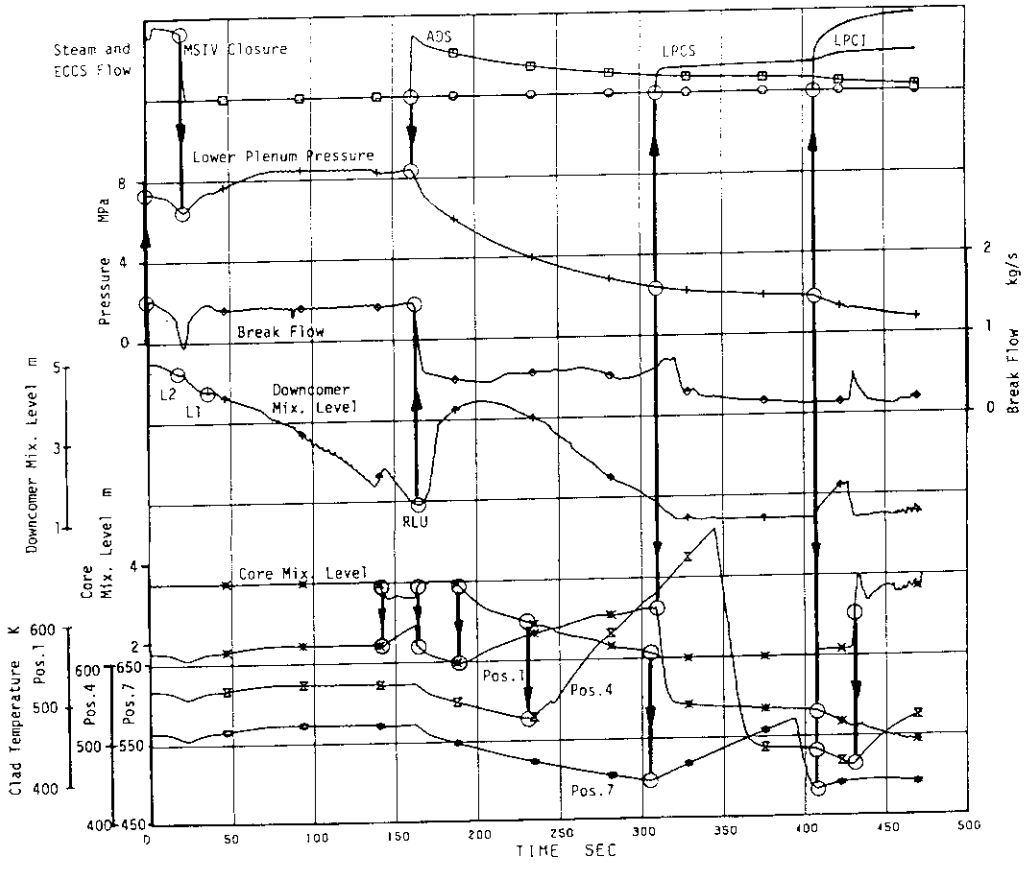

Fig.4.6 Scenario in JINS Calculation

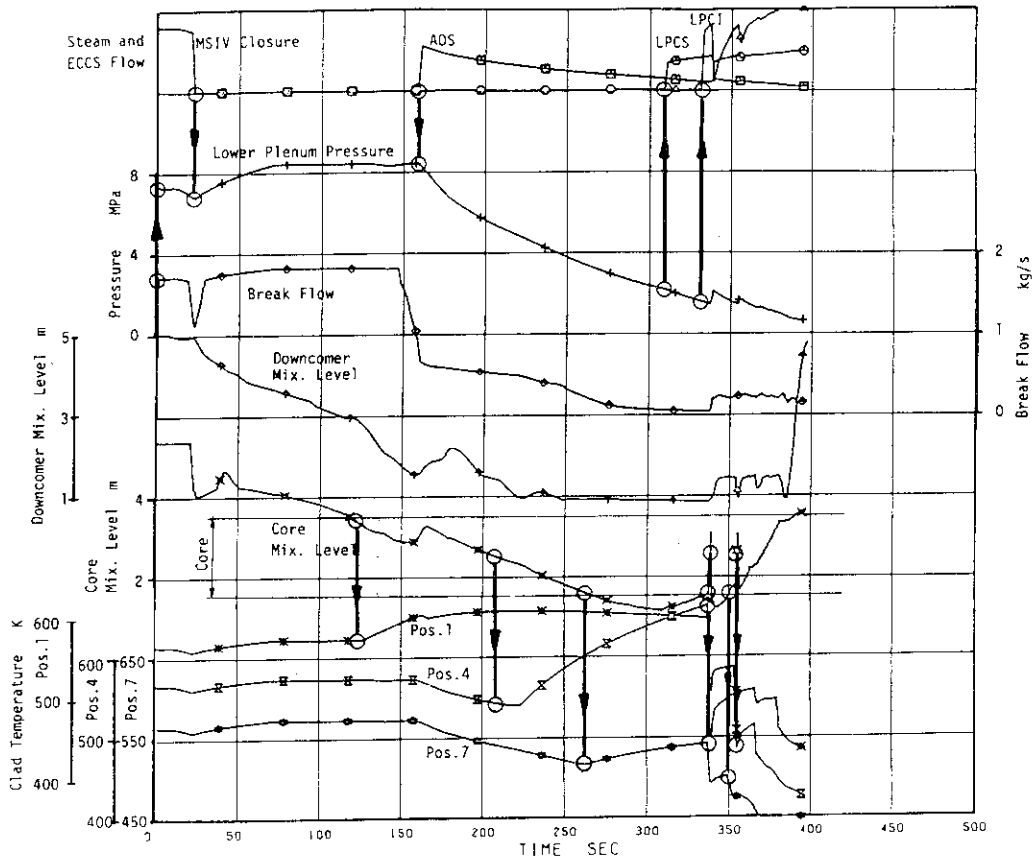

Fig.4.7 Scenario in JAERI-C Calculation

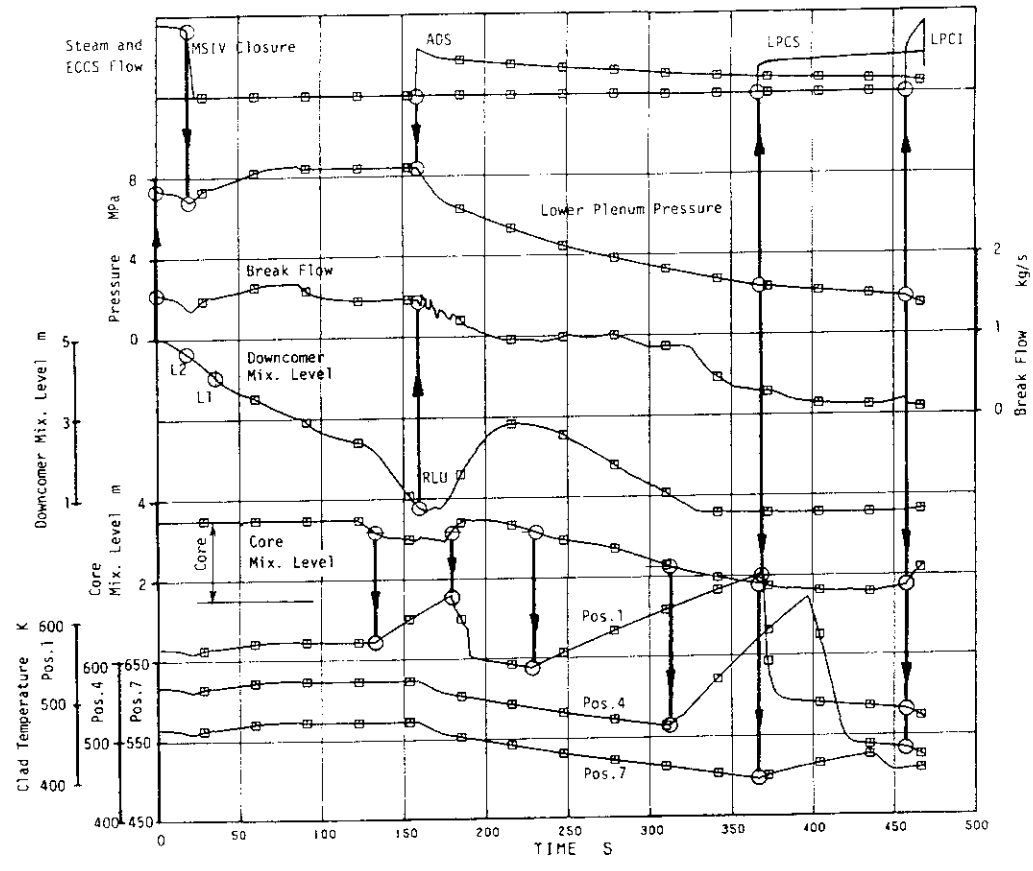

Fig.4.8 Scenario in JAERI-A Calculation

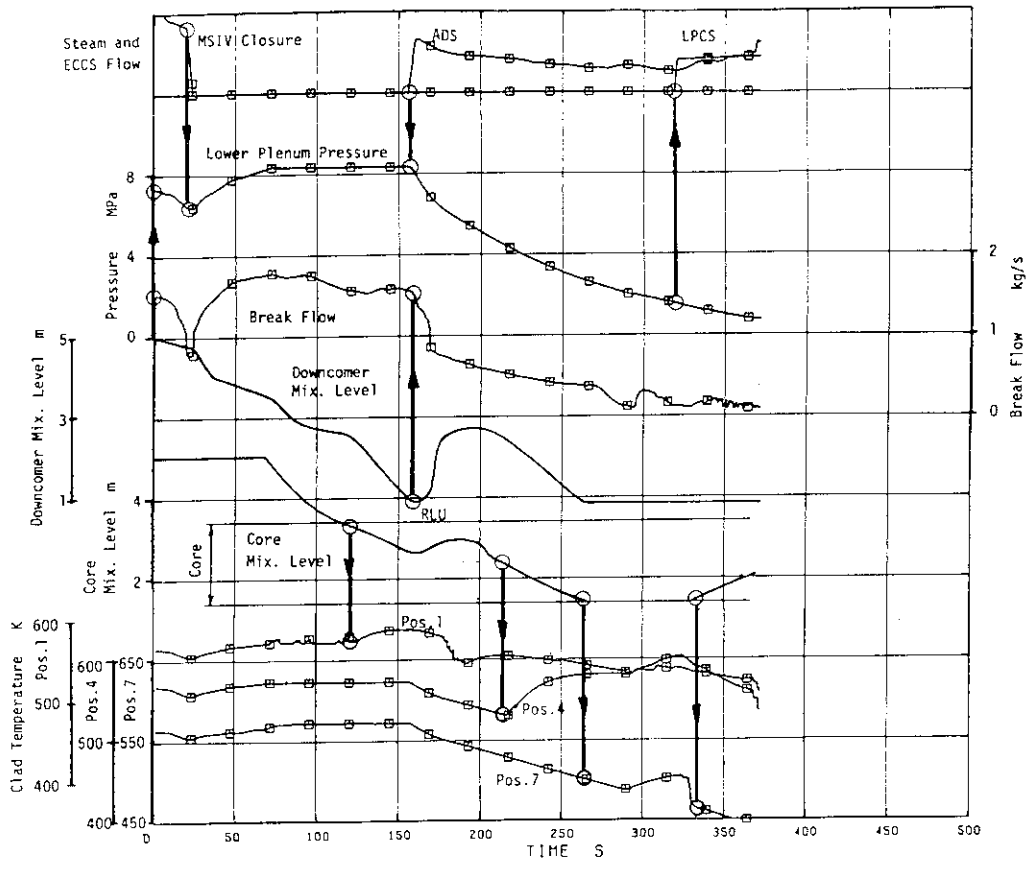

Fig.4.9 Scenario in JAERI-R Calculation

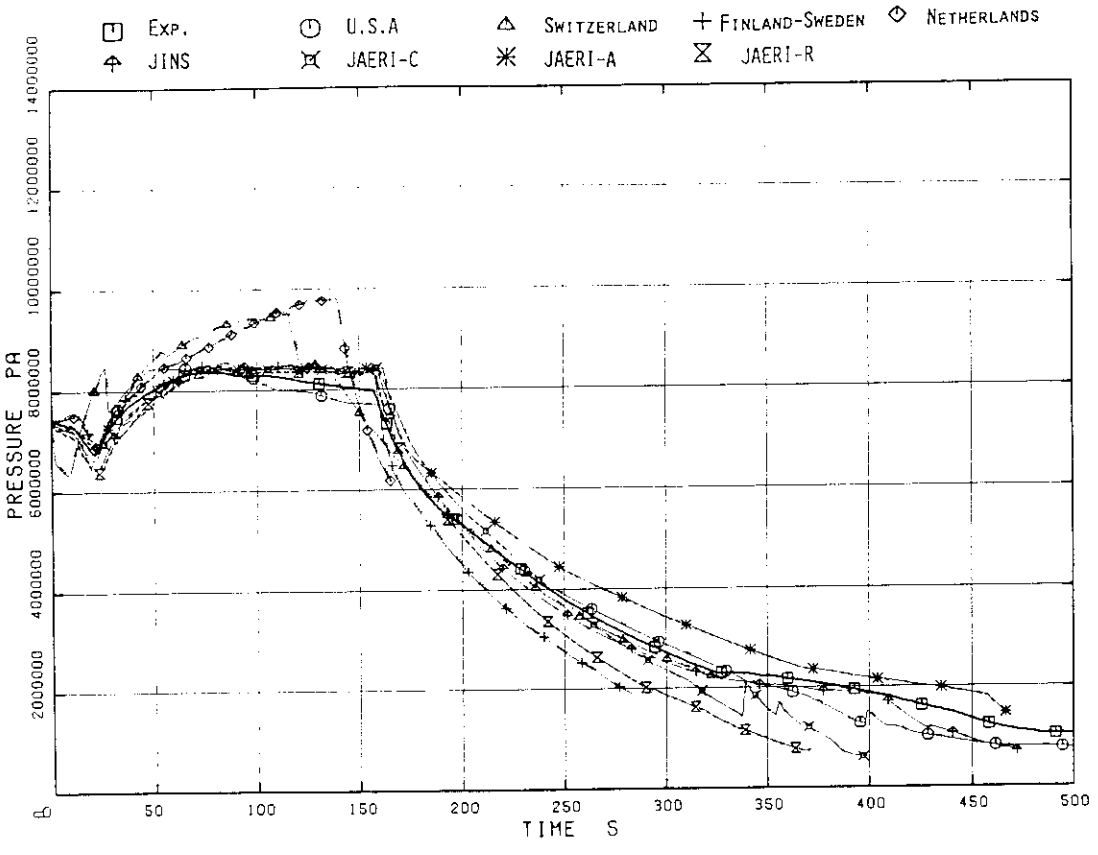

Fig.4.10 Lower Plenum Pressure

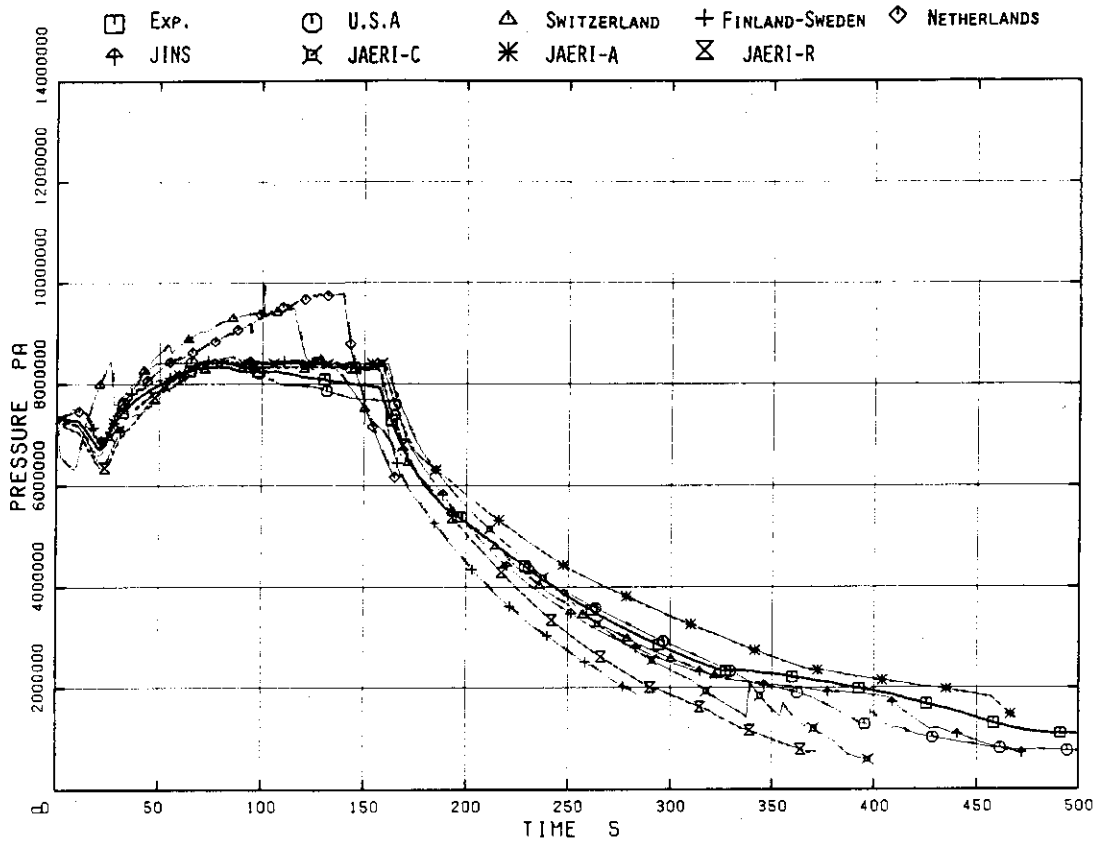

Fig.4.11 Steam Dome Pressure

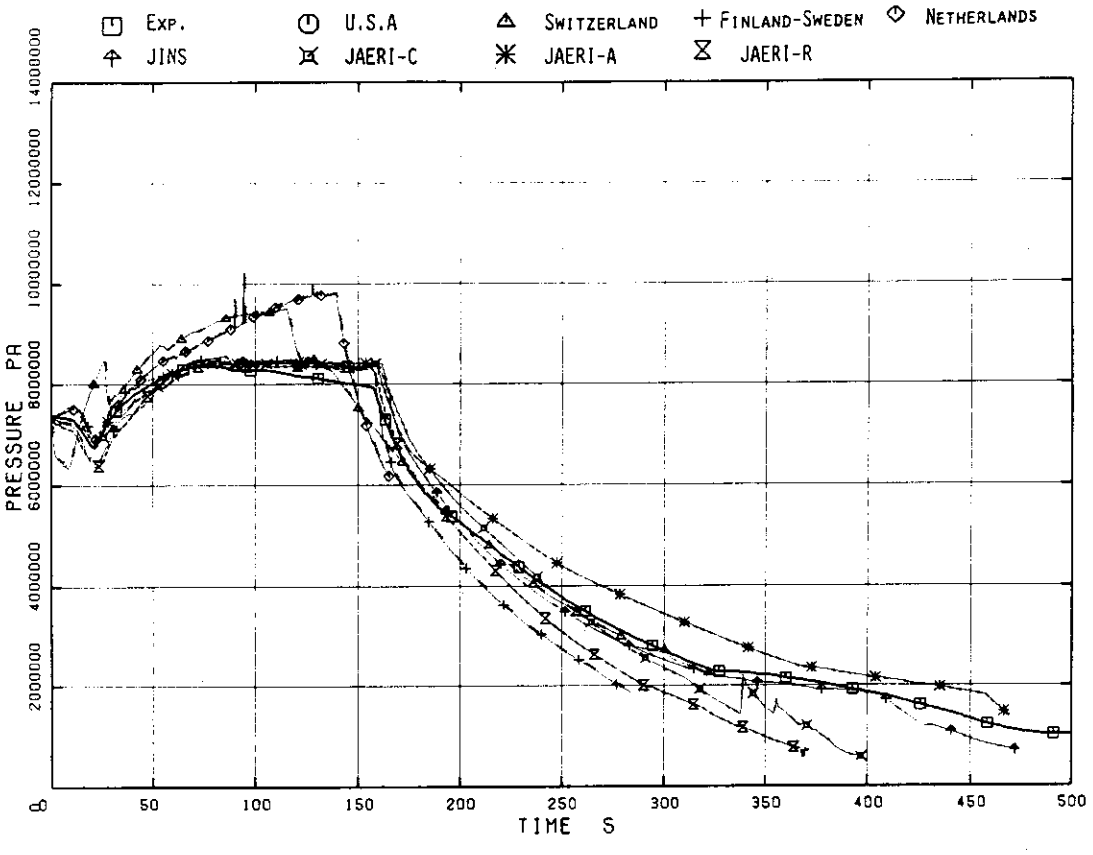

Fig.4.12 Break Upstream Pressure

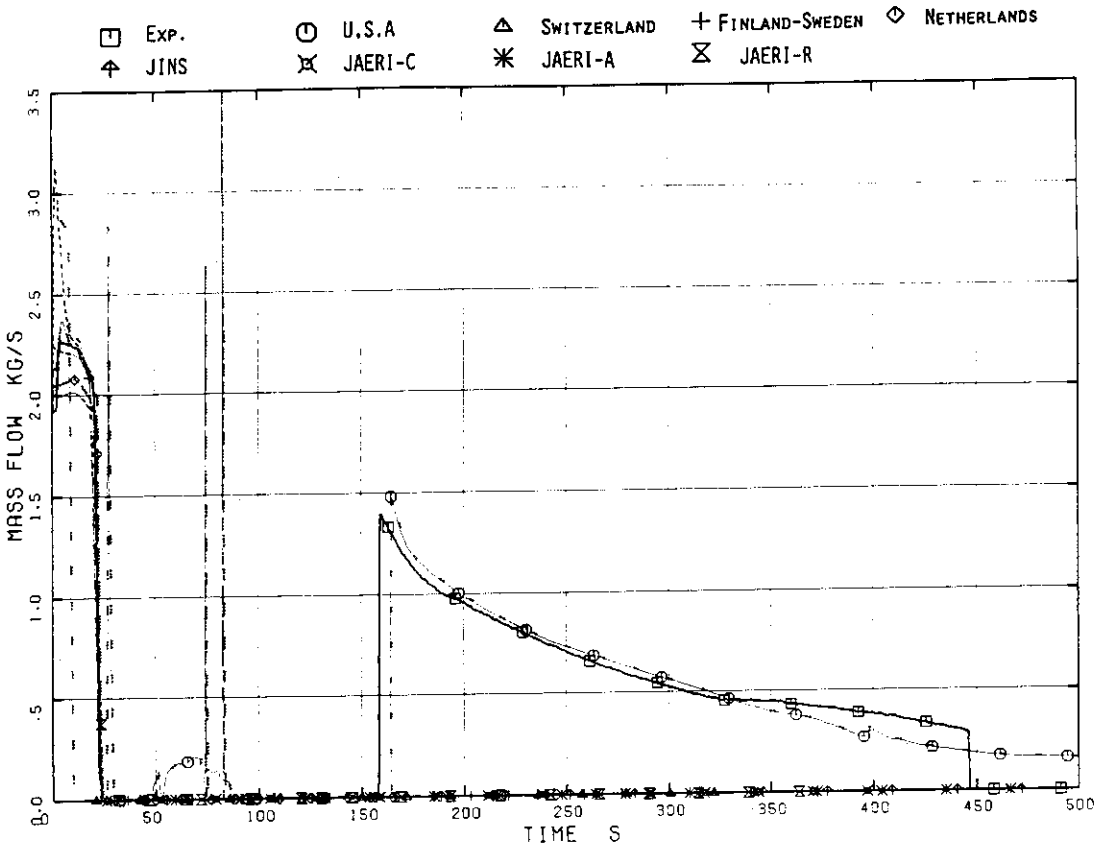

Fig.4.13 Main Steam Line Flow Rate

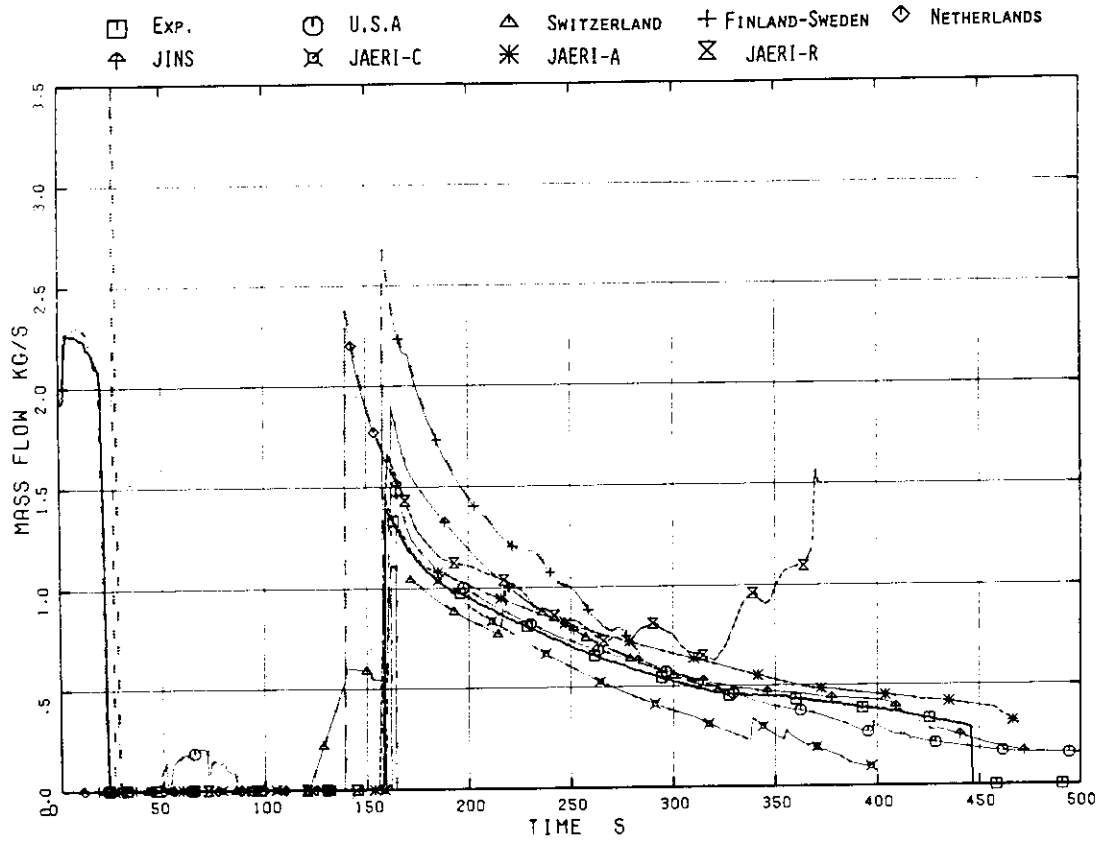

Fig.4.14 ADS Line Flow Rate

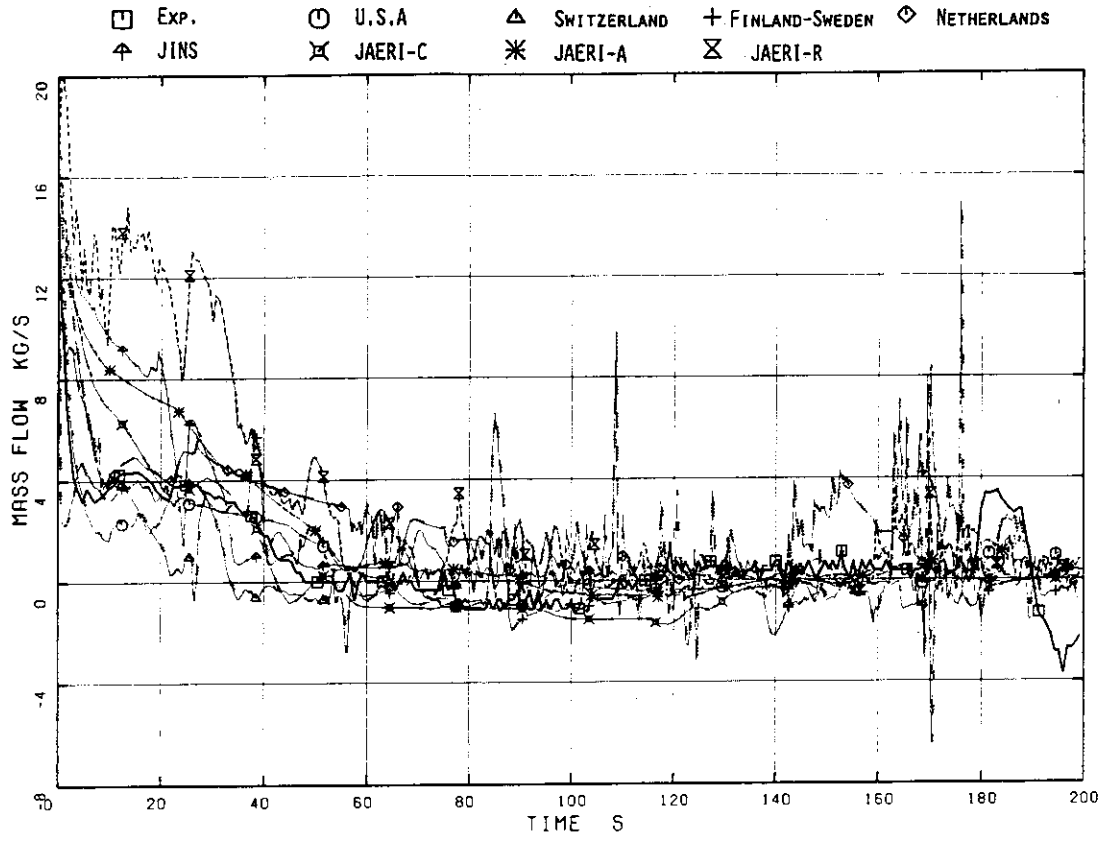

Fig.4.15 Total Core Inlet Flow Rate (0 - 200 s)

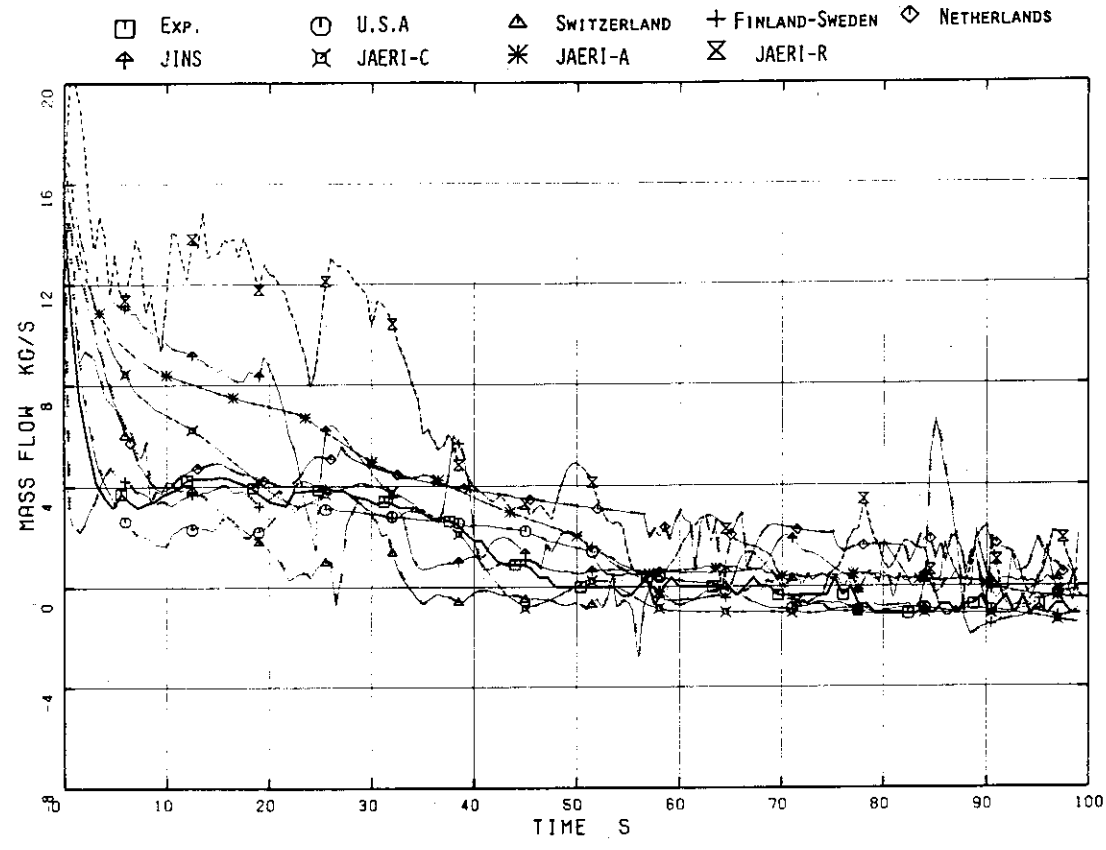

Fig.4.16 Total Core Inlet Flow Rate (0 - 100 s)

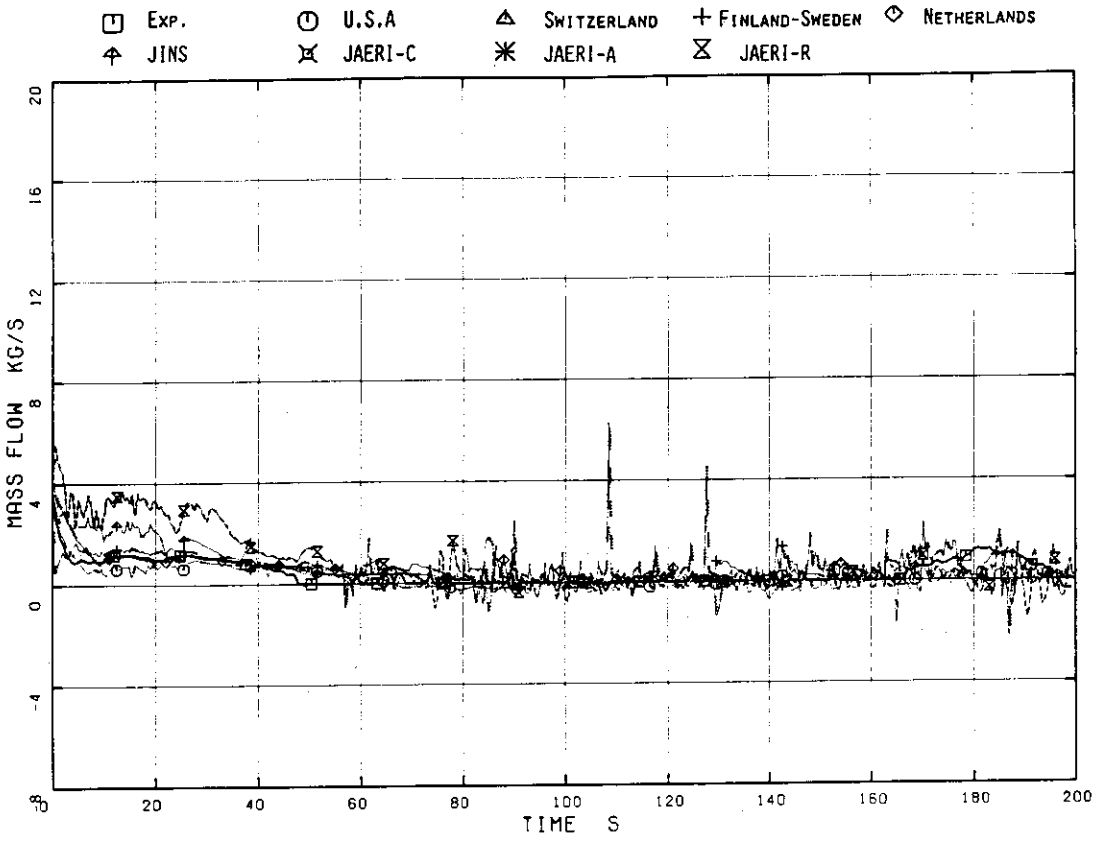

Fig.4.17 High Power Channel Inlet Flow Rate

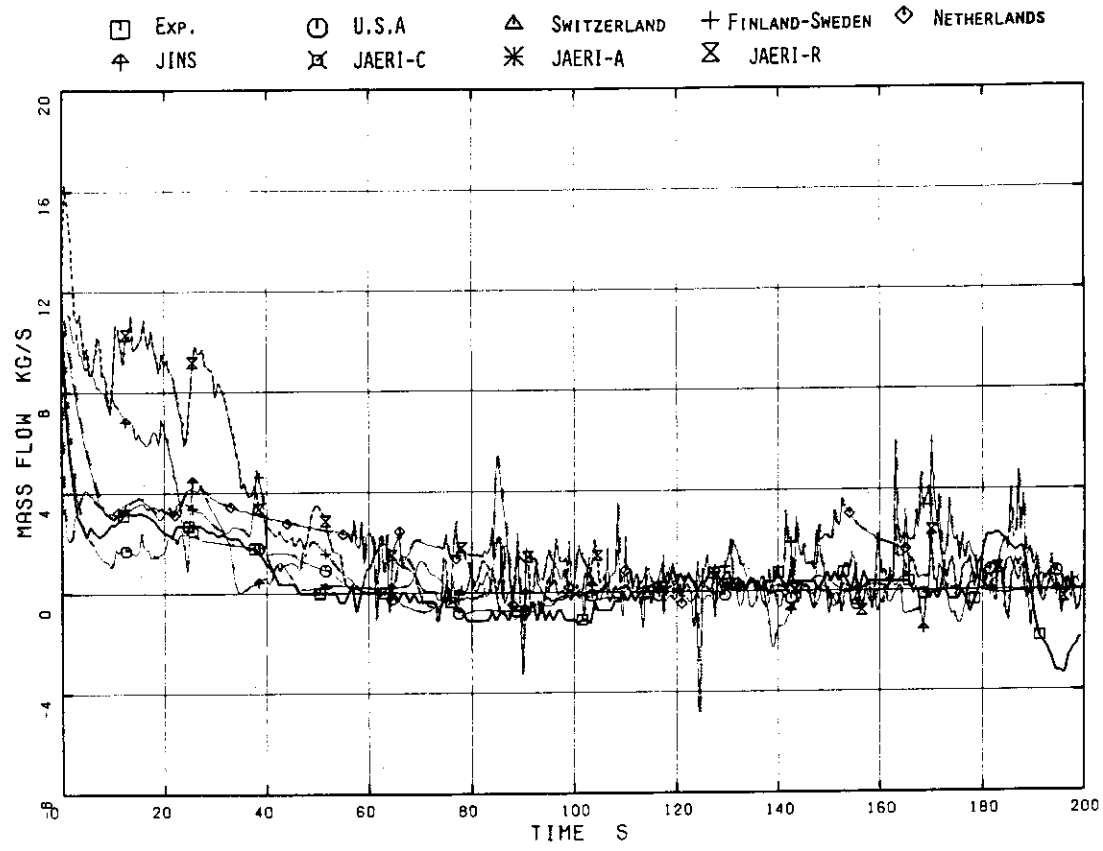

Fig.4.18 Average Power Channel Inlet Flow Rate

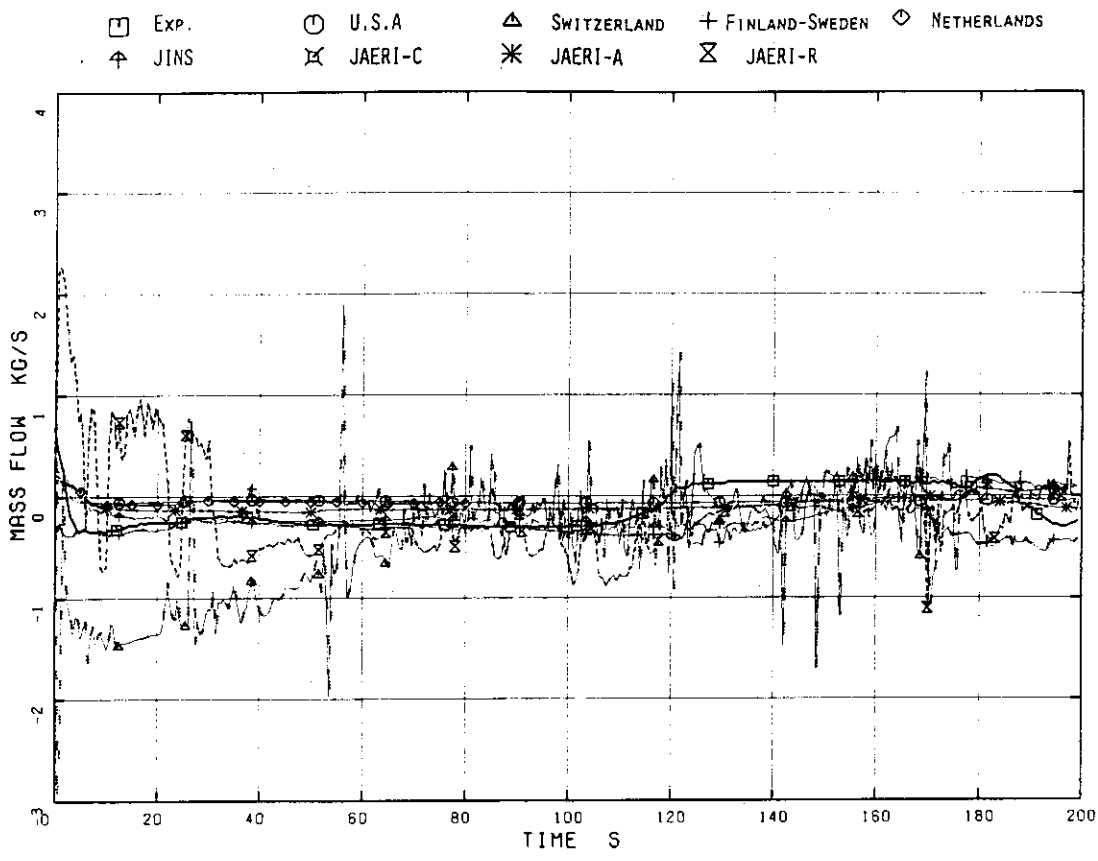

Fig.4.19 Guide Tube Inlet Flow Rate

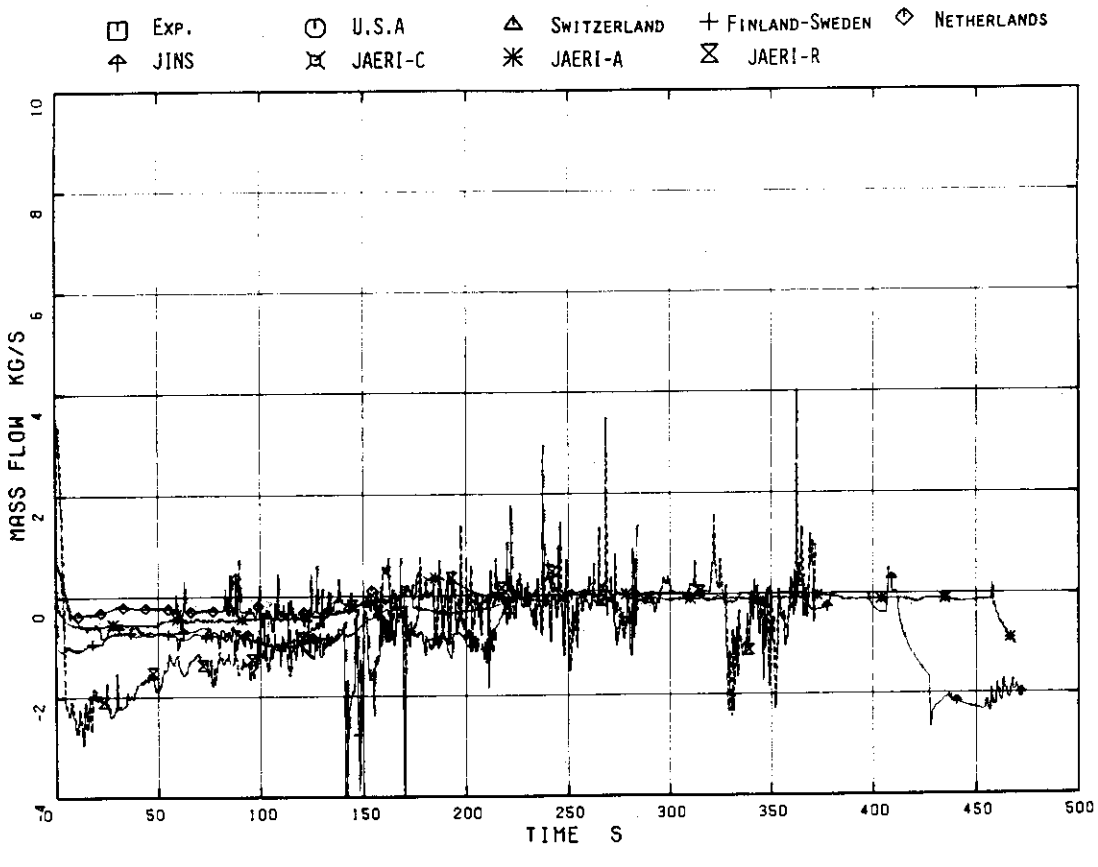

Fig.4.20 Flow Rate from Core to Bypass

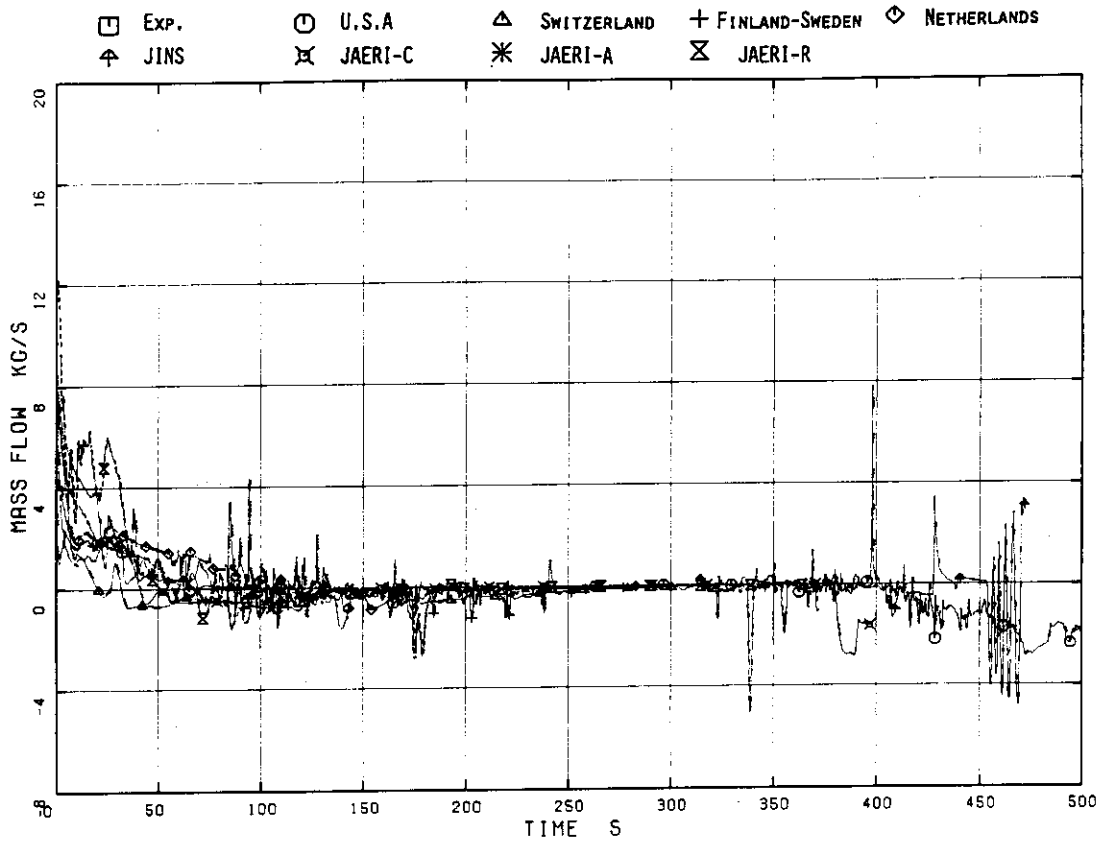

Fig.4.21 Intact Loop Jet Pump Outlet Flow Rate

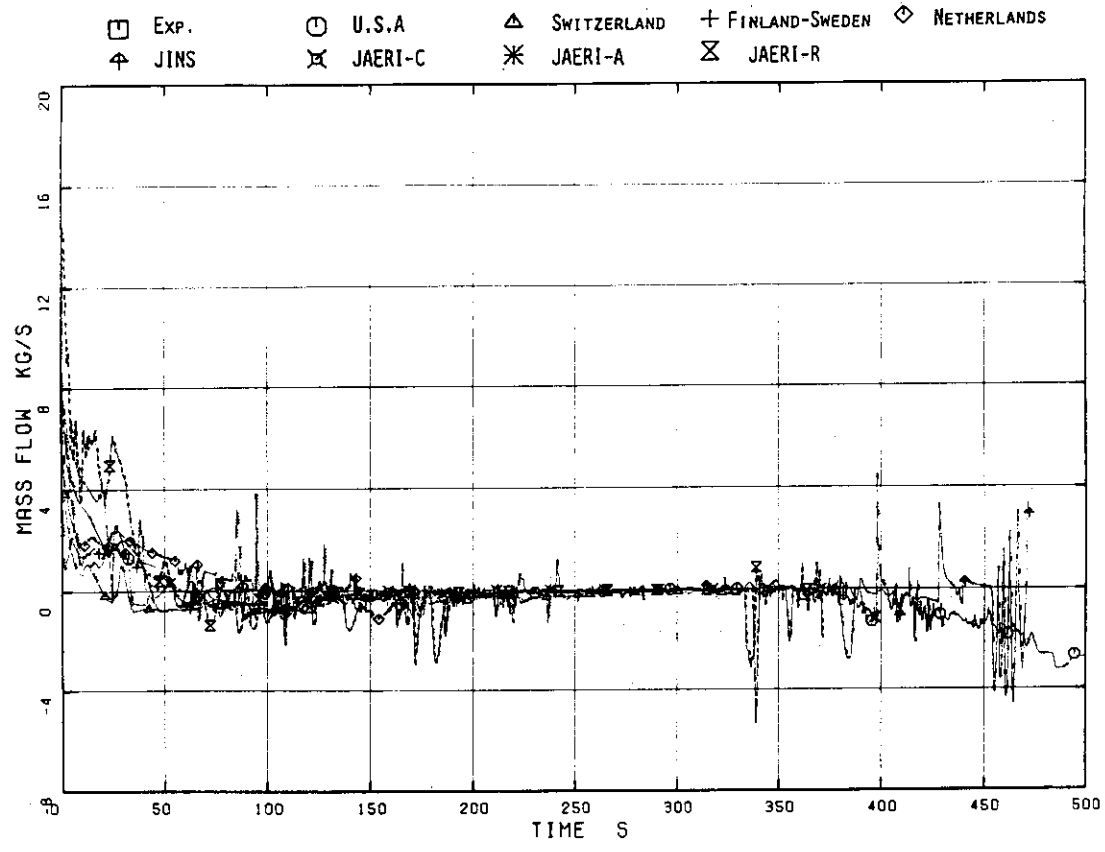

Fig.4.22 Broken Loop Jet Pump Outlet Flow Rate

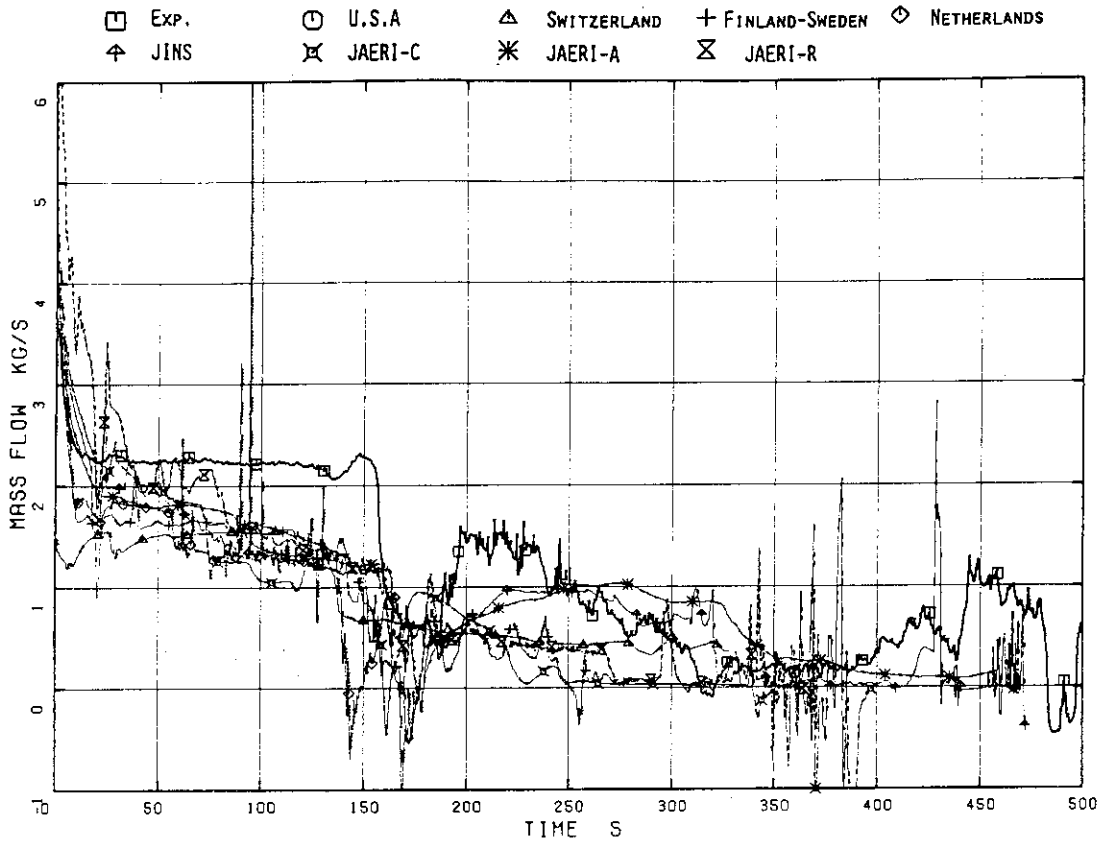

Fig.4.23 Vessel Side Break Flow Rate (Low Range Drag Disk)

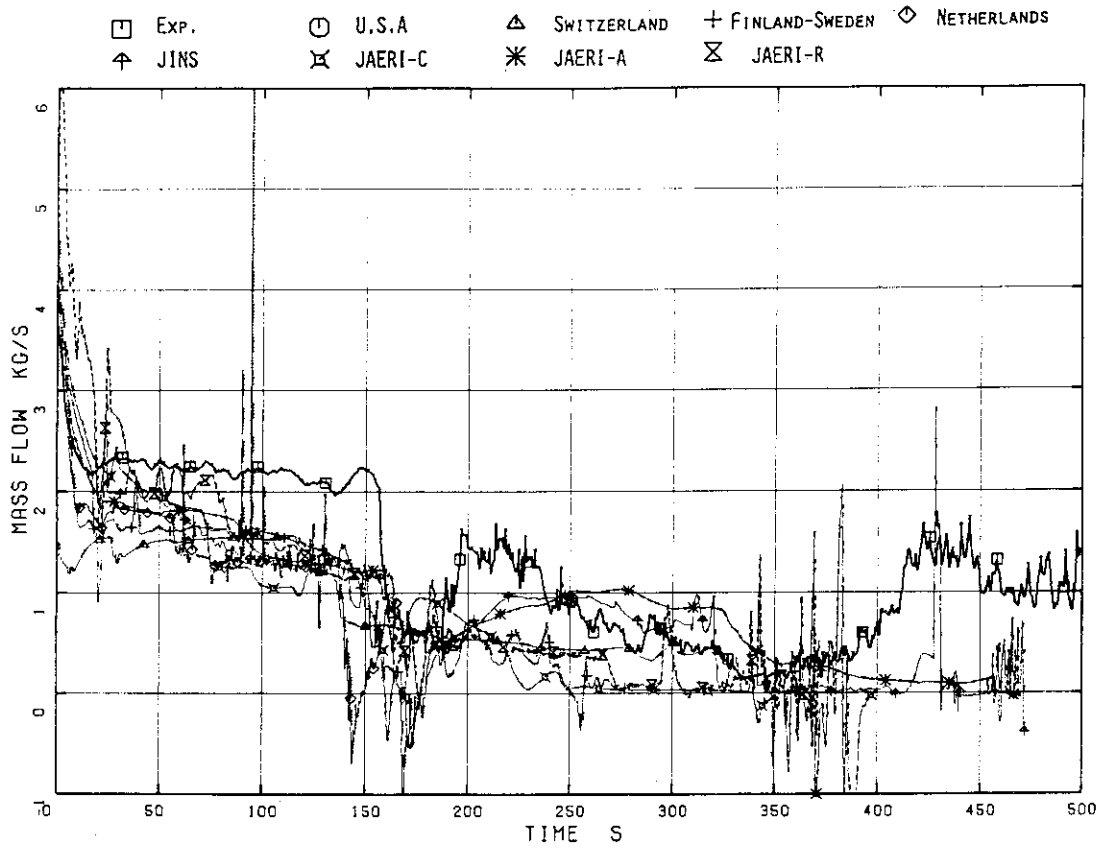

Fig.4.24 Vessel Side Break Flow Rate (High Range Drag Disk)

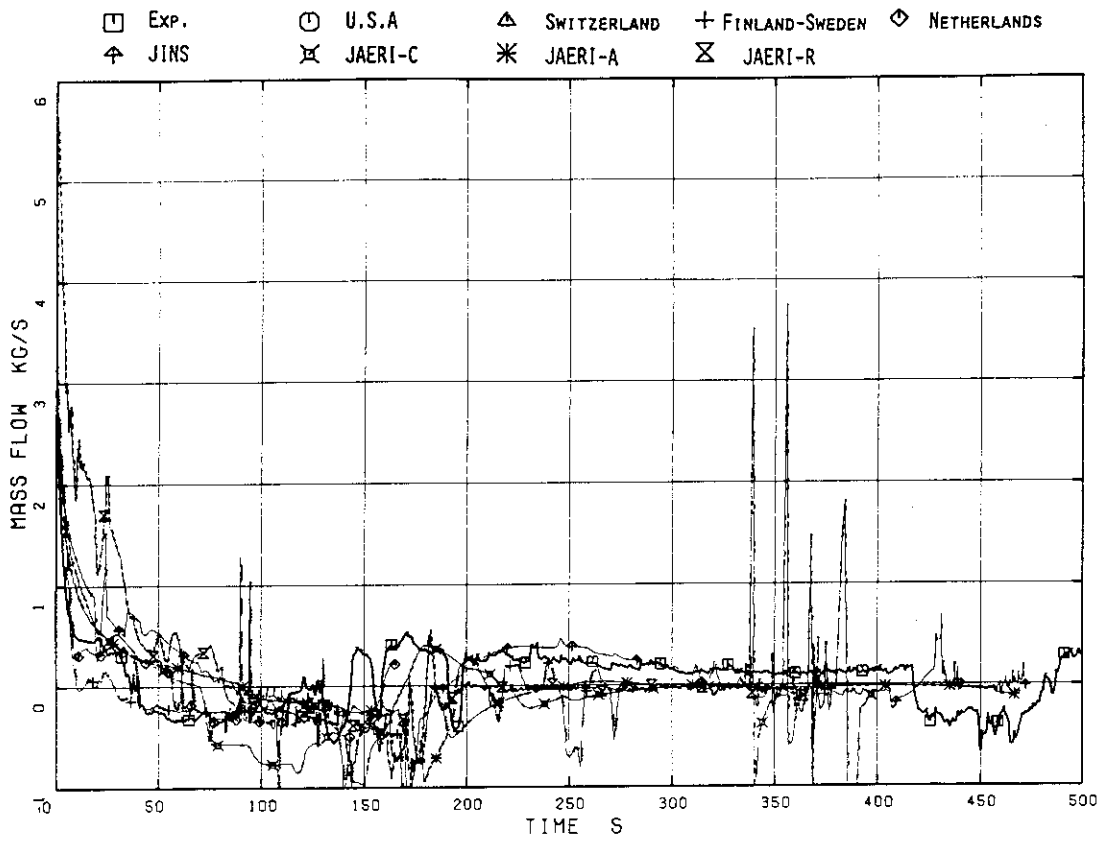

Fig.4.25 Pump Side Break Flow Rate (Low Range Drag Disk)

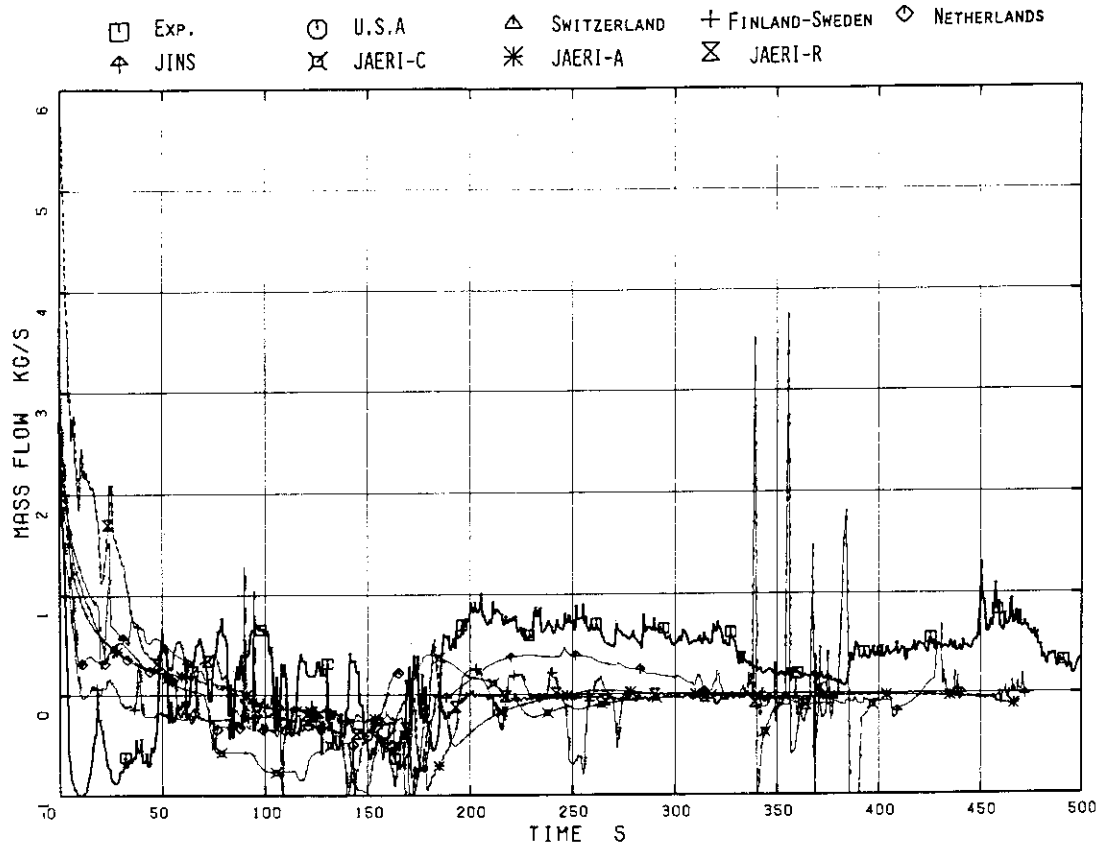

Fig.4.26 Pump Side Break Flow Rate (High Range Drag Disk)

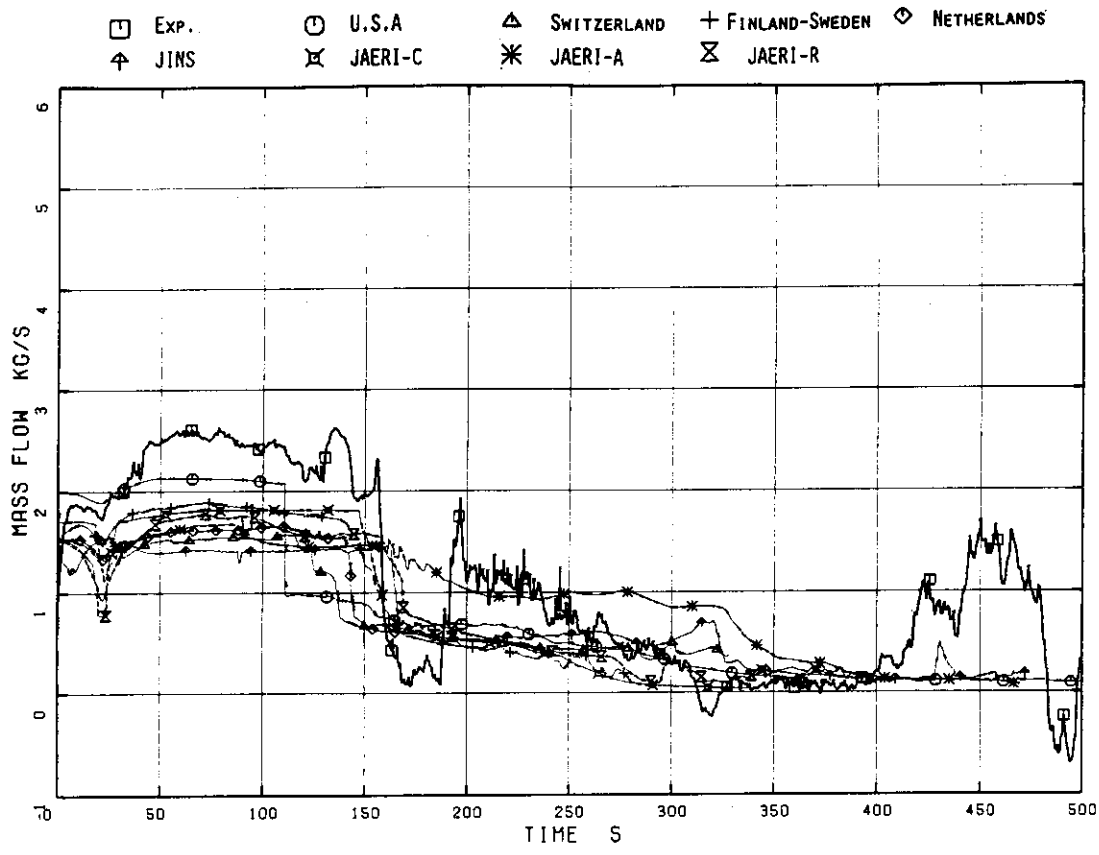

Fig.4.27 Break Flow Rate (Low Range Drag Disk)

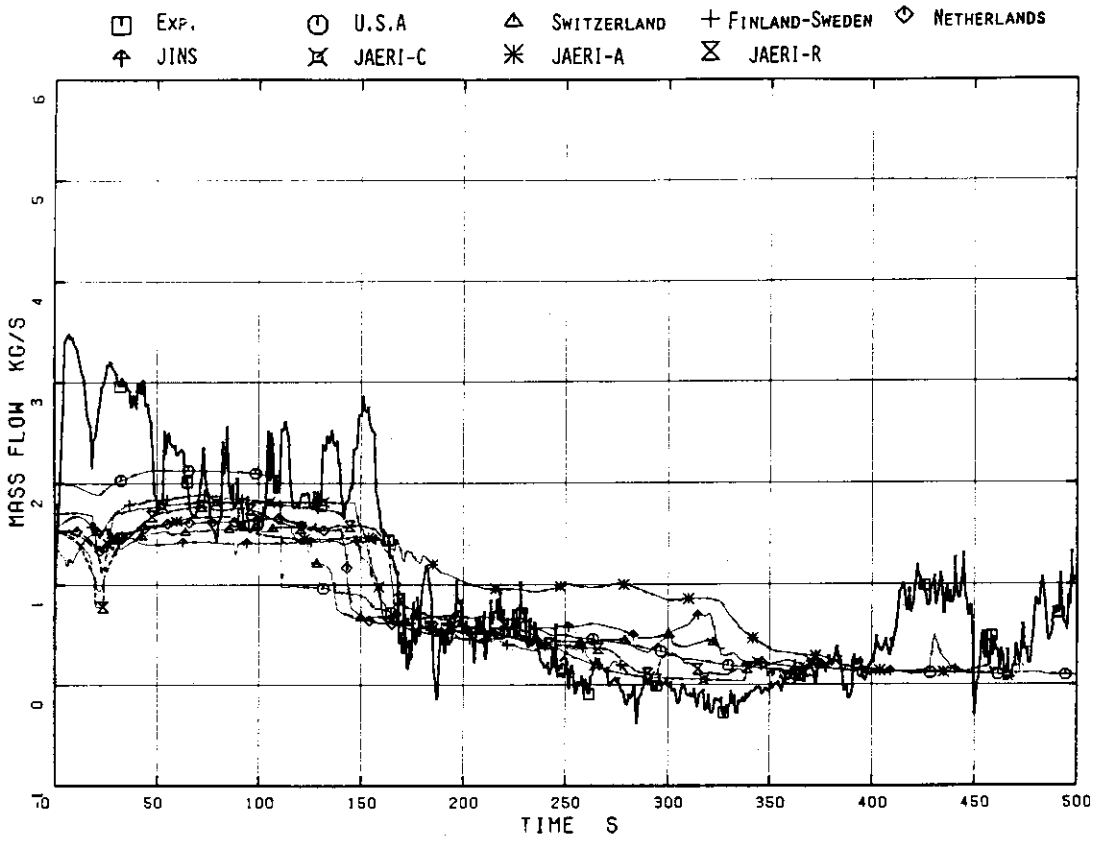

Fig.4.28 Break Flow Rate (High Range Drag Disk)

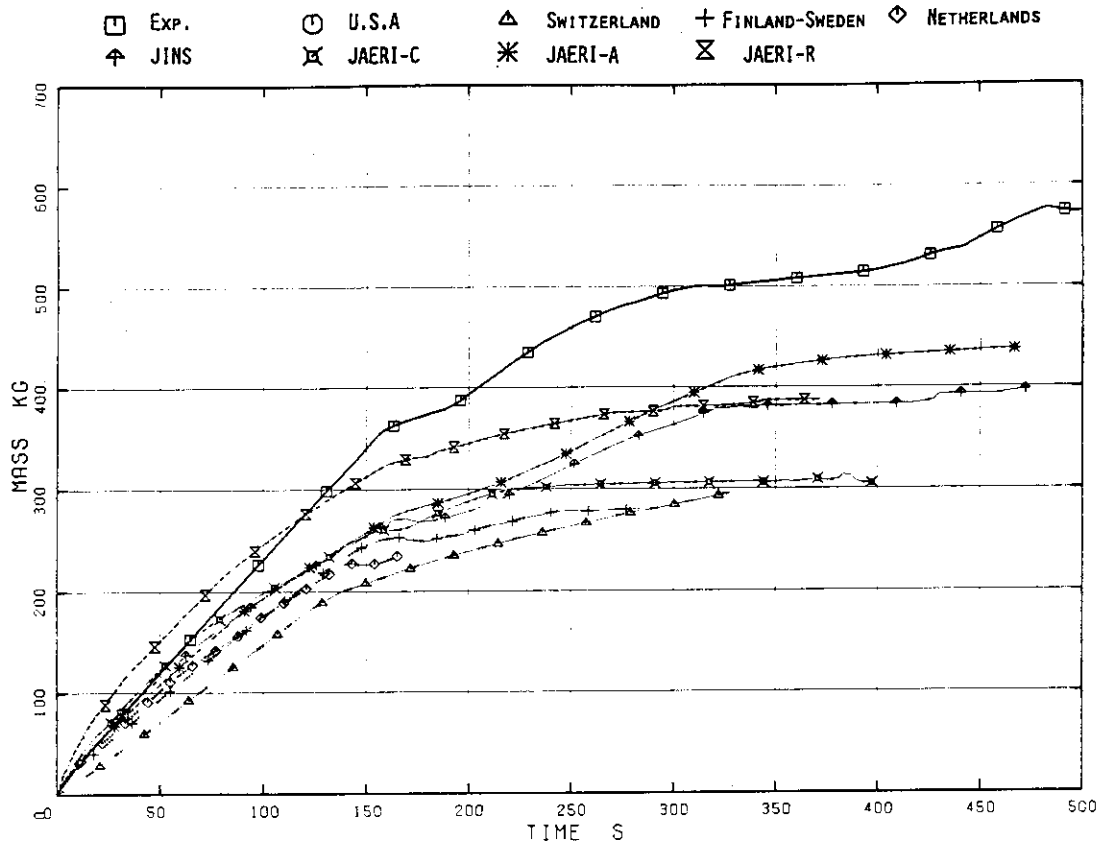

Fig.4.29 Integrated Flow of Vessel Side Break Flow (Low Range Drag Disk)

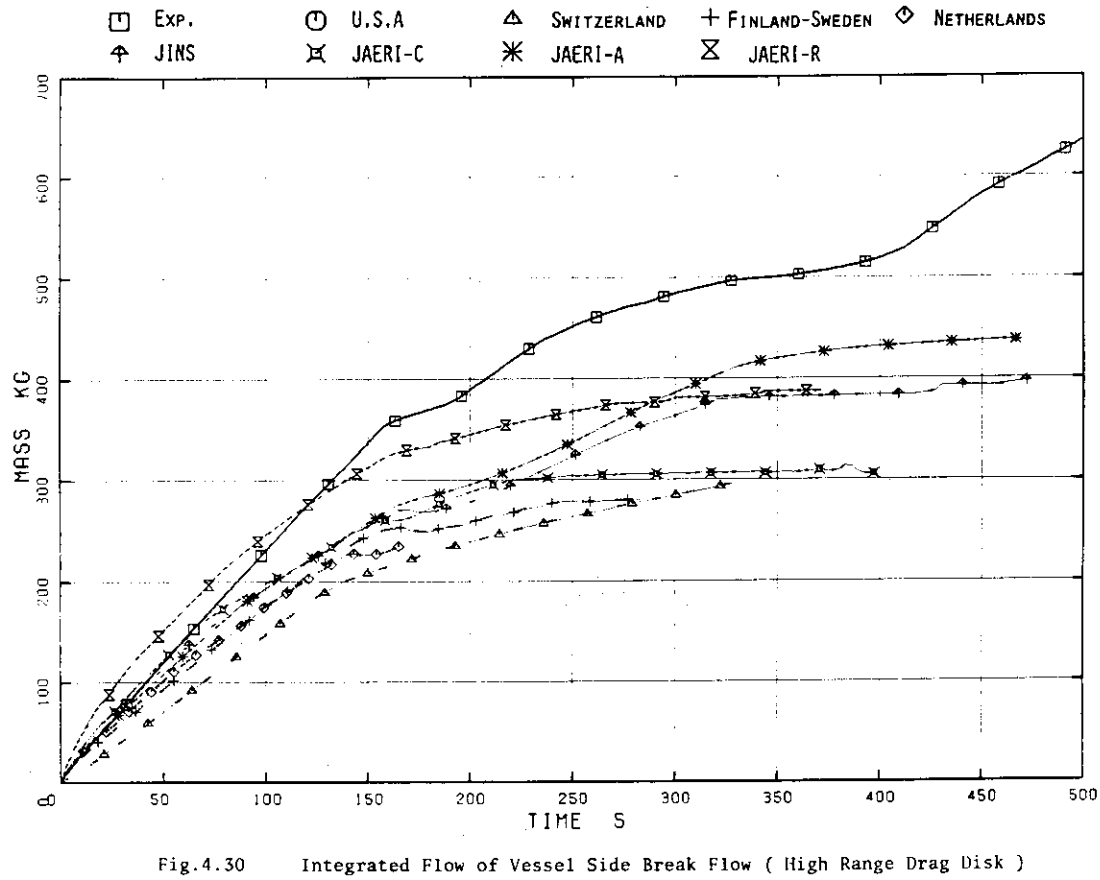

Fig.4.30 Integrated Flow of Vessel Side Break Flow (High Range Drag Disk)

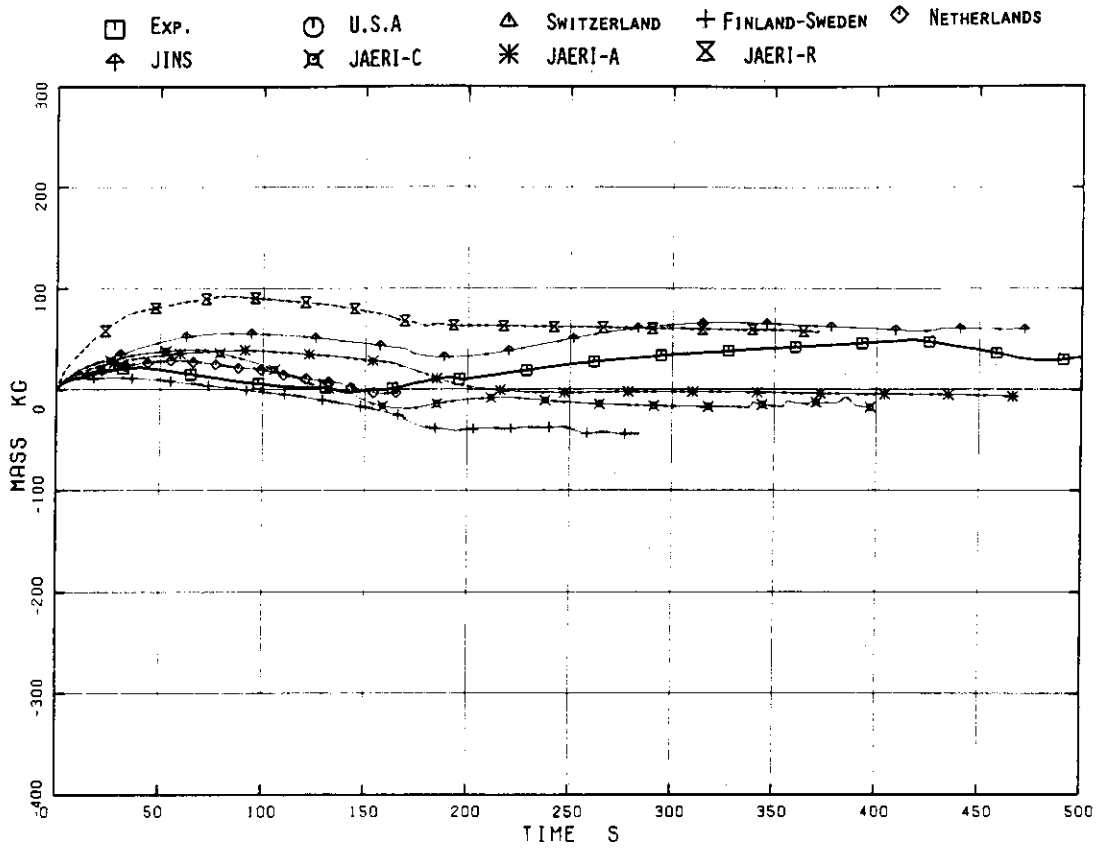

Fig.4.31 Integrated Flow of Pump Side Break Flow (Low Range Drag Disk)

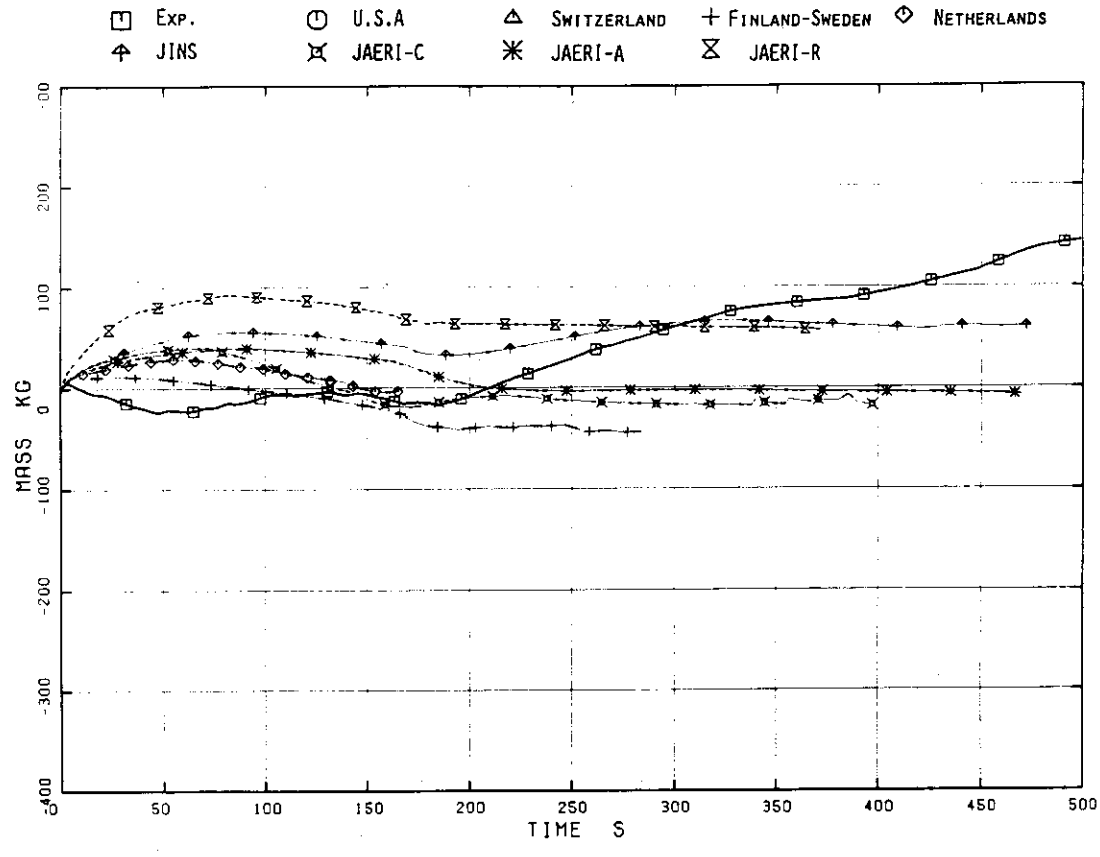

Fig.4.32 Integrated Flow of Pump Side Break Flow (High Range Drag Disk)

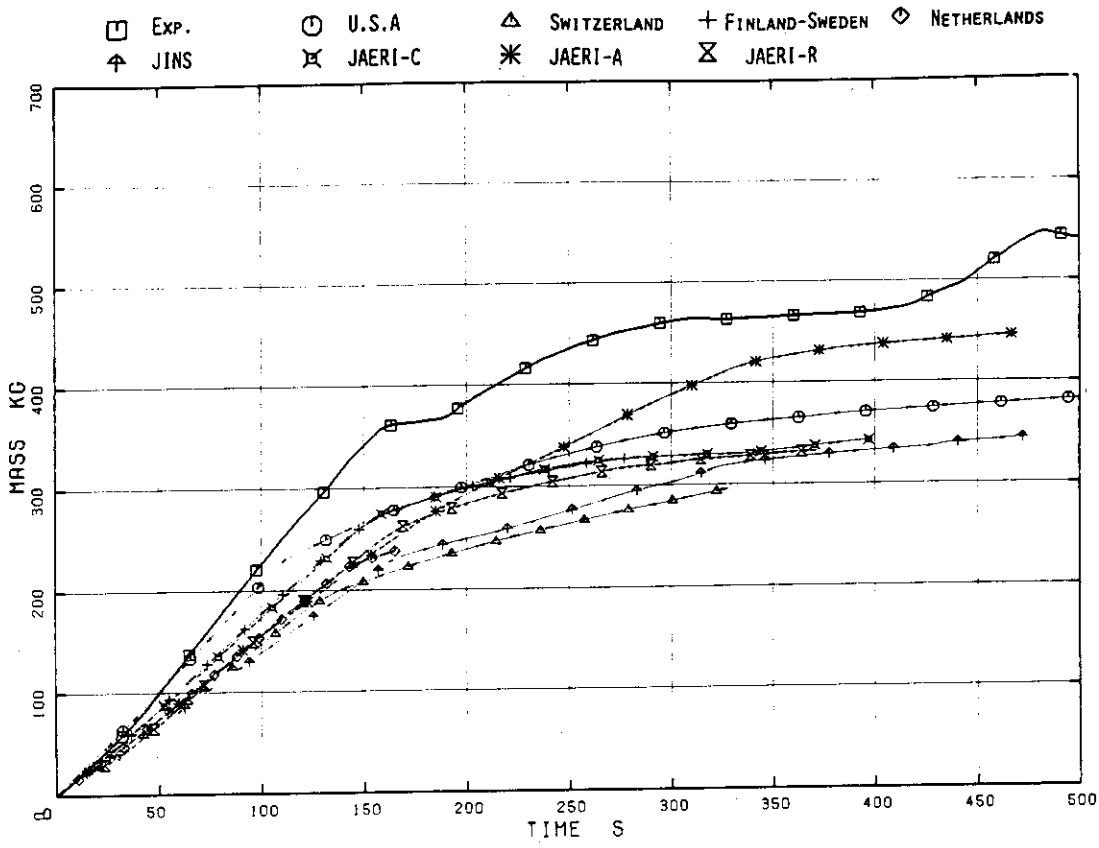

Fig.4.33 Integrated Break Flow Rate (Low Range Drag Disk)

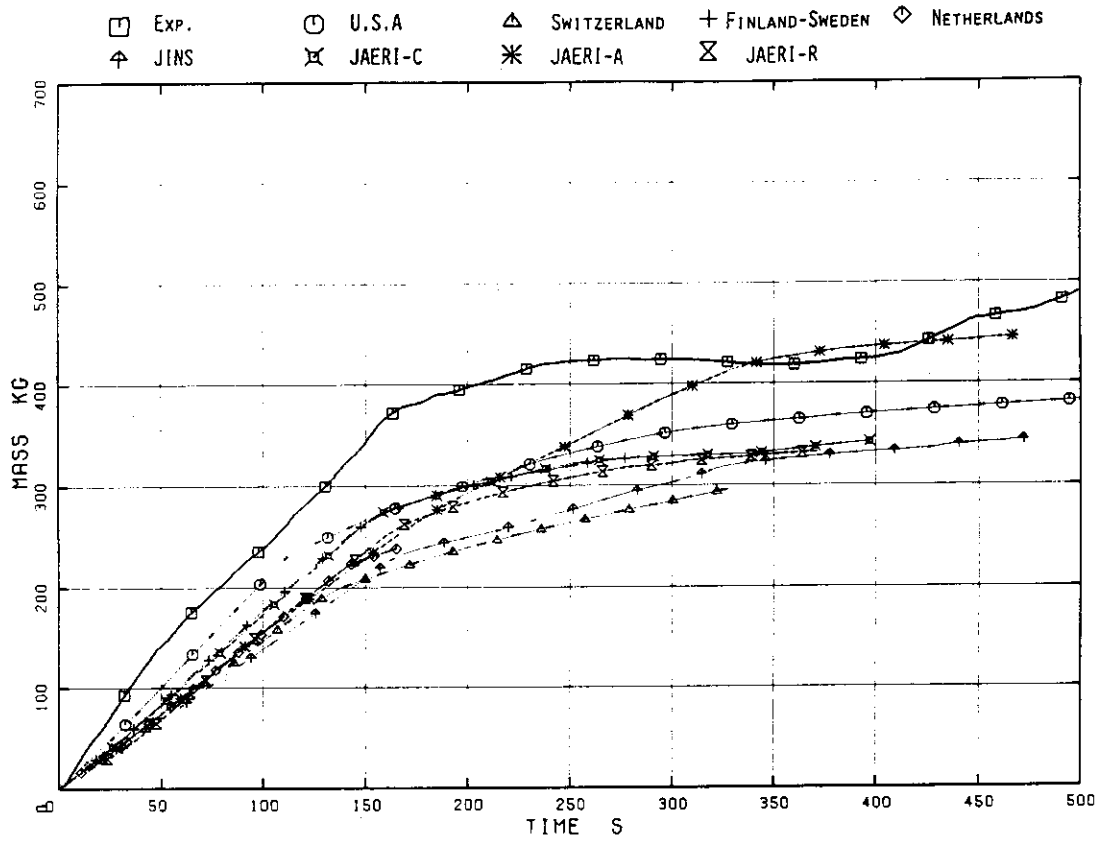

Fig.4.34 Integrated Break Flow Rate (High Range Drag Disk)

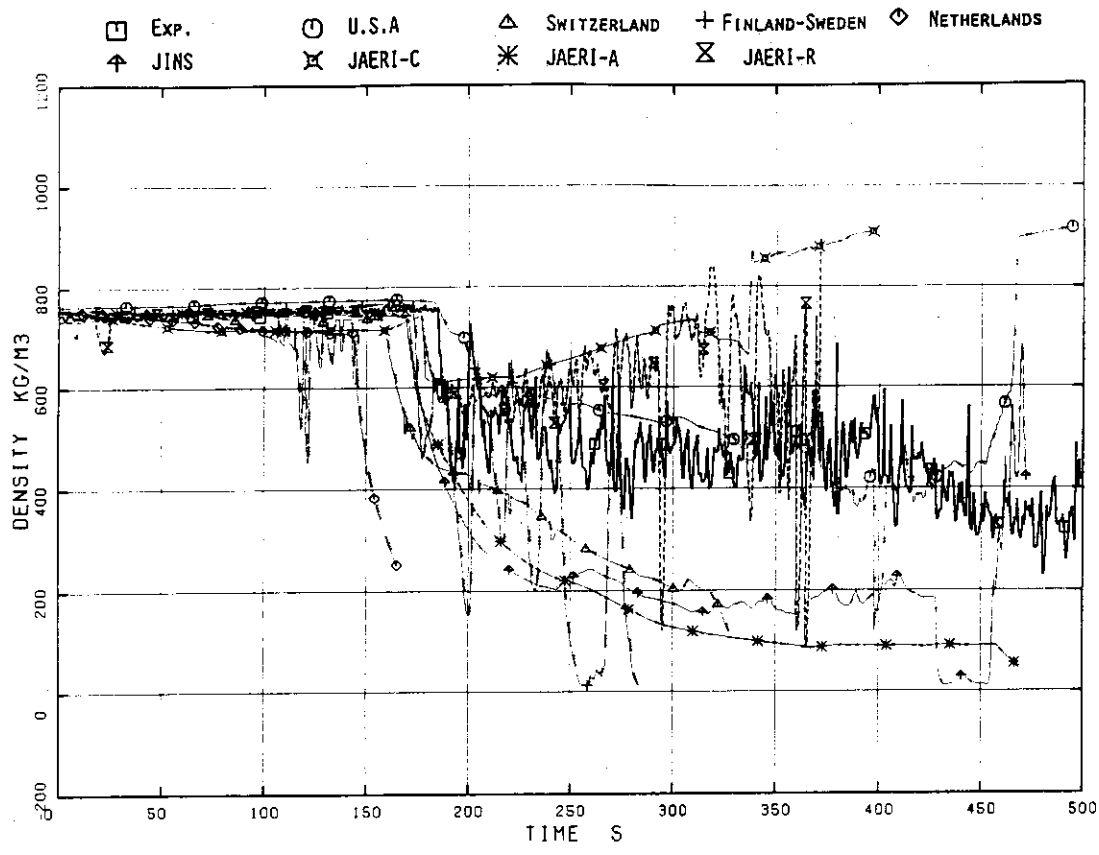

Fig.4.35 Intact Loop Jet Pump Outlet Fluid Density

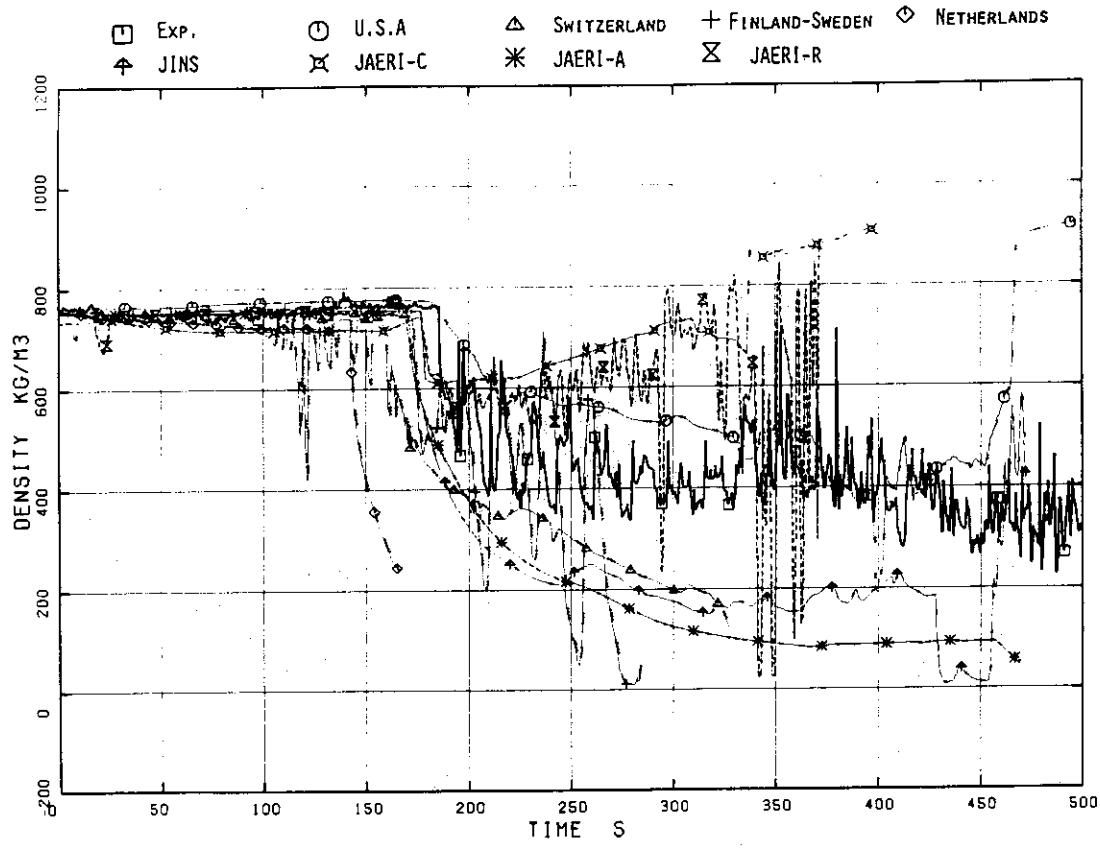

Fig.4.36 Broken Loop Jet Pump Outlet Fluid Density

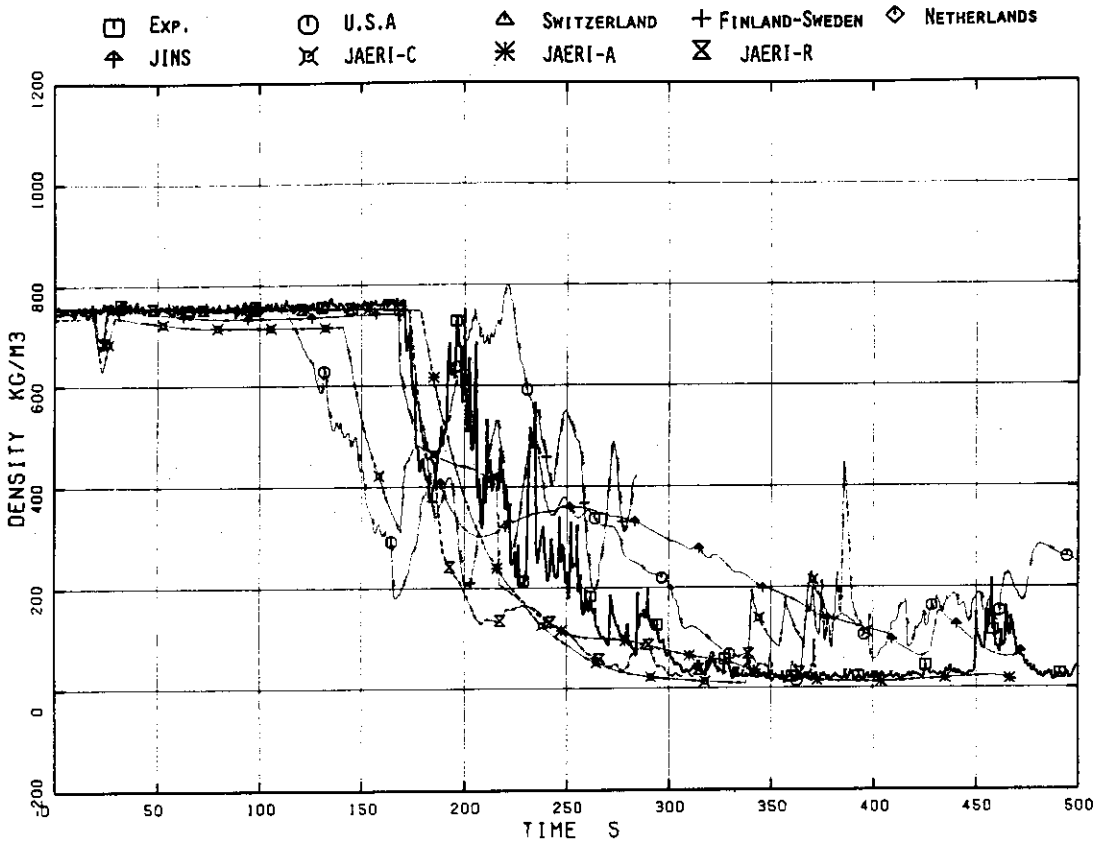

Fig.4.37 Density of Vessel Side Break Flow

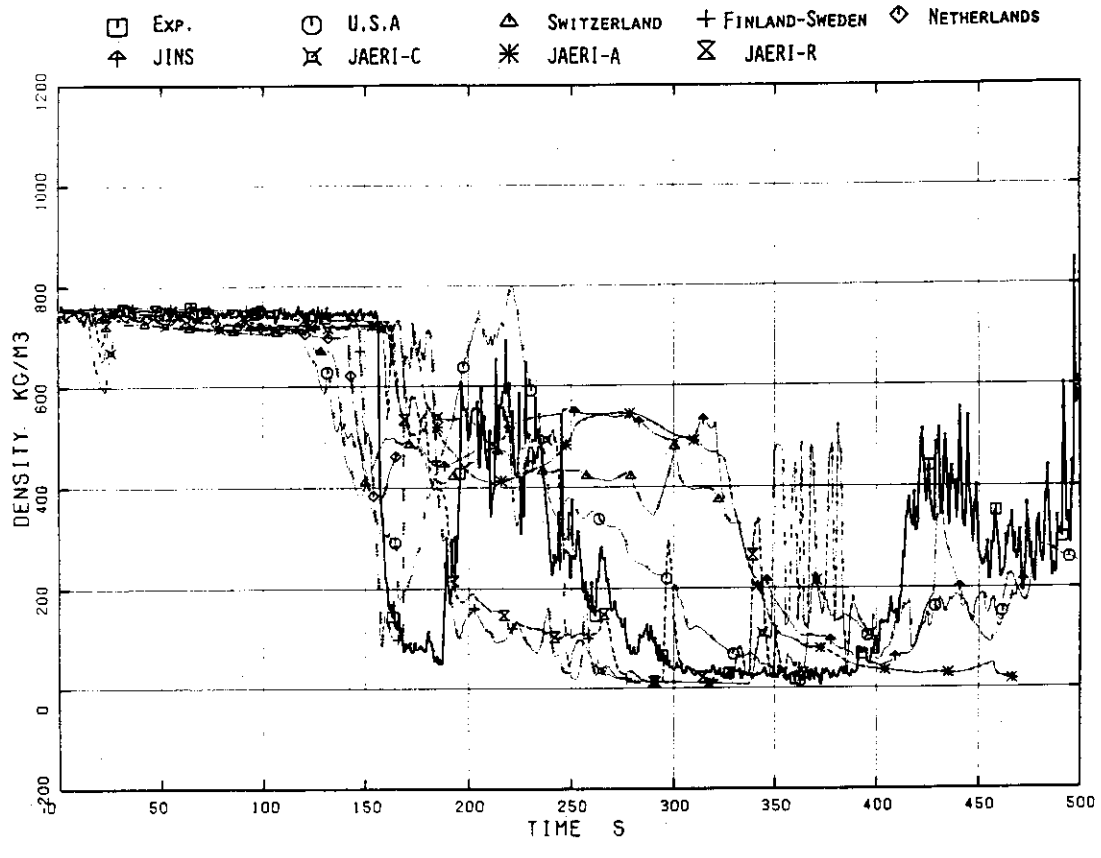

Fig.4.38 Density of Pump Side Break Flow

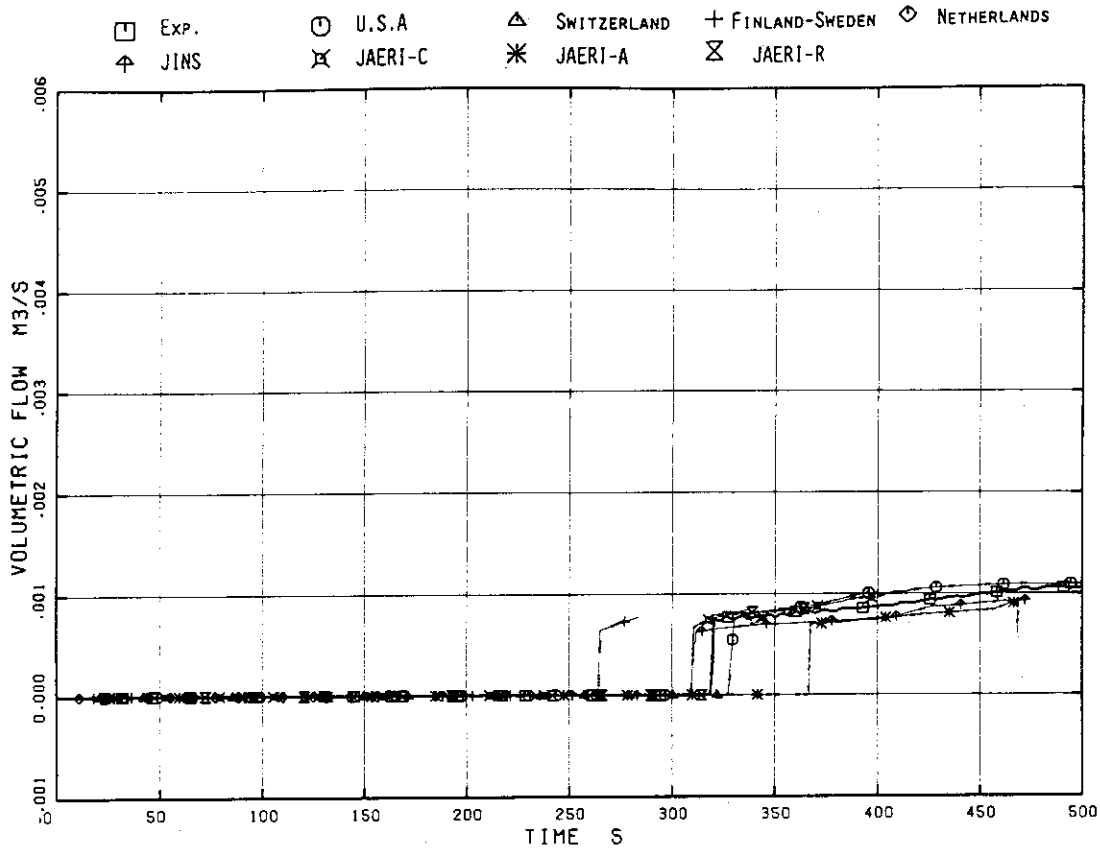

Fig.4.39 LPCS Flow Rate

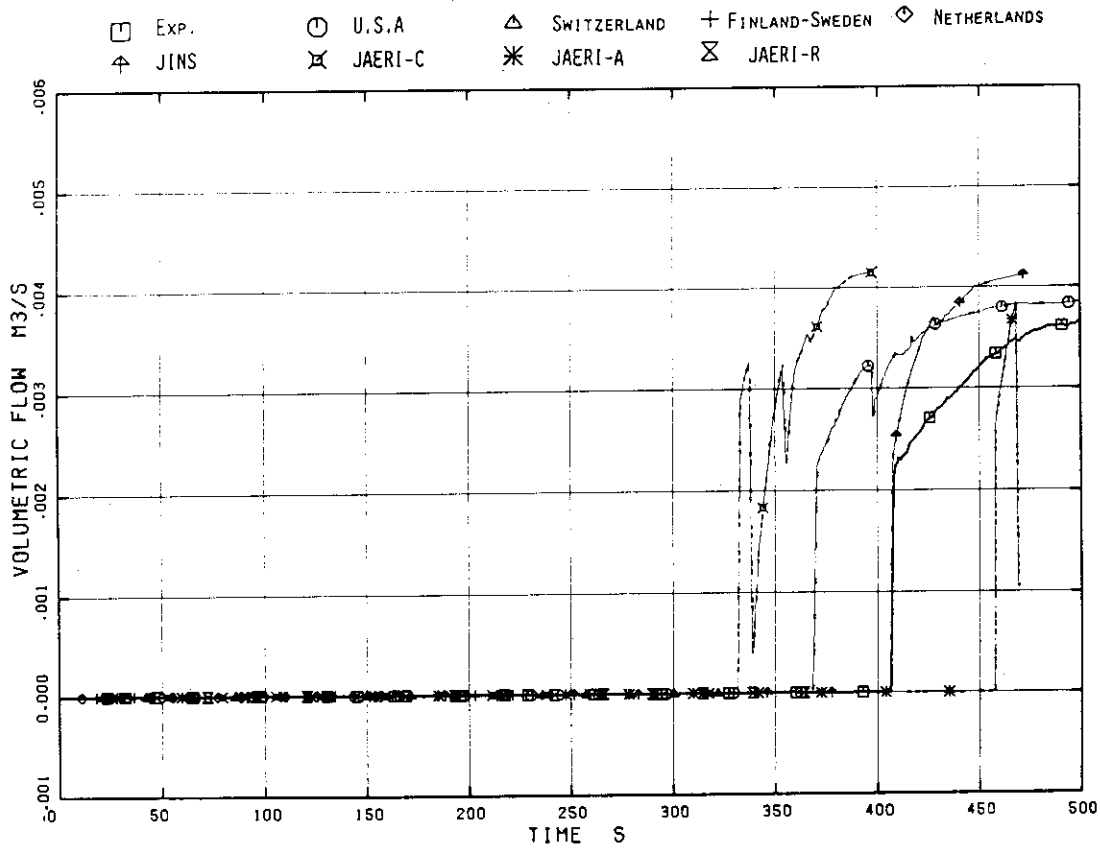

Fig.4.40 LPCI Flow Rate

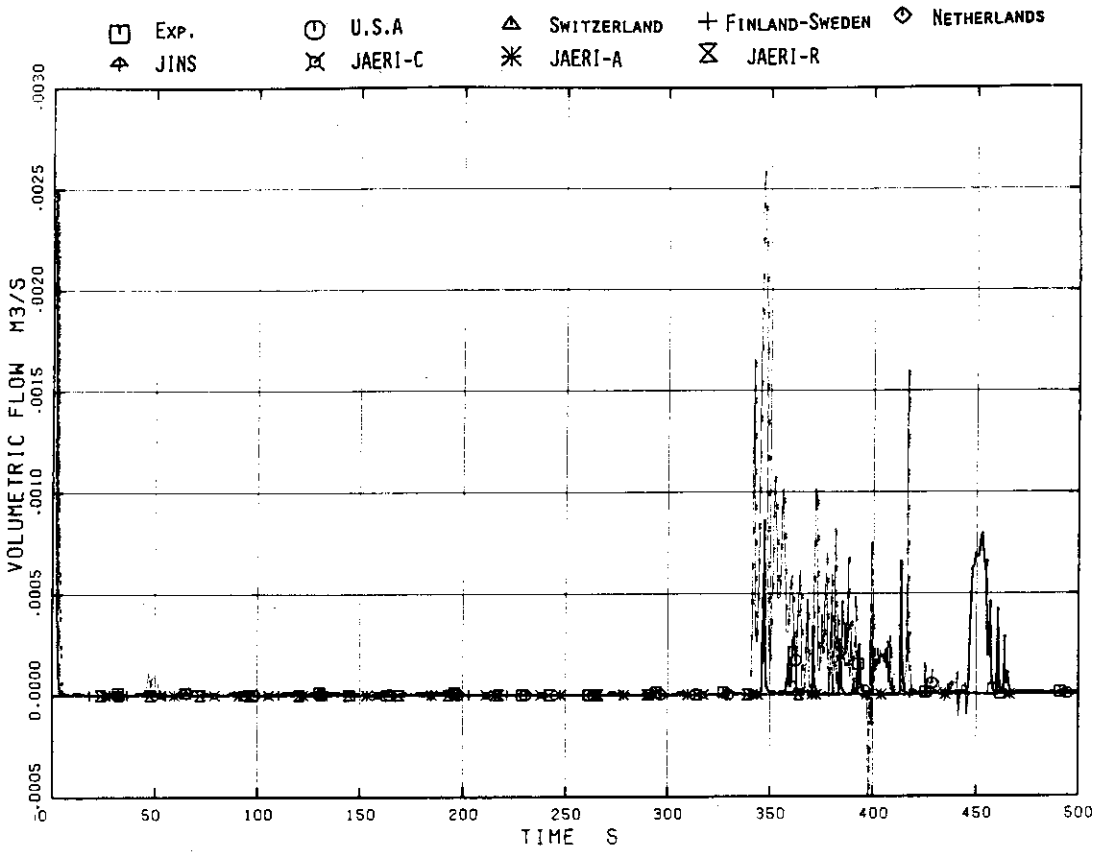

Fig.4.41 Feedwater Flow Rate

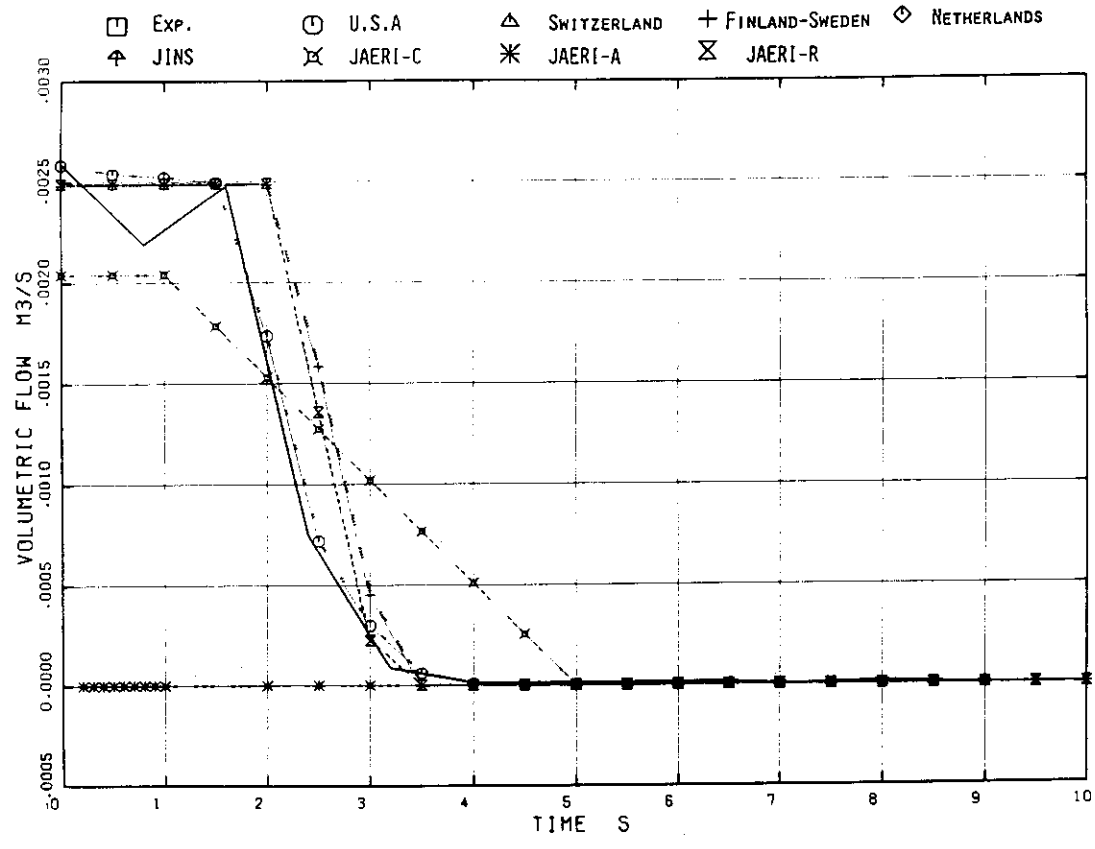

Fig.4.42 Feedwater Flow Rate

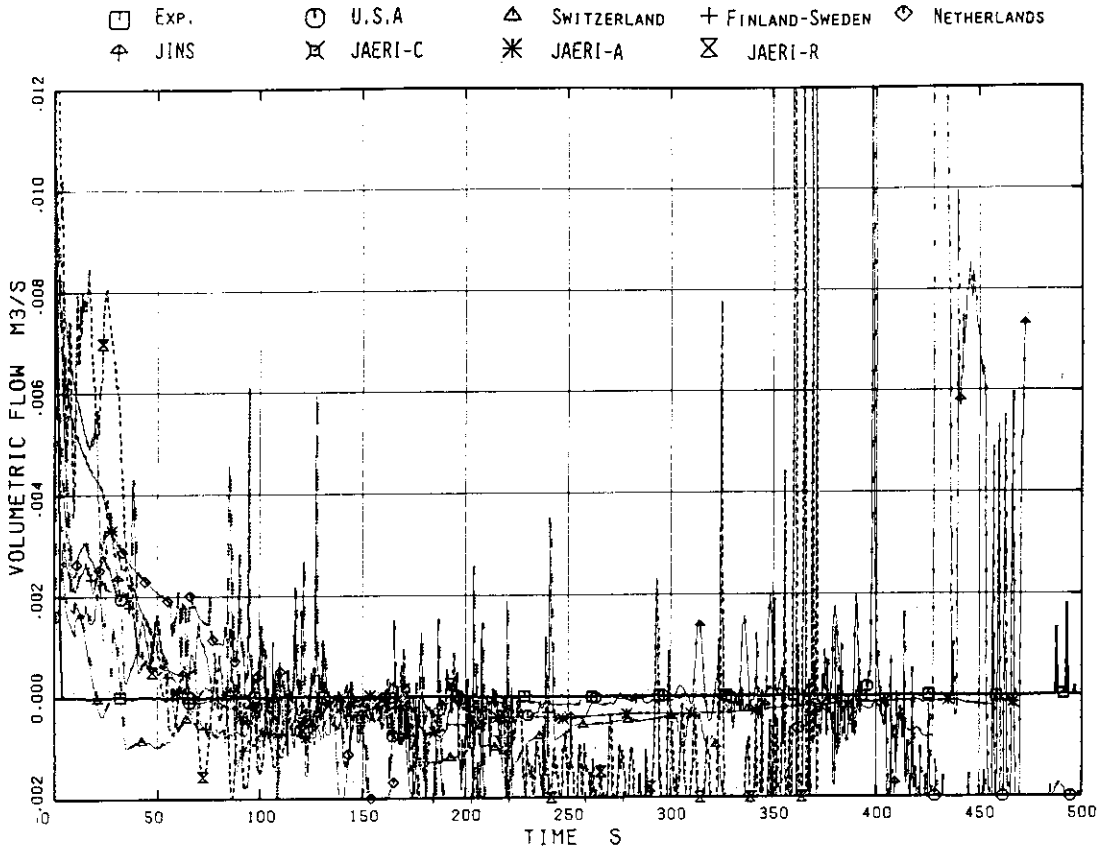

Fig.4.43 Intact Loop Jet Pump Discharge Flow Rate

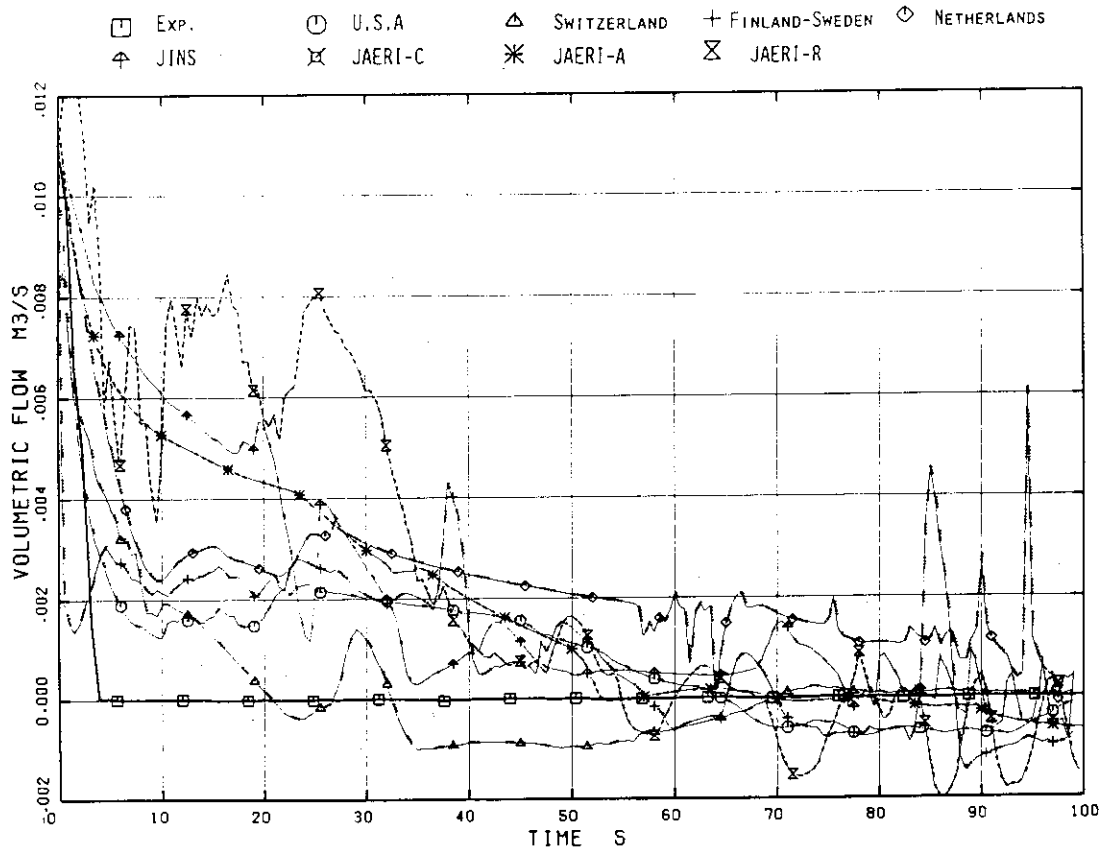

Fig.4.44 Intact Loop Jet Pump Discharge Flow Rate

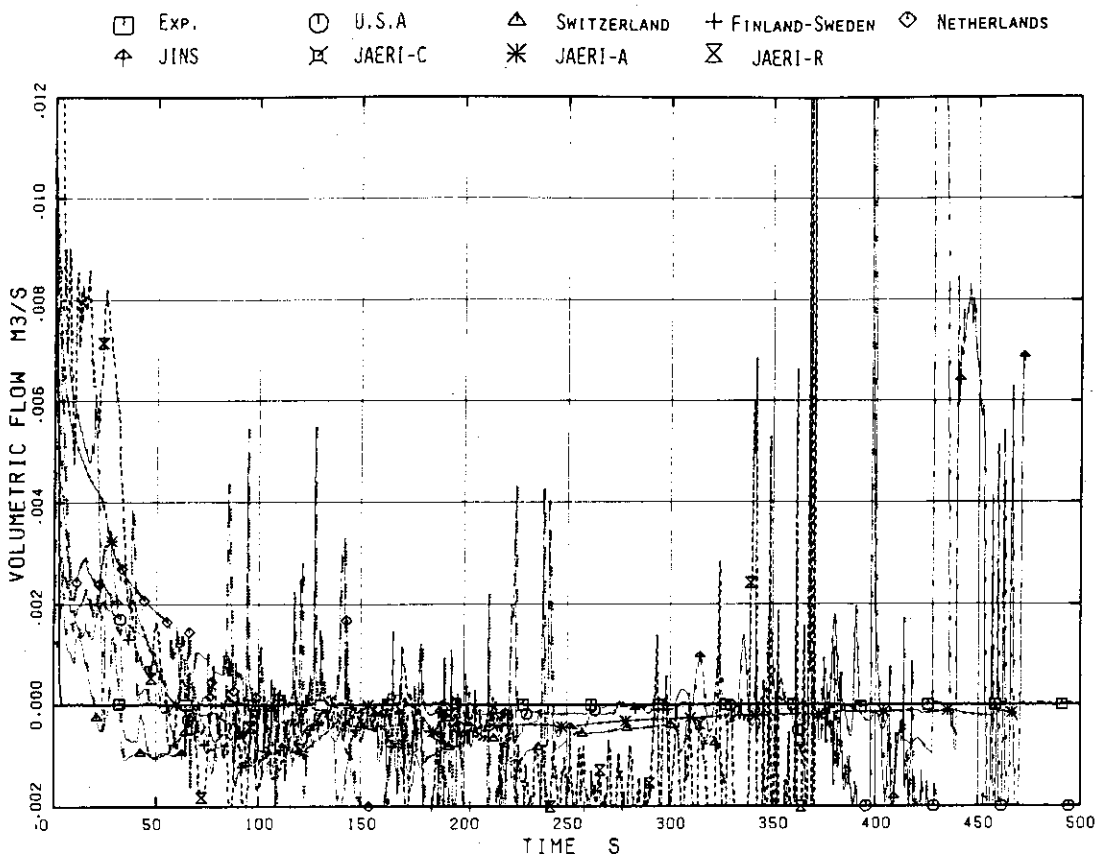

Fig.4.45 Broken Loop Jet Pump Discharge Flow Rate

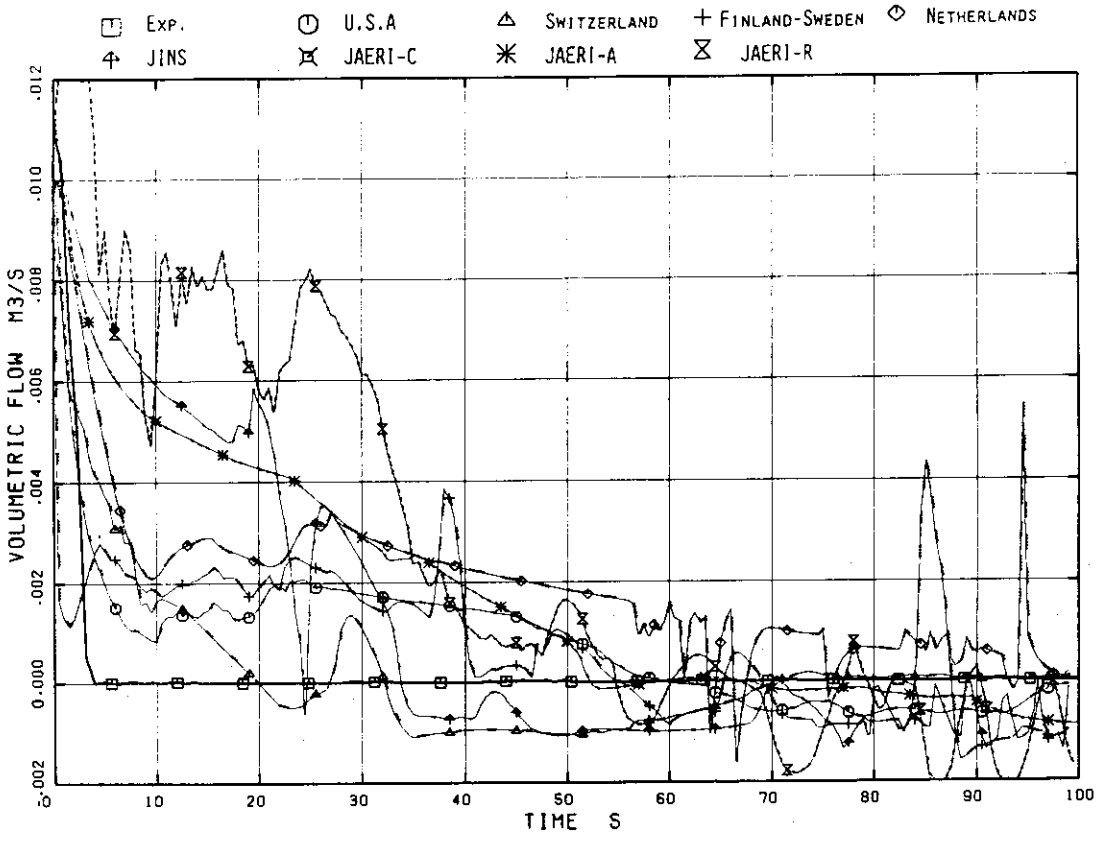

Fig.4.46 Broken Loop Jet Pump Discharge Flow Rate

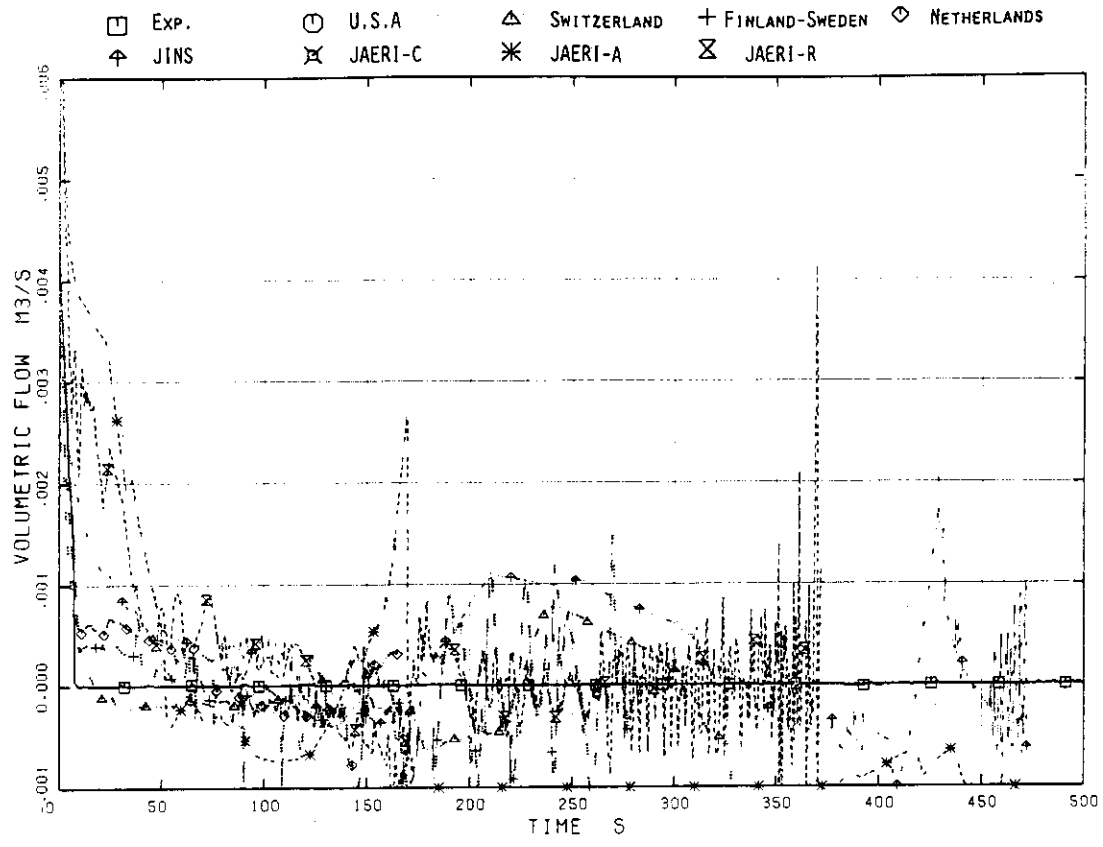

Fig.4.47 Intact Loop Recirculation Pump Flow Rate

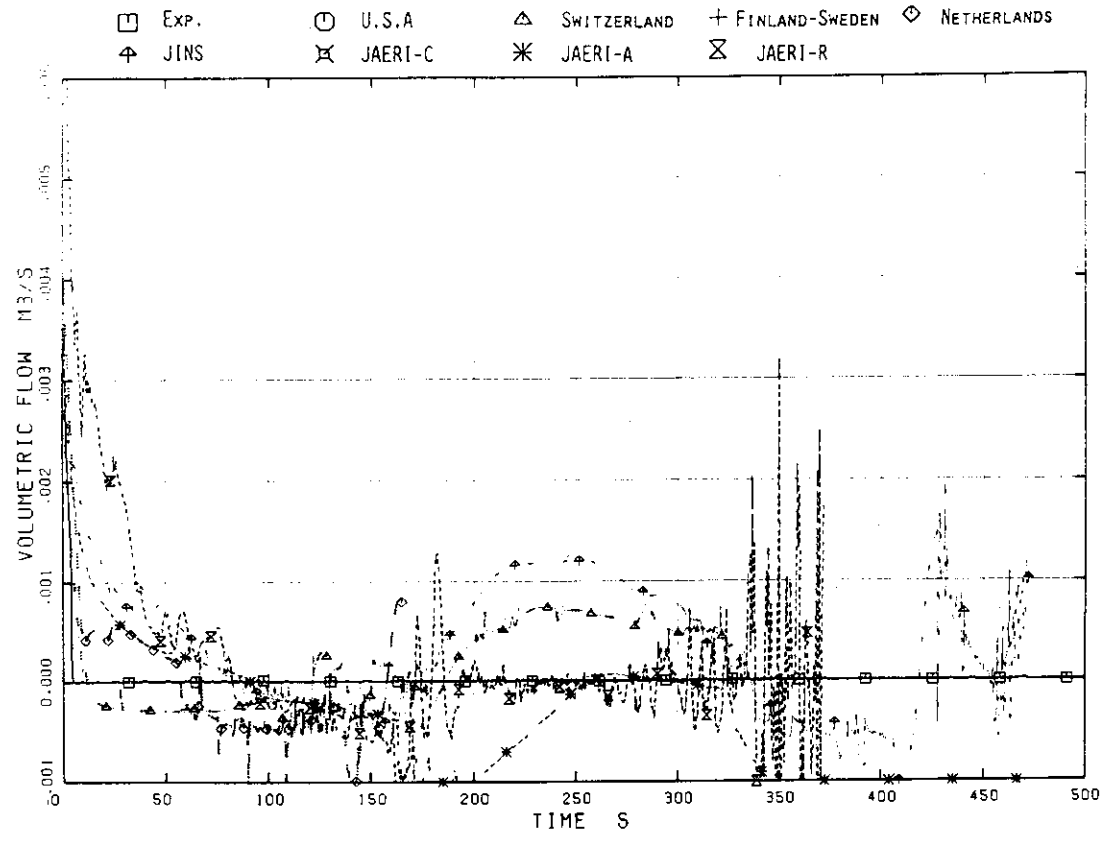

Fig.4.48 Broken Loop Recirculation Pump Flow Rate

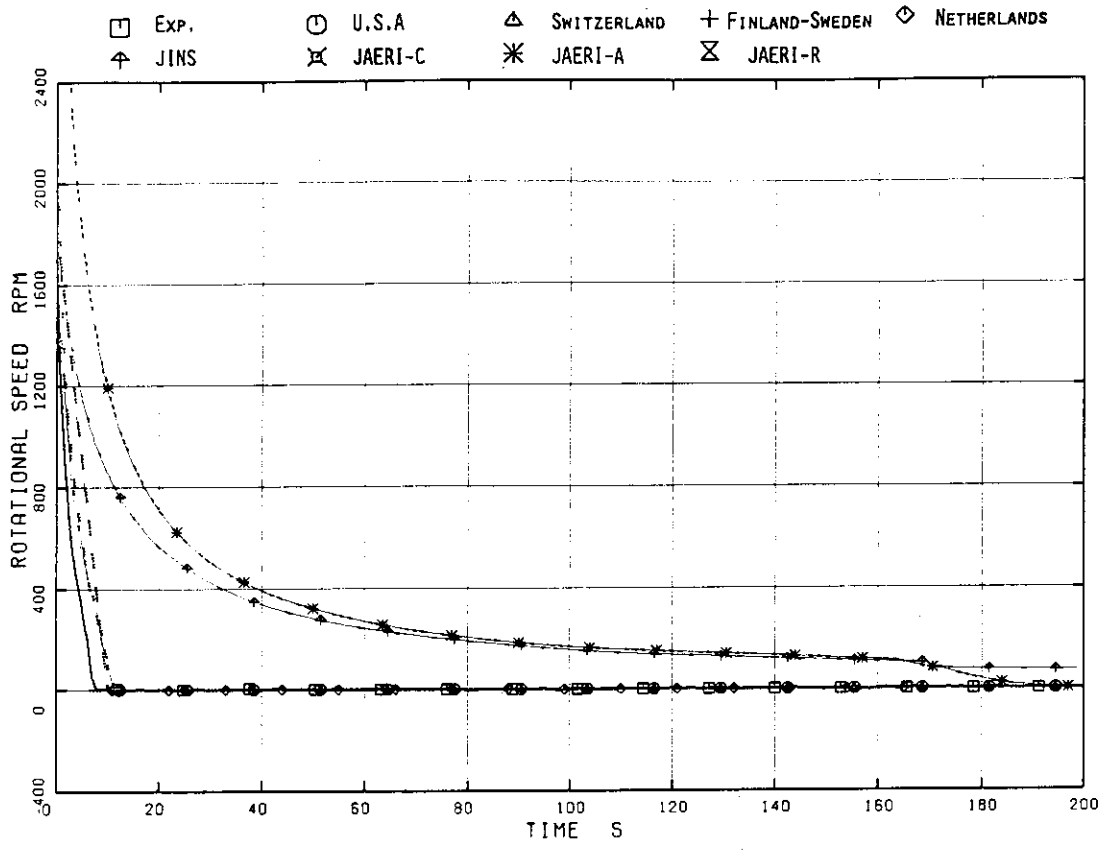

Fig.4.49 Intact Loop Recirculation Pump Speed

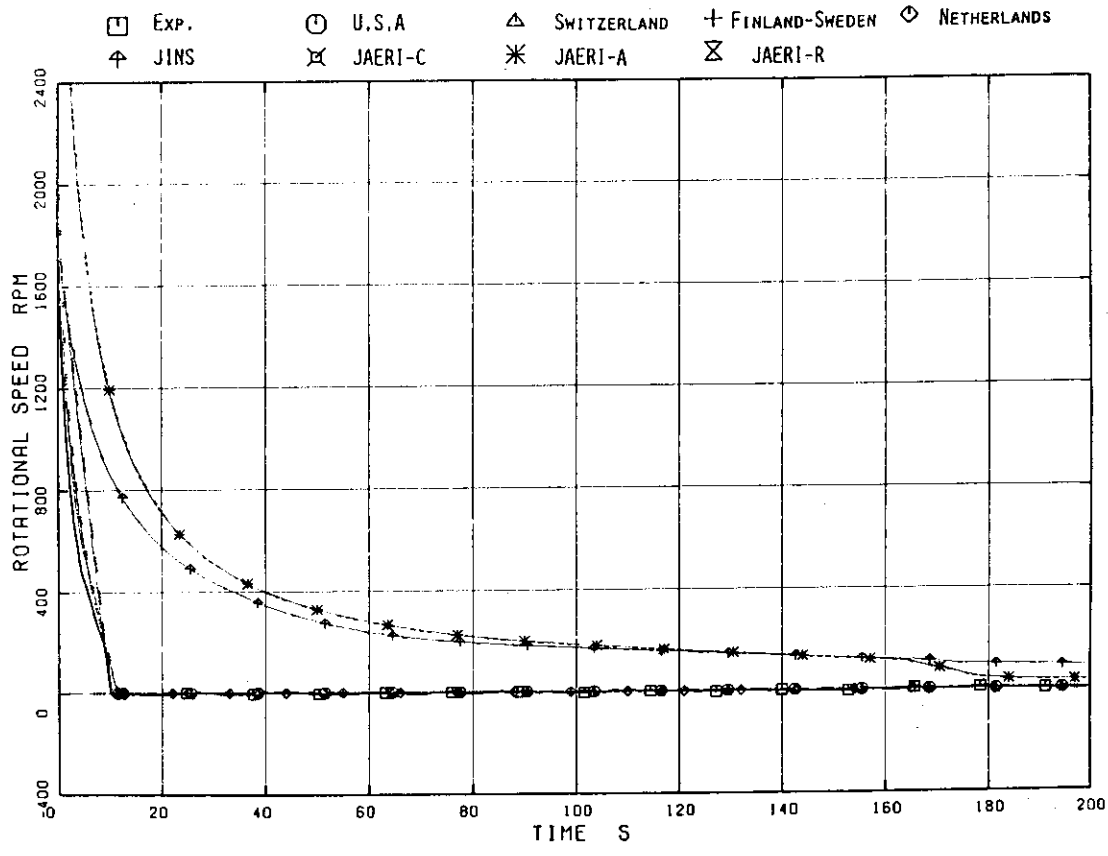

Fig.4.50 Broken Loop Recirculation Pump Speed

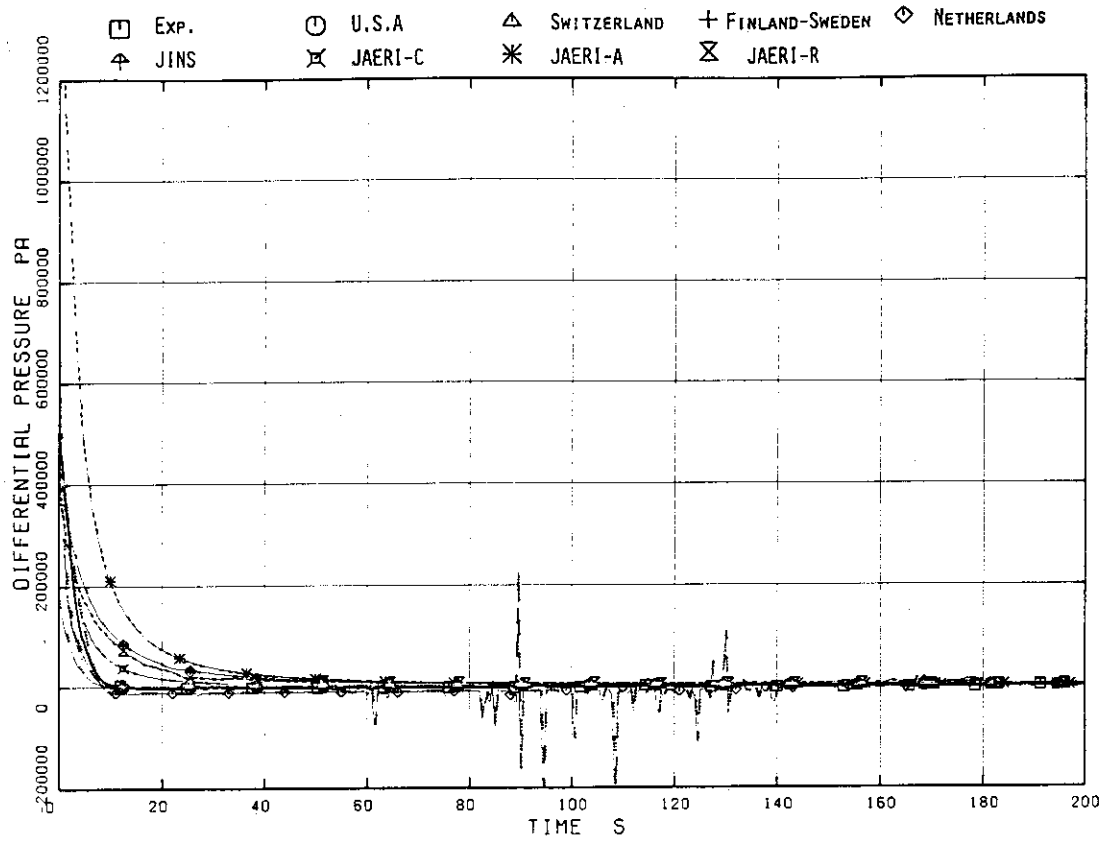

Fig.4.51 Intact Loop Recirculation Pump Head

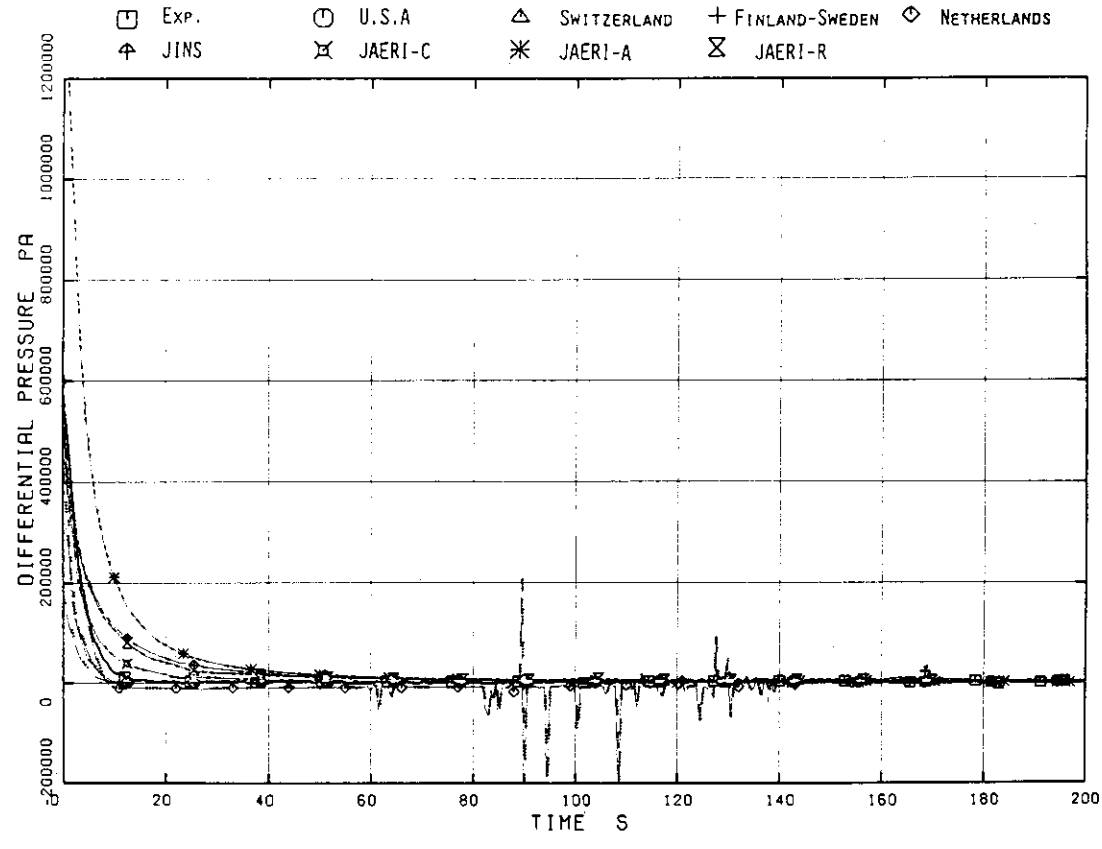

Fig.4.52 Broken Loop Recirculation Pump Head

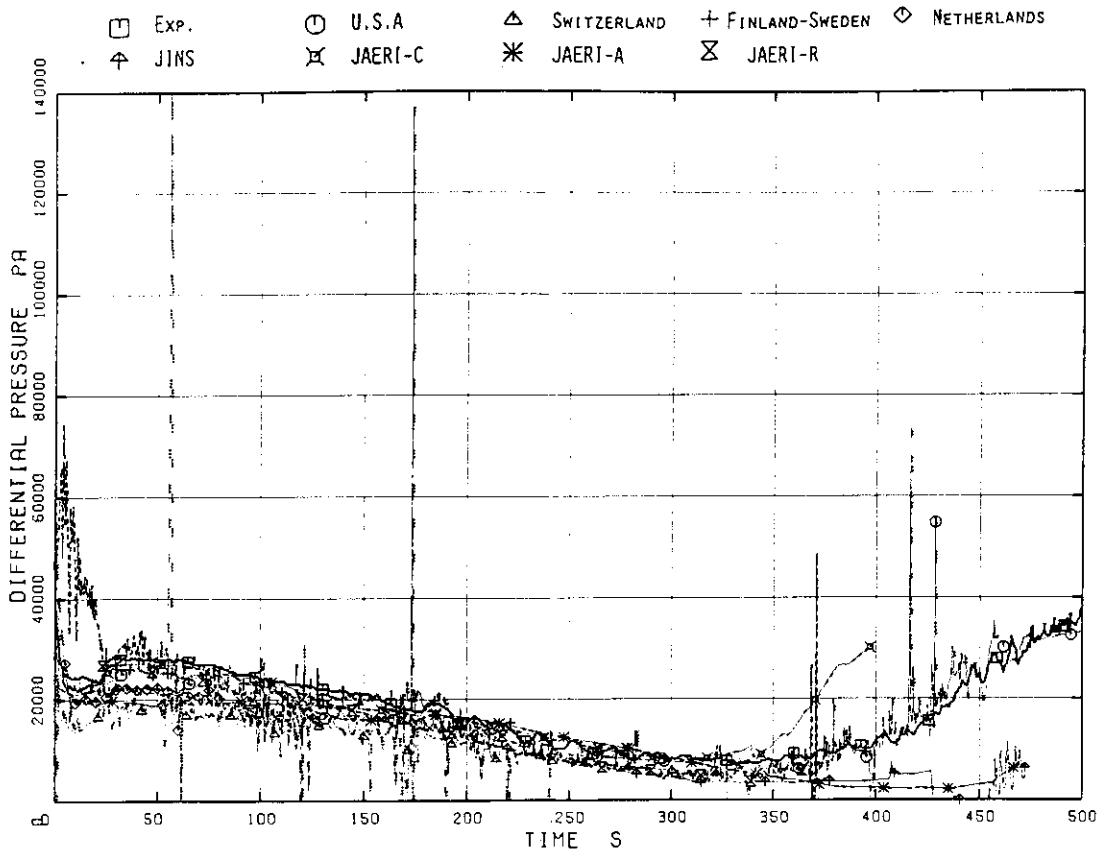

Fig.4.53 Differential Pressure between Lower Plenum and Upper Plenum

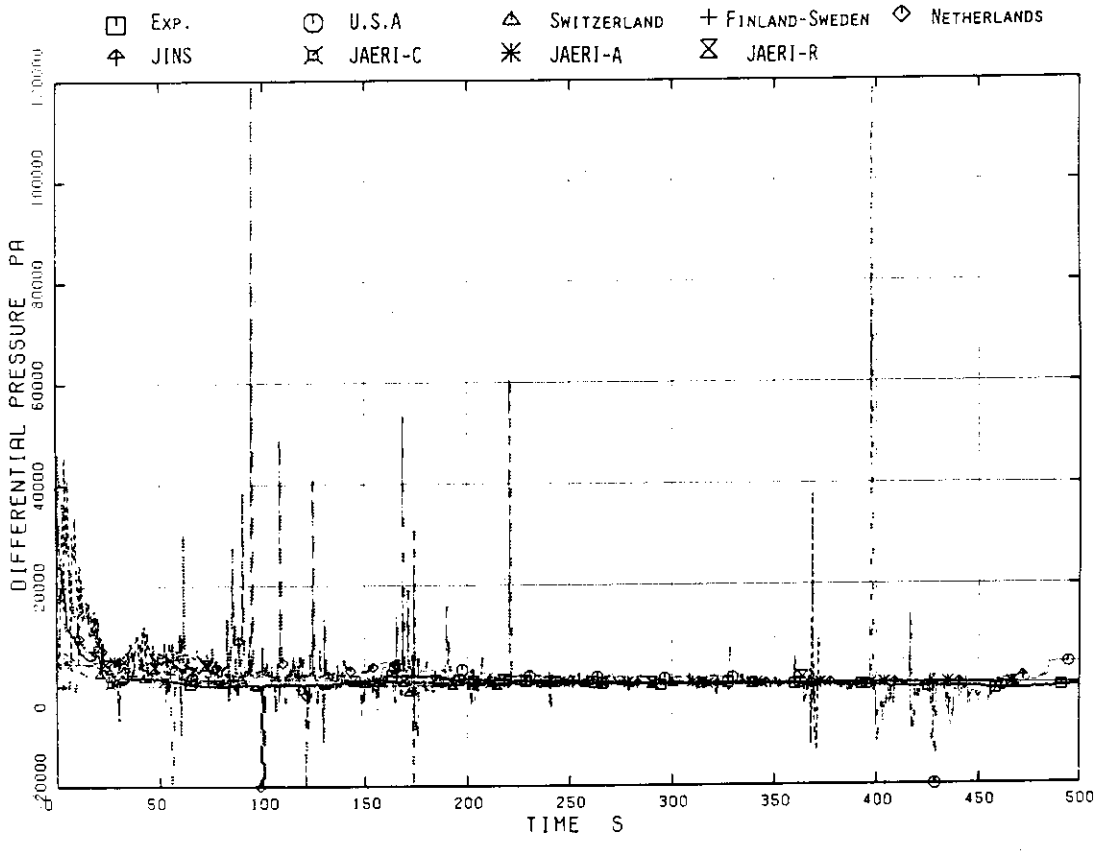

Fig.4.54 Differential Pressure between Upper Plenum and Steam Dome

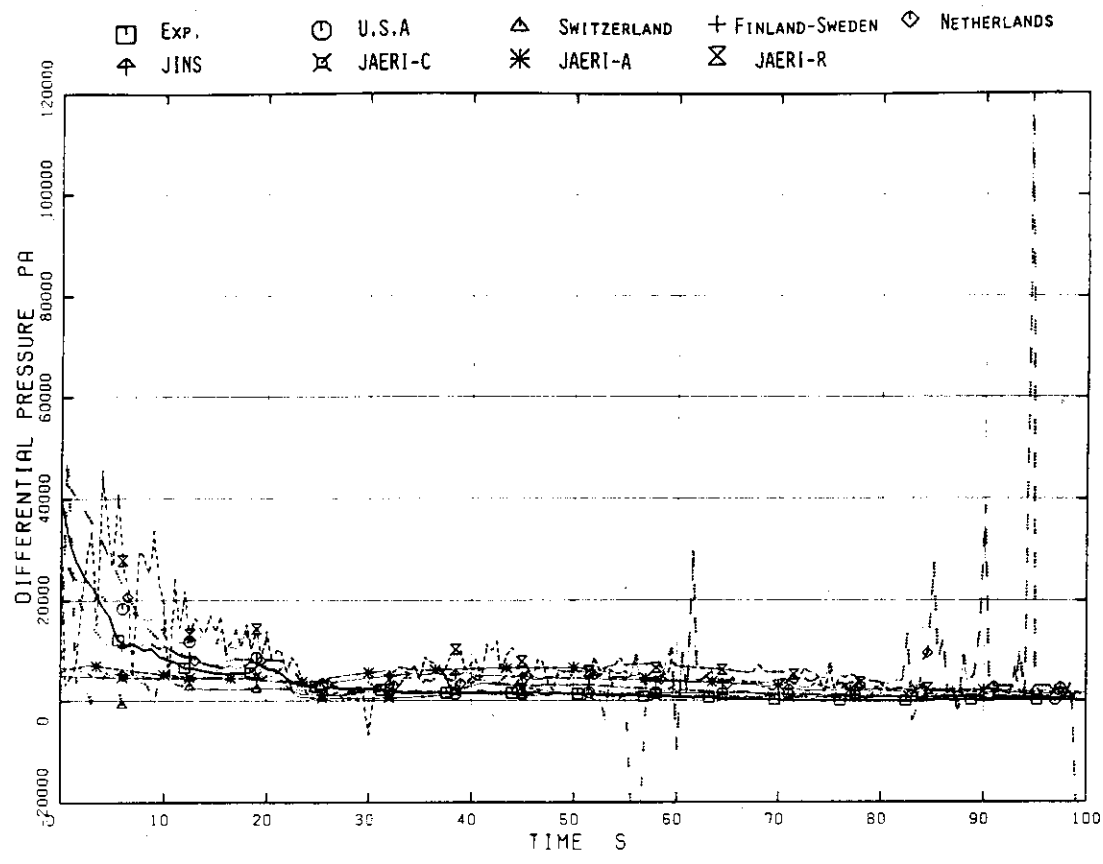

Fig.4.55 Differential Pressure between Upper Plenum and Steam Dome

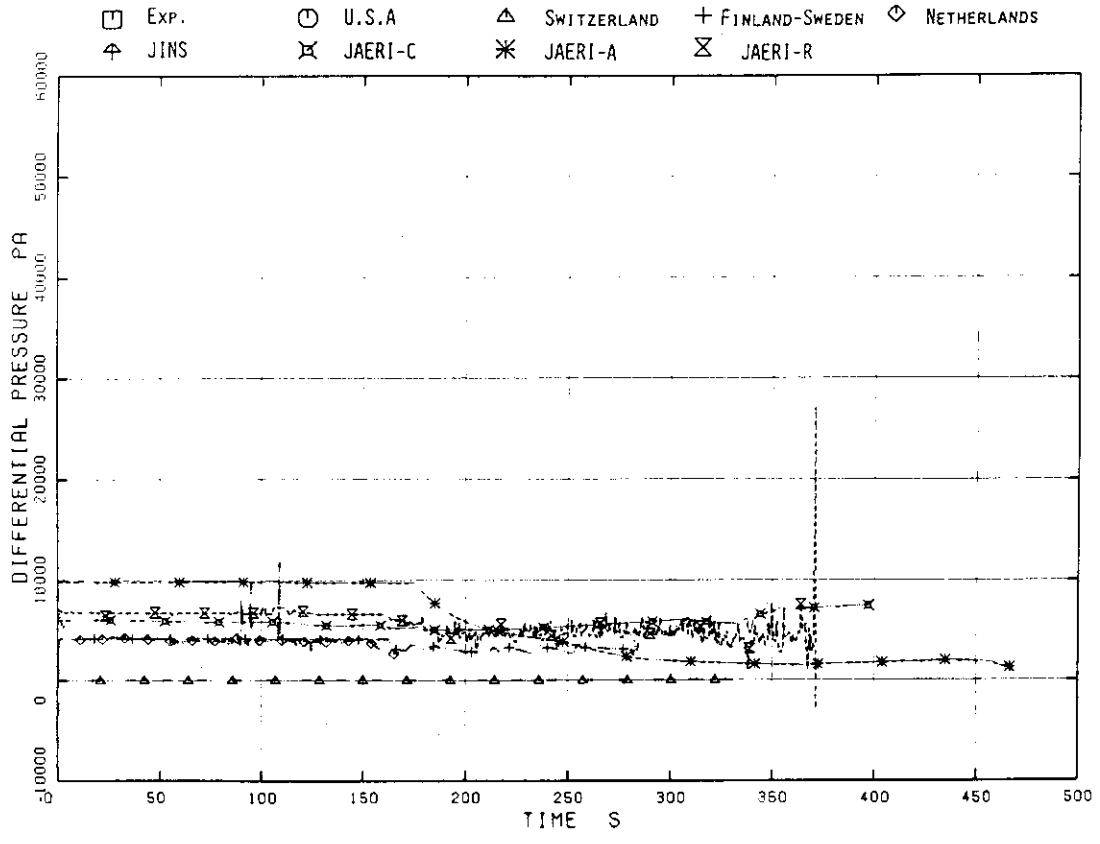

Fig.4.56 Lower Plenum Head

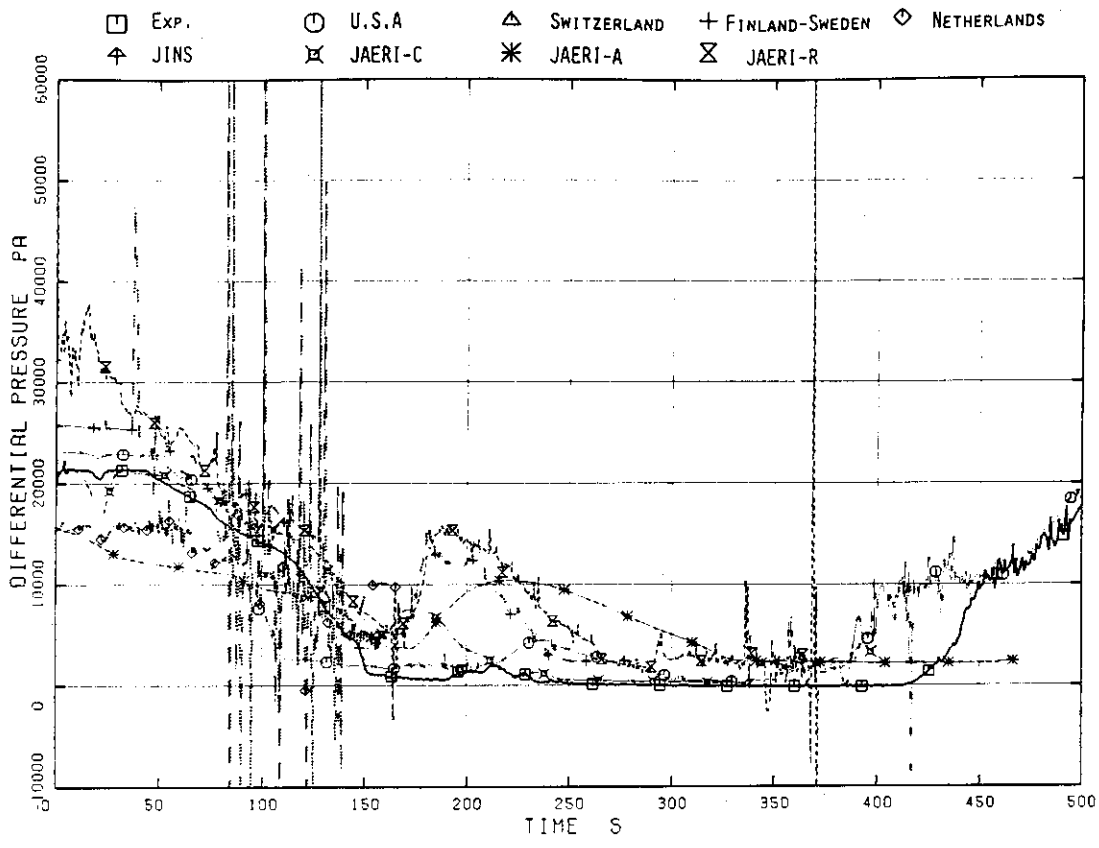

Fig.4.57 Downcomer Head

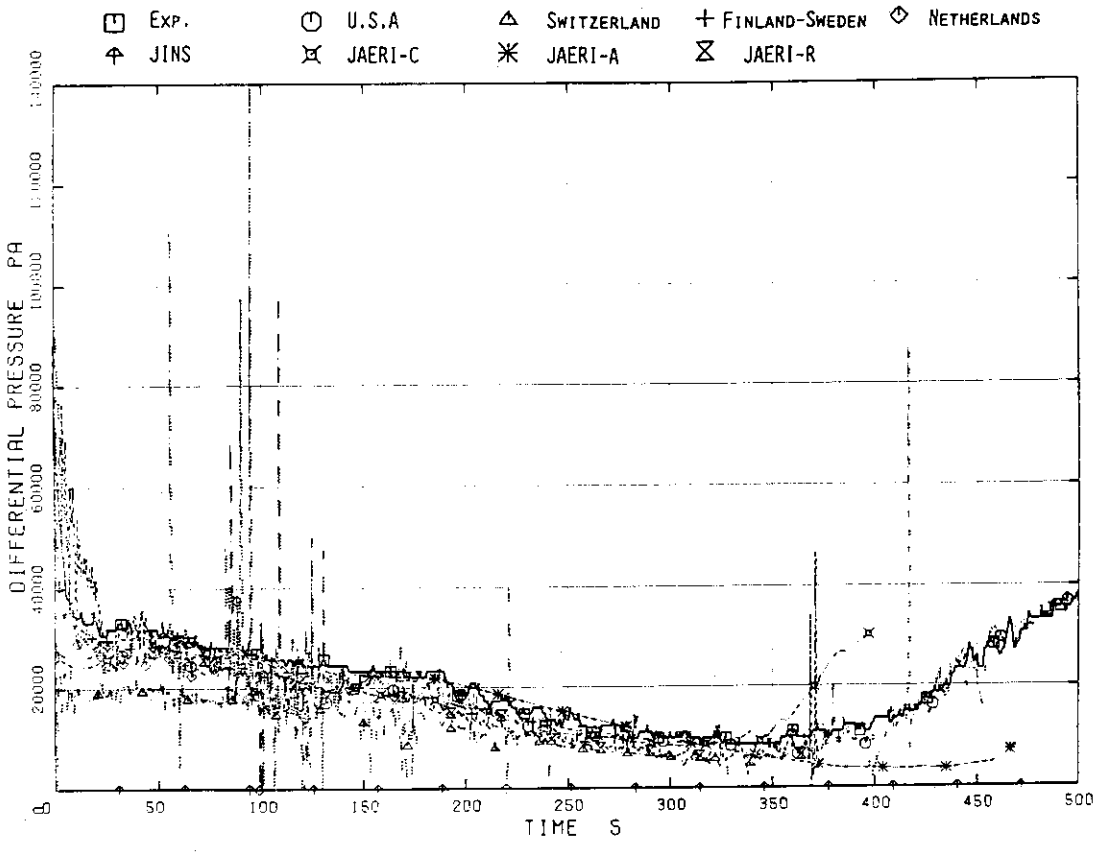

Fig.4.58 Differential Pressure between Pressure Vessel Bottom and Top

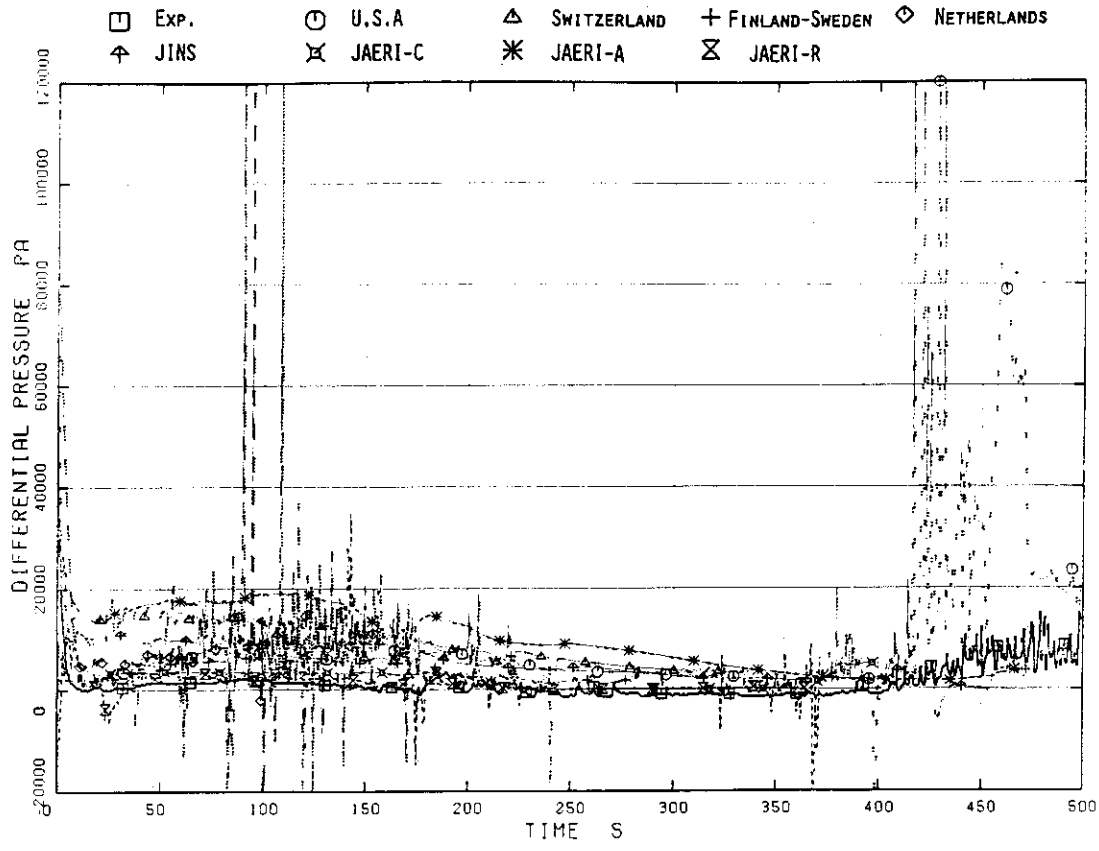

Fig.4.59 Diffrential Pressure between Intact Loop Jet Pump Discharge and Suction

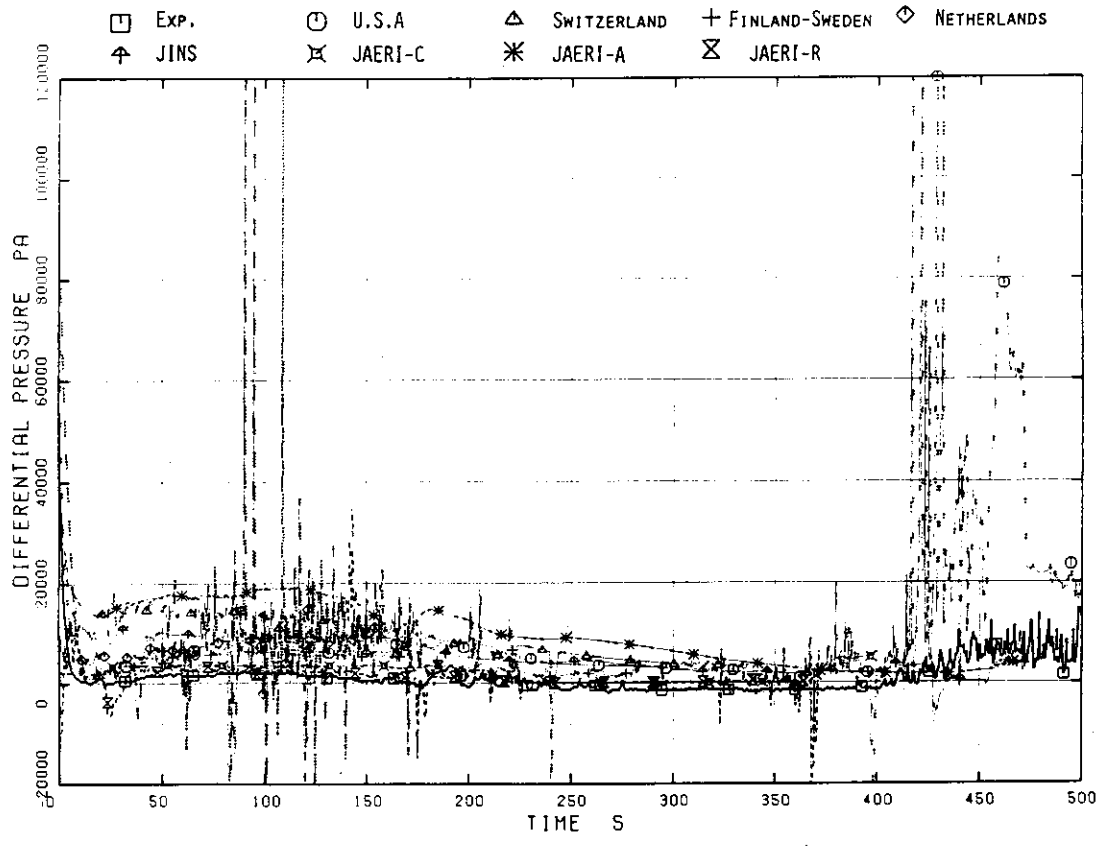

Fig.4.60 Diffrential Pressure between Intact Loop Jet Pump Discharge and Suction

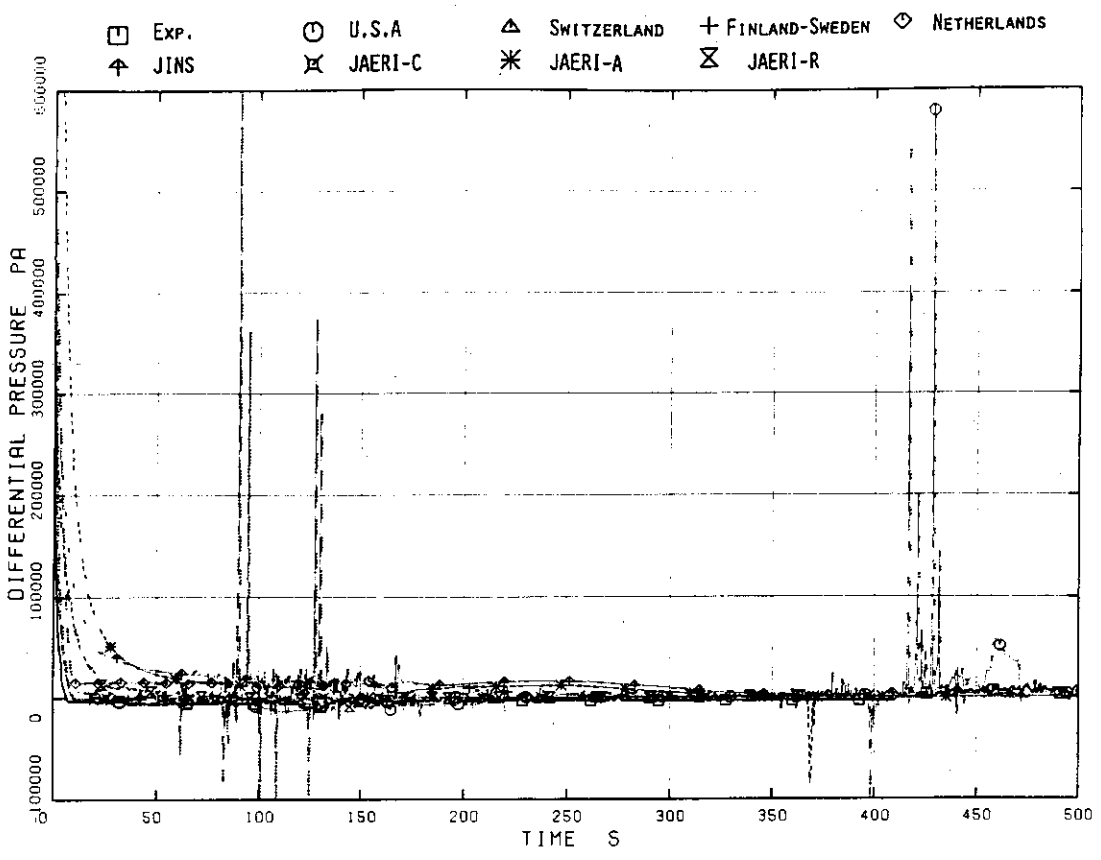

Fig.4.61 Differential Pressure between Intact Loop Jet Pump Drive and Suction

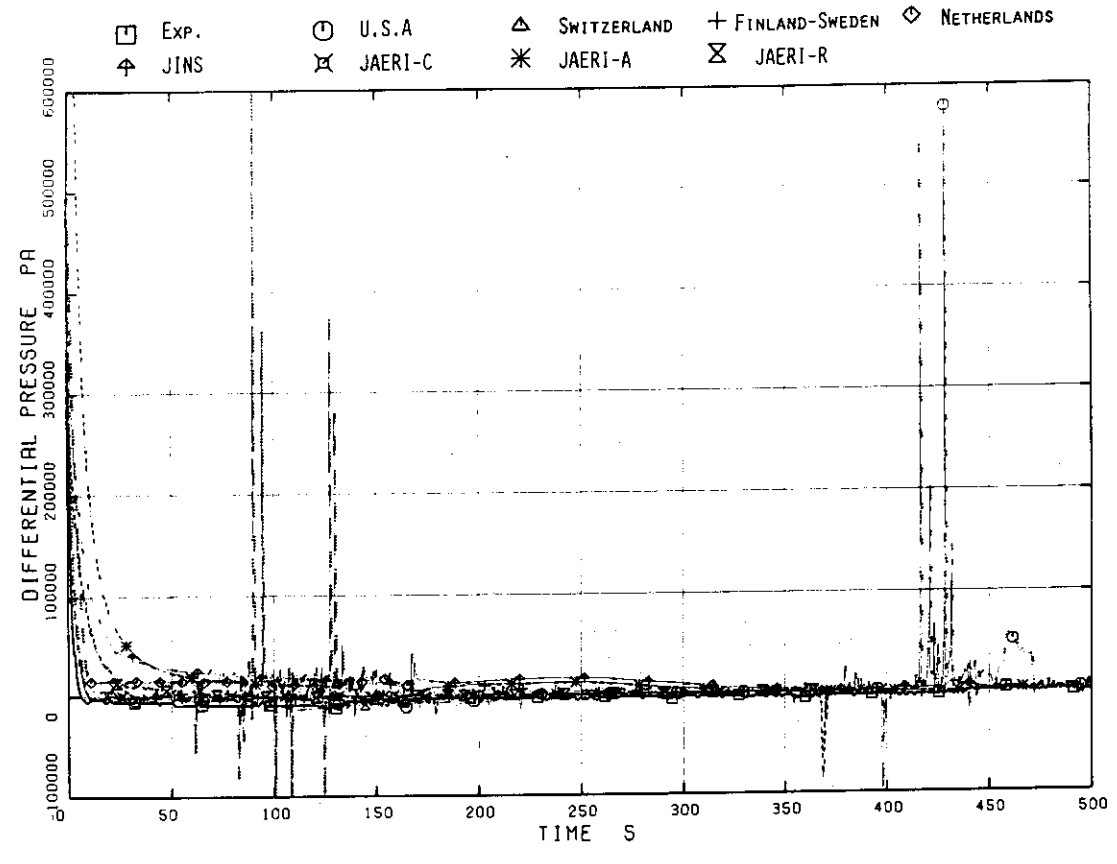

Fig.4.62 Differential Pressure between Intact Jet Pump Drive and Suction

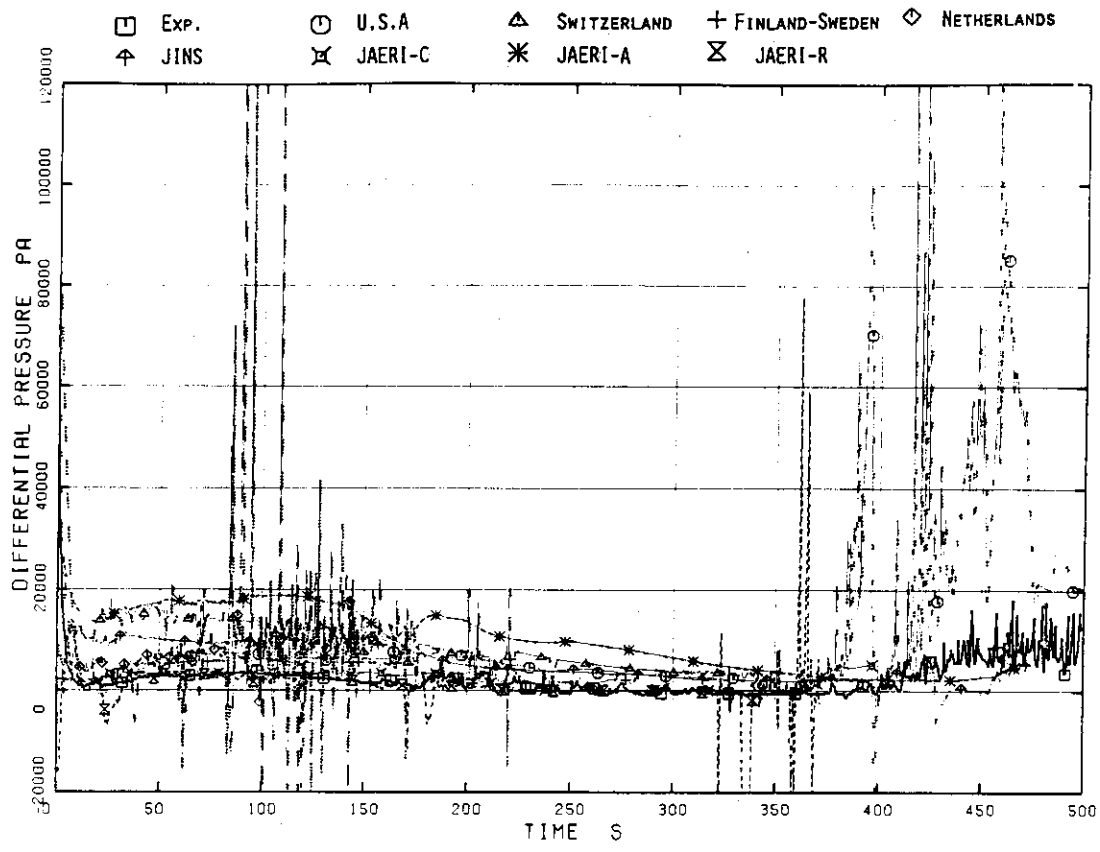

Fig.4.63 Differential Pressure between Broken Loop Jet Pump Discharge and Suction

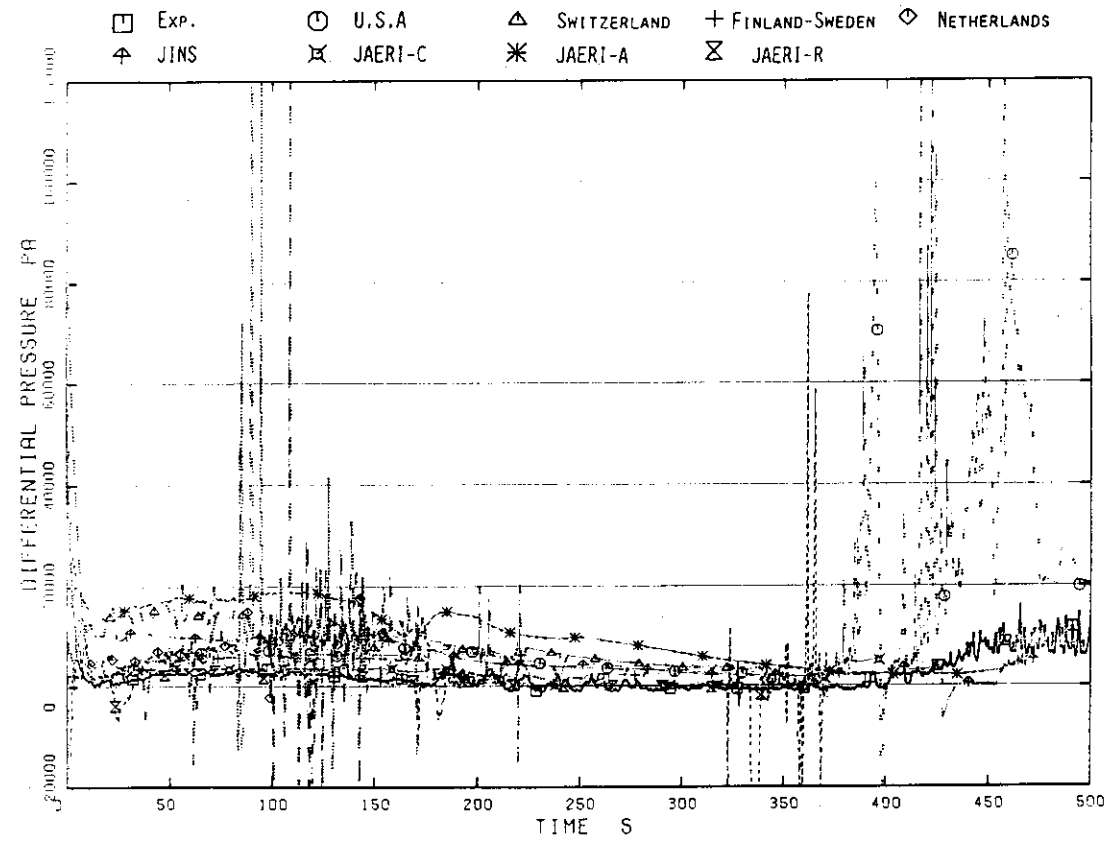

Fig.4.64 Differential Pressure between Broken Loop Jet Pump Discharge and Suction

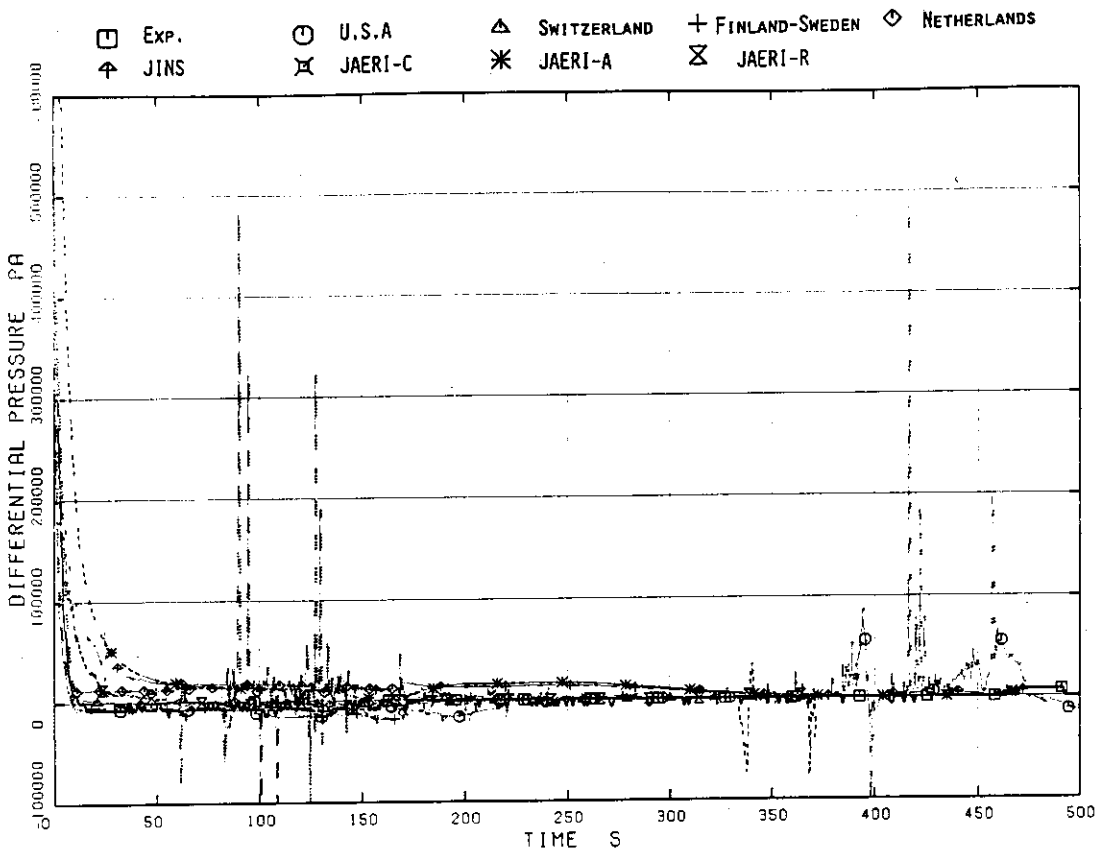

Fig.4.65 Differential Pressure between Broken Loop Jet Pump Drive and Suction

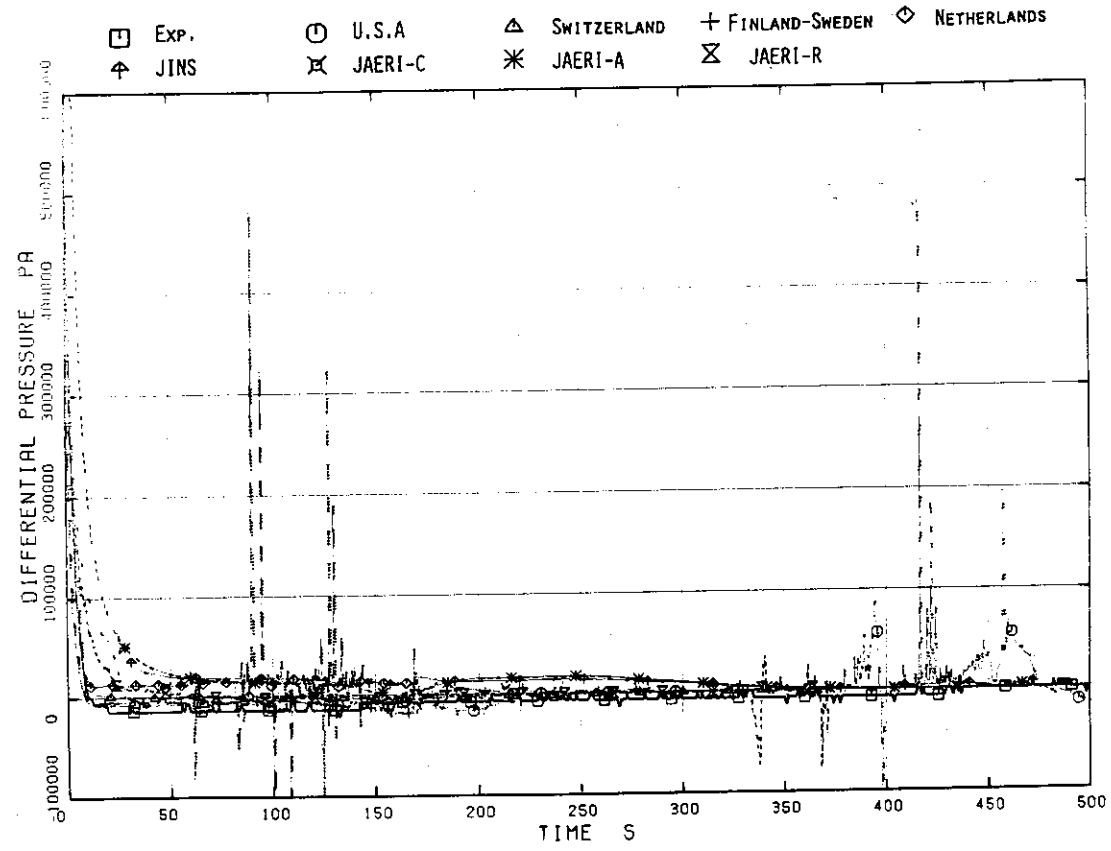

Fig.4.66 Differential Pressure between Broken Loop Jet Pump Drive and Suction

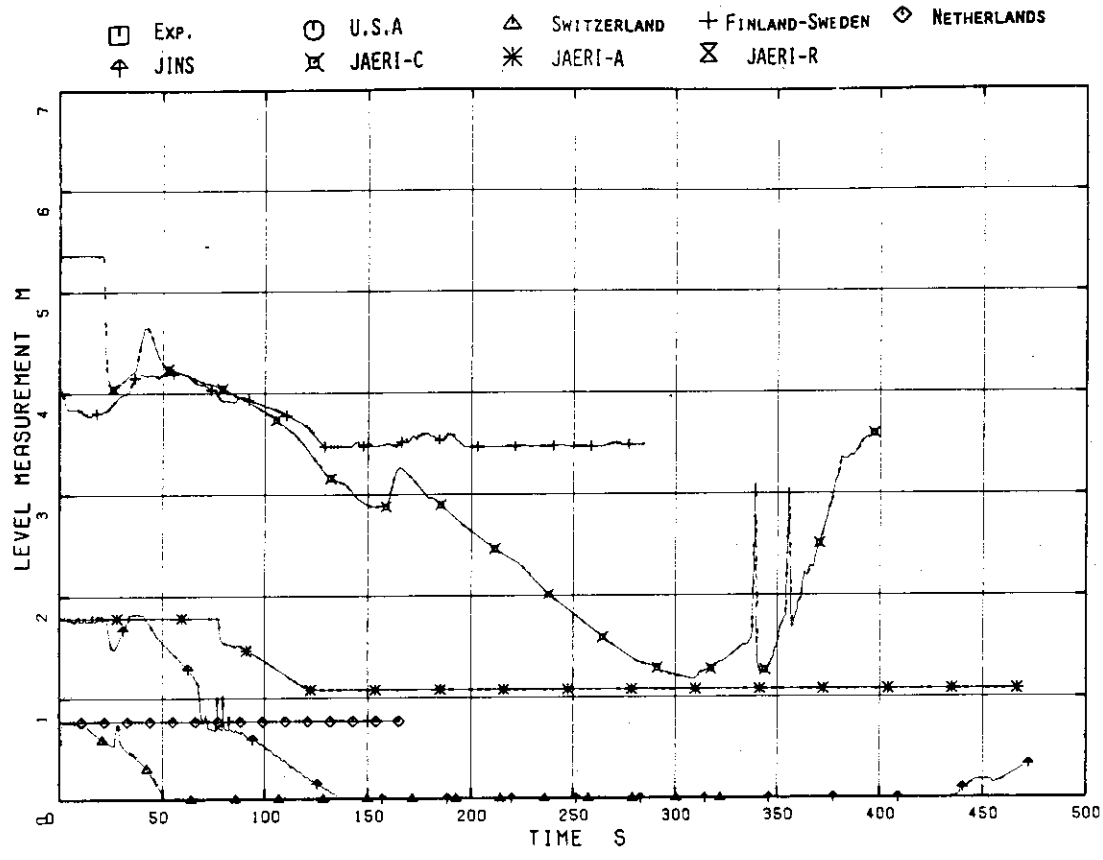

Fig.4.67 Mixture Level in Upper Plenum

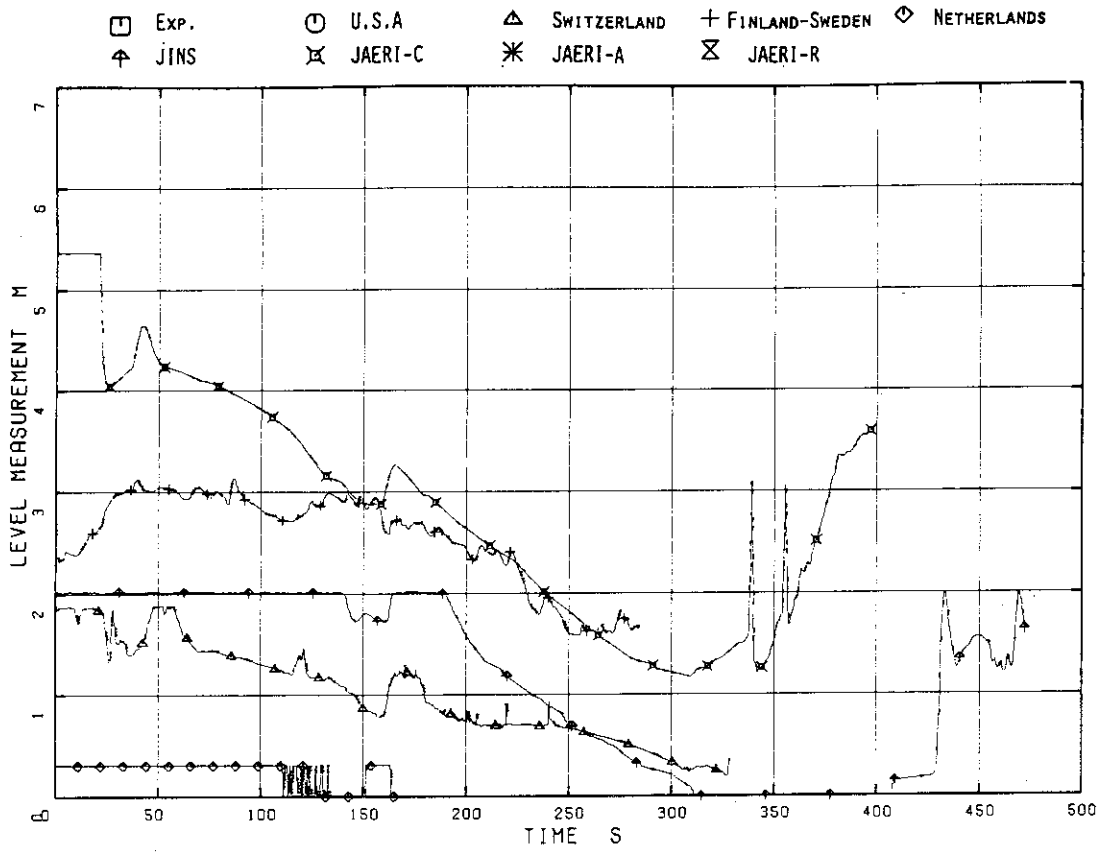

Fig.4.68(a) Mixture Level in High Power Channel

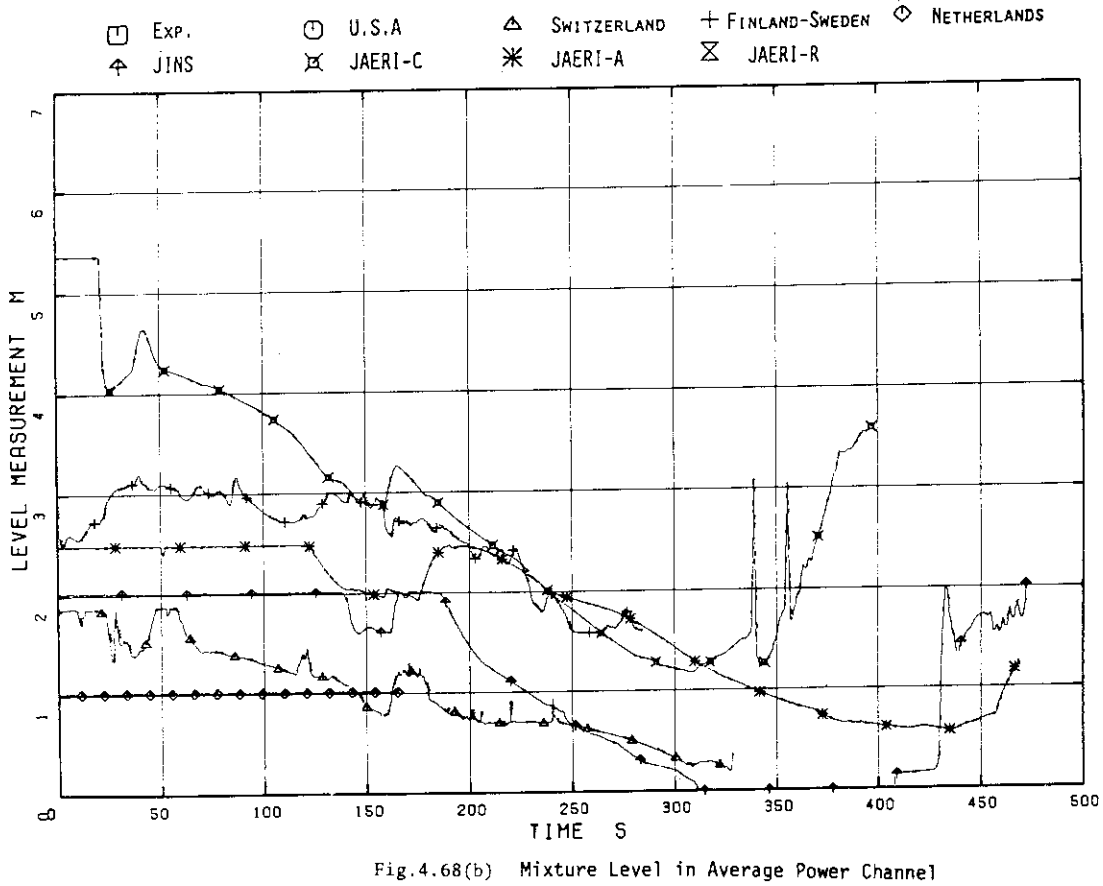

Fig.4.68(b) Mixture Level in Average Power Channel

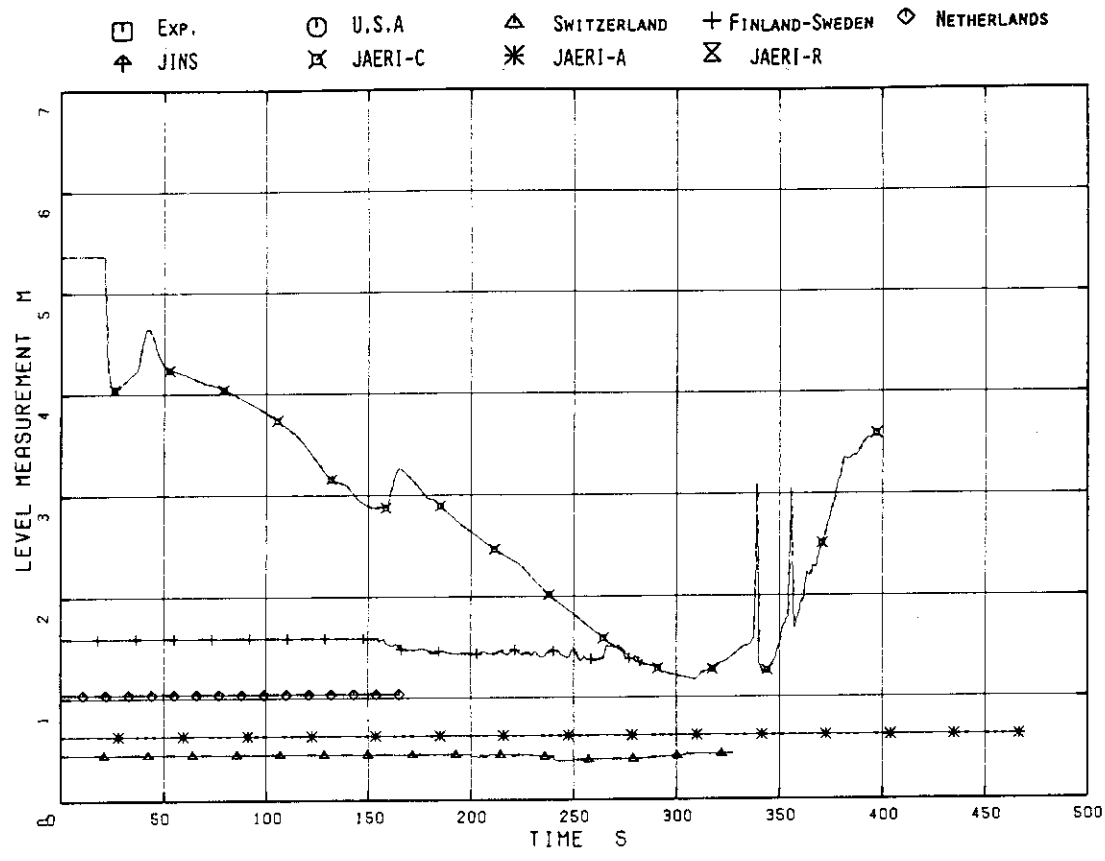

Fig.4.69 Mixture Level in Core Inlet Chamber

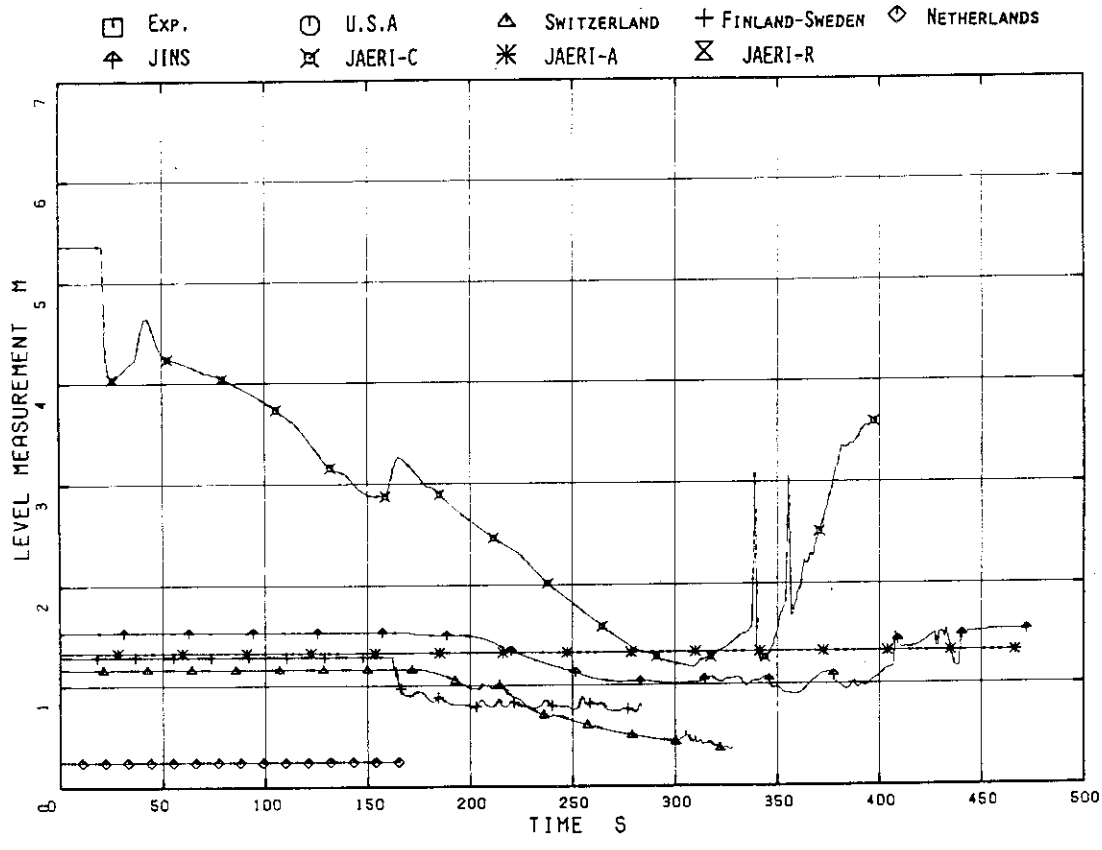

Fig.4.70 Mixture Level in Lower Plenum

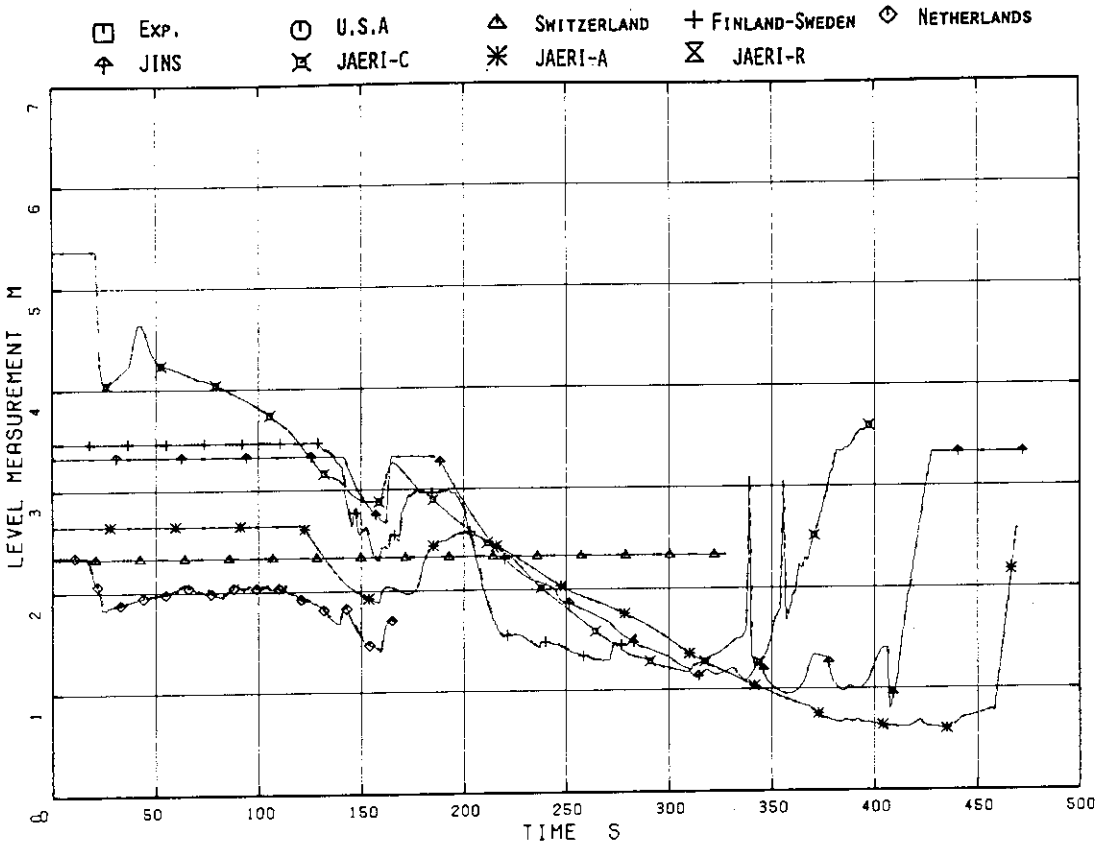

Fig.4.71 Mixture Level in Core Bypass

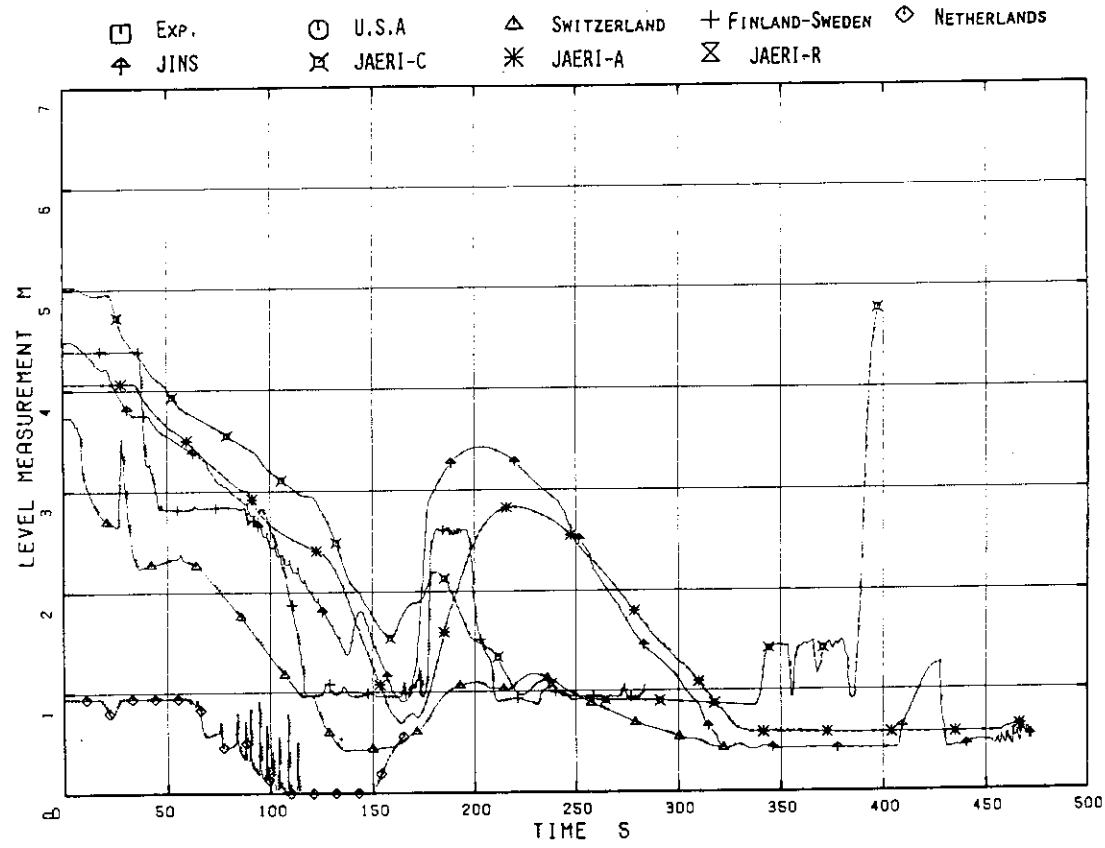

Fig.4.72 Mixture Level in Dowencomer

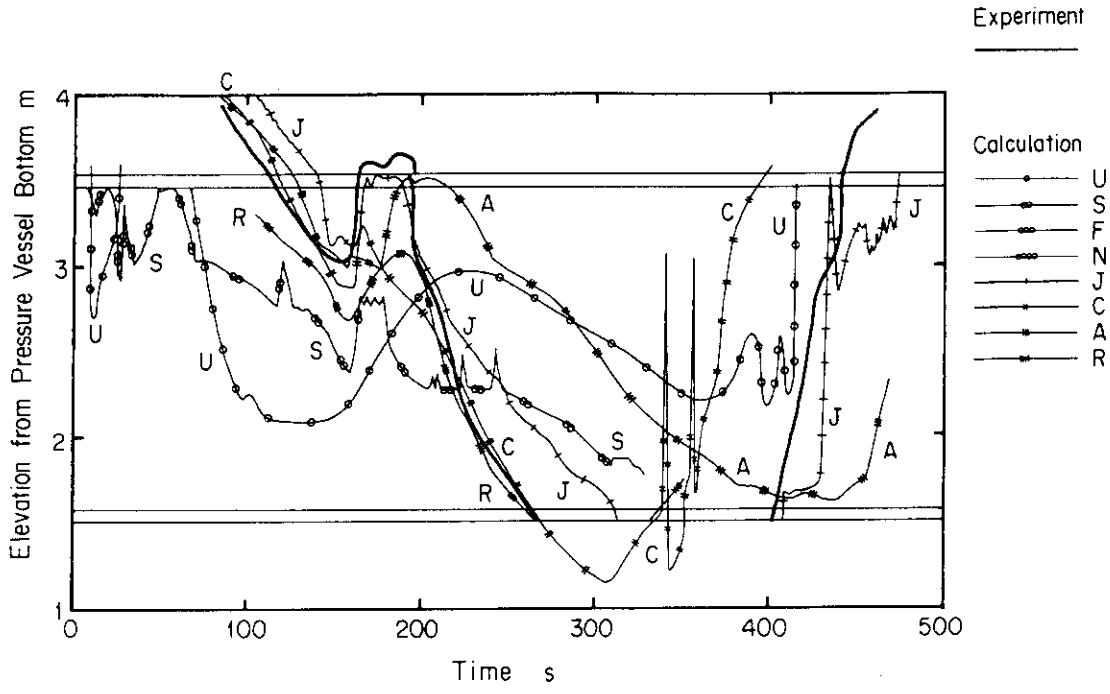

Fig. 4.73 Comparison of Calculated Mixture Level in the Core

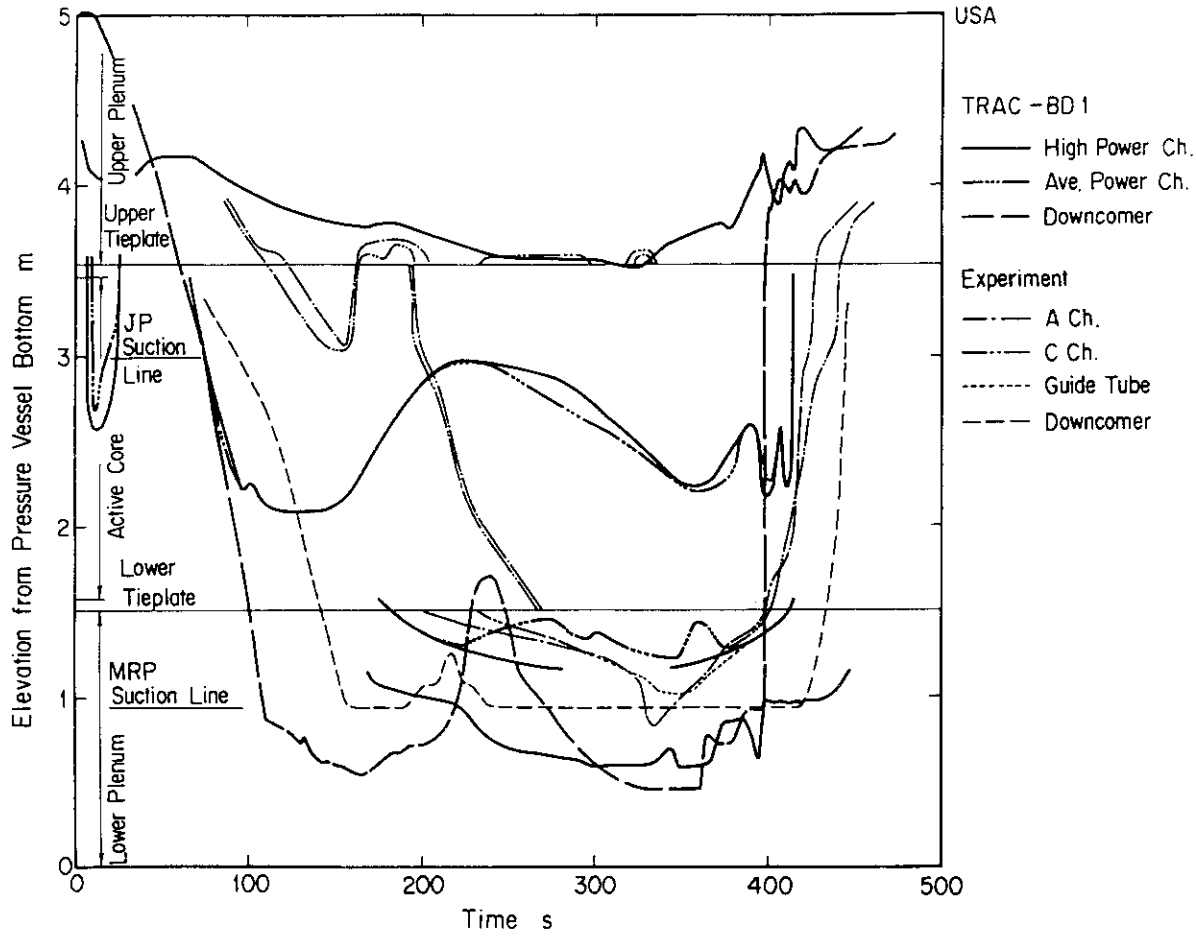

Fig.4.74 Mixture Level in USA Calculation

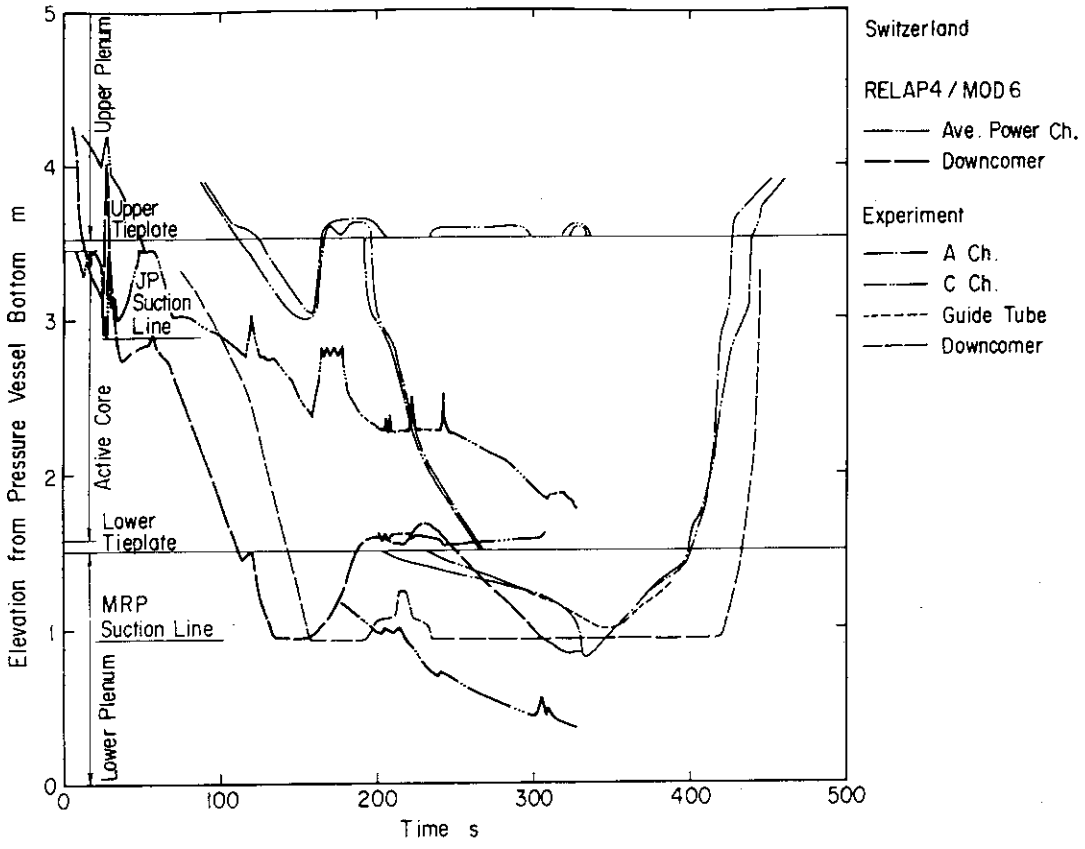

Fig.4.75 Mixture Level in Switzerland Calculation

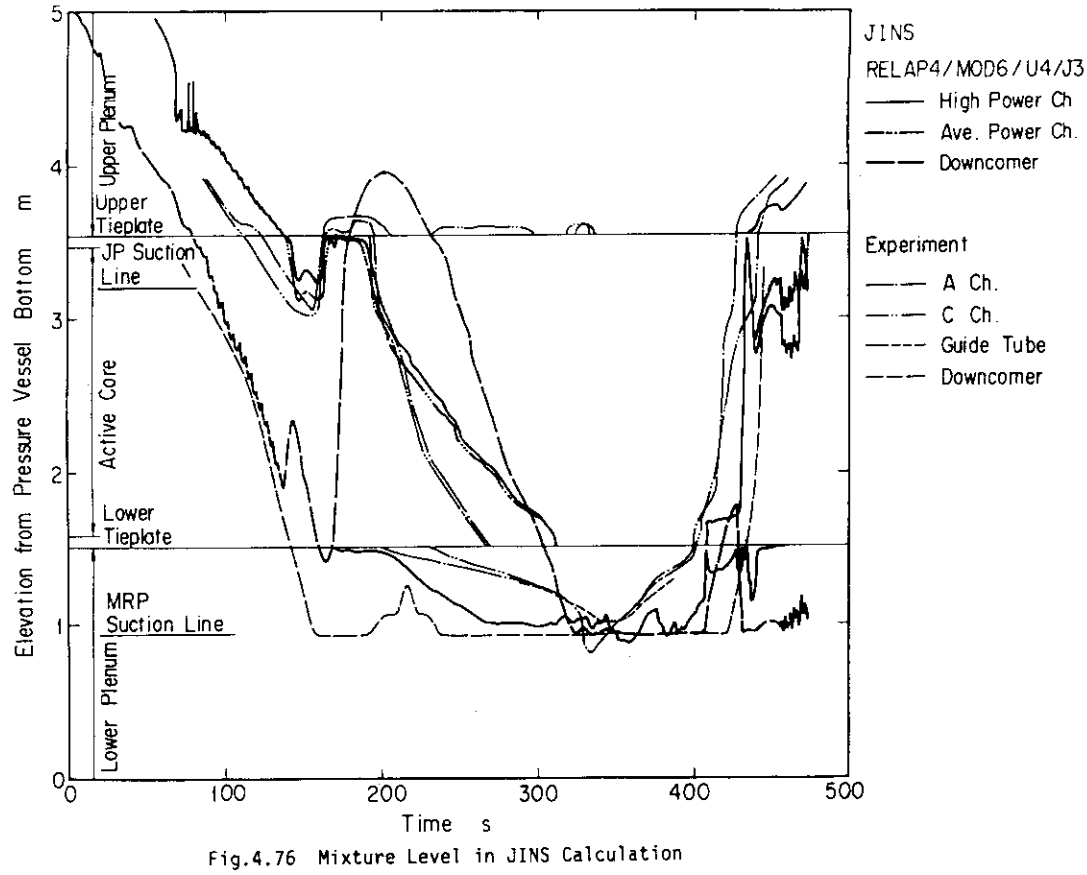

Fig.4.76 Mixture Level in JINS Calculation

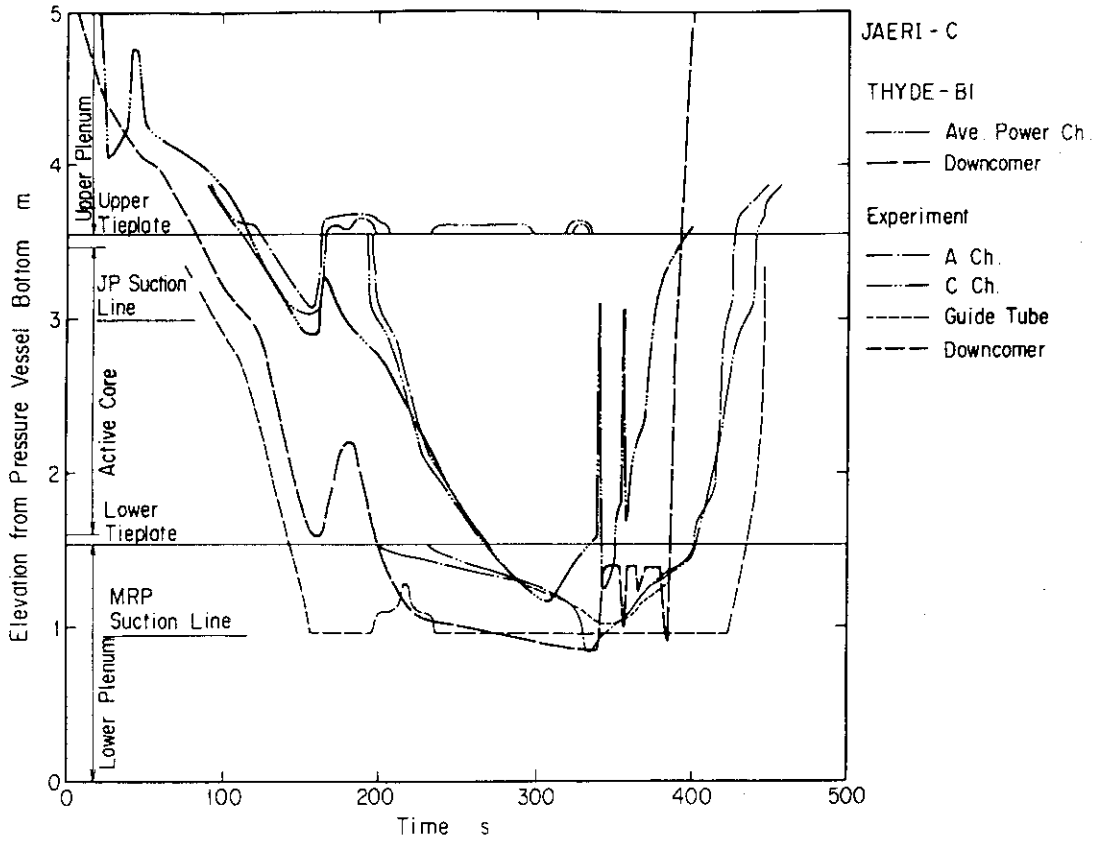

Fig.4.77 Mixture Level in JAERI-C Calculation

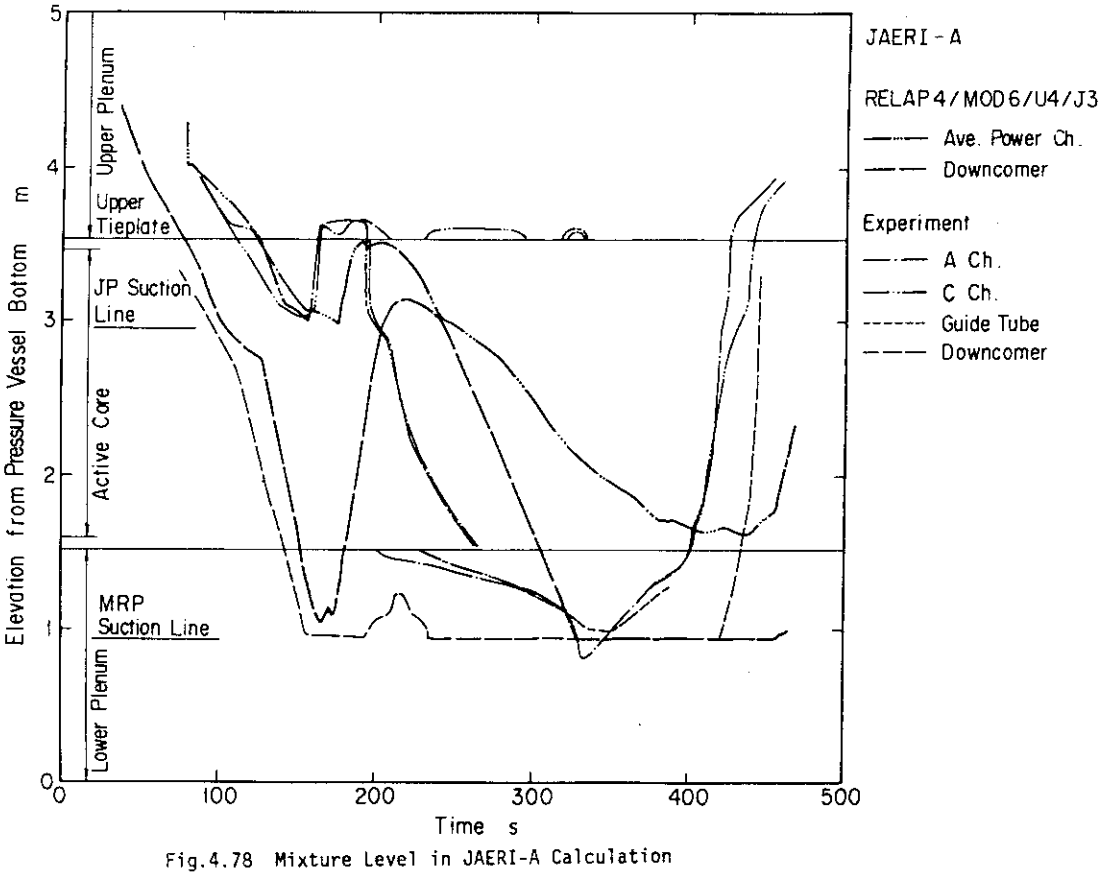

Fig.4.78 Mixture Level in JAERI-A Calculation

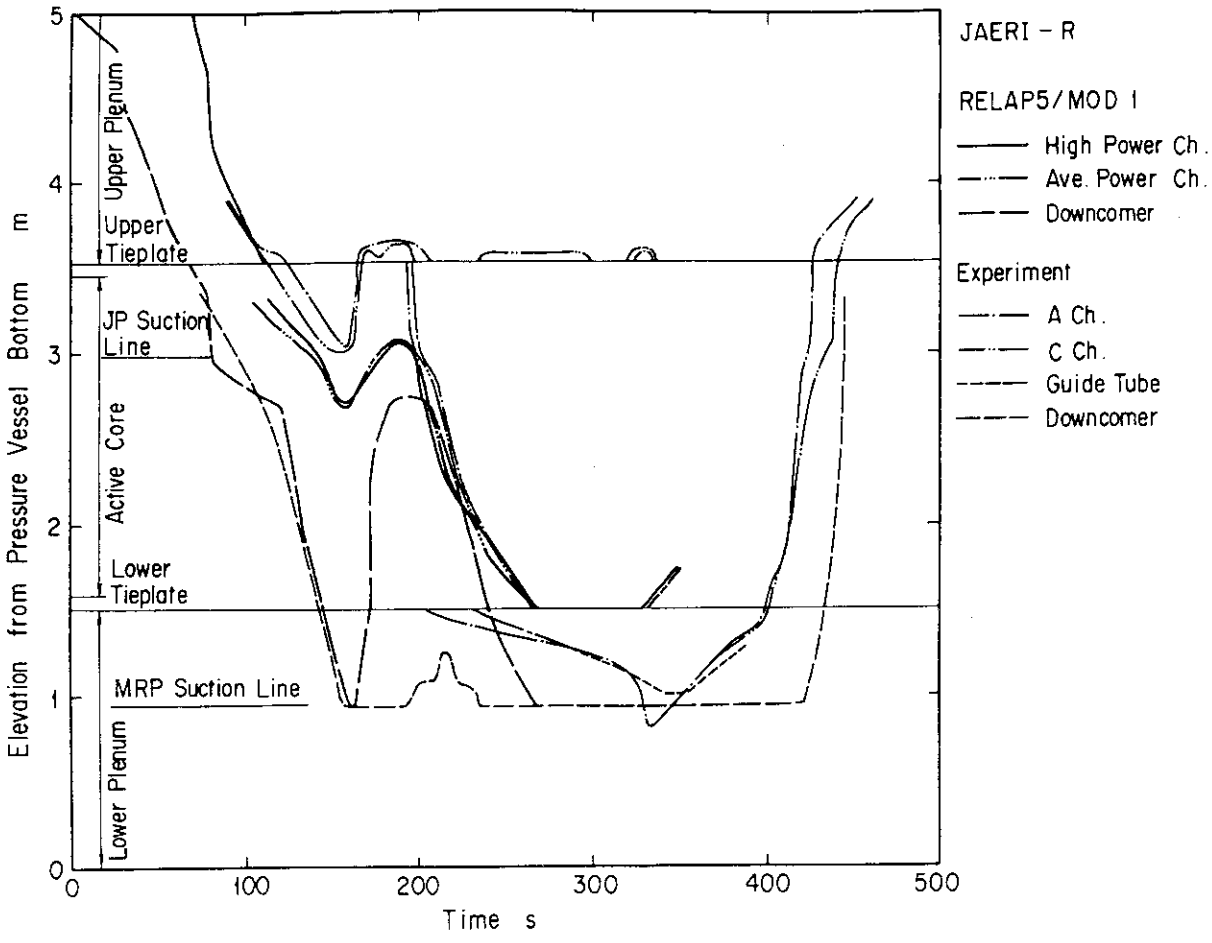

Fig.4.79 Mixture Level in JAERI-R Calculation

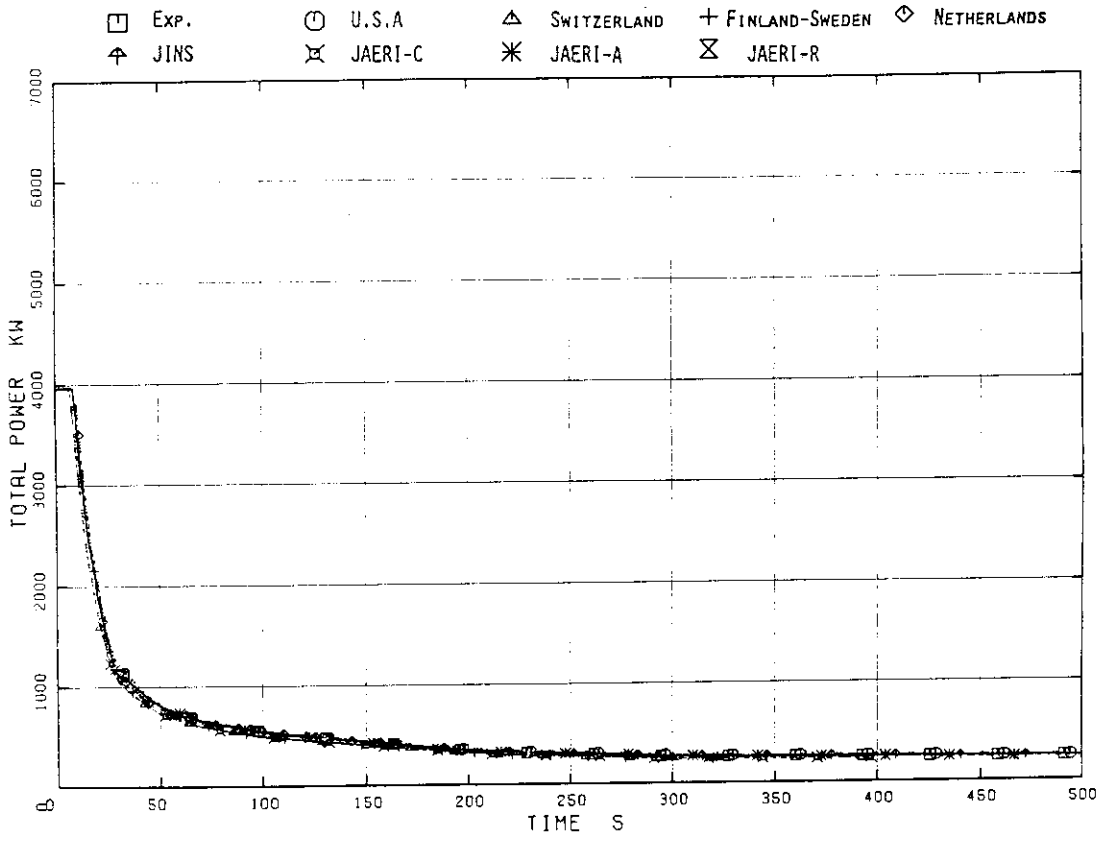

Fig.4.80 Core Power

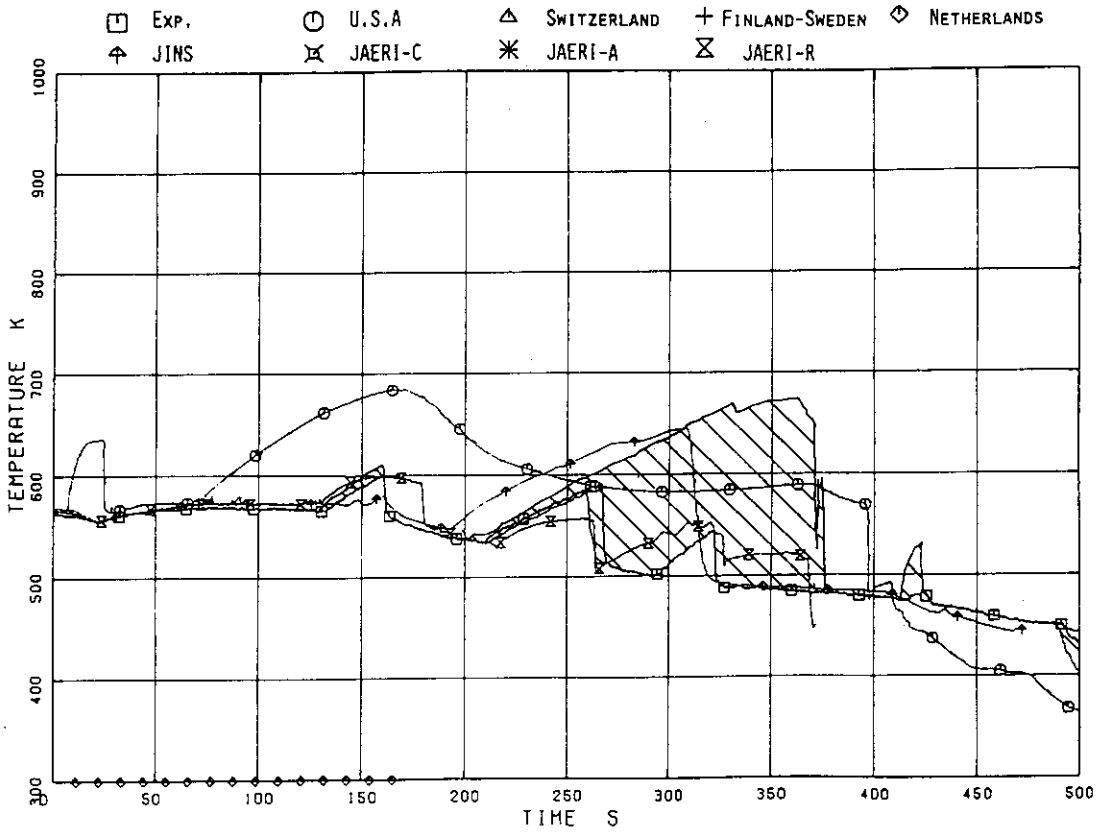

Fig.4.81 Rod Surface Temperature in High Power Channel ; L.P.F.=1.1 , Pos.1

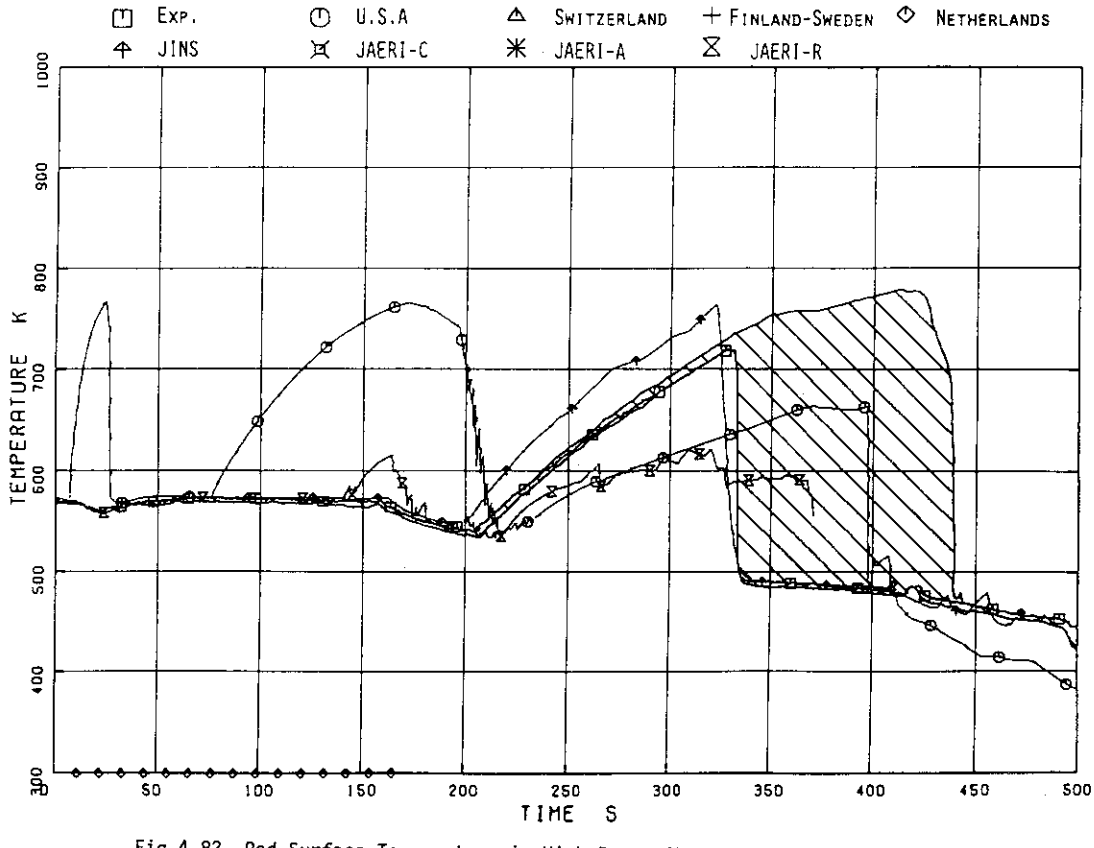

Fig.4.82 Rod Surface Temperature in High Power Channel ; L.P.F.=1.1 , Pos.2

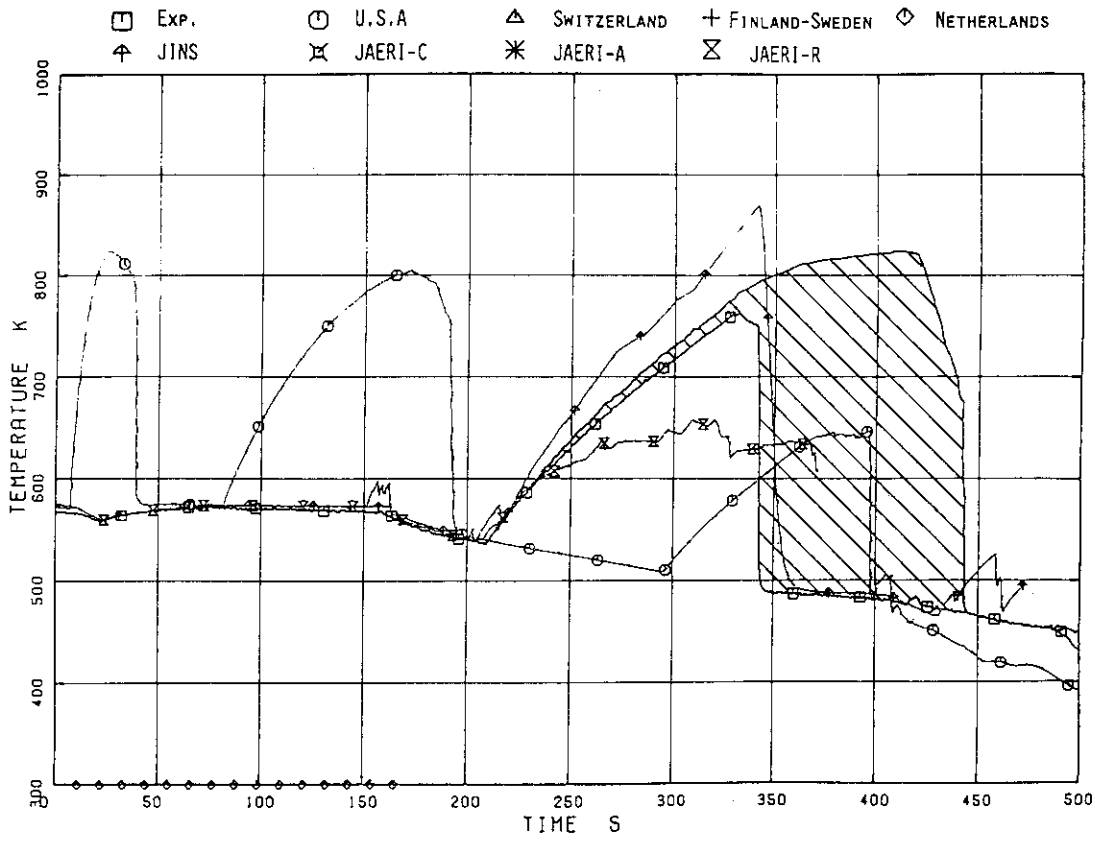

Fig.4.83 Rod Surface Temperature in High Power Channel ; L.P.F.=1.1 , Pos.3

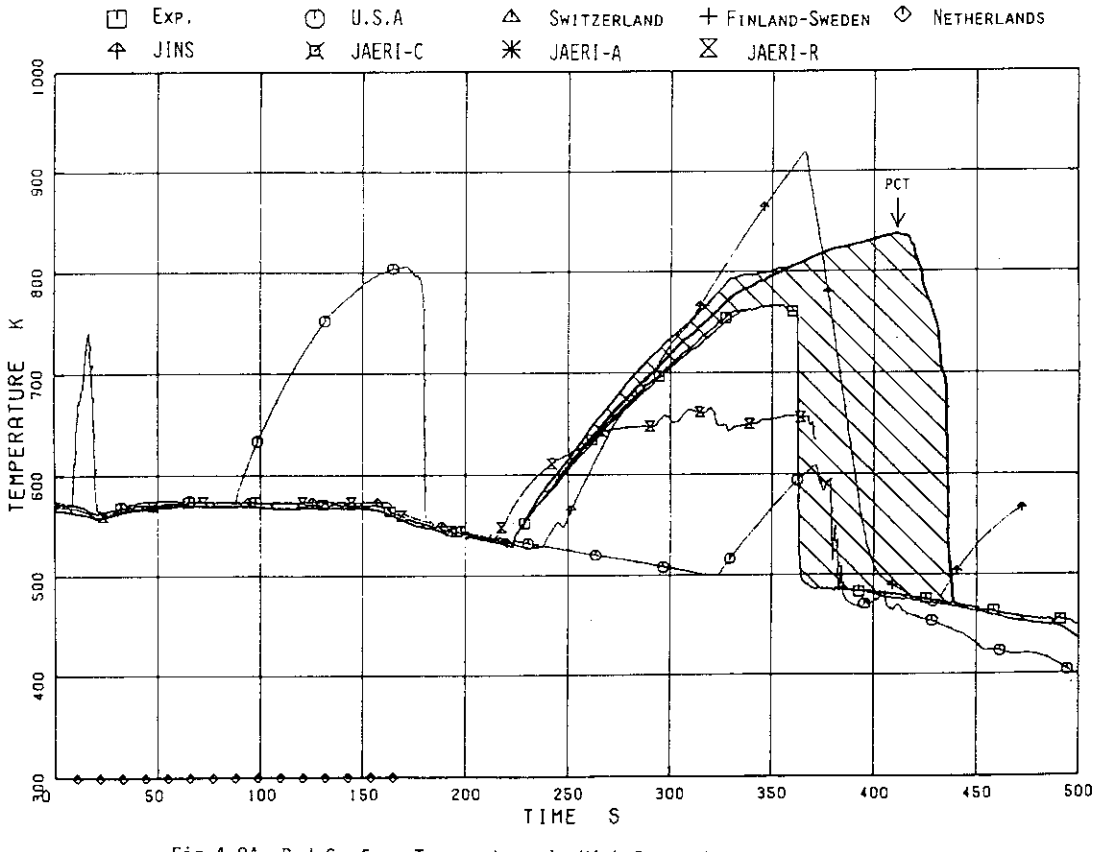

Fig.4.84 Rod Surface Temperature in High Power Channel ; L.P.F.=1.1 Pos.4

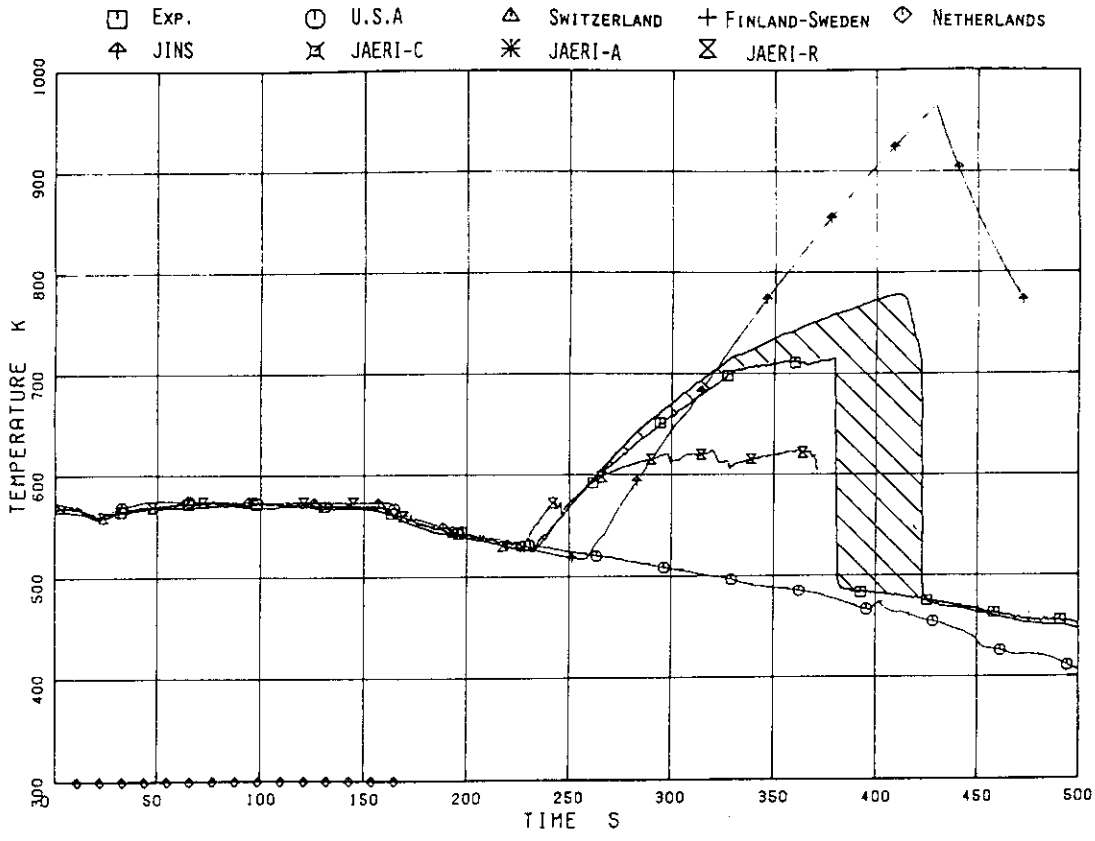

Fig.4.85 Rod Surface Temperature in High Power Channel ; L.P.F.=1.1 Pos.5

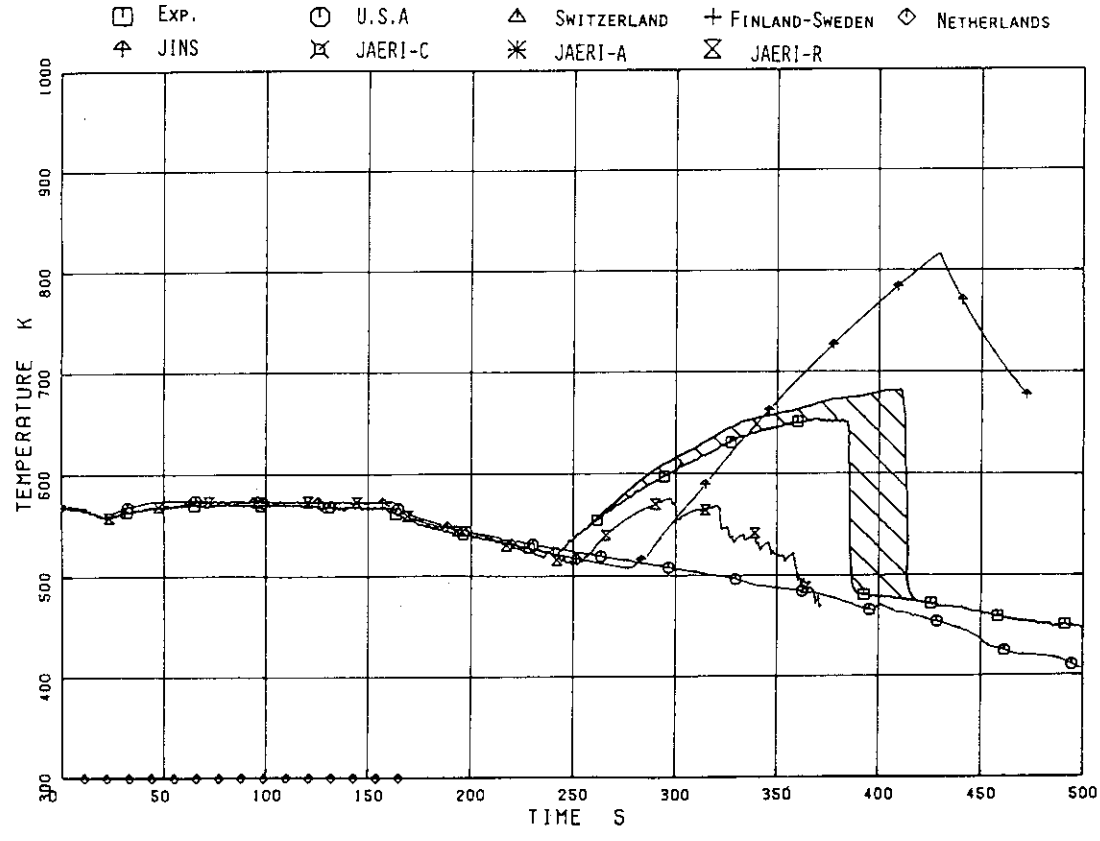

Fig.4.86 Rod Surface Temperature in High Power Channel ; L.P.F.=1.1 , Pos.6

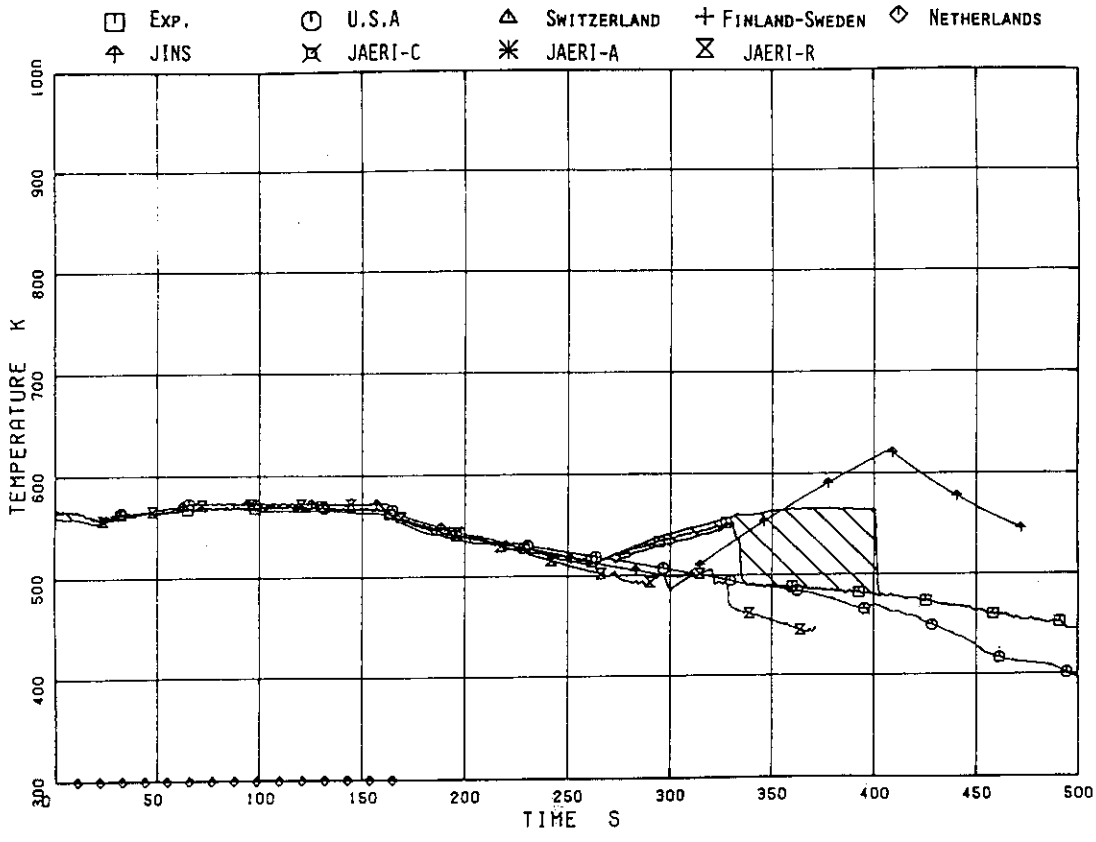

Fig.4.87 Rod Surface Temperature in High Power Channel ; L.P.F.=1.1 , Pos.7

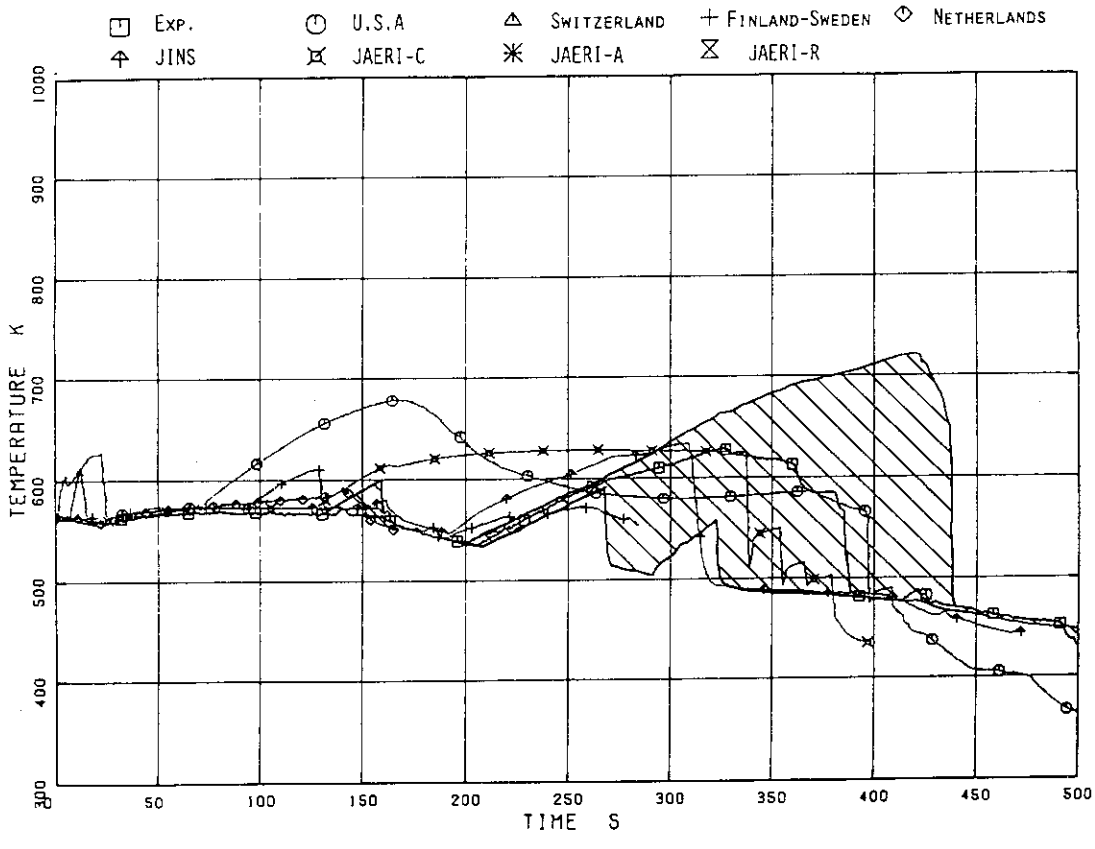

Fig.4.88 Rod Surface Temperature in High Power Channel ; L.P.F.=1.0 , Pos.1

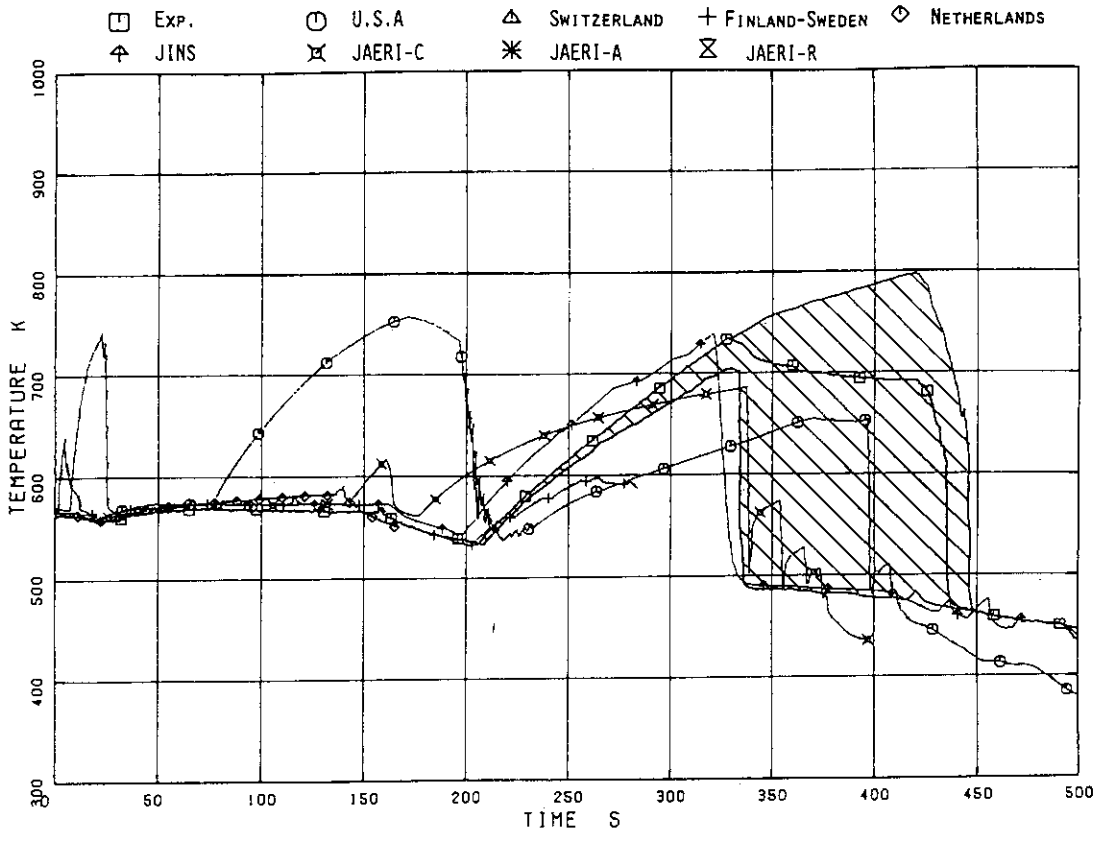

Fig.4.89 Rod Surface Temperature in High Power Channel ; L.P.F.=1.0 , Pos.2

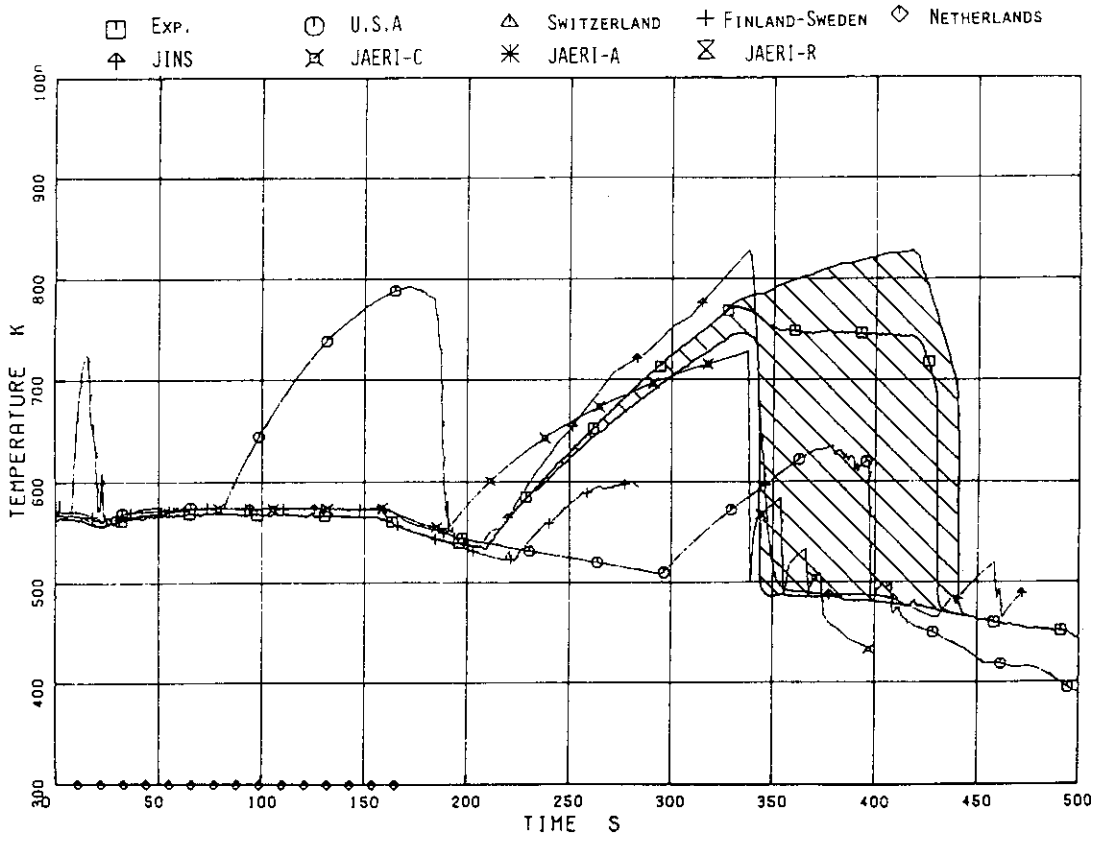

Fig.4.90 Rod Surface Temperature in High Power Channel ; L.P.F.=1.0 , Pos.3

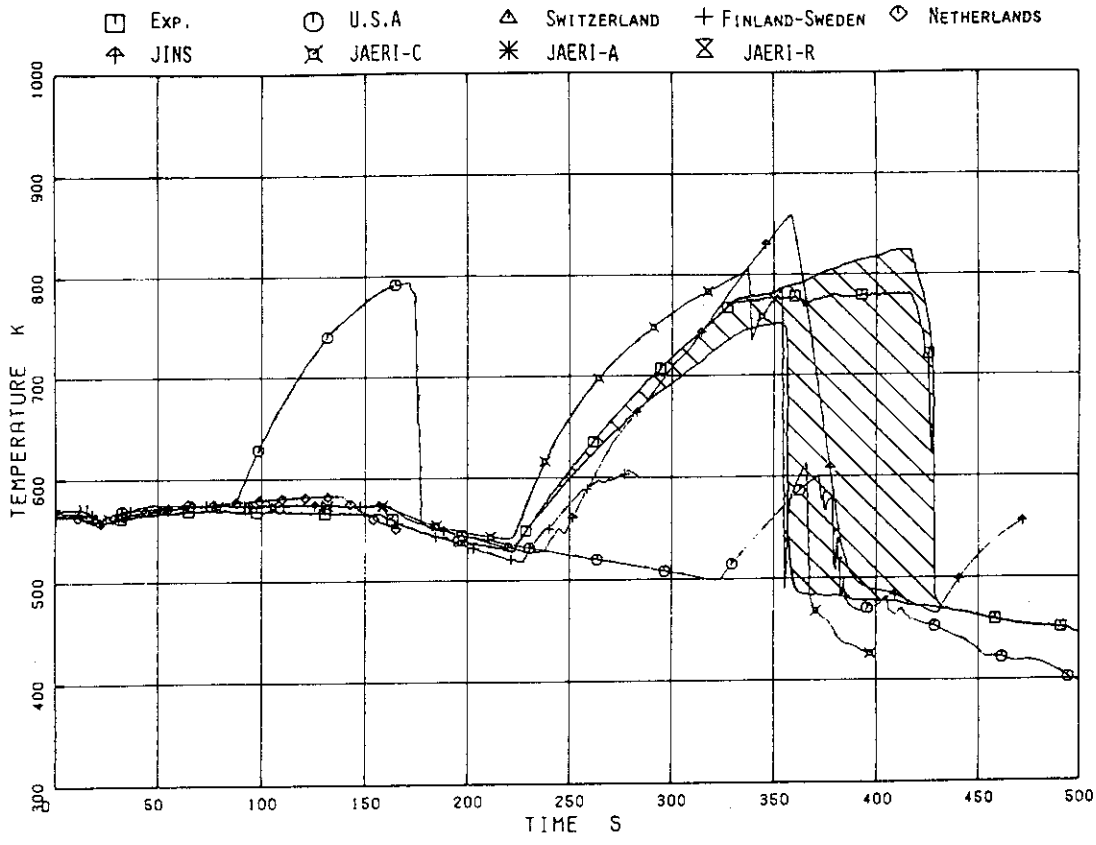

Fig.4.91 Rod Surface Temperature in High Power Channel ; L.P.F.=1.0 , Pos.4

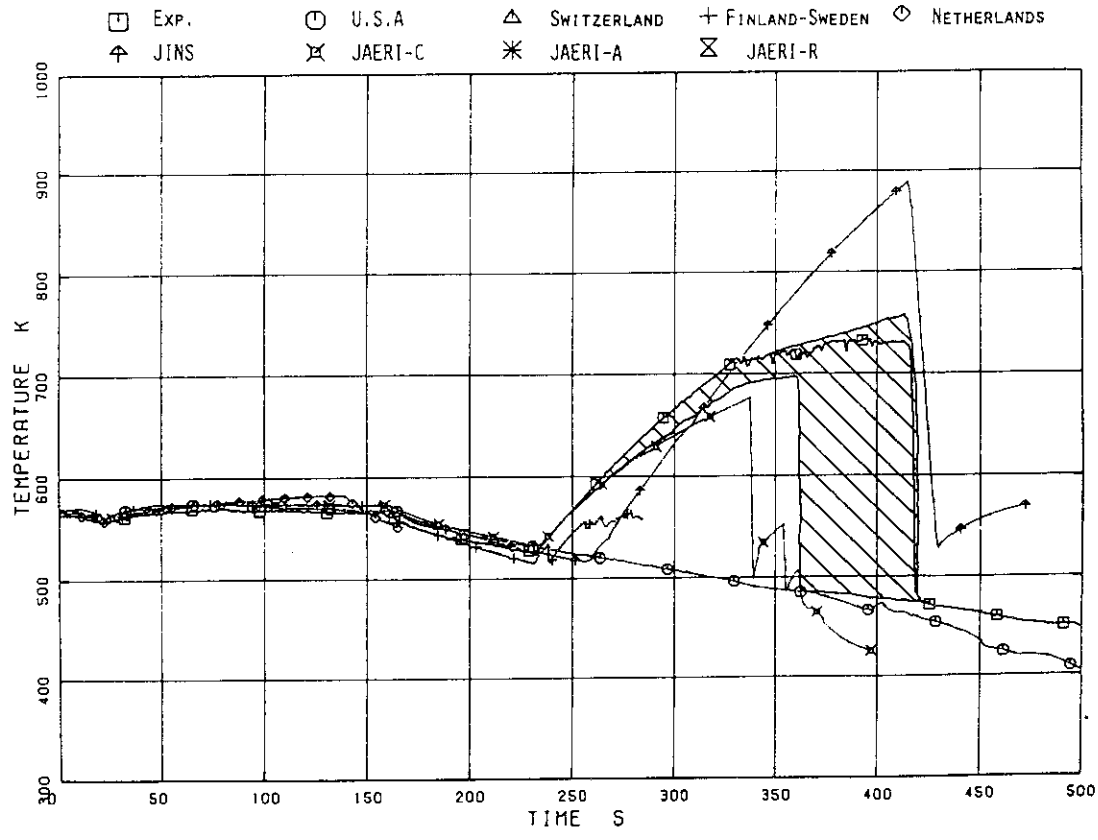

Fig.4.92 Rod Surface Temperature in High Power Channel ; L.P.F.=1.0 , Pos.5

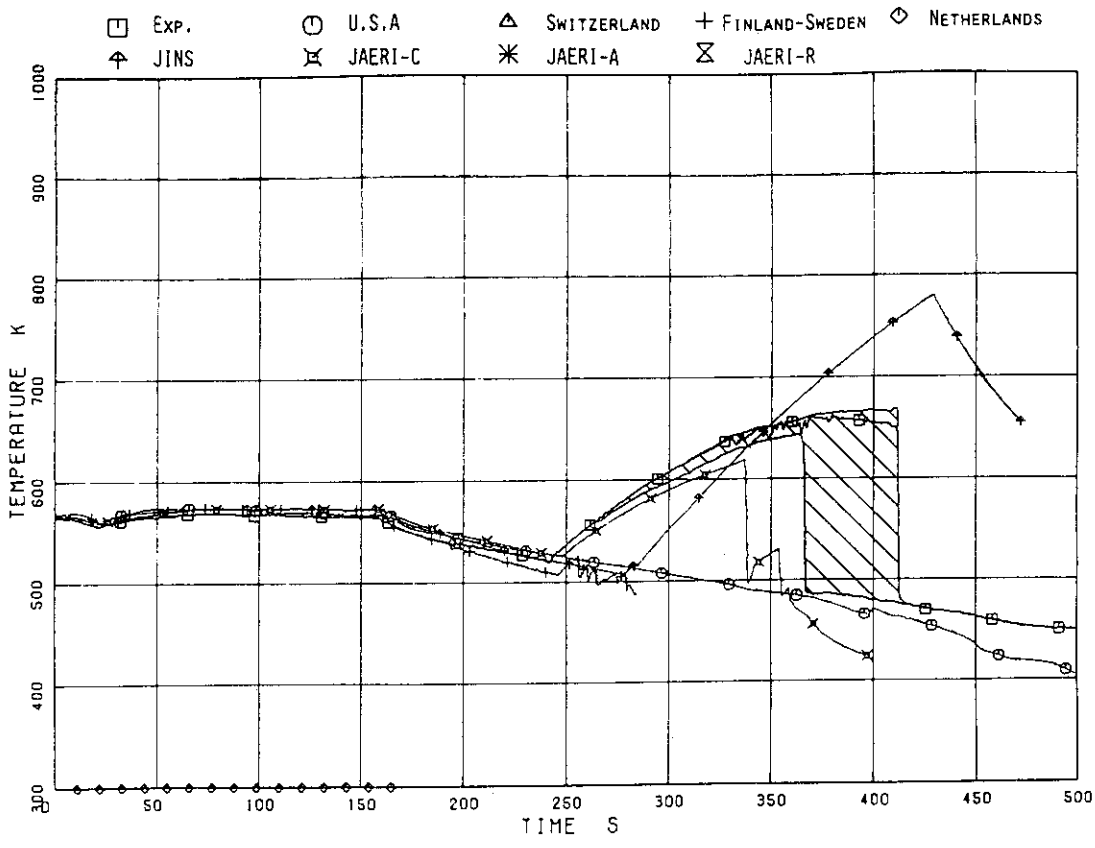

Fig.4.93 Rod Surface Temperature in High Power Channel ; L.P.F.=1.0 , Pos.6

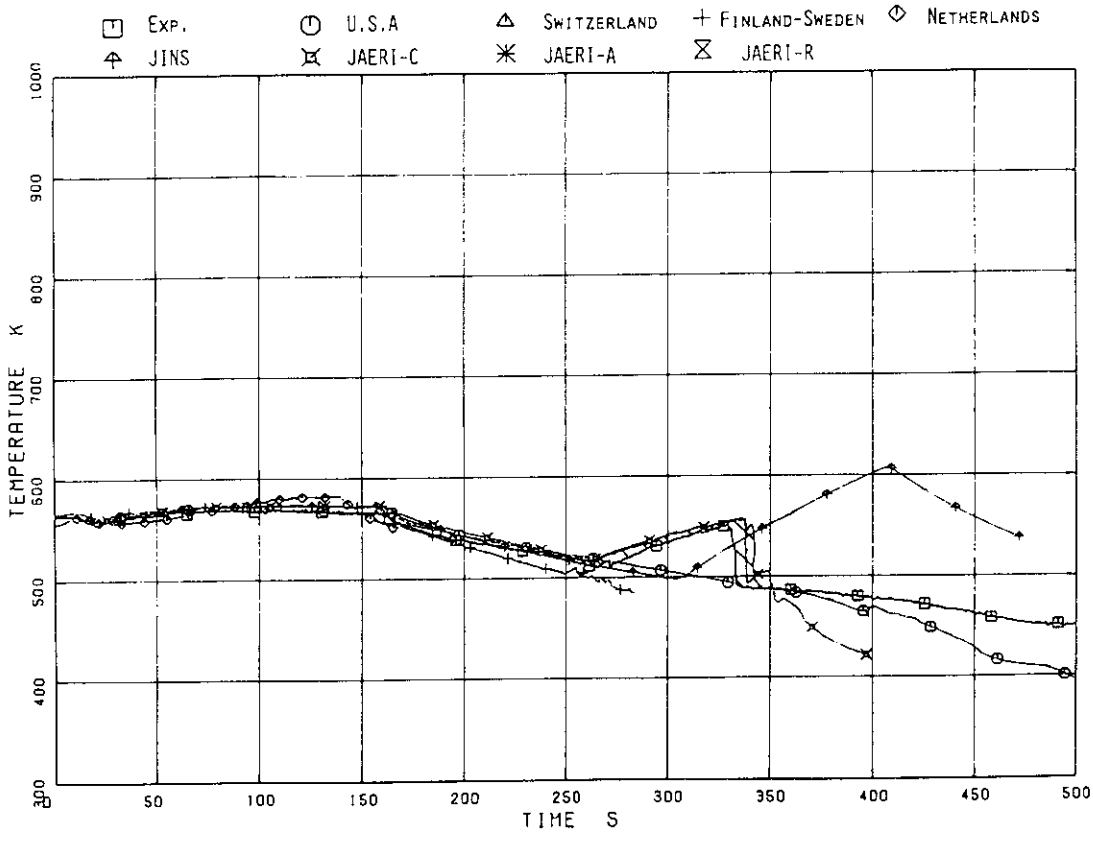

Fig.4.94 Rod Surface Temperature in High Power Channel ; L.P.F.=1.0 , Pos.7

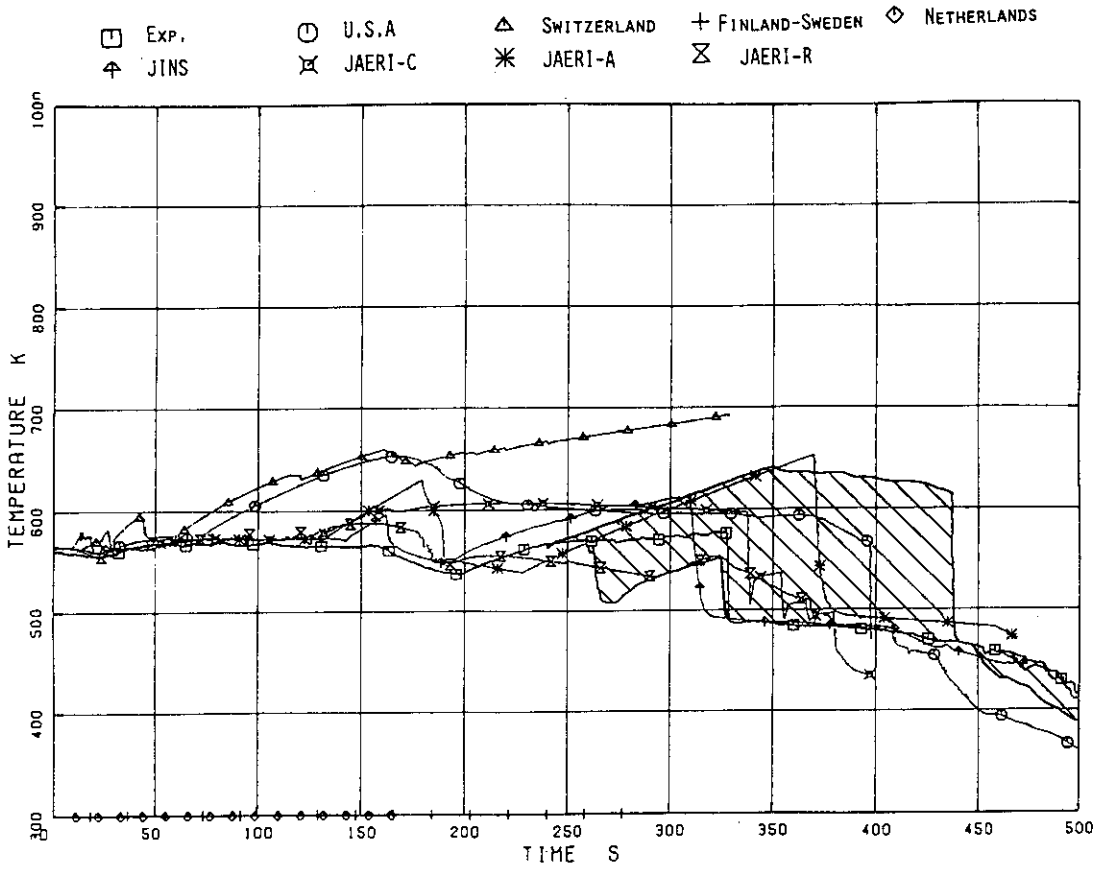

Fig.4.95 Rod Surface Temperature in High Power Channel

(L.P.F.=0.875 , Pos.1)

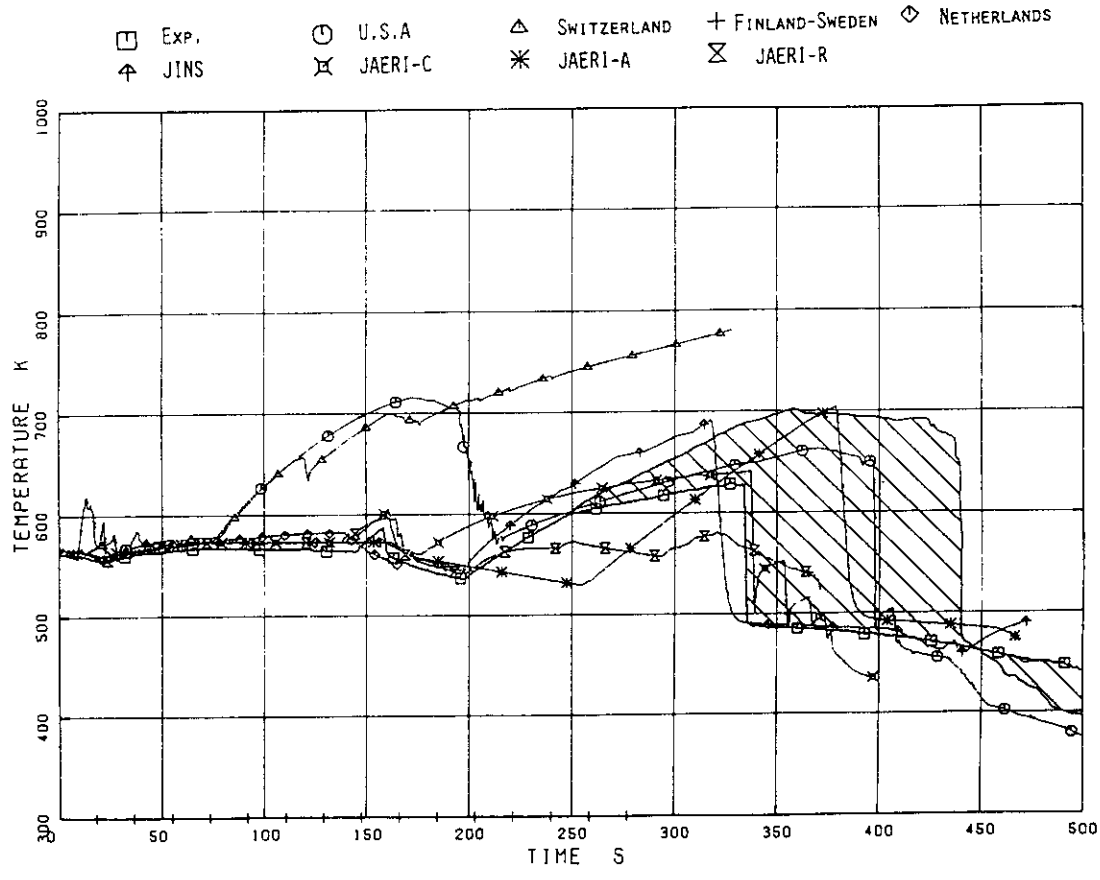

Fig.4.96 Rod Surface Temperature in High Power Channel

(L.P.F.=0.875 , Pos.2)

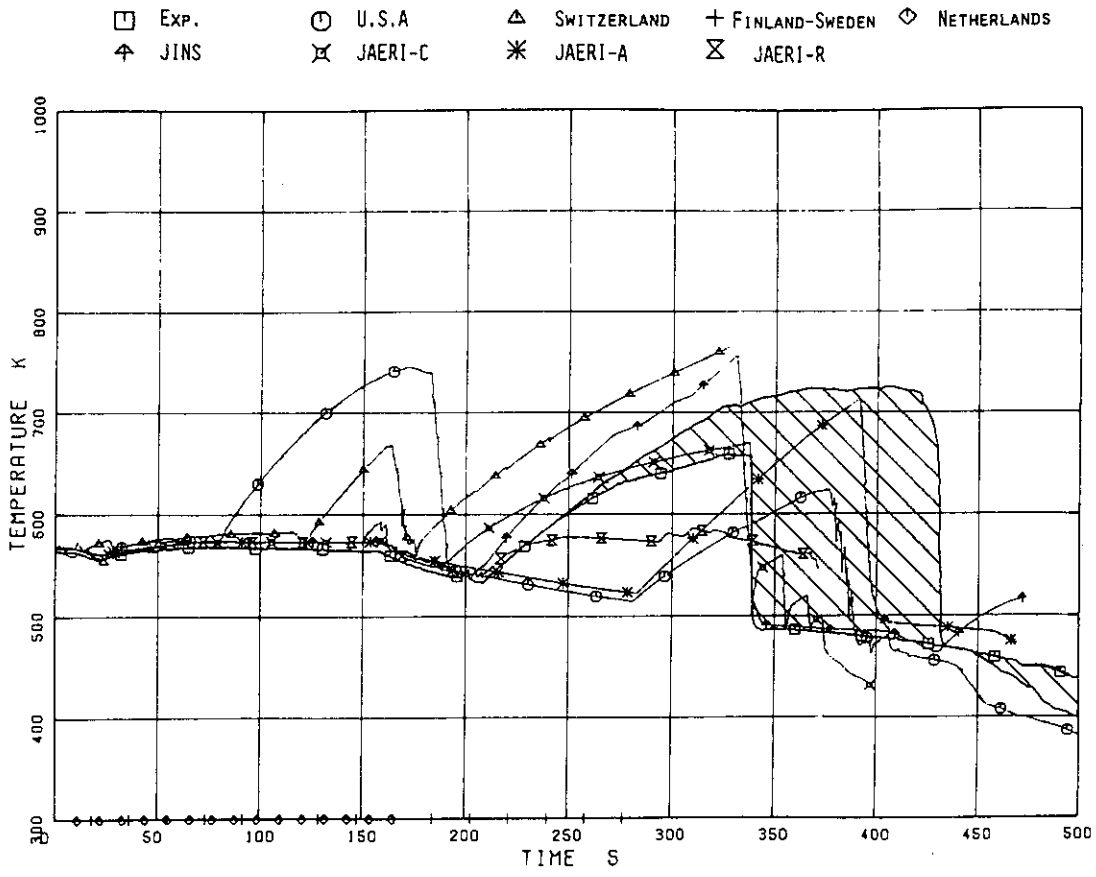

Fig.4.97 Rod Surface Temperature in High Power Channel

(L.P.F.=0.875 , Pos.3)

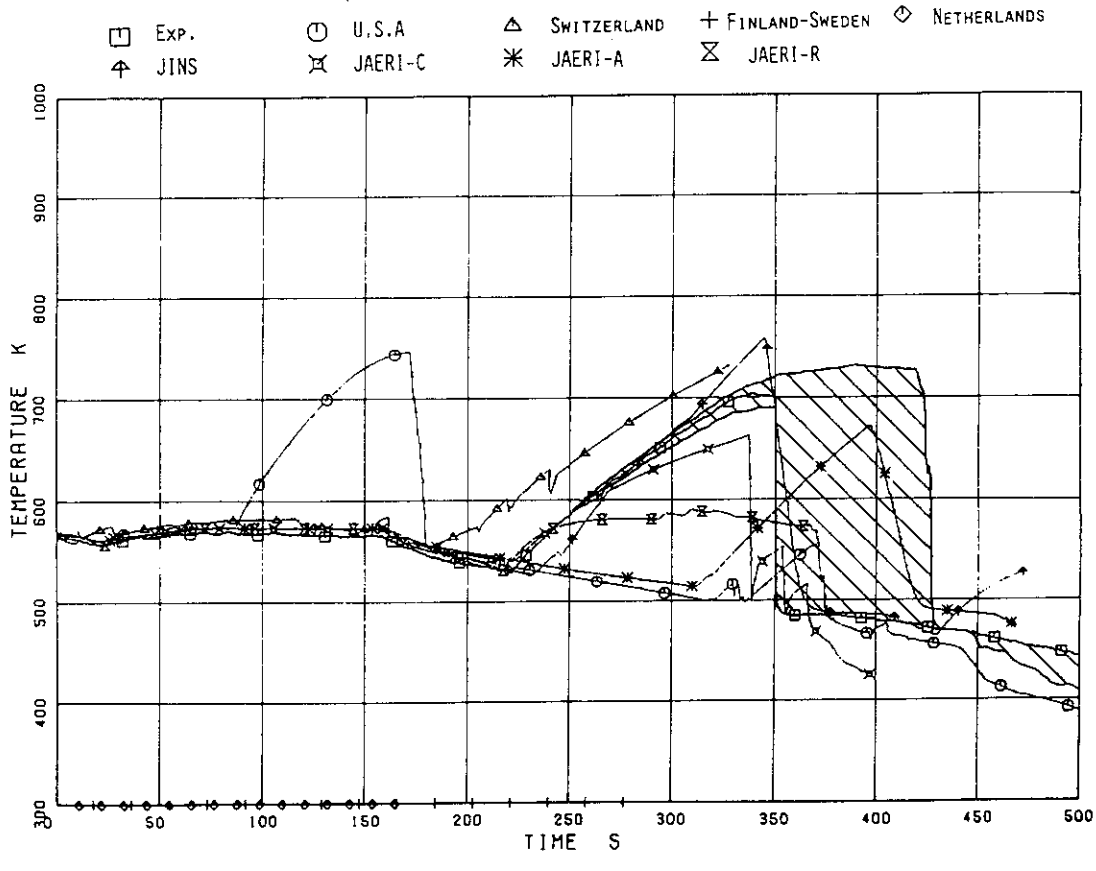

Fig.4.98 Ros Surface Temperature in High Power Channel

(L.P.F.=0.875 , Pos.4)

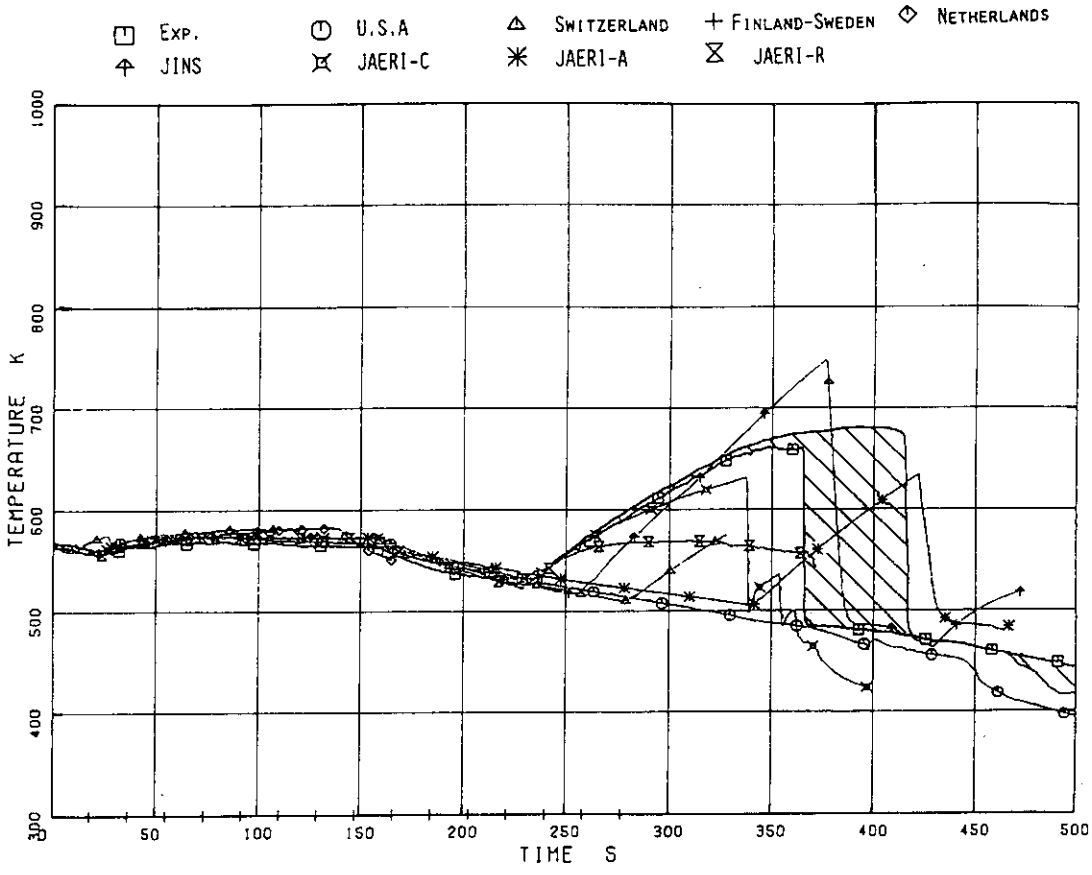

Fig.4.99 Rod Surface Temperature in High Power Channel

(L.P.F.=0.875 , Pos.5)

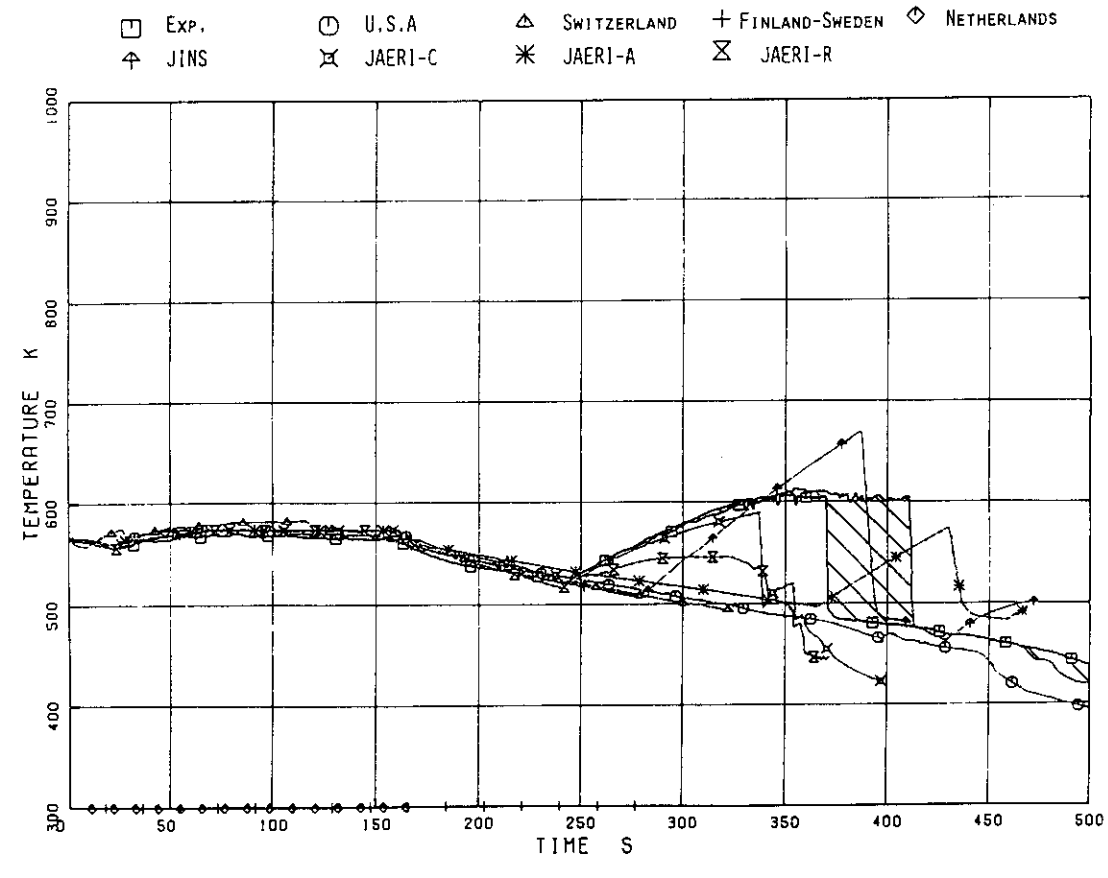

Fig.4.100 Rod Surface Temperature in High Power Channel

(L.P.F.=0.875 , Pos.6)

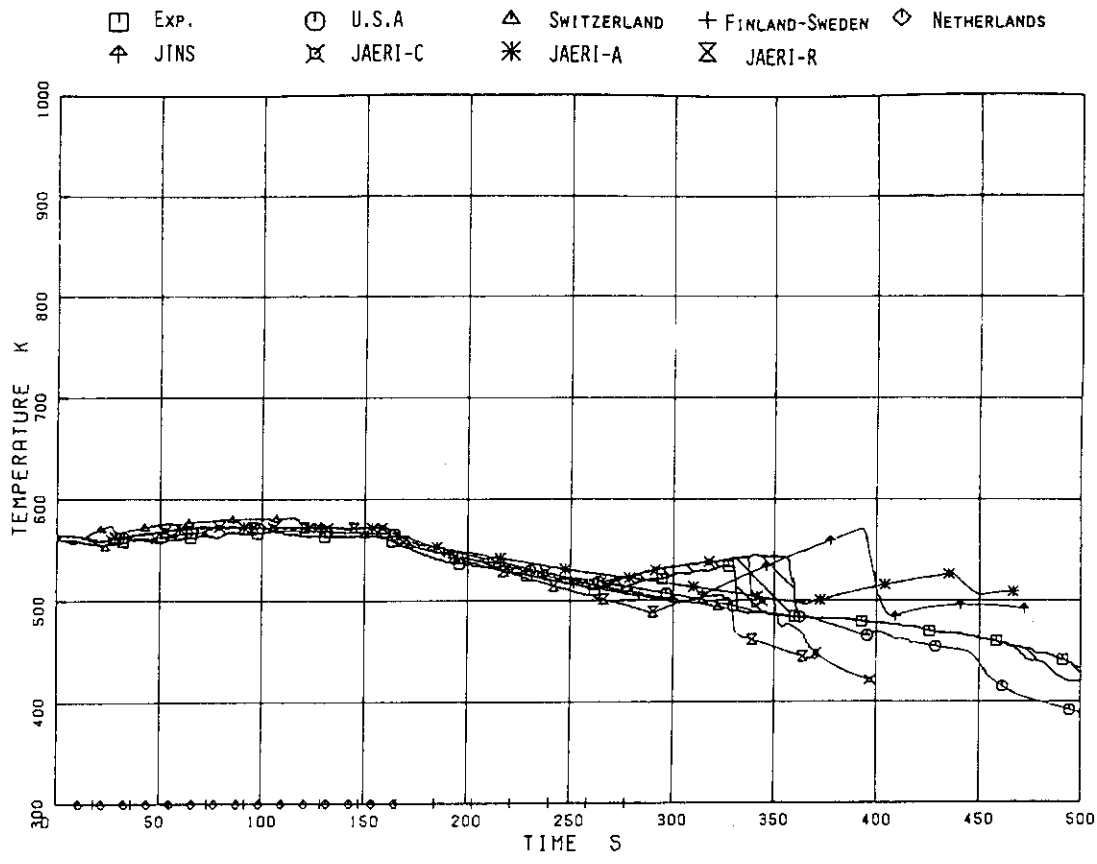

Fig.4.101 Rod Surface Temperarure in High Power Channel

(L.P.F.=0.875 , Pos.7)

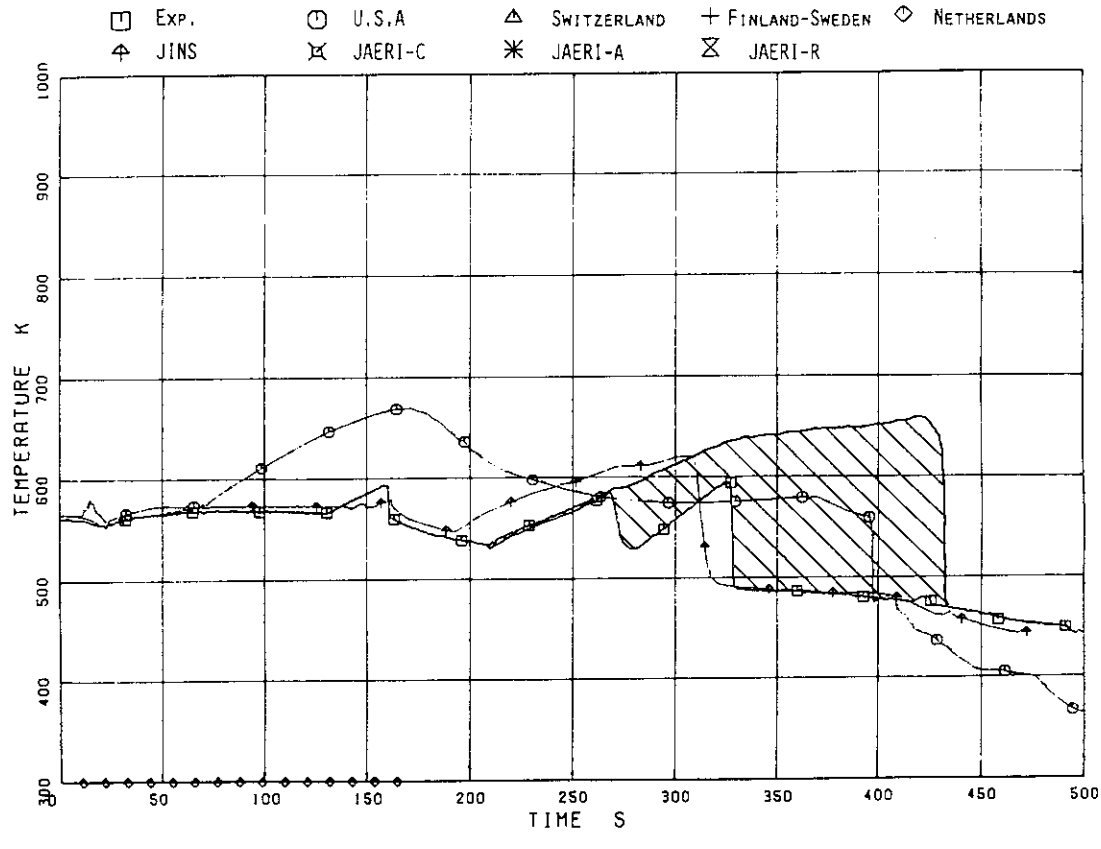

Fig.4.102 Rod Surface Temperature in Average Power Channel ; (L.P.F.=1.0 , Pos.1)

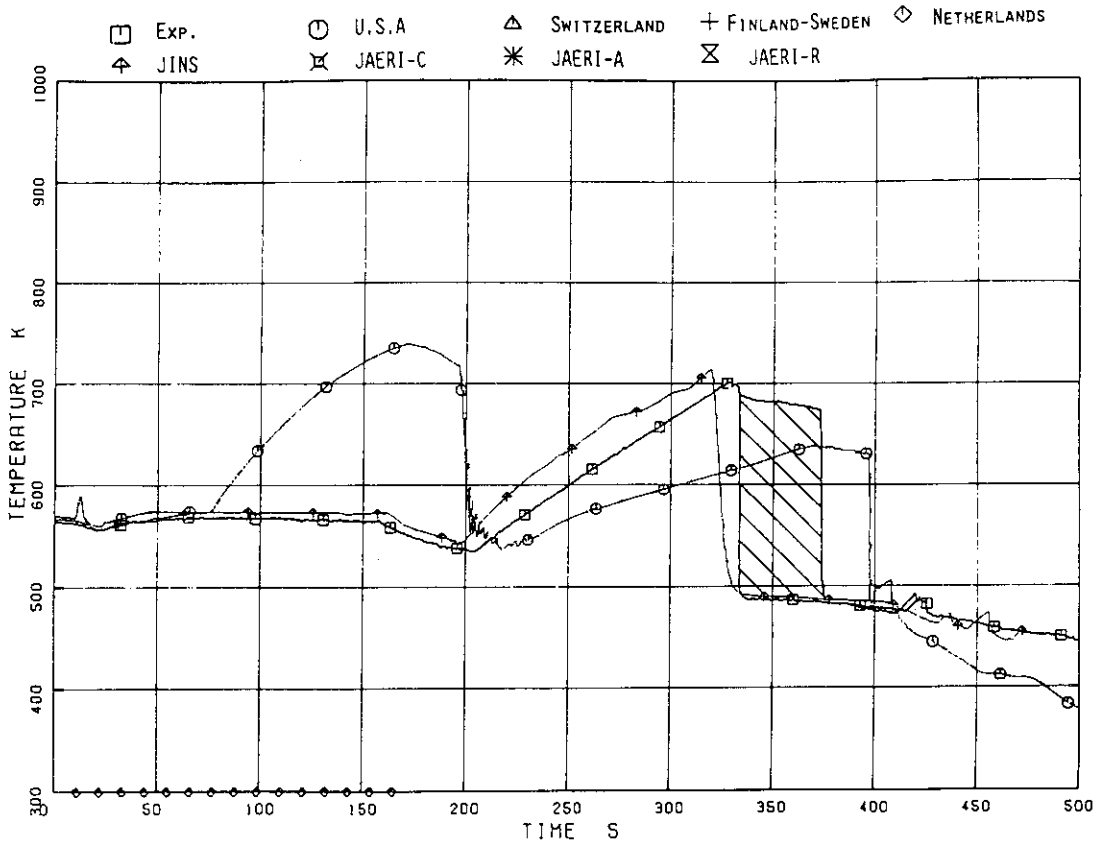

Fig.4.103 Rod Surface Temperature in Average Power Channel (L.P.F.=1.0 , Pos.2)

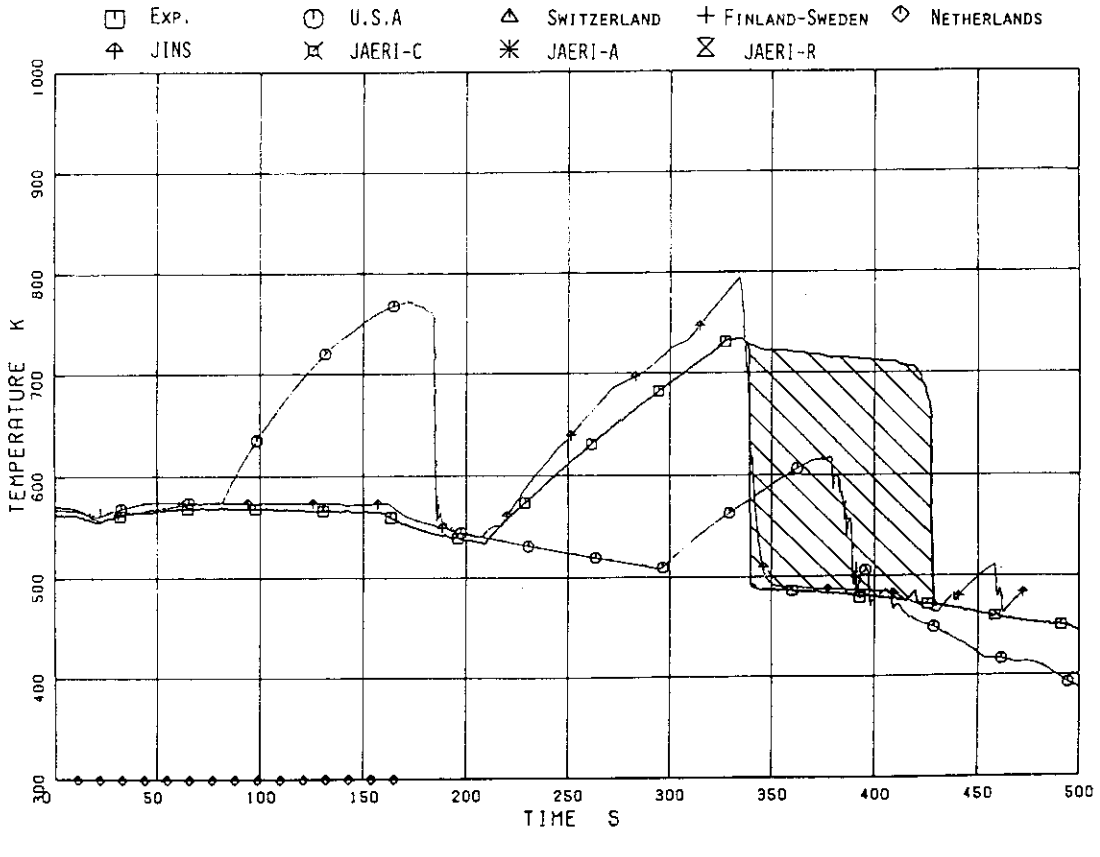

Fig.4.104 Rod Surface Temperature in Average Power Channel (L.P.F=1.0 , Pos.3)

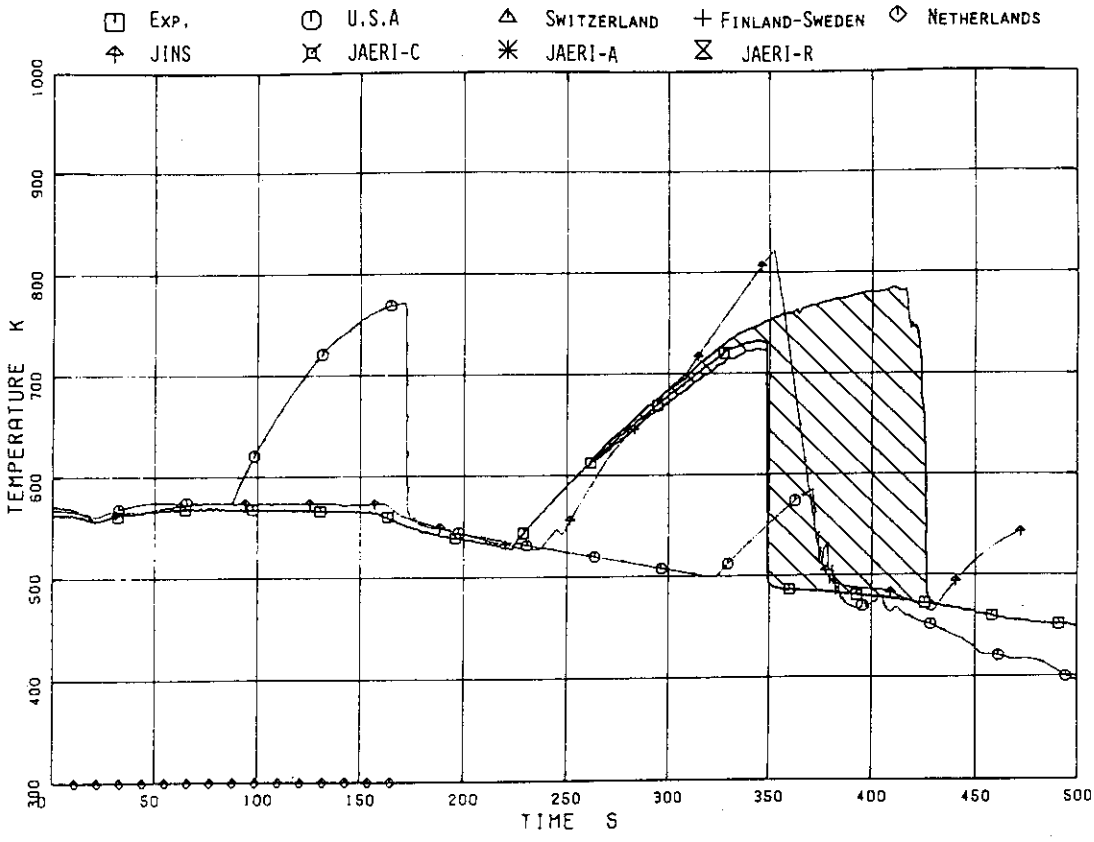

Fig.4.105 Rod Surface Temperature in Average Power Channel (L.P.F.=1.0 , Pos.4)

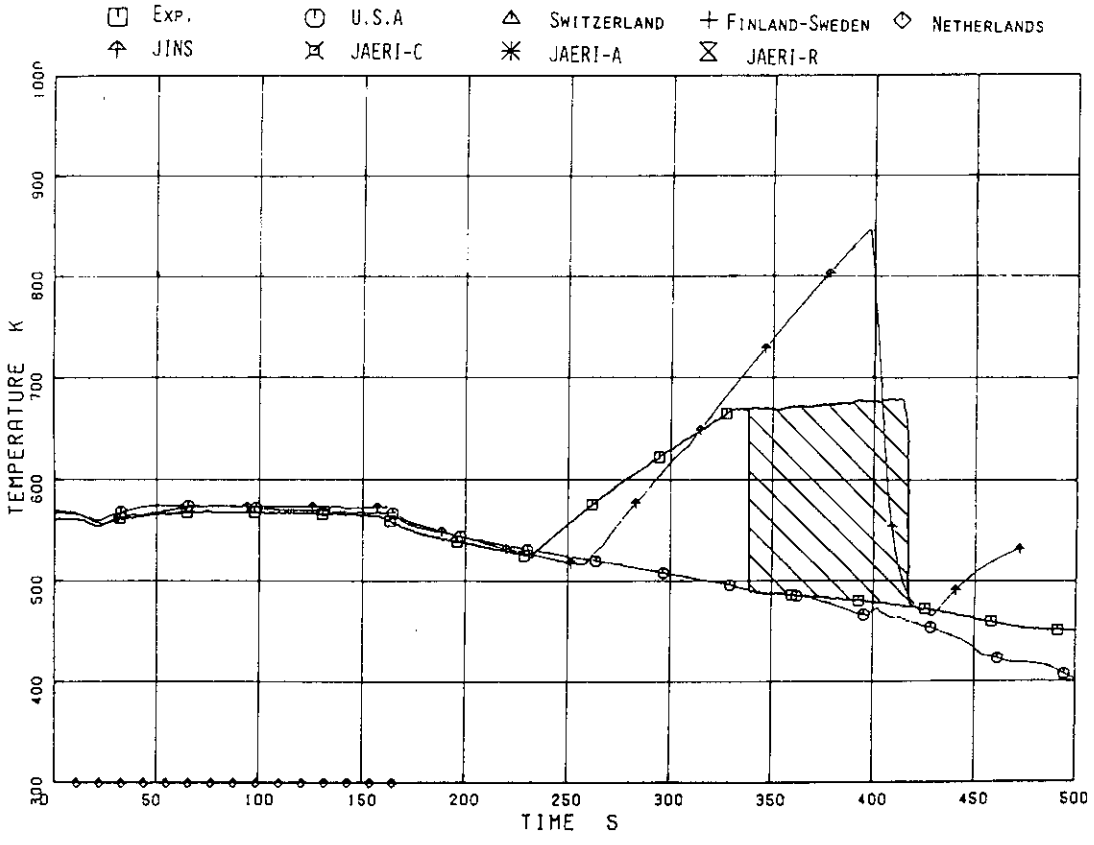

Fig.4.106 Rod Surface Temperature in Average Power Channel (L.P.F.=1.0 , Pos.5)

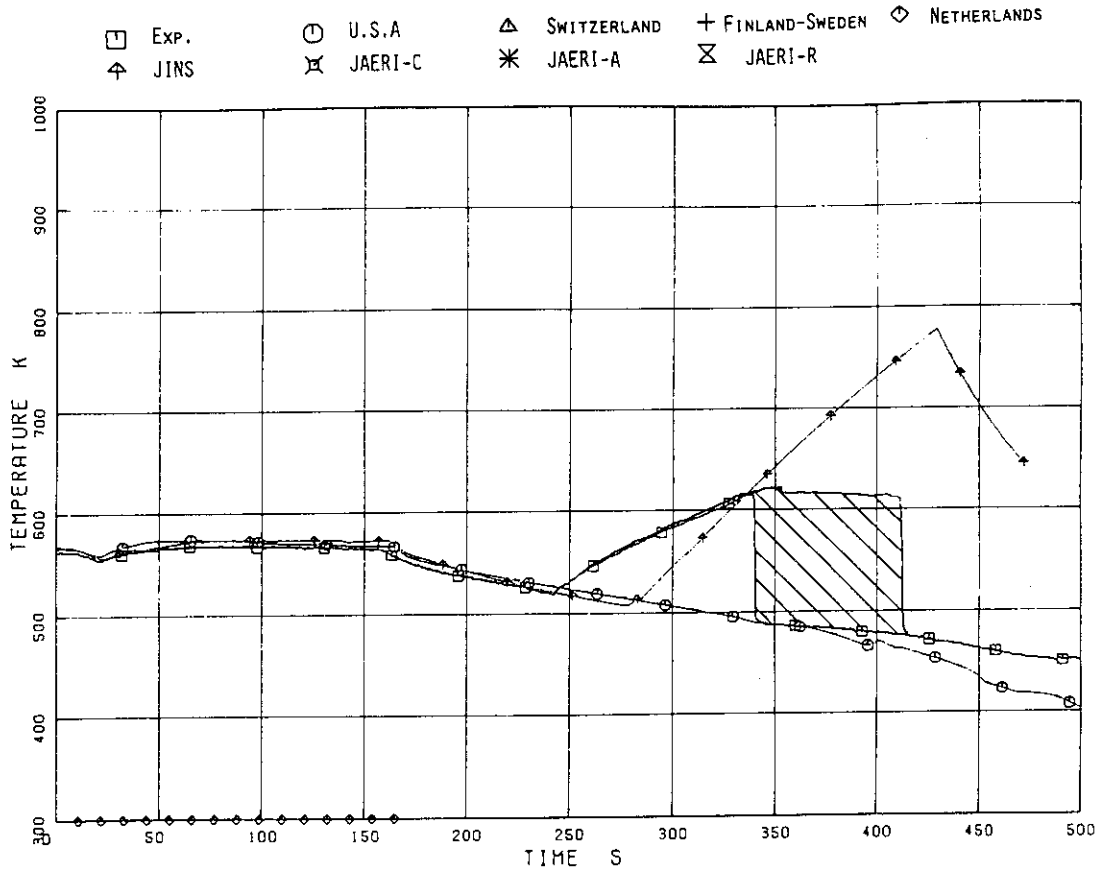

Fig.4.107 Rod Surface Temperature in Average Power Channel (L.P.F.=1.0 , Pos.6)

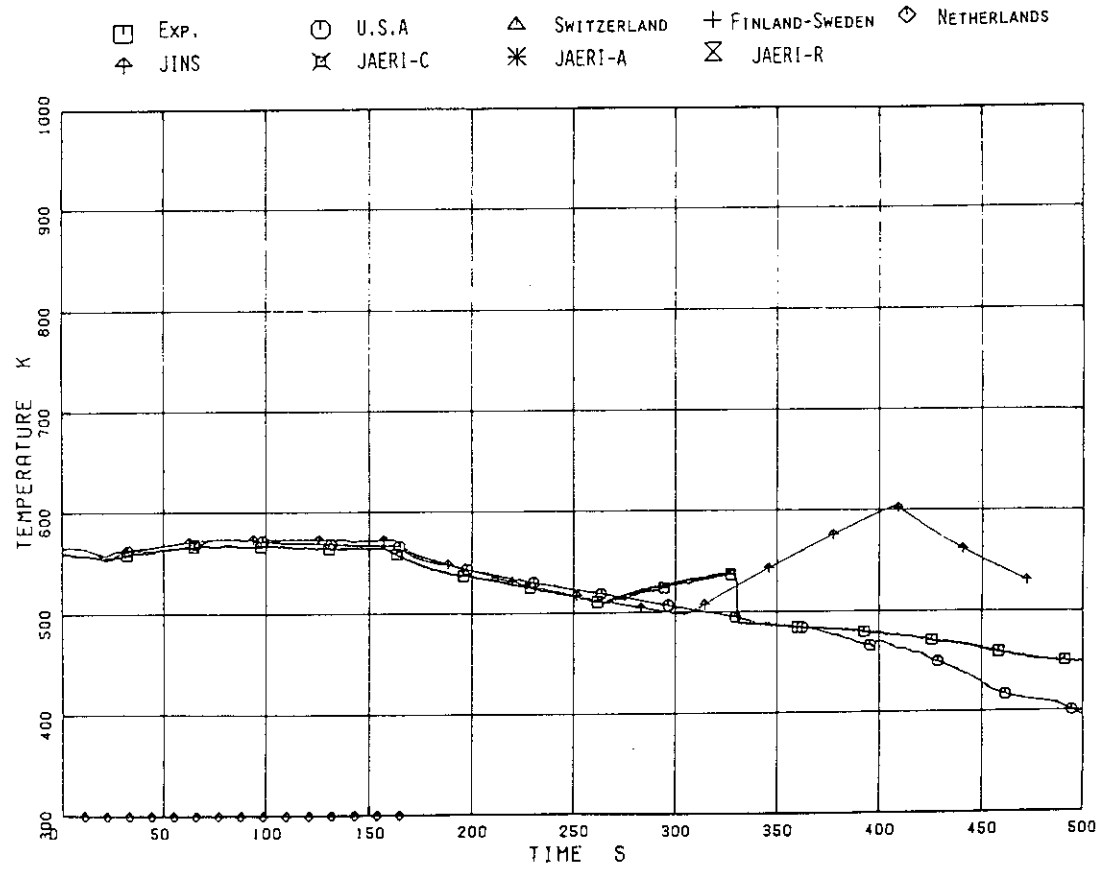

Fig.4.108 Rod Surface Temperature in Average Power Channel (L.P.F.=1.0 , Pos.7)

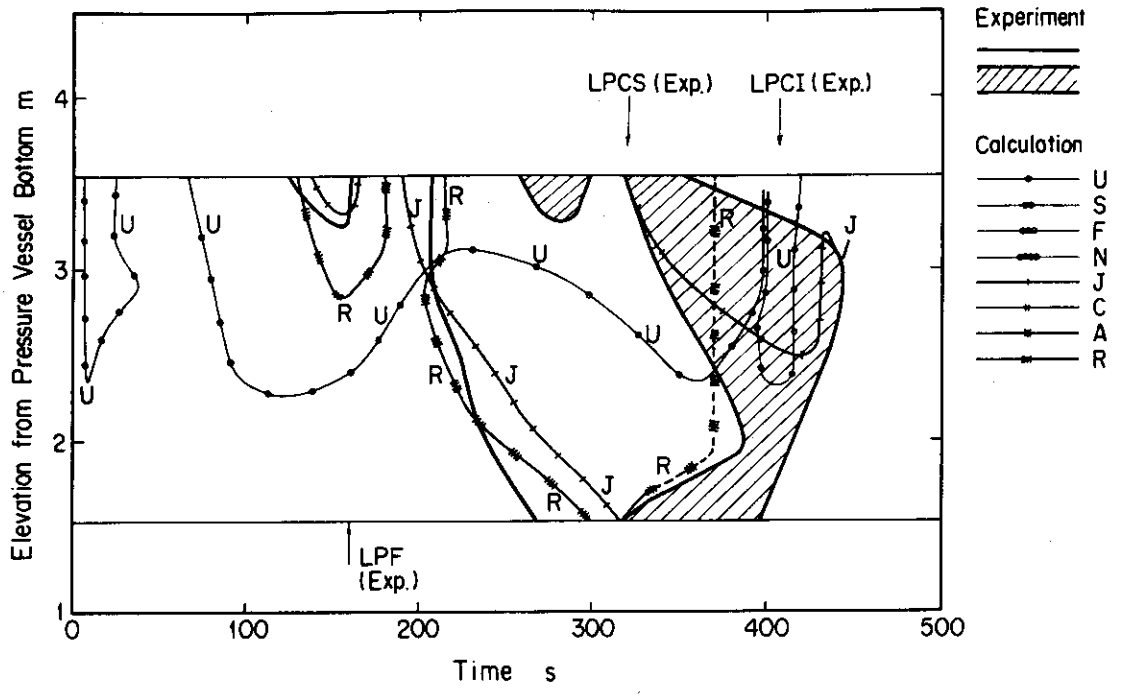

Fig.4.109 Dryout and Quench Front on the Peak Power Rod
(L.P.F.=1.1) in High Power Channel

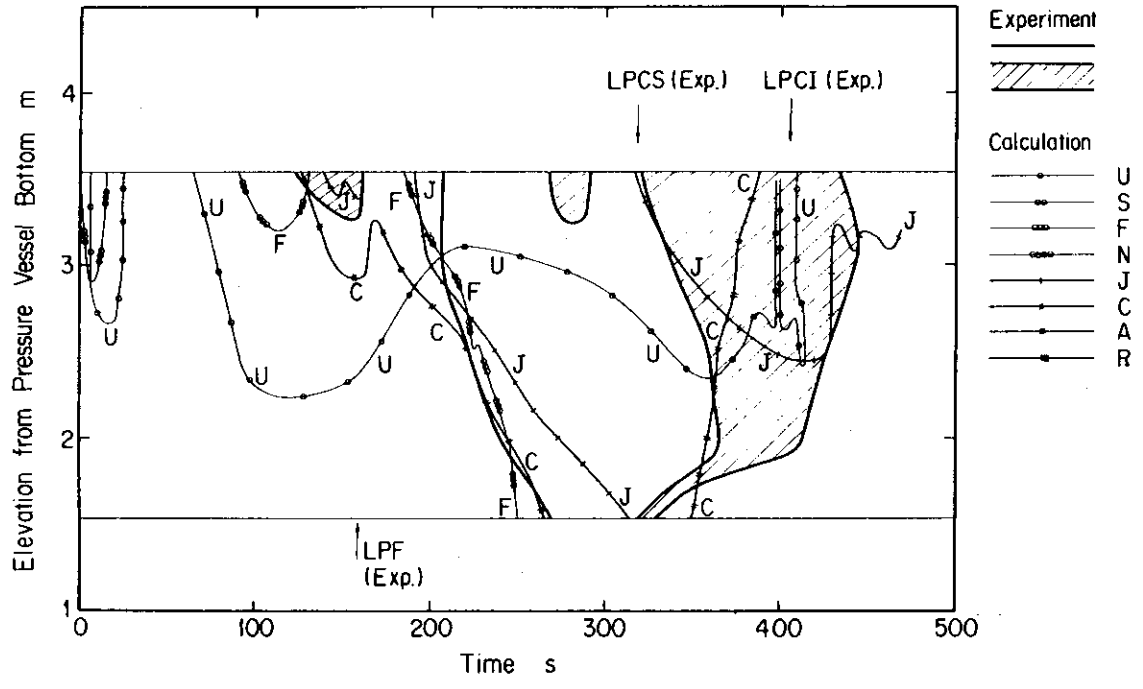

Fig.4.110 Dryout and Quench Front on the Average Power Rod
(L.P.F.=1.0) in High Power Channel

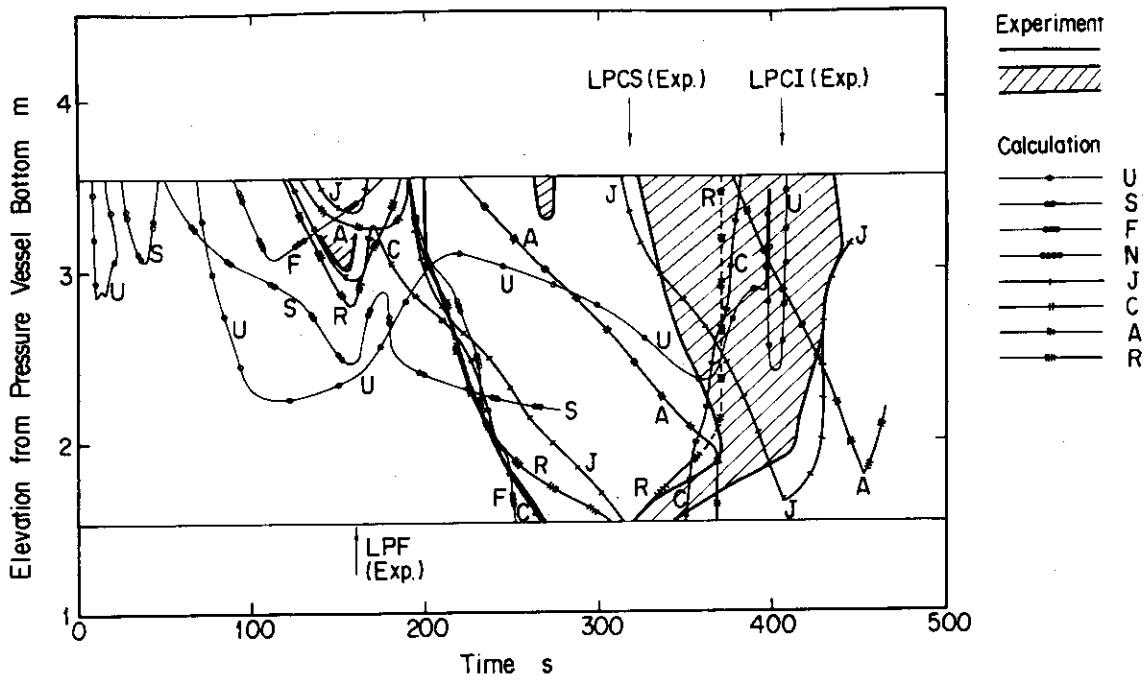

Fig.4.111 Dryout and Quench Front on the Average Power Rod
(L.P.F.=1.0) in Average Power Channel

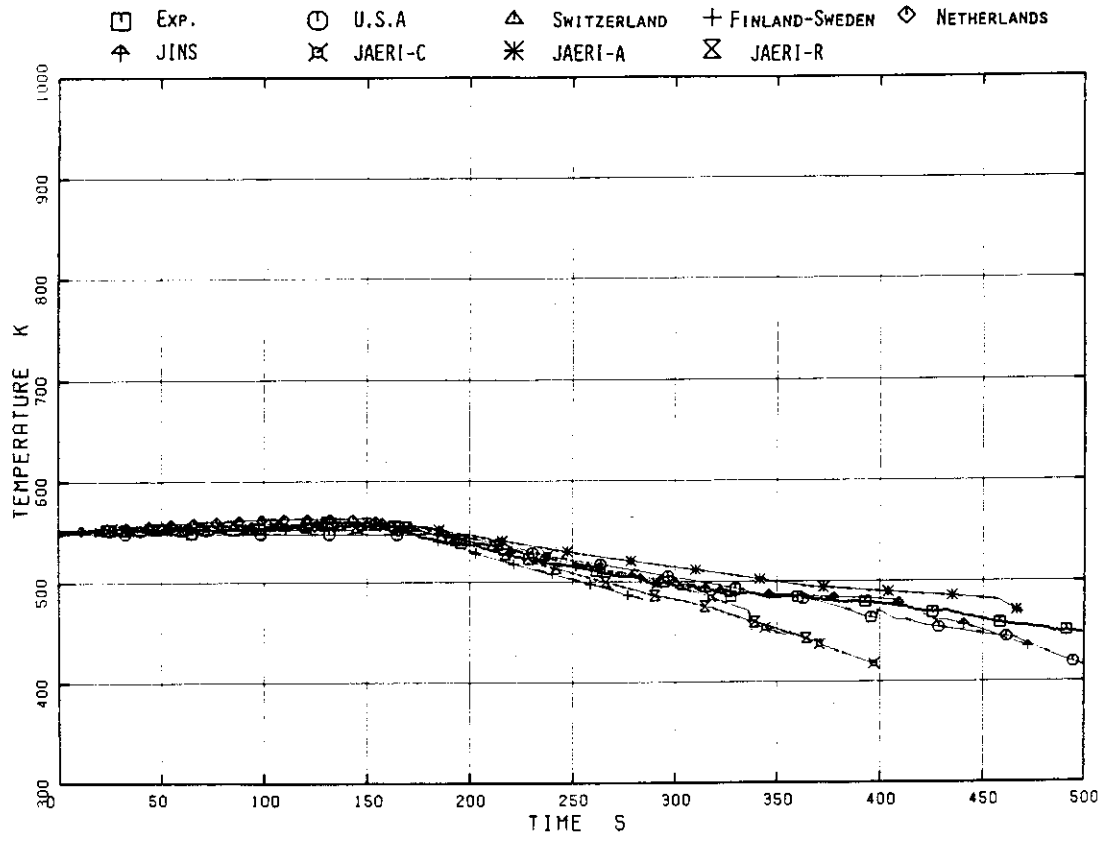

Fig.4.112 Lower Plenum Fluid Temperature

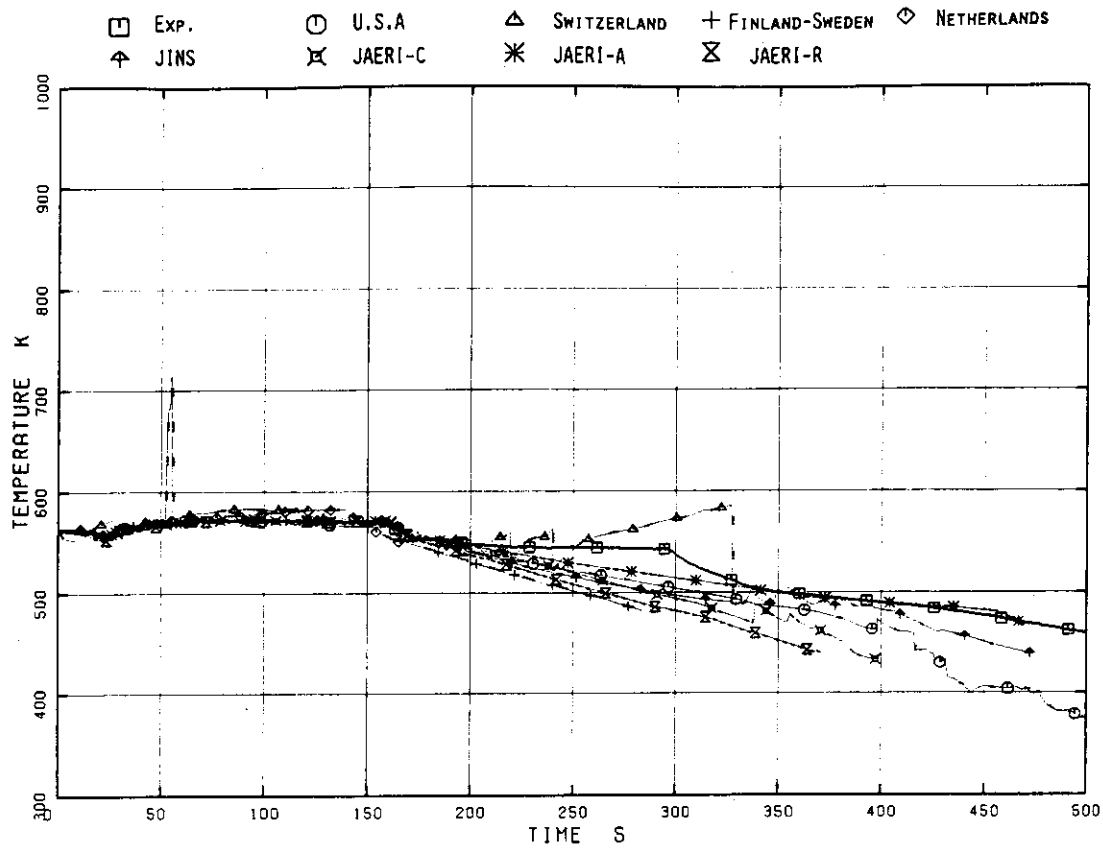

Fig.4.113 Upper Plenum Fluid Temperature

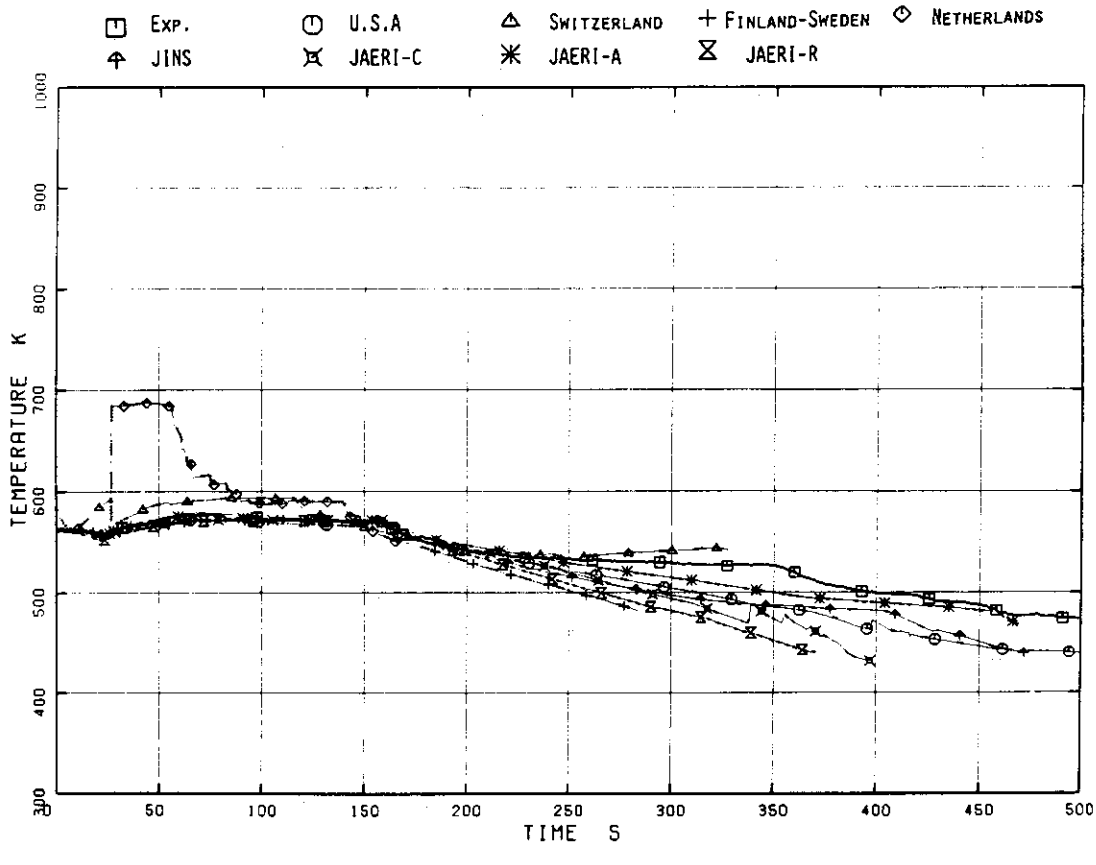

Fig.4.114 Steam Dome Fluid Temperature

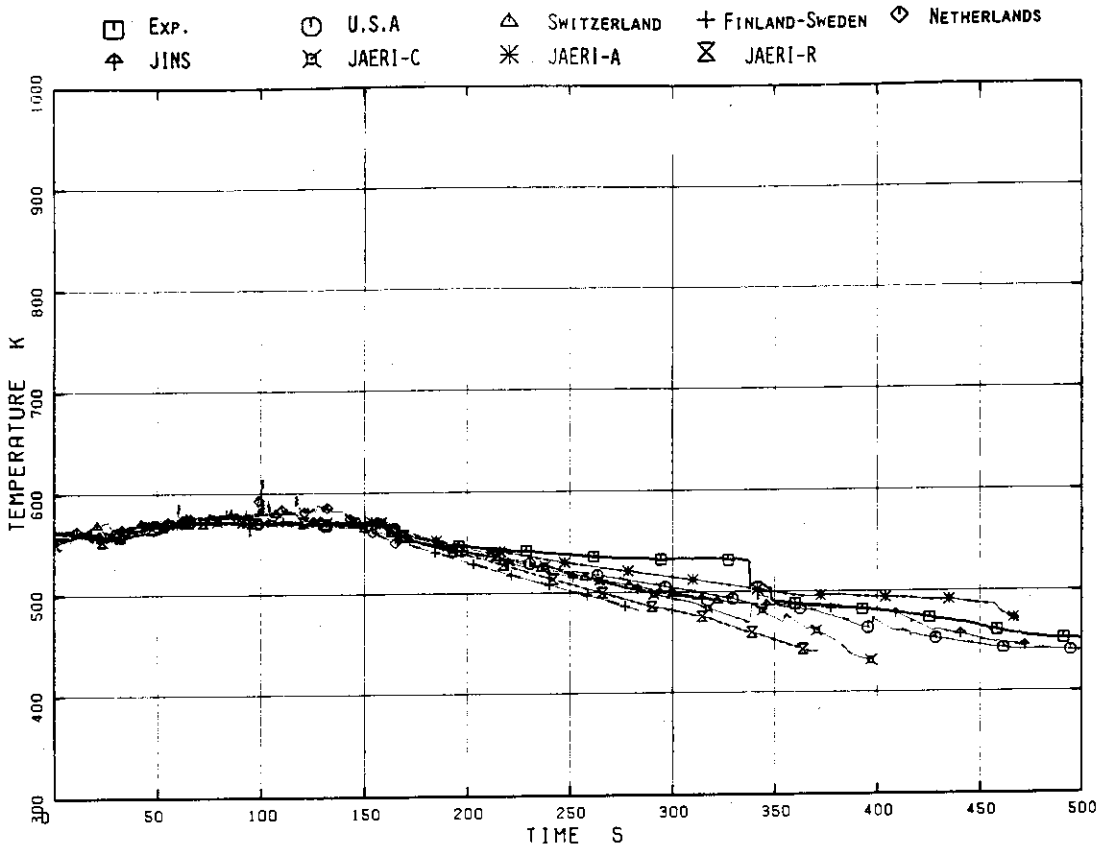

Fig.4.115 Upper Downcomer Fluid Temperature

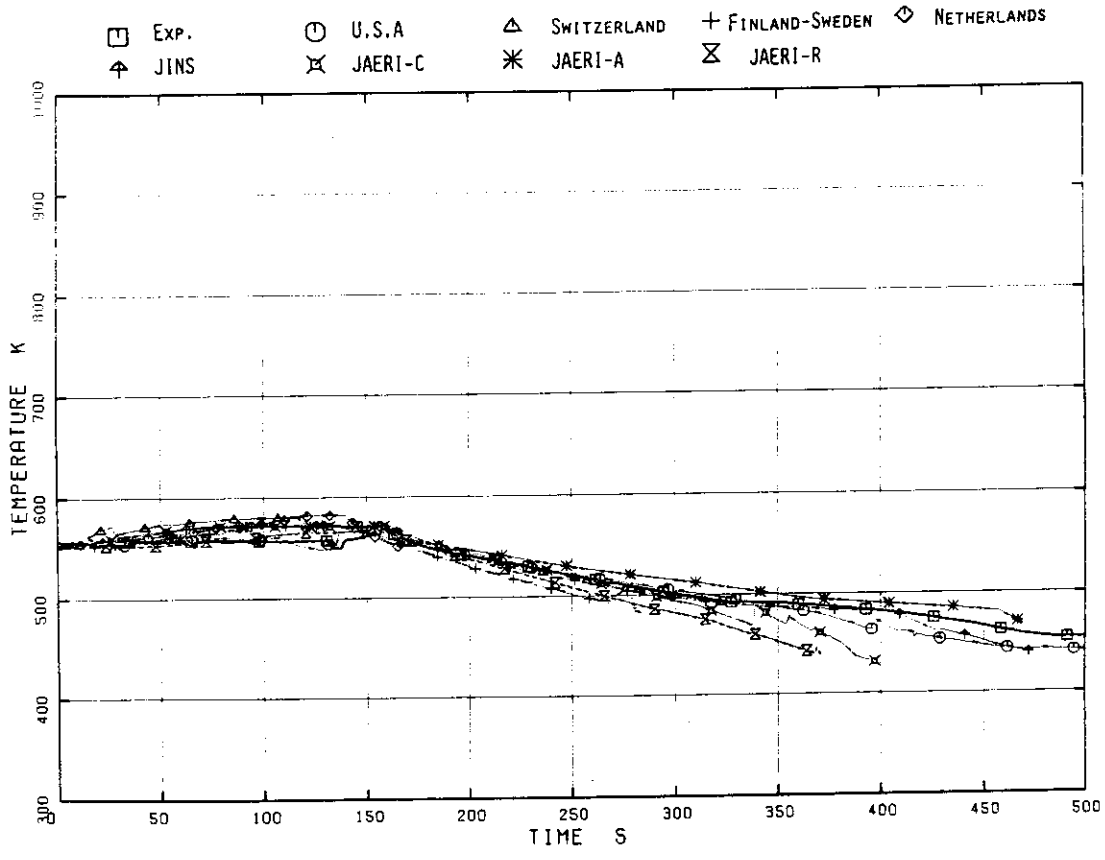

Fig.4.116 Lower Downcomer Fluid Temperature

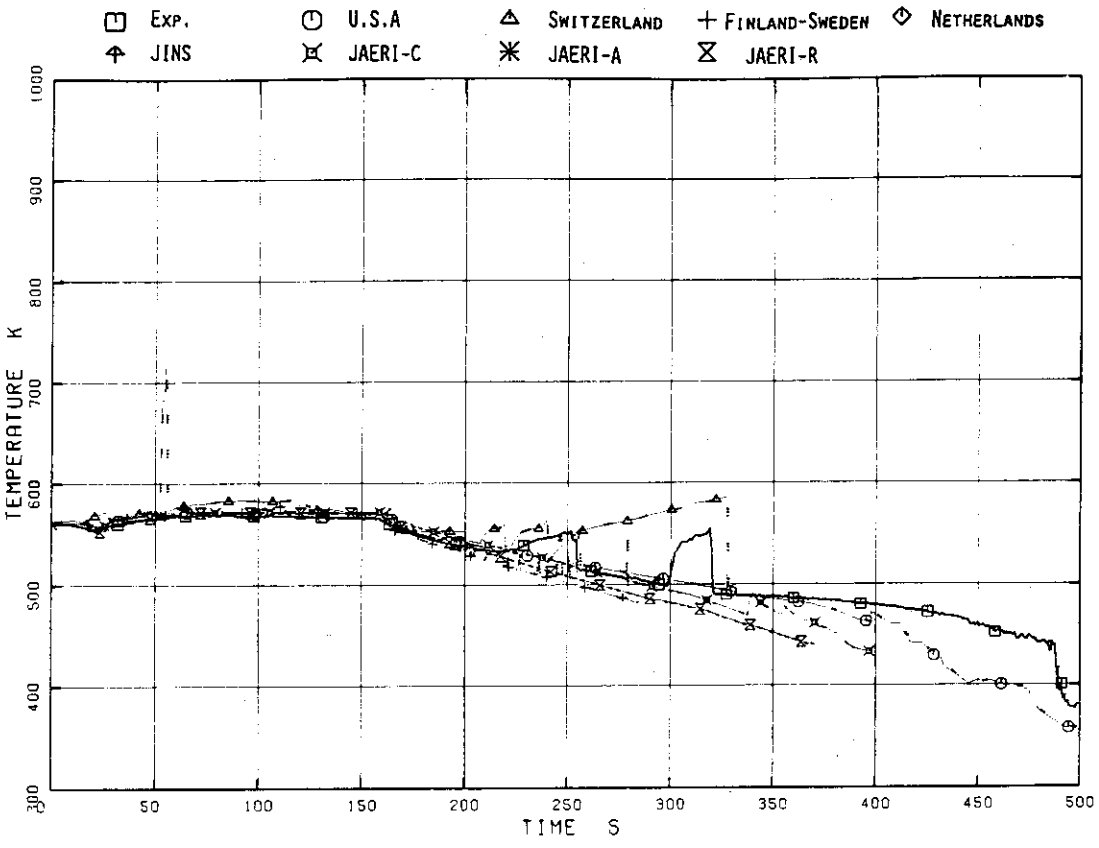

Fig.4.117 Fluid Temperature above Upper Tieplate

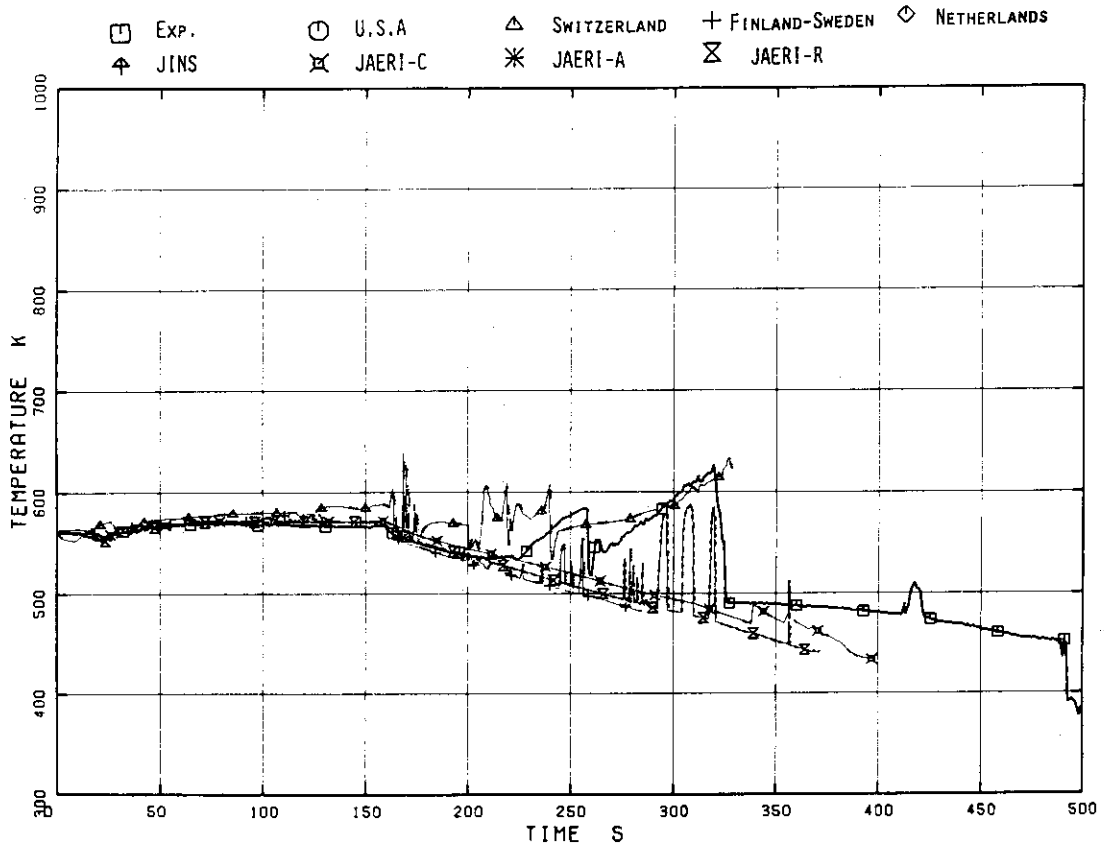

Fig.4.118 Fluid Temperature below Upper Tieplate

5. Conclusions

Comparisons between measurements from ROSA-III Test Run 912 and calculations from eight participants using five different computer codes have lead to the following conclusions.

The trends of the system pressure were calculated by most participants. However, a considerably higher pressure before ADS actuation without using the safety relief valve model in RELAP4/MOD6 was calculated by two participants. The system pressure after ADS actuation was considerably lower than the measured pressure as calculated by two participants and higher per one participant primarily due to insufficient modeling of the ADS flow.

The measured break flow has a large uncertainty of at least ±20 %, however, the accuracy of the integrated break flow calculation before the uncovery of the recirculation line outlet nozzle in the downcomer can be assessed by the timing of the rapid decrease in break flow. The time of the recirculation outlet nozzle uncovering calculated by most participants agreed with the measured time of 160 s within +10 s and -25 s. The break flow calculated by one participant was much higher than the other results and the time of the recirculation outlet nozzle uncovering (RLU) was 50 s earlier than the experimental result because the calculated break flow was adjusted to the data with large uncertainties. The break flow after RLU calculated by most participants was similar. However, one participant calculated the break flow to be approximately two times larger than the others because of the selection of an extraordinarily high transition quality (0,3) from the Henry-Fauske critical flow model to the homogeneous equilibrium model.

The measured total core inlet flow became negligibly small after 50 s. This trend was calculated by most participants. Quantitatively higher flow rates were calculated by the four participants who used incomplete data of the ROSA-III recirculation pump, without measured torque data. The other four participants are considered to have used the experimental pump coastdown curve (pump speed vs. time) and calculated the core inlet flow rate accurately. However, the calculated flow rate was less than the measured flow rate for a certain time period in the analyses of three participants out of four.

The mixture level transient in the core was calculated well by selecting the parameters carefully for the Wilson's bubble rise velocity and the void distribution below the mixture level by RELAP4/MOD6/U4/J3 or THYDE-B1. RELAP5/MOD1 calculated the mixture level transient in the core well which indicates the adequacy of the interphasial friction correlation and the flow regime map used in the code. The mixture level was defined for the advanced code as the level separating the regions with the void fraction greater and less than 0.95. There were significant differences between the measured mixture level transient and the calculated one by TRAC-BD1 which indicates the necessity for the improvement of the two-phase flow models in the code.

There is a strong correlation between the heater rod surface temperature transient and the mixture level transient in the core. Temperature rise or dryout corresponds to exposing of the heater rod surface to steam above the mixture level and temperature turnaround corresponds to the covering of the surface by a two-phase mixture below the mixture level. The trends of the heater rod surface temperatures calculated by TRAC-BD1 and RELAP4/MOD6 (Switzerland) were in poor agreement with measured results because of a poor prediction of the mixture level transient. No rewetting was calculated at the top part of the core by LPF and no dryout was calculated at the bottom part of the core. The trends of dryout and rewetting were calculated well by RELAP5/MOD1, RELAP4/MOD6/U4/J3 and THYDE-B1. However, a considerable delay in the dryout was calculated in one of the RELAP4/MOD6/U4/J3 analysis (JAERI-A) because of inappropriate selection of parameters for the mxiture level calculation. The temperature increase rate after dryout was larger than the experimental value because the evaluation model heat transfer correlations were used in RELAP4/MOD6/U4/J3 after initiation of LPCS. The peak cladding temperature (PCT) was calculated 125 K higher than the measured PCT in one of the RELAP4/MOD6/U4/J3 analysis (JINS). Top-down quenching was calculated in the RELAP4/MOD6/U4/J3 analysis, however, the heater rod surface temperature started to rise again after reflooding because of a conservative heat transfer coefficient used after reflooding. The temperature increase rate after dryout calculated by RELAP5/MOD1 and THYDE-B1 was lower than the measured increase rate. In the THYDE-B1 analysis the shroud inside region is expressed by one node, therefore, no super-heated steam condition can be calculated, resulting in the lower heater rod surface temperature after

dryout. The RELAP5/MOD1 code uses the heat transfer correlation for the laminar natural convection after dryout. The applicability of this heat transfer mode to the region after dryout should be assessed.

Acknowledgment

The authors are grateful to K. Yamano and H. Gotoh of Information System Laboratory and N. Fujita of Nippon Computer Bureau Corporation for their valuable assistance in plotting the results and preparing the report.

dryout. The RELAP5/MOD1 code uses the heat transfer correlation for the laminar natural convection after dryout. The applicability of this heat transfer mode to the region after dryout should be assessed.

Acknowledgment

The authors are grateful to K. Yamano and H. Gotoh of Information System Laboratory and N. Fujita of Nippon Computer Bureau Corporation for their valuable assistance in plotting the results and preparing the report.

References

(1) Anoda, Y., et al., "ROSA-III System Description for Fuel Assembly No.4", JAERI-M 9363, (1981).

(2) Kumamaru, H., et al., "Quick Look Report for ROSA-III 5% Small Break Test, Run 912", Internal Report, (1981).

(3) Anoda, Y., et al., "Experiment Data of ROSA-III Integral Test Run 912 (5% Split Break Test without HPCS Actuation)", JAERI-M 82-010, (1982).

(4) Sobajima, M., et al., "Instrumentation and Data Processing for ROSA-III Test", JAERI-M 8499, (1979).

(5) Abe, N. and Tasaka, K., "Electric Power Transient Curve for ROSA-III Tests", JAERI-M 8728, (1980).

(6) EG&G, "TRAC-BD1, An Advanced Best Estimate Computer Program for Boiling Water Reactor Loss-of-Coolant Accident Analysis," NUREG/CR-2178 (Volume 1 ∿ 4) (1981).

(7) EG&G, "RELAP4/MOD6, A Computer Code Program for Transient Thermal-Hydraulic Analysis of Nuclear Reactors and Related Systems, User's Manual," CDAP-TR-003 (1978).

(8) EG&G, "RELAP5/MOD1 Code Manual," NUREG/CR-1826 (Volume 1,2) (1980).

(9) Yoshida, K., et al., "RELAP4/MOD6/U4/J3, A JAERI Improved Version of RELAP4/MOD6 for Transient Thermal-Hydraulic Analysis of LWR Including Effects of BWR Core Spray," JAERI-M 9394 (1981).

(10) Muramatsu, K., "Computer Programs, THYDE-B1 for Analysis of Small Break LOCA of a BWR and THYDE-B-REFLOOD for Analysis of Reflood Phase," JAERI-M 8119 (1979) (in Japanese).